UNIVERSITY OF SOUTHAMPTON
FACULTY OF ENGINEERING AND THE ENVIRONMENT

Civil, Maritime and Environmental Engineering and Science

Energy Extraction from Shallow Tidal Flows

Jack William Giles

Thesis for the degree of Engineering Doctorate

Industrial sponsor
IT Power Ltd.

December 2013

Abstract

Over the past decade within the renewable energy sector a strong research and development focus has resulted in the growth of an embryonic tidal stream energy industry. Previous assessments of the tidal stream resource appear to have neglected shallow tidal flows. This resource located in water depths of 10-30m is significant because it is generally more accessible for energy extraction than deeper offshore tidal sites and hence a good location for first generation tidal stream arrays or fences. The close proximity to shore may lead to improvements in construction feasibility and economic prospects. The objective of this project is to investigate several aspects concerning the exploitation of shallow tidal flows for energy extraction. Fundamental to this project is the importance of developing research alongside and in conjunction with industrial shallow water prototype projects.

The key objectives are: (1) The development and understanding of the use of artificial flow constraint structures in the form of specifically-shaped foundations (herein described as "ramp-foundations") that constrain the flow leading to an increase in the magnitude and quality of power from marine current energy convertors (MCEC) operating in shallow tidal flows. (2) The investigation of seabed and free-surface proximity effects on the downstream wake structure of a MCEC. (3) Commercial shallow water device optimisation; utilising project results to aid with the design and development of full-scale commercial demonstrators.

Through theoretical and scaled experimental modelling, and commercial collaboration the project has concluded ramp-foundations could be utilised to locally increase tidal flow velocities and increase MCEC output across a tidal cycle in shallow flows. Predicted power benefits are in the region of 5-22% depending on lateral and vertical ramp channel blockage ratios. The ramp width or overall array width must therefore be tuned to the channel width to maximise power benefits. Ramp-foundations will thus only be technically viable in relatively narrow channels or ideally in MCEC arrays or tidal fences.

Results have shown that the downstream wake length is dependent on and varies with the vertical flow constraint and it is critical that the downstream array spacing of MCECs are tuned to the local flow depth. An optimum device height to flow depth ratio to minimise wake length has been identified.

It is hoped that this ramp-foundation concept and the relationship between boundary proximity and wake length will continue to help with the development of a niche shallow tidal energy market.

List of Contents

Appendix A

GILES, J., MYERS, L., BAHAJ, A. S., O'NIANS, J. & SHELMERDINE, B. 2011a. Foundation-based flow acceleration structure for marine current energy converters. IET Renewable Power Generation, 5, 287-298.

Appendix B

GILES, J., MYERS, L., BAHAJ, A. S. & SHELMERDINE, B. 2011b. The downstream wake response of marine current energy converters operating in shallow tidal flows. World Renewable Energy Congress 2011. Linkoping, Sweden.

Appendix C

GILES, J., MYERS, L., BAHAJ, A. S., SHELMERDINE, B. & PAISH, M. 2011c. The Commercialisation of Foundation-based Flow Acceleration Structures for Marine Current Energy Converters. 9th European Wave and Tidal Energy Conference. Southampton, UK.

List of Figures and Tables

Nomenclature

a	Axial induction factor or distance between two nodes (node arm length)
A	Quadratic fit coefficient
A_d	Area of actuator disk (MCEC area)
ADCP	Acoustic Doppler Current Profiler
ADV	Acoustic Doppler Velocimeter
B	Tidal constant or quadratic fit coefficient
b	Distance between streamlines
C	Tidal constant or quadratic fit coefficient
c	Blade chord length or Linear fit coefficient
Cd	Drag coefficient
CFD	Computational Fluid Dynamics
C_p	Power coefficient
C_{pmax}	Power coefficient at Betz limit
C_t	Thrust coefficient
d	Total flow depth
D	MCEC rotor diameter or Actuator Disk diameter
dB	Decibel
d_c	Critical depth
E	Specific Energy
F	Force
Fd	Froude number
G	Gravitational constant ($6.6x10^{-11}$ m^2N/kg^2)
g	Acceleration due to gravity ($9.8ms^{-2}$)
GIS	Geographic Information System
GW	Gigawatt
HAT	Horizontal axis turbine
Hz	Hertz
I	Turbulence intensity
k	Roughness height
KE	Kinetic Energy
kW	Kilowatt
kWh	Kilowatt hour
LAT	Lowest Astronomical Tide
LB	Lateral blockage ratio (device width to channel width ratio)

LDV	Laser Doppler Velocimeter
m	Mass or linear fit coefficient (m_1 = first mass & m_2 = second mass)
MCEC	Marine current energy convertor
MCT	Marine Current Turbines Ltd.
Mnp	Mean neap peak tidal velocity
Msp	Mean spring peak tidal velocity
MW	Megawatt
MWh	Megawatt hour
n	Number of streamlines
N	Number of data points in sample or Newtons
NPV	Net Present Value
OTEC	Ocean thermal energy conversion
P	Pressure
PE	Potential Energy
$\mathbf{P_{gain}}$	Power gain from ramp-foundations
PSCD	Pulse Stream Commercial Demonstrator
PV	Present Value
Q	Total flow rate
q	Flow rate between a pair of streamlines or discharge per unit width
r	Radius, Radial distance to object
R	Ratio of flood to ebb tide
$\mathbf{R_L}$	Ramp width to channel width ratio
$\mathbf{R_V}$	Ramp height to flow depth ratio
$\mathbf{R^2}$	Coefficient of Determination
Re	Reynolds number
ROC	Renewables Obligation Certificates
SNR	Signal to Noise Ratio
t	Time or maximum thickness as a fraction of the blade chord
$\mathbf{T_0}$	Diurnal period
$\mathbf{T_1}$	Spring-neap period
TW	Terawatt
U	Axial velocity
$\mathbf{U_{(t)}}$	Axial velocity with regards to time
u(x)	Velocity component, x direction
$\mathbf{u_*}$	Shear velocity
$\mathbf{U_0}$	Free-stream velocity

$\mathbf{U_d}$	Velocity at actuator disk
$\mathbf{U_{t(z)}}$	Axial velocity with respect to height above channel bed and time
$\mathbf{U_w}$	Downstream wake velocity
V	Mean velocity or velocity along streamline
v(y)	Velocity component, y direction
VAT	Vertical axis turbine
VB	Vertical blockage ratio (device height to flow depth ratio)
$\mathbf{V_{gain}}$	Velocity increase or gain from ramp-foundations
W	Channel width
w(z)	Velocity component, z direction
x	Downstream direction or Position along blade chord
y	Across channel direction or Half blade thickness at point x
$\mathbf{Y_2}$	Surface drop
$\mathbf{y_{ramp}}$	Ramp width
z	Height above channel bed
$\mathbf{Z_2}$	Ramp height

$\boldsymbol{\delta}$	Boundary layer thickness
$\boldsymbol{\theta}$	Rotation angle
$\boldsymbol{\lambda}$	Length of shortened node arms or filtering constant
$\boldsymbol{\mu}$	Dynamic viscosity or bed friction coefficient
$\boldsymbol{\nu}$	Kinematic viscosity
$\boldsymbol{\pi}$	Pi
$\boldsymbol{\rho}$	Density
$\boldsymbol{\sigma}$	Standard deviation of sample
$\boldsymbol{\tau}$	Shear stress
$\boldsymbol{\varphi}$	Velocity Potential Function
$\boldsymbol{\psi}$	Stream Function

Declaration of Authorship

I, Jack William Giles

declare that the thesis entitled

Energy Extraction from Shallow Tidal Flows

and the work presented in the thesis are both my own, and have been generated by me as the result of my own original research. I confirm that:

- this work was done wholly or mainly while in candidature for a research degree at this University;
- where any part of this thesis has previously been submitted for a degree or any other qualification at this University or any other institution, this has been clearly stated;
- where I have consulted the published work of others, this is always clearly attributed;
- where I have quoted from the work of others, the source is always given. With the exception of such quotations, this thesis is entirely my own work;
- I have acknowledged all main sources of help;
- where the thesis is based on work done by myself jointly with others, I have made clear exactly what was done by others and what I have contributed myself;
- parts of this work have been published as:

GILES, J., MYERS, L., BAHAJ, A. S., O'NIANS, J. & SHELMERDINE, B. 2011a. Foundation-based flow acceleration structure for marine current energy converters. IET Renewable Power Generation, 5, 287-298.

GILES, J., MYERS, L., BAHAJ, A. S. & SHELMERDINE, B. 2011b. The downstream wake response of marine current energy converters operating in shallow tidal flows. World Renewable Energy Congress 2011. Linkoping, Sweden.

GILES, J., MYERS, L., BAHAJ, A. S., SHELMERDINE, B. & PAISH, M. 2011c. The Commercialisation of Foundation-based Flow Acceleration Structures for Marine Current Energy Converters. 9th European Wave and Tidal Energy Conference. Southampton, UK.

GILES, J. W., MYERS, L., BAHAJ, A. S. & O'NIANS, J. 2009. An experimental study to assess the potential benefits of foundation based flow acceleration structures for marine current energy converters. 8th European Wave and Tidal Energy Conference. Uppsala, Sweden.

MYERS, L., BAHAJ, A. S., GERMAIN, G. & GILES, J. 2008. Flow boundary interaction effects for marine current energy conversion devices. World Renewable Energy Congress X. Glasgow.

Signed: ……..

Date: …….

Acknowledgements

I would like to thank the following people and groups who have all been instrumental throughout my Engineering Doctorate:

I would like to express my sincere gratitude to my supervisor Luke Myers for his continuous support and advice throughout the project. I thank him for always making time to chat and for having the belief in me in the first instance to undertake this Engineering Doctorate.

My supervisor and head of research group AbuBakr Bahaj for his support and motivation. I would also like to thank him for making this project a reality and giving me the opportunity to be part of the Sustainable Energy Research Group team.

Everyone at the Bristol office of my industrial sponsor IT Power. Particularly over the two years while based in Bristol they provided support, advice, encouragement, friendship and laughter. Specifically I would like to say a big thank you to my industrial supervisor Bob Colclough who has endlessly answered questions, provided advice and inspired me to try windsurfing!

My friends from the Civil Engineering research office; Mark Leybourne, Tassos Papafragkou Jonathan Dewsbury, Kevin Briggs, Cath Harvey, Nick Bakker (aka Nick the Greek), Gabi Wojtowitz, Pascal Galloway, Despoina Teli, Davide Magagna and Nicolas Choplain (aka Nick the French). They have all provided inordinate friendship and help throughout the doctorate with academic advice, fun filled times, cycling trips, games of golf, holidays and eventful sailing adventures!

Friends from Clifton Lawn Tennis Club for providing a welcomed escape from thesis writing and a constant source of laughter. Sincere thanks to Bob Hill for proof reading this thesis from cover to cover.

Special thanks to family friend Alan White for his inspirational engineering help and advice along the way.

My family and Fiona for their boundless support and belief in me to complete this doctorate. In particular I would like to thank my parents and grandparents because without them I would never be where I am today.

Chapter 1

1 Introduction

1.1 Renewable Energy

Renewable energy can be defined as, "energy obtained from natural and persistent flows of energy occurring in the immediate environment" (Twidell and Weir, 2006). There are numerous types of renewable energy technology including photovoltaic generation, hydro-power, wind power, biomass fuels, biofuels, wave power, tidal power and geothermal energy.

In recent years there has been a significant increase in the development and deployment of renewables. This has primarily been driven by increased environmental awareness and government policy. The UK government first pledged in its 2003 Government White Paper on energy (DTI, 2003) to increase the quantity of the UK's electricity generated from renewable energy. The government specified that 10% of the UK's energy would be generated from renewable sources by 2010 and hoped that this would reach 20% by 2020. These targets were reiterated in the 2007 White Paper (DTI, 2007). The primary objective of this increase was to reduce the production of Greenhouse gases; electricity generation produces approximately 30% of the UK's carbon dioxide emissions (Postnote, 2007). Greenhouse gases are thought to be contributing to the global warming effect by causing global temperature rise. In response with the Climate Change Act 2008 the Government set a legally binding target for 80% reduction in carbon emissions by 2050, with the objective of moving towards a more energy efficent and low carbon economy (Great Britain, 2008). The Government's 2011 Energy White Paper (DECC, 2011) sets a commitment to provide a secure, low carbon and affordable future energy supply network. The paper focuses on decarbonising electricity supply by providing 15% of energy from renewables by 2020, increasing Carbon Capture and Storage (CCS) and providing a new system of long term contract incentives for low carbon technologies. Over the next two decades the UK is expected to require 30-35 GWs of new electricity generation capacity and two thirds of this by 2020 (DTI, 2007). At present the majority of the UK's electricity (86.0% in 2012) is generated from fossil fuel and nuclear power stations, with many of these reaching the end of their useable life (DECC, 2012). The security of energy supply is influenced by various factors, the key ones being the available reserves of fossil fuels and the world's over-dependence on fossil fuels, with statistics showing a 88% world fossil fuel dependence in 2009 (BP, 2010).

Reserve levels of oil, coal and gas have been predicted at 35, 107 and 37 years respectively. Although coal reserves are currently abundant, barriers exist because of environmental problems and the slow development of clean coal technologies (Shafiee and Topal, 2009). A major concern is the limited abundance of oil and gas reserves; crude oil is described as being the most important primary world fuel and made up 34.8% of world energy consumption in 2009 (BP, 2010). In 2010 the UK depended on natural gas for 46.3% of its electricity needs (DECC, 2011a), Watson and Scott (2009) highlight the risks of security of supply and attacks on international pipelines that surround the use of imported natural gas. To meet the required future generation capacity, heavy investment will be required in the UK's power industry. A large investment is likely to be in renewable energy (DTI, 2005). In the last 20 years there has been a shift in the UK energy mix with an increased reliance on gas and a reduction in coal-fired power stations (Postnote, 2007); the introduction of the EU's Large Combustion Plant Directive has made the operation of existing coal fired stations difficult due to imposed restrictions on emissions. Since the 2007 White Paper there has been renewed government interest in renewing the UK nuclear energy industry. Although nuclear power has low carbon emissions, major problems exist with decommissioning, disposal of radioactive waste and threats from terrorist attacks on nuclear infrastructure (Venables, 2008). In 2012 the UK generated 11.3% of its electricity from renewable sources, an increase from 5.8% in 2008 (DECC, 2012).

Although the fuel cost for renewable technology is often zero, the capital cost can be considerable. However, government subsidies exist to help. The Renewables Obligation (RO) is a government subsidy which acts as a support mechanism for renewable technology; it allows renewable energy to be competitive with non-renewable sources such as coal, gas and nuclear power (DTI, 2007). For renewable technology to succeed it must become cost competitive with non-renewable sources. It is essential that low cost and reliable electricity is supplied to the consumer.

Providing energy security includes utilising a diverse range of reliable energy sources with a stable energy cost per unit of generated energy. This is a vital consideration because governments must provide a safe and reliable mix of energy for their nation (HM Government, 2009). Indigenous non-renewables also contribute to diversity but their inherent centralisation can leave them exposed to large scale failures, whereas renewables tend to be dispersed in nature, increasing their security. The UK has been stated as having some of the best renewable resources in Europe, particularly in terms of wind and marine resources (DTI, 2007).

1.2 Marine Renewables

The oceans are a vast and powerful source of energy which could potentially be harnessed to supply more than enough energy to meet worldwide demand for electricity (Pelc and Fujita, 2002). This energy is stored in the form of heat, wind, currents, waves and tides. Marine renewables can be subdivided into four main technologies - tidal energy, wave energy, ocean thermal energy conversion and offshore wind.

Marine renewables have key advantages over land-based renewables. The oceans are a virtually untapped resource which could provide clean energy on a grand scale without manifesting conflicts that are associated with land-based renewables. Many countries, such as the UK, have limited land area suitable for developing onshore renewable energy; hence conflicts over land use, planning consent, noise pollution and visual impacts are common place. Despite this benefit, constructing technology in a harsh marine environment will present many technical challenges. Devices will need to be designed to survive more extreme weather events than those occurring onshore and the technology must not damage the marine environment which is already suffering from pollution, overfishing, habitat loss and climate change (Wilson and Downie, 2003). Placing technology far offshore creates questions regarding the economics and the logistics of long subsea cables and the associated transmission losses. The operation and maintenance of plant located far from shore with limited weather windows must be considered.

Offshore wind is now an established technology and is one of the cleanest energies available. Winds over the oceans generally have greater velocities and are less turbulent than onshore winds; enabling greater device efficiency. With higher levels of generation, the additional construction and operation costs may be offset (Gaudiosi, 1999). With space onshore at a premium in many countries, offshore wind is looking attractive. Moreover, in terms of turbine and farm size there is virtually no limit (Breton and Moe, 2009). Despite the benefits, there are several logistical difficulties associated mainly with construction and maintenance. It has been estimated that it costs 1.5-2 times more for offshore construction and due to inaccessibility repairs can be 5-10 times more expensive than land-based farms (Breton and Moe, 2009). In 2007 European Union members set a target to install 50GW of offshore wind energy in Europe by 2020 (EWEA, 2007). Currently the majority of deployments have

Figure 1-1: Offshore wind,
image from: http://www.vestas.com

occurred in Denmark and the UK. The UK has leases allocated for farms totalling up to 40GWs with the Round 1 and 2 schemes totalling 7.7GW and in 2010 the Government issued leases for up to 31.8GWs in its Round 3 scheme (Toke, 2011). Offshore wind power has now entered the stage of large-scale development (Zhixin et al., 2009). In May 2010 in the UK 1 GW of offshore wind was operational, 1.5GW was under construction, 2.6GW was 'approved but not built' and 43.7GW was in the planning process (DECC, 2010).

Ocean thermal energy conversion (OTEC) generates power by utilising the thermocline that is present in deep oceans. The greatest ocean temperature differences occur near the equator, in the tropics, and this is where the resource is greatest. Utilising the first law of thermodynamics - conservation of energy - heat stored in the warm surface water is used to create steam to drive turbines and the cold deep water is pumped to the surface to re-condense the steam (Boyle, 2004). The benefit of OTEC is an almost limitless supply of energy from the constant temperature difference between the surface and deep water, giving potential for constant base load generation (World Energy Council, 1994). It has been theoretically predicted that there is potential to produce 10TW of power, approximately equal to global demand (Pelc and Fujita, 2002). However as the temperature differences are very small the device efficiency will also be small and the technology is unlikely to be economic without significant subsidies. In addition to generating electricity the technology can be used to desalinate sea water and thus the greatest potential is likely to be for small island communities which need both domestic electricity and fresh water.

The potential for generating electricity from ocean waves has been acknowledged for many years. Large energy fluxes can occur in deep ocean waves and can average between 50-70kW per metre width of the wave (ABP, 2008). Ocean waves are driven by the wind but waves act as an effective store for wind energy because waves show less variability. Due to this higher predictability, energy delivery to the grid can be more reliable than wind power (Elliott, 2009). The Carbon Trust estimates the practical UK offshore wave energy resource to be 50 TWh/year and the near shore/shoreline resource to be 8 TWh/year (Carbon Trust, 2006b). The UK is considered to be one of the best locations for large-scale wave energy extraction due to the fact that it lies at the end of a long fetch across the Atlantic (Cooper et al., 2005). There are difficulties associated with the harsh

Figure 1-2: Pelamis,
image from: http://www.pelamiswave.com

marine environment. More specifically the irregularity of waves, survival of devices in extreme weather conditions and peak power is generally only available at deep water sites located some distance offshore. Devices must be designed to withstand extreme events that will at most only occur infrequently, meaning considerable construction costs without the benefit of increased generation capacity. Despite over 1,000 patented proposals wave power is still not a commercialised technology and will require considerable development and investment to reach this stage (Clément et al. 2002).

Tidal energy's regularity of supply is its major advantage over other renewables, with tides being driven by predictable forces generated by the moon and sun. Tidal energy extraction can be sub-divided into tidal range and tidal stream technologies. Tidal range technology includes barrages and lagoons which exploit tidal potential energy. Seawater is trapped at high-water by a dam or barrier and then released at low-water through turbines. Sites of high tidal range, such as the Severn estuary, provide inordinate potential for power generation (Falconer et al., 2009). It has been estimated that tidal barrages across estuaries and tidal lagoons could provide up to 20% of UK electricity (Elliott, 2009). Despite their vast energy potential, tidal barrages have significant capital costs, are very site specific and can significantly damage the marine environment (Pethick et al., 2009). Tidal stream energy exploits mainly the kinetic energy present in a tidal flow. Energy can be extracted using individual tidal turbines or multiple turbines can be deployed in an array or tidal fence which stretches across a channel. Early turbine designs operated in a similar manner to horizontal axis wind turbines albeit with different rotor configurations (Figure 1.3). In addition a number of vertical axis MCEC designs have also gained influences from early vertical axis wind turbines. This technology has the benefits of reducing capital costs and environmental impacts associated with tidal barrages. Extraction is generally only economic at specific sites where tidal flow velocities have been enhanced by constraining topography (Fraenkel, 2002). An estimate of the practical tidal stream energy resource in the UK is 18 TWh/year and it is expected that the combined contribution from wave and tidal stream could be up to 20% of UK electricity demand (Carbon Trust, 2006b). Tidal energy may be predictable but it is still variable due to spring and neap tides, where neap velocities are significantly reduced. Device installation in the harsh marine environment is a concern, where access is limited with narrow weather windows and short slack

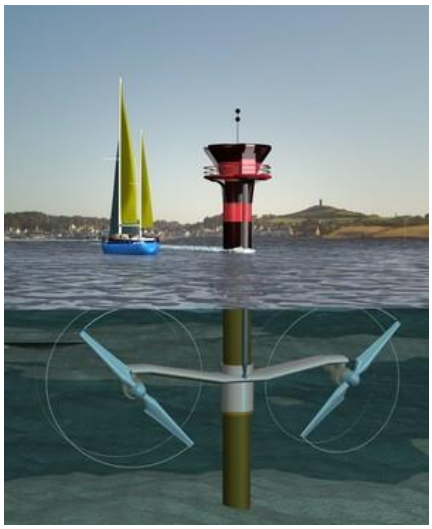

Figure 1-3: SeaGen, image from: http://www.marineturbines.com

tide periods. Tidal range technology is now well understood but tidal stream energy is still in its infancy with only a few full-scale demonstration projects deployed.

1.3 Tidal Power

1.3.1 Introduction

Utilising tidal energy is not a modern manifestation; tidal mills are known to have been operating in the time of the Domesday Book in 1086 (Bryden, 2006). The first significant tidal power plant was La Rance in France which has been operational since 1967 with an installed capacity of 240MW and an average output of 100MW (Garrett and Cummins, 2004). Since La Rance there have only been a few small tidal range installations but in recent years there has been significant interest in tidal stream technology with a number of full-scale demonstration projects being deployed. Tidal stream technology is not yet fully commercialised and it might be said that tidal stream technology is at a similar stage to that of wind energy 25 years ago. Figure 1-4 shows a timeline for commercial and full-scale tidal energy technology. It can be seen that in recent years the majority of development has been with tidal stream technology and now with developers looking seriously at tidal stream arrays. Despite this there is still interest in developing tidal barrages and tidal fences, such as those proposed for the Severn Estuary.

The periodic nature of tides is advantageous in terms of the predictability for power generation, but tidal ranges and flows are still highly variable. This variation occurs from the interaction of the gravitational attraction between the Earth and Moon and also the Earth and Sun. Larger lunar tidal ranges and flows take place when the Earth, Sun and Moon are aligned, these are termed “spring tides” and happen twice per lunar month at times of new and full moon. The highest spring tides occur after the equinoxes in March and September when the Sun crosses the Earth’s celestial equator. When the Sun/Earth and Moon/Earth’s directions are perpendicular to each other, “neap tides” with smaller tidal ranges and flows occur. The spring tidal range is approximately twice that of the neaps, meaning that power output from tidal devices will be considerably lower during periods of neaps. In mid-ocean areas the tidal range is less than one metre with little potential for tidal energy extraction. It is only when tidal flows are constrained by topography or resonance effects arise, that tidal ranges or flows are suitable for energy extraction. This only transpires at specific sites, such as straits between islands, shallows between open seas, around headlands, bays or estuaries (Fraenkel, 2002).

Until recently the major renewable energy developments have been with wind energy. Wind is unpredictable, so for a large scale wind energy industry a larger reserve margin for standby power plant would be required. Wave energy is slightly more predictable than wind but is still

likely to require standby plant with a significant reserve margin. Energy from tidal energy is much more predictable and hopefully the resource will be less dependent on standby power plants. It has been stated that marine energy has the potential to contribute considerably to the UK's energy demand (Fraenkel, 2002).

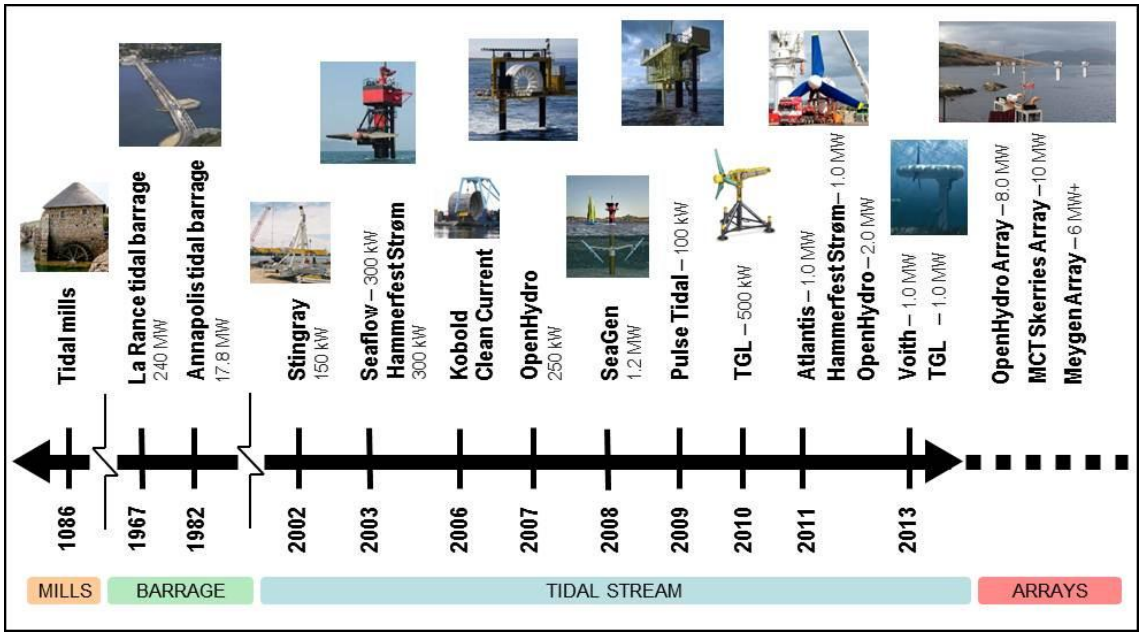

Figure 1-4: commercial and full-scale tidal energy timeline

The UK Government offers financial incentives for marine renewables including the Renewables Obligation Certificates (ROCs). The Energy Act 2008 (OPSI, 2008) introduced banding of the ROCs, which proved advantageous for marine renewables where the number of ROCs/MWh was increased from 1 to 2 to encourage development. The Scottish Government offers increased incentives for marine renewables with 3 and 5 ROCs/MWh for tidal and wave energy respectively (SQW Energy, 2008). On 20th October 2011 the UK Government announced a further re-banding of the ROCs to help new technologies reach the market. Wave and tidal stream will be given 5 ROCs/MWh for deployments of less than 30MW. Early in 2012 one ROC was equivalent to £42.37/MWh.

1.3.2 Tidal Barrage

Tidal barrages dam an entire estuary and the potential energy from the induced water level difference inside and outside the basin is harnessed with low head water turbines.

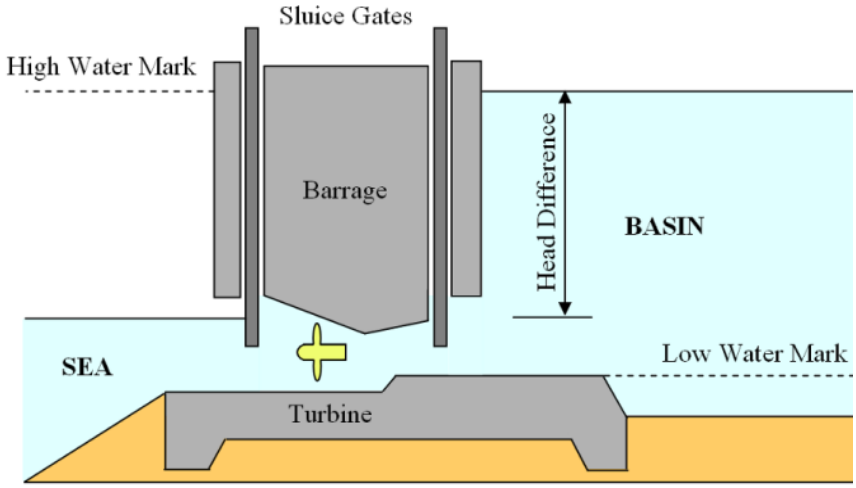

Figure 1-5: tidal barrage diagram

Although the cost of barrage construction is considerable, the extra extracted energy compared with tidal stream is thought to outweigh the initial investment (Hammons, 1993). Barrages can be operated in three main ways:

1. Ebb generation: this is the simplest method, where the basin fills during a flooding tide with the sluice gates open. Energy is then generated through the turbines once the tide starts to ebb and the basin empties. This gives two bursts of energy per day, which start approximately 3 hours after high-tide and last for 4-6 hours (Hammons, 1993).
2. Flood generation: the opposite of ebb generation where electricity is generated on a flooding tide as the basin fills. This is not as effective as ebb generation but a plant can be used to generate energy out of phase with an ebb generating barrage.
3. Two-way generation: this system combines an ebb and flood generating system, where energy can be generated on both the ebb and flood tides. Power output will generally be slightly less than pure ebb generation, except perhaps at very high tidal ranges. However, it would increase regularity of supply. Investment would only be economical in high spring tidal ranges (Frau, 1993) as these systems would involve more costly construction and two-way turbines.

A pumping system may also be used to increase the head difference and increase the average output, again adding additional cost. Twin basins can be used as an alternative to single-basin schemes and it has been stated that they enable almost continuous generation (Hammons, 1993). The development of tidal barrages has been limited mainly due to the large capital costs, long

construction times, visual and environmental impacts (Bryden, 2006). Sites are usually located in estuaries which have large areas of mud-flats exposed at low tide (Boyle, 2004). The presence of the barrage will affect the tidal regime inside the basin and is likely to have a significant effect on the ecological characteristics of the estuary. In general the power generation potential of barrages is great, for example the proposals for the Severn Estuary; but so are the obstacles of high capital cost, environmental impacts, regularity of supply and grid integration (Hammons, 2011). Tidal barrages around the word are rare, but include La Ranch (France – 240MW), Annapolis (Canada – 17.8MW) and Jiangxia (China 3.2MW). There are a number of new tidal barrage schemes proposed in China and South Korea including the 1,320MW Incheon Tidal Power Station, the 254MW Sihwa Lake Tidal Power station and a range of smaller schemes.

1.3.3 Tidal Stream

Tidal streams can be exploited using a range of different technologies, including horizontal axis turbines, vertical axis turbines, oscillating hydrofoils and venturi devices. The industry is not yet fully commercialised and currently only pre-commercial demonstrators have been tested at sea (Bahaj, 2011). The next critical stage of development will see farms of turbines being deployed. There is a diversity of research being conducted. Although a great deal of fundamental theory can been gained from the wind energy industry, there are principal differences that must be investigated. Of key importance is the vertical constraint of the flow with the close proximity of the bed and water surface boundaries (Myers et al., 2008, Giles et al., 2011). The main obstacles for commercialisation are economics, reliability and installation and maintenance in a harsh marine environment.

Tidal stream technology has some appreciable benefits over other forms of renewables including the high predictability of tidal flows, which makes the resource attractive for grid integration. Despite this it must be remembered that although predictable the resource is still highly variable. This variability could be mitigated by utilising tidal phase shifts. Indeed, Hardisty (2009) shows how the phase shift between six different tidal stream deployment sites around the UK could be used to deliver an almost constant total power output across a 12 hour tidal cycle. The environmental impacts and construction costs associated with tidal stream would be lower compared with large tidal barrages, but the energy potential would be less. While the capital costs are likely to be lower, the cost of energy for a fence of continuous tidal stream turbines across the Severn Estuary has been estimated, by “The Severn Tidal Fence Consortium (STFC) as part of a government funded research project, at 20.4-25.9 pence/kWh (Giles et al., 2010). This can be compared with approximately 9.2-22.2 pence/kWh for a Severn

tidal barrage calculated by the Sustainable Development Commission (Knight and Hill, 2007). Both these calculations for the cost of energy included capital construction costs, operational costs and a range of discount factors to model different risk scenarios.

The well-known critical parameter for exploiting tidal streams and currents is the tidal flow velocity as power is proportional to the cube of the velocity. In open sea locations tidal velocities are very small, but when flows are concentrated in certain locations peak spring tide velocities are commonly in the range of 2-3m/s or more (Fraenkel, 2002). Resources become exploitable in regions such as estuaries (e.g. Seven Estuary), straits between islands (e.g. Pentland Firth), shallows between open seas and around headlands (e.g. Portland Bill). Hence the resource is very site specific and although the potential tidal resource has been estimated at 200-400TWh/year (Bahaj, 2008) only a small proportion of these will be feasible to extract. Initially development is expected to be restricted to the most accessible and economic tidal sites.

Although not fully commercialised the technology has seen some significant developments, with successful deployments of full scale prototypes and a number of proposals for first generation tidal stream farms. The forerunner appears to be Marine Current Turbines Ltd with its 1.2MW SeaGen twin rotor horizontal axis turbine which has been successfully installed and operated in Strangford Lough, Northern Ireland, since 2008 (MCT, 2013). This is the company's second generation device building on the experience gained with the 300kW Seaflow prototype installed and tested at Lynmouth, Devon, in 2003. Open Hydro, an Irish Company, successfully tested and exported electricity to the grid in 2006 with its 250kW open centred rim generator. This device was installed and tested at the European Marine Energy Centre (EMEC), Orkney. In late 2009 a 1MW Open Hydro turbine was installed in the Minas Passage of the Bay of Fundy, Canada, but in 2010 a forced recovery was required due to damage (Open Hydro, 2011). Later in 2011 Open Hydro installed a 2MW unit in Brittany, France, the first of a 8MW array. Other deployments include Pulse Tidal's twin oscillating hydrofoil device, installed in the Humber Estuary in 2009 (Paish et al., 2010), Clean Current's 65 kW horizontal axis turbine installed in Canada (Clean-Current, 2011), Verdant Power installed six, 35 kW turbines in the USA (Verdant-Power, 2012) and Hammerfest Strøm tested its 300kW horizontal axis turbine in Norway for five years and later installed its "HS1000" 1MW device at EMEC in 2011 (Hammerfest-Strøm, 2013). Another promising developer, Tidal Generation Ltd, deployed its 500kW horizontal axis device at EMEC in 2010 (TGL, 2013) and now in 2013 has installed a 1MW turbine.

In addition to individual deployments there are plans for operational larger-scale device arrays in the near future. Scottish Power Renewables has partnered with Hammerfest Strøm and hopes

to develop 105MW of capacity at two sites in Scotland. The Islay site plans to have a 10MW array and the Duncansby Head site a further 95MW (Hammerfest-Strøm, 2013). MCT Ltd is working with RWE npower to deploy a farm of seven 3rd generation 1.5MW SeaGen turbines off the coast of Anglesey and this array is anticipated to come online by 2015/16 (MCT, 2013). A developer called MeyGen Limited has consent awarded for a 86MW tidal energy project in the Pentland Firth, Scotland, initial plans are for a pilot project of 6 devices. EDF Energy has partnered with Open Hydro and following the installation of their first unit are in the process of installing three further scaled-up 2MW 16m diameter devices off the coast of Brittany in the Paimpol-Bréhat tidal farm project (Open Hydro, 2013). EDF's and Open Hydro's project will be the world's first tidal stream array, representing a key milestone for the industry. With the backing and partnerships from large energy companies the future for tidal stream energy looks promising in and around the UK.

1.3.3.1 Horizontal axis turbines

Horizontal axis turbines usually have two or three rotor blades which generate lift. This results in axial rotation which drives a generator (Bryden and Melville, 2004). They have to be aligned to the current by either rotating the device or pitching the blades through 180°. In general the top and bottom 25% of the flow depth should be avoided (Figure 1-6). Examples include MCT's twin rotor SeaGen turbine (MCT, 2013) and Tidal Generation Ltd.'s three bladed turbine (TGL, 2013). Figure 1-6 shows a pile mounted turbine. The surface piercing monopile allows the turbine and nacelle to be raised out of the water for maintenance.

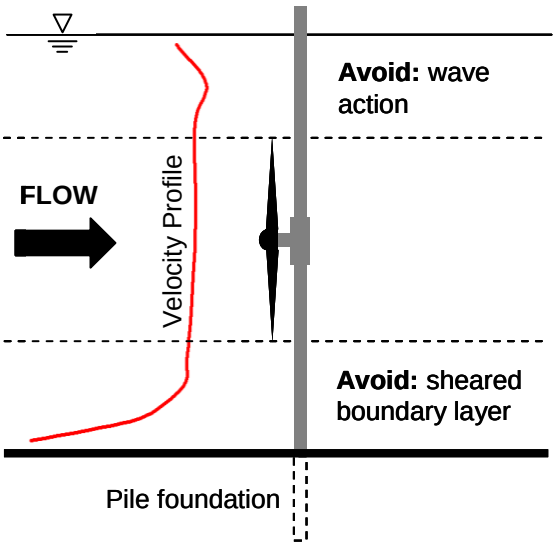

Figure 1-6: Horizontal axis turbine (piled foundation)

1.3.3.2 Vertical axis turbines

Vertical axis or cross flow turbines (Figure 1-7) have blades mounted parallel to the axis of rotation. They may also be mounted horizontally in the water, resembling a water wheel. Principal advantages are: the drive train can easily be located above the water line and the vertical axis can exploit flows from any direction. Drawbacks include: they are difficult to stop in an emergency and have greater sensitivity to cavitation (Fraenkel, 2002). Figure 1-7 shows a floating device which could enable easier installation and in the event of maintenance the whole device could be floated to shore. Negatives include concerns over wave interactions and anchoring. Examples of commercial vertical axis turbines include the Kobold turbine (KOBOLD, 2009) and the Neptune Proteus device (Neptune Renewable Energy, 2010).

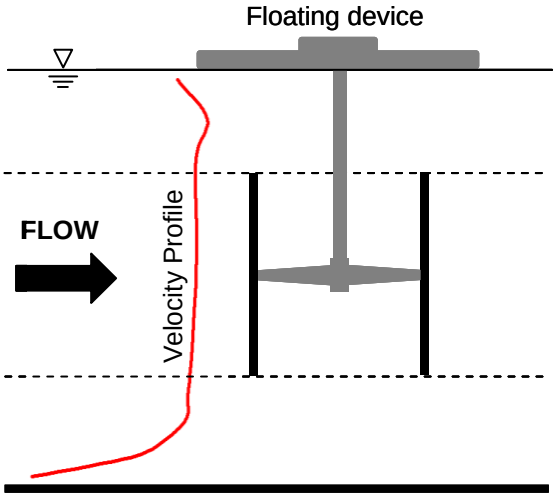

Figure 1-7: Vertical axis turbine (Floating)

1.3.3.3 Reciprocating Hydrofoils

Reciprocating Hydrofoil devices are different as they do not use rotary motion. As flow passes the hydrofoil, lift is created and the hydrofoil reciprocates vertically (or horizontally). The hydrofoil is attached to a lever arm which drives the power take-off. In a previous prototype hydraulic power take-off was used. These devices are particularly suited to shallow flows as they can sweep through most of the water depth. The main concern is that the hydrofoil requires an active control system that adjusts the blade pitch to produce optimal power throughout the cycle (Bryden and Melville, 2004). A single hydrofoil 150kW device called “Stingray”, developed by Engineering Business Ltd., was tested in Yell Sound off Shetland; further development of this device was put on hold. A twin hydrofoil prototype was deployed in the Humber Estuary during 2009 by Pulse Tidal Ltd (Paish et al., 2010). Figure 1-8 shows a gravity based foundation which

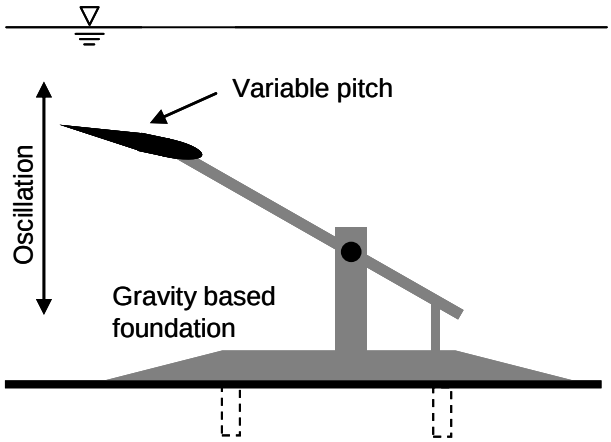

Figure 1-8: Reciprocating hydrofoil (gravity based foundation)

relies on its mass weight to hold the device in position. In some cases there may be additional fixing to the seabed. Gravity based foundations could be constructed as caissons and floated out from shore.

1.3.3.4 Others

There are many other novel devices but it seems the forerunners are currently horizontal axis turbines alongside a few vertical axis turbines and a handful of reciprocating hydrofoil devices. A slight modification to a horizontal or vertical axis device is a ducted turbine, where a venturi type duct is used to accelerate the flow through the turbine. There may be increased risk of inducing blade tip cavitation with a shrouded device because increased flow velocities tend to result in higher rotor speeds (Fraenkel, 2002). Lunar Energy has developed a shrouded device, claiming additional benefits of improved operation in yawed flows (Lunar Energy, 2011). Yawed flow occurs when tidal flows are not exactly perpendicular to the axis of turbine rotation and this can significantly affect turbine performance (Bahaj et al., 2007a).

1.3.4 Tidal Fence

A tidal fence can be defined as a continuous row of tidal energy extraction devices which span the entire width or a significant proportion of a tidal resource. Fences are a lower financial and environmental cost alternative to a tidal barrage (Shanahan, 2009). A variation on the fence is a "tidal pier". These are essentially tidal fences connected to shore at one end (Giles et al., 2010). A tidal fence takes tidal energy extraction technology and tunes its arrangement to make the best use of the available kinetic and potential energy, whilst optimising the scheme for minimum impact on the environment and the local stakeholders. By adjusting the impedance of the fence upon the flow the change in water level across the system can be controlled. Minimising this water level difference improves the ease of passage for shipping. At the low energy and blockage end of the spectrum (Figure 1-9, left), a fence mainly exploits the tidal kinetic energy and the fence could sustain two-way navigation at all times though a free gap. In the higher energy and blockage form (Figure 1-9, right), exploiting both kinetic and a proportion of potential energy, low head locks would be installed for navigation. The ability of a fence to be tuned is a key advantage over a conventional barrage. Impact on the environment and navigation can be adjusted at the design stage to find the best match between energy generation, loss of inter-tidal habitats and the impact on shipping activities. Ideally a fence would span the full width of a tidal channel but in reality, due to navigational requirements and safe passage for marine life, partial fences may be installed (Garrett and Cummins, 2008).

A tidal fence has been proposed for the Severn Estuary, UK. Work by the Severn Tidal Fence Group, presents a low blockage 390MW fence with a free passage navigation gap (Figure 1-9,

left). Further development by IT Power Ltd. has shown that by introducing a higher blockage fence, perhaps using shrouded turbines and additional substructure, (Figure 1-9, right) that the peak power could be increased up to approximately 1.5GW. Although the expected power output is lower than other proposed Severn Estuary barrages, the project would have a much reduced environmental impact and lower construction costs.

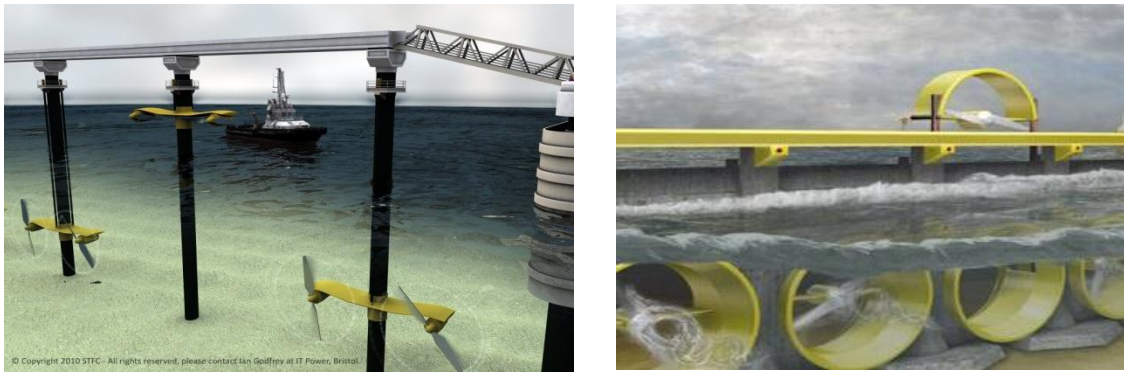

Figure 1-9: impressions of a tidal fence. Low blockage (left). High blockage (right)

1.3.5 Tidal Lagoon

Artificial lagoons are isolated containment structures that can be deployed in tidal estuaries to exploit tidal potential energy. They use the same principles as a tidal barrage by establishing a head difference between the lagoon and estuary to drive low head turbines.

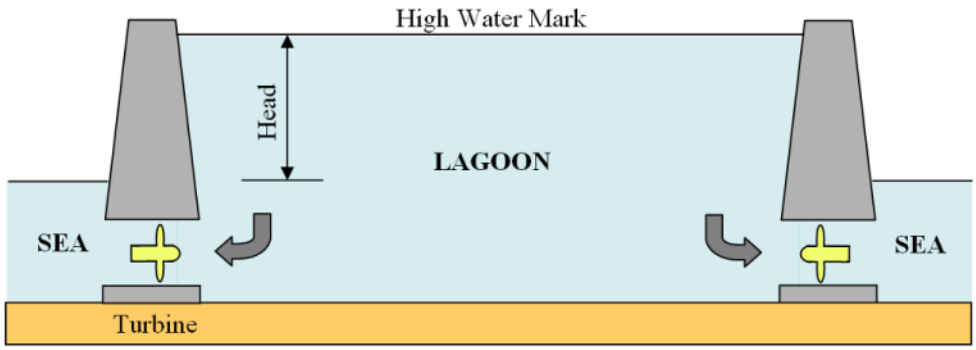

Figure 1-10: tidal lagoon cross section

The principal advantages are that lagoons do not require the damming of an entire tidal estuary and a number of isolated lagoons could be deployed within an estuary without obstructing shipping traffic or causing significant alteration to the ecosystem (Bryden, 2006). The drawback is that a much longer containment structure would be required to that of a barrage for the same area of entrapment. Bryden (2006) states the UK potential for installed capacity could be as high as 6GW. Lagoons have been proposed as an alternative to a barrage for the Severn Estuary tidal scheme.

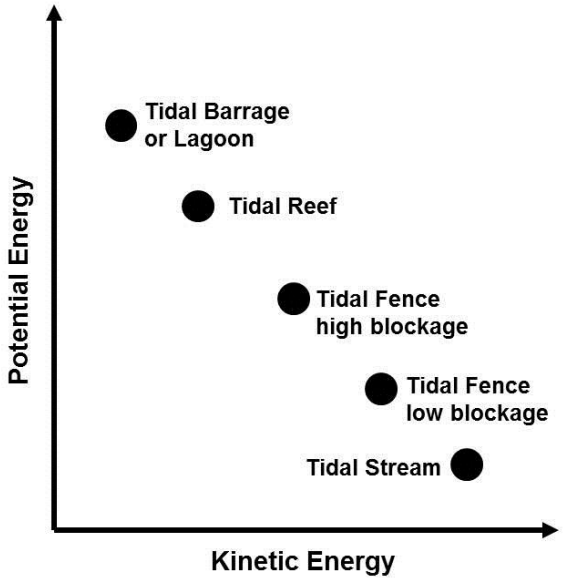

Figure 1-11: tidal technology energy utilisation

1.4 Shallow Tidal Flows

Shallow tidal flows might be described as flows with a depth of less than 30 metres, commonly found close to the shore or in bays and estuaries (Hardisty, 2007). They are significant because they are generally more accessible for energy extraction than deeper offshore tidal sites, hence a good location for first generation tidal stream arrays, barrages or fences. Their often closer location to shore improves the construction feasibility and economic prospects. Constructing in deep offshore sites that are long distances from the shore is very challenging due to short weather windows and large travelling distances. In addition at deeper locations it may be technically difficult to harness a large fraction of the available energy, whereas in shallow areas a MCEC can be designed to occupy a greater proportion of the vertical water column. Some shallow flows are located close to population centres and electrical grid connections, reducing connection costs and transmission losses. Many sites are located away from major shipping channels due to depth limitations. The UK has a good shallow water tidal resource (Figure 1-13); although in many regions the flow velocity is not currently sufficient for economic energy extraction. Examples of shallow tidal flow sites in the UK are the Humber Estuary, large areas of the Bristol Channel, the Channel Islands and the Mersey Estuary. Sites located in sheltered estuarine locations are favourable as wave loadings will be reduced and the environment is less demanding for installation. In the Humber Estuary, Pulse Tidal has installed and operated a prototype tidal energy convertor (Paish et al., 2010) that has been specifically designed to exploit shallow tidal flows (Figure 1-12).

When deploying farms/arrays of devices in shallow tidal flows, it is critical to understand the influence of bounding surfaces on the downstream wake development behind Marine Current Energy Convertors (MCECs). The downstream row spacing and packing density of devices must be optimised and tuned to the local flow depth to maximise array performance. In deeper flows (>50m) wake is anticipated to persist further downstream than in intermediate-depth tidal sites (30-50m) because of less flow augmentation occurring above and below the MCEC. In shallow flows (<30m) wake length is again expected to persist further downstream due to the close proximities of the seabed and free-surface.

Figure 1-12: Pulse Stream 100 shallow flow prototype

Figure 1-13 presents results showing potential UK sites for device deployments in shallow tidal flows. The data for bathymetry and mean spring peak velocities were obtained from the BWEA "Marine Energy Resource Atlas" (ABP, 2008, Cooper et al., 2005) and the layers were manipulated using geographic information system (GIS) software. Suitable sites cover an area of 3643 km^2, however these results must be treated with caution as the data resolution is only 2 km. This means results are potentially downgraded in locations close to the shore and in estuaries (Blunden, 2009). For example the Humber Estuary, Manai Straits and other regions known to be suitable are excluded due to the large resolution. In addition this data does not consider tidal range and this may reduce the times at which devices can operate at some locations due to surface exposure ("ventilation"). Hence the increased risk of cavitation and possibly ventilation is of concern in shallow flows.

The extent of the UK shallow water resource is largely unknown because resource assessments such as Black and Veatch Consulting Ltd (2004, 2005) ignored tidal sites with depths of less than 20m and the "Marine Renewable Energy Atlas" does not have a sufficiently high spatial resolution to fully characterise the shallow water resource.

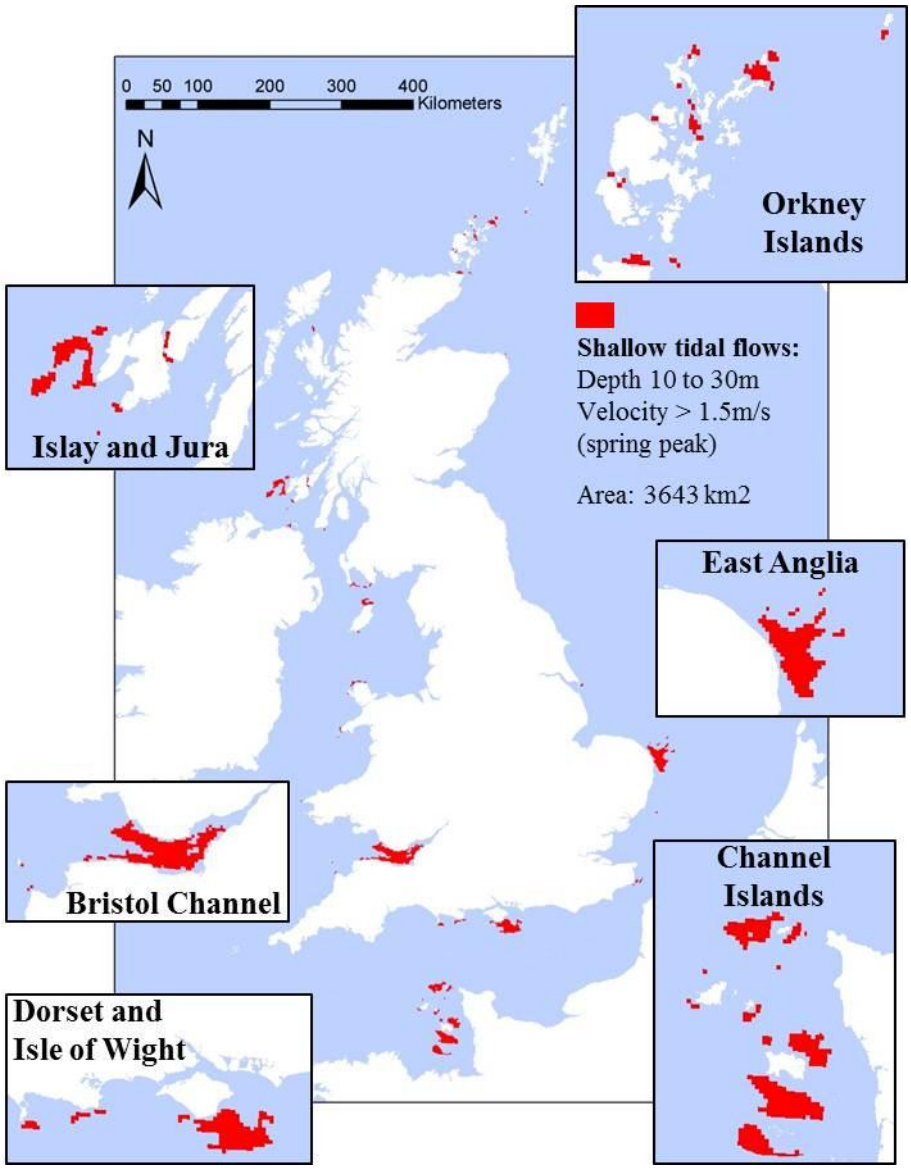

Figure 1-13: Potential UK shallow tidal energy sites, 10-30m

1.5 Objectives

The scope of this project encompasses several objectives concerning the exploitation of shallow tidal flows for energy extraction. Research and development to date has been limited with the initial focus and technology development being associated with intermediate-depth tidal flows in the region of 30-40m. Highlighted research areas of particular importance are the close proximity of bounding surfaces in shallow flows and the insufficient tidal flow velocities in some regions. The objectives are to investigate the following:

1. **Artificial flow constraint:** many shallow tidal flows do not presently have sufficient flow velocities for feasible energy extraction. This package of work aims to investigate the concept of using artificial flow constraint structures in the form of specifically-shaped foundations (herein described as "ramp-foundations"). These raised foundation structures will confine the flow and increase the incident velocity at the plane where the marine current energy convertor (MCEC) extracts energy. The result being an increase in the magnitude and quality of power from a shallow water MCEC.
2. **Wake structure in shallow flows:** the MCEC swept height to flow depth ratio can have a significant effect on the wake length behind MCECs. This objective aims to characterise this phenomenon. It is critical to comprehend the influence of the bounding surfaces on the wake length as this will influence the optimum packing density in device arrays.
3. **Commercial shallow water device optimisation:** this work will form an important industrial link with objectives 1 and 2. Pulse Tidal Ltd.'s 1.2MW MCEC, the "Pulse Stream Commercial Demonstrator (PSCD)", is being designed with an integral ramp-foundation to augment the flow. Informing the design for the ramp-foundation has been a large focus of this project and shows a direct commercial application of the ramp-foundation concept.

Chapter 2

2 Review of Current Literature

2.1 Tidal stream energy

2.1.1 Resource

A detailed understanding of the extent and potential of the tidal stream energy resource is essential for successful development of a tidal stream energy industry (Iyer et al., 2009, Couch and Bryden, 2006). Unfortunately because of the large scales involved and complexities such as the interaction of devices with natural flows, resource estimates to date contain many assumptions and in reality are only rough approximations of resource potential. Improvements have been made with the methods employed in recent reviews but unfortunately there appears to be a downward trend in energy estimates as factors such as feasible extraction limits are considered as opposed to the technically-extractable resource in early estimates. It must be emphasised to date that most resource estimates have been based on admiralty tidal flow data (Bryden, 2006) that has a limited spatial resolution even with interpolation (Bahaj, 2011) and has no consideration for the vertical velocity profile which is very important for site and device selection.

There are three main methods of resource assessments which are detailed by Black and Veatch Consulting Ltd (2004), Bryden (2006), Hardisty (2007) and Bahaj (2008):

1. **Array method:** this was the basis of most early assessments and works on the idea of developing a farm of turbines where each device extracts an equal amount of energy that is purely dependent on the device efficiency, device size and site packing density. It purely considers free-stream velocities and there is no consideration for the amount of available energy in the channel. Hence there is risk of over estimation by extracting more energy than actually exists.
2. **Flux method**: the array method is limited as it provides a poor estimate of the resource and the site potential. The Flux method considers the energy that enters the tidal site but is independent of array layout and device type. It considers the available channel energy and constrains the amount that can be extracted. It can be further enhanced by defining a percentage extraction limit to take account of flow modification from the MCECs. This

method is widely accepted, but it is still limited by the fact that it does not directly include the physical influence of the MCECs presence and would only provide accuracy for channels with low MCEC area to channel area ratios.

3. **Analytical method:** this method uses numerical modelling to characterise tidal flows at specific sites. A high resolution picture can be developed by combining sparse tidal data with known fluid dynamics (Bahaj, 2008). In addition it is possible to model the effects of turbine arrays on the flow. This method was used by Blunden and Bahaj (2006) to characterise Portland Bill and parameterised the turbine array as added roughness. An analytical estimate was also conducted by Bahaj and Myers (2004) for the Alderney Race, Channel Islands. The results from Acoustic Doppler Current Profilers (ADCPs) could also be integrated into these models to improve their localised accuracy. Garrett and Cummins (2007, 2008) develop an analytical method which models MCECs as an additional frictional force to that applied by the seabed. A recent paper by Vennell (2011a) analytically investigates the resource potential of two very different tidal channels in New Zealand. Analytical methods are an on-going area of research.

Early resource assessments utilising un-disturbed kinetic energy (KE) flux do not accurately replicate the power potential of a channel (Vennell, 2011a) except where devices occupy a small percentage of the channel cross-section (Trowse and El-Hawary, 2009), which would only occur in channels with extremely large cross-sections such as the Pentland Firth. For estimates with improved accuracy the influence of the MCEC's physical presence must be modelled (Bahaj, 2011). Vennell (2011a) discusses the unreliability of KE methods and how with different channel types the methods can both under estimate and overestimate potential. These KE methods may be suitable for locating areas of strong resource potential but in terms of estimating accurate power potential more detailed localised modelling is required. In reality flux methods will be unsuitable for future tidal stream resource assessments, particularly given that first generation tidal stream farms are likely to be deployed in shallow and intermediate-depth tidal stream sites. It is anticipated that more comprehensive 1D, 2D and possibly 3D analytical models will form the basis of all future resource assessments. Trowse et al. (2009) present a review and the key limitations of these analytical methods. Both 1D and 2D models are a significant improvement on KE flux methods because they include the flow impedance effects from MCECs. The key limitation of a 1D model is the fact that it can only model an array/fence that spans the entire channel width. A 2D model can be used to provide a more accurate estimate for isolated arrays with free-flow channel gaps for navigation, environmental and economic constraints. A 2D model is depth averaged and to account for the sheared boundary layer and that many MCECs will only occupy the middle region of the water column a 3D

model would be required. 3D models add significant complexity, cost and computing resource to the process.

In principal there is no substitute for collecting data in the field using devices such as ADCPs (Bahaj, 2008); this is an on-going process but is currently not economically feasible on a large scale (Iyer et al., 2009). Wyatt (2009) describes the technique of using HF radars to measure surface currents with a spatial resolution of up to 300m and the added advantages of being land based. Wyatt claims the accuracy is equal to ADCPs but without the profiling capabilities. This method only measures surface currents that may be useful in deeper flows but would not be suitable for shallow resources because of their highly sheared velocity profile. It might be possible to use HF radars in conjunction with ADCP profiles, enabling a detailed flow model to be interpolated using surface currents and a discrete number of ADCP profiles. These real-time measurement techniques are expected to be critical for future site-specific resource assessments which will be required for tidal array site selection (Bahaj, 2011).

The majority of resource estimates to date have been conducted for UK waters although there are a limited number for European and Global assessments, but these have a much higher degree of uncertainty due to a lack of independent estimates and variability between those that exist (Black and Veatch Consulting Ltd, 2004). Blunden and Bahaj (2007) and Blunden (2009) provide a detailed review of UK resource assessments since the 1970s and the associated limitations of different approaches. Blunden (2009) also describes the tasks involved with resource assessments and the importance of an iterative process including site selection, device choice, layout optimisation and investigating the geographical extent of the flow modification. Couch and Bryden (2006) present a methodology for characterising resources into five main types and indicate that selection of suitable tidal sites can be largely based on three parameters: local water depth, proximity to grid connections and the resource persistence. Large mean spring and neap tidal velocities are highly sought-after as power yield is proportional to the cube of velocity. Resource assessments to date have tended to neglect shallow water tidal flows, which is unfortunate as this resource could be critical for first generation tidal stream farm deployments due to their often close proximity to shore.

UK Resource

Early studies by Fraenkel and Musgrove (1979) and Wyman and Peachey (1979) based on Admiralty Chart data and basic analysis of kinetic energy through tidal channels, such as the Pentland Firth, estimated the UK resource to be 14.7-18.7 GW respectively. During the 1980s Evans (1987) developed a new approach to resource assessments using a two-dimensional finite

difference numerical model to estimate kinetic energy flux and select suitable sites. This is an array method or as Blunden (2009) describes a 'pre-generator' resource assessment technique, as there is no consideration for the effects of multiple devices on the flow characteristics.

During the 1990s two key reports were identified and Blunden (2009) emphasises that these reports have formed the basis of methodologies for subsequent resource assessments. ETSU (1993) estimated the UK resource to be 6.9 GW and selected sites based on the following two requirements: spring peak tidal stream velocities greater than 2m/s and depths of greater than 20m. This means that a large proportion of the shallow tidal resource was ignored during this study. This again used an array method and in total 33 sites were identified around the UK based on velocities taken from tidal stream diamonds and tidal stream atlases. The later European Commission (1996) report estimated the UK resource to be 3.9 GW and used a similar array method which was limited by the fact it neglects to model the energy extraction and physical influence that the farm has on the flow. In this study peak flow velocities of greater than 1.5 m/s were considered exploitable. Blunden (2009) identifies some key flaws with these studies; both are based on tidal stream velocities from admiralty charts which are only available at discrete points and the authors have interpolated between points neglecting any localised flow effects. Not only is the resolution low, but using linearly interpolated velocities can cause accentuated errors when estimating power because of the cubic relationship. The estimate by the European Commission (1996) was considerably lower than ETSU (1993) primarily because of different assumptions such as a much lower turbine packing density. This highlights the fact that because of differences in underlying assumptions it is difficult to directly compare resource assessments (Blunden, 2009), particularly those derived from an array method.

More recent resource assessments by Black and Veatch Consulting Ltd (2004) and its later Phase II report (Black and Veatch Consulting Ltd, 2005) present an improved flux based method. The Phase II report presented a better resource estimate as a number of sites were duplicated in the Phase I report giving an inflated prediction. The authors conducted a review of previous work including ETSU (1993) and European Commission (1996), concluding that these array methods significantly over-estimated the UK resource potential because they failed to consider the effects of energy extraction on the flow. In response, a flux method is proposed and implemented to give a UK resource estimate of 2.5 GW. Based on work presented in Bryden and Couch (2006) and Bryden et al. (2007) a 'Significant Impact Factor' (SIF) of 20% is defined because most tidal sites are constrained, hence only a proportion of the available resource can be extracted. The SIF is defined as the maximum amount of kinetic energy that can be extracted from a tidal channel without causing major disruptions to the flow. This factor was later revised in Black and Vetch's Phase II report (Bryden et al., 2007) to take account of its

variation at specific tidal sites and as a result the potential resource reduced by approximately 20% to 2.1 GW. The authors admit that there is still a great deal of uncertainty around the estimate and expect the uncertainty to be in the region of ±30%taking into account the projected nature of the SIF factor and uncertainty surrounding the total energy resource. The input data for the Black and Veatch reports was initially based on ETSU (1993) and European Commission (1996) estimates and so omits any sites with depths less than 20m. This means that a significant proportion of shallow flows are still ignored despite the fact that many first generation sites could be located in shallows. It is concluded that the UK has a considerable percentage of the global tidal resource and up to 40% of this is concentrated in the Pentland Firth and Channel Islands, with many depths exceeding 40m.

In 2004 the independent "Marine Renewable Energy Atlas" was published. The atlas is a marine energy resource assessment, including tidal stream, undertaken for the UK Department of Trade and Industry to assist the government with strategic planning of offshore renewables. Details of the atlas can be found in ABP (2008) and Cooper et al. (2005). Tidal data was used from the Proudman Oceanographic Laboratory giving a resolution of approximately 2km. The atlas serves its purpose to assist with potential tidal stream site selection. However as highlighted by Blunden (2009) & Bryden et al. (2007) the coarse resolution means that localised flow effects such as those found around headlands and through narrow straits are not characterised. This means that the atlas cannot be used for detailed resource assessments or for a detailed estimation of the potential shallow tidal resource.

It is clear on a UK scale that the predicted resource has decreased considerably over time but is still bounded by a degree of uncertainty and is very much open to interpretation. Methods to date have come with wide ranging assumptions surrounding the effects of energy extraction on the flow. It seems these assumptions and uncertainties will only be mitigated by more detailed localised analytical models.

European Resource

Resource estimations for Europe are limited but the European Commission (1996) report extends its estimates to 57 European sites using the same method that it employed for estimating the UK potential. The total non-UK European resource was stated as 1.9GW. The European Commission (1996) considers its value to be a reasonable first approximation even though the figure is less than the predicted UK resource. It is postulated that this is partly because much of the European resource is located in Mediterranean regions where tidal ranges and flows are limited. To validate this estimate further work is required, ideally using a flux based method

(Black and Veatch Consulting Ltd, 2004). Hardisty (2007) states that North Western Europe has large potential for tidal stream power, however this statement is not accompanied with supporting figures. Grabbe et al. (2009) present a review of the tidal current energy resource in Norway and conclude that it is favourable given Norway's extensive coastline, islands, inlets and deep fjords.

Global Resource

Estimates of global tidal energy resources are limited and are subject to high uncertainty (Black and Veatch Consulting Ltd, 2004). An early estimate of 5000 GW was presented by Isaacs and Seymour (1973) but is generally considered too high. Black and Veatch Consulting Ltd (2004) consider the extractable non-European global resource to be approximately 13.7 GWs but there is a great deal of uncertainty attached to this. At this time it is not possible to draw reliable conclusions for the global resource because of the lack of estimates and a high degree of variation between the inadequate available estimates.

Hardisty (2009) presents a broad review of potential tidal stream sites across various regions of the globe, including North-West Europe, North America, Australia, New Zealand, Indonesia and China. It is clear from this review that potential for tidal stream energy stretches across the Globe but is very site-specific. The review relies heavily on Admiralty Chart data and tidal diamonds, which will not provide sufficient resolution to fully characterise the global resource. Harries et al. (2006) describe the tidal resource in Australia, with the majority of this being located in the Kimberley region in the north-west. Jo et al. (2010) present a review of the current status of tidal stream energy in Korea and highlight the potential in this region, particularly the strong currents on the west coast with a tidal range of up to 10m. Dong et al. (2010) describe China's vast tidal current potential with its long 18,000km coastline and numerous constrained tidal channels. A huge resource of nearly 14GWs in 130 channels is reported, but given an absence of independent review this figure is likely to reduce significantly.

Summary

It seems clear that all resource assessments to date have discounted a large proportion of the potential shallow water resource. Hardisty (2007) indicated, based on Black and Veatch's estimate, that the shallow water and estuarine resource makes up 20% of the total estimate. However Black and Veatch disregarded all sites with depths less than 20m and hence it is important to understand the definition of shallow tidal flows. Hardisty (2007) is thus defining a shallow resource to have a depth range of 20-30m but the author of this project defines shallow flows at 10-30m depth. With new shallow water extraction devices emerging disregarding the

10-20m depth range could be limiting in terms of the shallow tidal resource estimation. In addition the Marine Renewable Energy Atlas does not have sufficient spatial resolution to fully resolve the shallow water resource close to the shore and in estuaries which are areas highly suited for farm deployments due to their close proximity to land (Blunden, 2009).

Resource assessments are still surrounded by a high degree of uncertainty, personal interpretation and a lack of spatial resolution, largely because of the absence of data and the range of assumptions used in different methods (Iyer et al., 2009, Blunden, 2009). Iyer et al. (2009) highlights the importance of localised resource measurement because local flow characteristics of tides are governed by topography, bathymetry and fluid interactions at particular sites. Interpolation of sparse tidal data will inevitably lead to errors. In the past there has been a tendency to state peak tidal flow velocity values for sites, which leads to overestimation of the resource (Couch and Bryden, 2006). However this has been rectified by using mean peak velocities in more recent assessments such as Black and Veatch Consulting Ltd (2005). It seems that despite the lack of detail for European and Global resources the tidal stream resource is promising and in particular the UK offers great potential. It is anticipated that the thrust of new research in this area will focus on localised analytical methods for specific tidal array deployment sites. This will be driven by the industries need for more accurate localised estimates that model the interaction effects of MCECs on tidal channel flow and the resulting influence on power. Despite this, general flux based resource assessments have been invaluable for identifying sites with worthy prospects for high energy yield.

2.1.2 Blockage and limits of energy extraction from tidal streams

The term “blockage” can be defined as the percentage occupation of the flow cross section with MCECs and the resulting proximity of the bounding surfaces within that flow. Blockage is not only influenced by the number of deployed MCECs but also the porosity/solidity of these devices. High blockage/impedance will result in the greatest energy extraction due to higher device thrust but this scenario will have the biggest impact on flow modification causing the free-stream velocities to increase or decrease in different locations. Blockage effects are generated when bounding surfaces or other MCECs/objects affect the path of streamlines around and through the MCEC. Any flow moving towards a bounding surface will be re-directed into the stream-wise direction and increased blockage could potentially force more flow through the MCEC by constraining the streamlines entering the swept area. The effects are important for accurate power prediction, particularly for MCECs deployed in shallow flows. Blockage can be subdivided into three broad interrelated scales:

1. Device scale blockage: this is local scale flow modification of the fluid surrounding MCECs, such as velocity increases above and below the device.
2. Array scale blockage: these are the flow modification effects that occur within a farm of MCECs. For example in a closely packed array velocity increases between devices can be seen (Myers et al., 2011b).
3. Global scale blockage: this can be defined as the large scale flow modification effects of an entire array. For example a "high solidity array" that creates large global flow constraint in a highly blocked channel will create significant velocity increases on either side of the farm. In addition if farm solidity is too high and the channels either side are free-flowing the energy extraction potential could reduce. This occurs because flow is diverted away from the MCECs influence and in fact reducing device solidity in this situation would increase farm energy yield. This leads on to the topic of tuning farm solidity to maximise energy yield which will be discussed further.

The level of tidal channel blockage or flow constraint can be defined by three ratios:

1. Area blockage ratio: this one-dimensional parameter can be defined as the ratio of MCEC or array cross-sectional area to the total channel cross-section. It is the classical correction parameter for blockage effects, traditionally used for wind turbines. However for tidal flows it loses validity as soon as the rotor to channel area becomes asymmetric in either the vertical or lateral planes.
2. Vertical blockage ratio (VB): the ratio of MCEC height to the channel flow depth. This ratio is important for MCECs because vertical blockage is much more critical with devices occupying a large proportion of the total fluid depth. This would very much be the case for shallow flows (Myers and Bahaj, 2010).
3. Lateral blockage ratio (LB): the ratio of MCEC or array width to the overall channel width. Decoupling of vertical and lateral blockage effects will be important, particularly given the prospects of development in very shallow and wide resources such as the Severn Estuary. Many first generation sites are likely to involve high vertical blockage but relatively low lateral blockage; hence these effects will require independent investigation.

Initial resource assessments based estimates purely on the undisturbed kinetic flux of tidal flows. No consideration was made for the effects of flow modification or blockage resulting from the MCEC extracting energy from the flow (Bryden and Couch, 2006). For site selection the effects of energy extraction on the underlying hydraulic nature of the environment must be considered particularly in channels where MCECs occupy a large percentage of the cross-section (Bryden and Couch, 2006). Bryden et al. (2005) present a one-dimensional open channel flow model that suggests that extraction of 10% of the kinetic energy flux would produce flow

retardation of under 3% but up to 6% for extraction rates of 20%. It is suggested that 10% extraction is used as a "rule of thumb" guideline for developers but the author also states that the analysis is not detailed enough to suggest accurate extraction limits. The authors also note that the model is limited by its simple one-dimensional nature and expanding it to two or preferably three-dimensions would enable more complex tidal sites to be modelled. Although simplified the model demonstrates the importance of considering the influence of energy extraction on the flow. In the case of small cross-section shallow flows it is likely to be even more critical as larger percentages of the total channel energy could be extracted.

Garrett and Cummins (2008, 2007) develop one-dimensional theory further and reinforce the problems surrounding resource estimates using kinetic energy flux and state the importance of considering MCEC blockage and structural drag. Adding devices to a channel will initially increase power but as more are added and more energy is extracted the current velocities will be reduced from the increased MCEC drag. Hence it will be important to establish the optimum number of devices to achieve peak channel power. Three different flow scenarios are considered; a complete tidal fence, a single turbine and a partial tidal fence. As with earlier work by Garrett and Cummins (2005) and Bryden et al.(2005) a tidal fence is essentially a MCEC with a specific drag occupying the entire channel cross-section. This of course does not consider the localised blockage effects such as wake interaction or bypass flow between turbines and around arrays. Garrett and Cummins (2008, 2007) develop the theory further to consider single turbines and partial fences which are in reality required for navigational, economic and ecological reasons. Maximum power would occur for the "tidal fence" scenario, when MCECs are deployed in smaller numbers there will be losses associated with downstream wake merging and the surrounding flow. Garrett and Cummins (2008) state that these losses could be in the region of 1/3 to 2/3 of a "tidal fence" as the device area to channel area blockage increases. Again the authors state some model limitations including the one-dimensional nature, which ignores the channel cross flow and the fact that supporting structures will add drag for no energy return.

Vennell (2010, 2011b) developed the work by Garrett and Cummins by investigating how the internal configuration of MCECs in the tidal channel can effect the channel's maximum energy extraction potential. Vennell concludes that to achieve maximum energy yield from a specific channel, the flow though the MCECs must be optimised through device solidity tuning, hence adjusting the overall channel blockage. The model is limited by the fact that it is still 1D and devices can only be tuned as a complete row of devices, but the author states the 1D results form important foundations for the development of 2D and 3D farm models. Vennell concludes that to maximise power potential devices must occupy the largest percentage of the channel

cross section and then be tuned to reduce impedance to the flow. This may be impractical except in very densely packed tidal fences because of navigational and environmental constraints.

Although one-dimensional, work by Garrett and Cummins, Bryden et al. and Vennell highlight the importance of considering tidal farm blockage effects and its resulting influence on energy extraction. Energy yield is essentially governed by the amount of fluid that is entrained through the MCEC's swept area and traditional wind energy theory states that for an unbounded flow the induction factor (flow velocity reduction through the swept area) approaches 1/3 of the free-stream velocity. In a tidal flow induction factors close to this would occur for an isolated turbine but could approach 1 for a farm blocking the majority of the channel cross-section. Turnock et al. (2011) shows that for high channel blockage ratios, the MCEC power coefficient (C_p) can exceed the Betz Limit (C_p =16/27). In reality the C_p value of an isolated un-constrained MCEC will be below the Betz limit due to losses associated with blades, the drivetrain and other losses. A good value for C_p would approach 0.4 (Myers, 2005). Marine Current Turbines' SeaGen device has been reported to have reached peak C_P values of 0.48 (Fraenkel, 2010). In a heavily constrained flow such as with a tidal fence the C_p value could well exceed the Betz limit . This exceedance occurs because a high degree of blockage restricts streamline expansion and more flow is directed through the MCEC swept area. The MCEC is also harnessing not only the kinetic energy but additionally some potential energy in the flow. Theory proposed by Betz only considers unbounded flows extracting only kinetic energy (Betz, 1920).

Blockage effects are very site specific, for example in shallow flows due to their small cross section, high device blockage in arrays causing large drag forces could result in a significant reduction in power. Shallow channels could therefore be defined as "drag dominated channels" because tidal farm impedance will have a significant impact on power production. Salter and Taylor (2007) introduce the idea of inertia dominated channels such as the Pentland Firth where adding turbines will have little effect on flow velocity because of the huge flow velocities and vast channel cross sectional area. Given the large depths in the Pentland Firth it is unlikely that first or even second generation MCECs will be deployed; hence blockage research should perhaps focus more on shallow and intermediate-depth sites.

Garrett and Cummins (2004) and Draper et al. (2010) describe how there must be a compromise for the impedance of MCECs themselves. If a turbine offers no flow resistance then no power will be generated and if resistance is too high flow could be forced around the turbine. If flow speed around the turbine is increased this means that there are lateral flow components upstream of the turbine and efficiency will be reduced. The degree of this effect will of course be dependent on the channel geometry, in open sites the flow magnitude around devices would be

larger compared with a very long narrow channel. In a long narrow channel a static head will form upstream until there is sufficient energy to overcome the MCEC impedance.

Whelan et al. (2009) develop a flow field model, using actuator disks, for flow around a horizontal axis tidal stream turbine and develop a blockage correction method taking into account the close proximity of the water surface and seabed. Specifically the close vicinity of bounding surfaces in shallow tidal flows is considered and significant increases in power coefficient occur because more flow is entrained through the rotor (Whelan et al., 2007). The model was one-dimensional, hence ignores lateral flow effects which will be significant in some flows and the authors state that the model only replicates highly blocked cases and needs development for high tip-speed ratios. The 1D model could however be applied to a tidal fence or central regions of a large tidal array. Whelan et al.'s blockage correction validation consisted of a very narrow experimental channel with a very high lateral blockage ratio of 0.66. This is reasonable for a tidal fence application but for further investigation into lateral blockage, studies need to be conducted in wider channels (Whelan and Stallard, 2011). This will be particularly important for many asymmetrical shallow flow sites where the lateral channel dimension is large. Belloni and Willden (2011) and Myers et al. (2011a) confirm the expectation that increasing percentage channel area occupied by turbines will result in increased turbine performance (e.g. power gain) because in constrained channels the flow cannot expand naturally around the device and hence more fluid is entrained through the energy capture zone of the MCEC.

Bahaj et al. (2005) present some blockage correction factors for scaled turbine tests in a cavitation tunnel based on work by Barnsley and Wellicome (1990). Equations are given for blockage correction of power, thrust and tip-speed ratio. The work is limited because the correction factors only consider area blockage and not the decoupled effects of vertical and lateral channel blockage. Durgun and Kafali (1991) and Bai (1979) discuss and provide solutions for blockage correction in experimental scale channels. Durgun and Kafali (1991) present a systematic method for correction although they state that for area blockage ratios greater than 0.064 the method will produce unrealistic results. Unfortunately when testing model turbines in restricted channels the ratio in most cases will be much higher than 0.064.

All these blockage specific studies to date consider 1D theory (e.g. a MCEC occupying a certain percentage of the overall channel cross-section) and the specific effects of decoupling vertical and lateral blockage are not fully implicit particularly in shallow flows. For example the effects of deploying MCECs in very shallow/wide or very deep/narrow channels requires further investigation.

Summary

Understanding the influence of blockage effects for device scale, array scale and global scale will be critical for geometrically optimising farms to increase device power potential. Much of the research to date has involved area blockage, but the effects of de-coupling lateral and vertical blockage are expected to be of paramount importance for future research, particularly with the first commercial arrays on the threshold of deployment. Vertical blockage effects, such as wake dissipation, will be critical where devices occupy large proportions of the vertical water column. This is likely to be the case for most early tidal stream deployments in shallow and intermediate-depth sites. Lateral blockage effects will have a heavy influence on the global flow around and through tidal arrays, hence affecting device performance and also wake dissipation. Many first generation sites are likely to involve high vertical blockage but relatively low lateral blockage; hence these effects will require independent investigation. Understanding global flow effects surrounding large device arrays will also be important for ensuring velocities are within navigational and environmental limits.

2.1.3 Flow augmentation

Many tidal regions may be suitable for energy extraction in terms of location but many do not possess sufficient tidal flow velocities. A solution to this problem could be to artificially increase the flow velocity by fabricating physical flow structures. These flow augmentation structures work on the fundamental principle that power is proportional to velocity cubed, hence for any small increase in flow speed there will be a considerably higher increase in device power. Research directly related to tidal energy is sparse although there have been some studies investigating the application of ducted turbines. In addition to this open channel hydraulics such as flow over submerged objects and bed forms could be applied to the tidal environment.

The shrouded Rotech turbine designed by Lunar Energy (2011) incorporates a flow augmentation duct with the objective of increasing the energy conversion from the flow by enhancing the incident velocity across the rotor. These shroud type structures magnify the incident flow velocity by utilising the venturi duct principle of flow continuity, the turbine is located in the central flow constriction of this duct. The shroud also aims to have a straightening effect on the flow streamlines through the rotor, hence reducing energy losses from tidal flow miss-alignment. Setoguchi et al. (2004) present an experimental investigation into a two-way fluid energy diffuser. This is effectively a circular duct that tapers from either end to form a venturi and the turbine is placed in the central straight duct. The diffuser has what the authors term external “brims” at either end of the duct, which are raised at the downstream end to create

a back pressure and lowered at the upstream end to create a nozzle. This effect forces more flow through the central duct and results indicate that flow could be enhanced by up to 1.3 times the free stream velocity (this theoretically equates to approximately 2.2 times the power or 120% turbine power gain). Results are promising but the experimentation does not consider the global effects of the turbine on the flow and the additional drag force caused by the "brim" is likely to increase device cost through increased foundation/mooring loads. The calculated turbine power benefits only consider localised 1D flow effects of a venturi, the potentially large addition to channel drag at a global scale when shrouded turbines are installed in large arrays is not considered. Both Thorpe (2005) and Klaptocz et al. (2007) present experimental and numerical investigations into ducted turbines both concluding that ducted turbines are beneficial for MCEC performance. Thorpe (2005) looks at the Rotech turbine and concludes that not only does the duct give velocity increase benefits, it also improves the efficiency of exploiting yawed flows because the duct re-directs the oncoming flow streamlines into a more orthogonal path onto the turbine rotor. Klaptocz et al. (2007) describe an experimental and numerical investigation into vertical side wall concentrators for a vertical axis turbine. Both approaches conclude that ducts have the ability to increase peak power by augmenting the flow through the turbine rotor. Roddier et al. (2007) describe a 1:40 scale experimental test investigating circular and elliptical vertical side wall acceleration structures. These were termed "Tidal Current Acceleration Structures" by the authors. The thrust on an actuator disk mounted between the vertical walls was recorded. Modelling the turbine with an actuator disk was considered more appropriate than simply measuring the un-obstructed velocity as the interference between the disk and walls must not be disregarded. The author was disappointed with the resulting maximum 50% thrust increase as over 200% was expected (these thrust gains theoretically equate to approximately 84% and 420% power gains respectively). It is stated that the initial estimate was too high because three-dimensional flow effects and channel blockage were not considered. 84% power gain is an extremely large increase in device power but the channel cross-section is small and the acceleration structures occupy a large proportion of the flow depth and cross-section. If these structures were deployed in a larger channel it is postulated the MCEC power benefits would reduce considerably. More recent work by Shives and Crawford (2010) and Belloni and Willden (2011) investigate the effects of ducted turbines when deployed in larger scale arrays in large tidal channels. It is concluded that when installed as single devices or small arrays ducted turbines could be beneficial, but for large scale arrays, the increased non-energy generated drag from the turbine ducts would reduce the power output compared with deploying un-ducted MCECs. Essentially there will be a balance point where arrays reach a critical size where ducts have no or even negative effects on power output. In this scenario the added drag from the ducting will force the global flow away from the influence of the MCECs. In addition to this the extra cost of the ducting needs to be recouped by any additional power

gains and a comprehensive techno-economic analysis would be critical. It could be said that in shallow tidal flows ducted turbine arrays are not the best solution of flow augmentation because of the channel flows sensitivity to the additional drag.

An alternative to a duct could be a seabed mounted flow modification structure. This could form an integral gravity based foundation that would effectively constrain the flow in the vertical plane and increase the magnitude of the velocity profile. Salter and Taylor (2007) state that for any reduction in channel width or depth, a high local flow velocity increase will result. Although there is no known work directly related to marine energy extraction, open channel hydraulics, channel bed obstructions and possibly submerged weirs could be applied. Starting with simple open channel hydraulics texts such as Chow (1959) and Chadwick et al. (2004); by utilising simple principles of specific energy and flow continuity it is clear that in a laterally constrained domain introducing a bed ramp will locally increase the flow velocity due to the reduction in channel cross-section. A small surface drop will result in the case of subcritical flows due to the reduction in specific energy across the ramp. This one-dimensional theory cannot be directly applied to tidal flows, except perhaps in a tidal fence application, as flows are generally laterally unconstrained, meaning lateral channel flow blockage effects must be considered. Ramp-foundations would be anticipated to be most applicable in shallow depth tidal flows because in deeper flows ramp heights would have to increase dramatically and hence capital costs, to provide meaningful power benefits. Open channel bed forms have been specifically addressed by Lyn (1993), Shen et al. (1990), Fadda and Raad (1997), Dyer (1986) and Dewey et al. (2005). Lyn (1993) presents mean velocity and turbulence characteristics across two types of bed form that were obtained using a laser-Doppler velocimeter. Of key note are graphs of vertical velocity profiles across the bed forms, showing how the lower sheared region is effectively removed by the bed form and how the boundary layer re-develops downstream. This profile development offers key insight into the potential flow augmentation benefits of ramp-foundations and the predicted requirement to optimise ramp length to allow for a well-developed energy extraction velocity profile. Ideally this optimum profile would form at the ramp centre-line so bi-directional flows could be exploited. Dewey et al. (2005) highlight the fact that with the temporal depth variation of tidal flows, it is important that a ramp-foundation does not induce critical depth conditions. This would result in very shallow and rapid flows unsuitable for energy extraction. Critical depth conditions would not be anticipated in typical tidal sites as Froude numbers are generally well below unity. For example for flow depths in the range of 10-30m unrealistic accompanying tidal flow velocities of 10 to 17m/s would be required to induce critical depth conditions. Bukreev et al. (2002) describe transcritical flow over the ramp and it is clear that high energy dissipating hydraulic jumps must be avoided for tidal energy extraction. Dyer (1986) describes how a rapidly constrained velocity

profile, such as one occurring at the crest of a ramp-foundation, will take an upward concave shape because the effects of inertia compared with friction are greater away from the bed. This work and the velocity profile results from Lyn (1993) show that a ramp-foundation would need to be sufficient in length to establish a stabilised uniform velocity profile suitable for energy extraction. Ideas about flow over bedforms are discussed, ramp-foundations would need a suitably smooth profiled to avoid the turbulent effects of inflow separation. The application of Dyer's (1986) theory may be limited because the bed form shapes represent bed ripples rather than smooth ramps. Weir flow theory can be found in Chow (1959), while Wu and Rajaratnam (1996) present an experimental study into submerged weir flow. However this studies sharp-crested weirs which show few similarities to a long submerged foundation ramp. A submerged bed obstruction has a much clearer resemblance to a ramp-foundation structure than a submerged weir mainly due to the ratio of flow depth to ramp height. Song et al. (2000, 2002) present experimental studies looking at the region of flow just downstream of a bed ramp structure. The phenomenon of separation will occur in this region with turbulent flows. An important conclusion for energy extraction above ramp structures is that this separation will not affect the nature of the upstream flow across the ramp surface. The separation bubble that forms at the trailing edge of the ramp will induce increased shear stress and turbulent intensity which could interact with the turbulent wake behind the MCEC and perhaps influence the downstream wake length. Aubertine et al. (2004) discuss similar experiments and describe how increasing bed roughness increases the size of this downstream flow separation region, but again this region does not appear to encroach into the energy extraction zone above the ramp. Abd-el-Malek and Masoud (1987) present a highly mathematical 2D potential flow model for flow across a ramp. Potential flow theory could be applied to a tidal ramp-foundation but due to its limitation of neglecting irrotational flow (and hence turbulent motion) it would be difficult to accurately model the MCEC's downstream wake. Potential flow could however be used to model the ramp-foundation in isolation of the MCEC.

Summary

It appears clear that ducted turbines provide flow augmentation benefits when considering localised turbine effects. There appears to be uncertainty regarding the balance point at which the added drag from the shrouding starts to have negative global effects on power potential when deployed in larger arrays. This added drag will be even more significant in shallow channels and hence might make this technology less suited to shallow flow deployment.

For MCEC ramp-foundations to be a reality a thorough understanding of their effects on laterally un-constrained flows is required. For example the effects of the lateral ramp width to channel width ratio on the power gain potential. It is likely that the concept would only be

applicable in shallow flows due to the large ramp heights that would be required in deeper flows to yield sizable MCEC power benefits. Ramp length would also need to be tuned to allow for a well-developed energy extraction flow profile to occur at the ramp centre-line.

Artificial flow augmentation structures could have the potential to make lower energy tidal resources exploitable.

2.1.4 Wake and arrangement within arrays

2.1.4.1 Wake structure

Knowledge of the downstream flow region (or wake) behind MCECs will be fundamental for optimising device spacing in farms/arrays and to understand environmental factors from changing the free-stream flow characteristics (Myers and Bahaj, 2010). MCEC wake constitutes a reduced velocity flow region downstream of the rotor that must hence expand to conserve momentum. The form is a gradually expanding cone (assuming a circular rotor) that is dissipated by turbulent mixing between the wake boundary and the faster moving free-stream flow. The region of wake behind a MCEC has been shown to persist with appreciable velocity deficits for 15-20 device diameters downstream (Myers et al., 2008). Bahaj et al. (2007b) and Blunden (2009) provide a detailed introduction into wake characteristics behind MCECs whereby the wake is characterised into the near wake, transitional wake and far wake regions. Features that affect the wake are detailed and include: device performance, ambient and device generated turbulence, bounding surfaces and free-stream flow speed. There appears to be a limited amount of work regarding the effects of ambient flow turbulence on wake structures but Jonsson et al. (2011) conclude that the presence of strong ambient turbulence at a MCEC deployment site would increase wake recovery, indicating the downstream device spacing could be reduced (also see section 2.1.4.2). This area requires more research but recreating representative turbulence at scale in the laboratory is very challenging because knowledge of turbulent structures at real tidal sites is limited.

Wake studies behind wind turbines are numerous and have been investigated for the past 30 years. Although the fundamental principles of wake dissipation through turbulent mixing (Baker et al., 1985) are exchangeable, for marine turbines, results cannot be directly applied due to key differences, in particular the close proximity of bounding surfaces (seabed and water surface). Burton et al. (2001) and Vermeer et al. (2003) provide background on the governing principles behind wind turbine wakes but again work is wind specific, hence they are only directly applicable to marine devices operating in almost unbounded flows such as perhaps the Pentland Firth.

Myers and Bahaj (2010) present experimental results using small scale mesh disk rotor simulators. Mesh disks or porous actuators are proven to be representative of the far wake region but not the near wake as rotor swirl effects are not simulated (Bahaj and Myers, 2013). They replicate the far wake well because wake dissipation is governed by turbulent mixing and the proximity of bounding surfaces in this region rather than mechanically-induced flow structures generated by the MCEC. The governance of turbulent mixing in the far wake is reinforced from results, presented by Myers and Bahaj (2010), showing that far wake recovery is largely independent of the thrust force exerted on the flow by a MCEC. It is shown that varying the thrust coefficient (Ct) value between 0.61 and 0.94 only has a significant effect on the near wake of less than 5 diameters downstream and beyond 7 diameters the velocity deficits were almost identical for all tested disks. Hence varying the Ct value of a MCEC is expected to only effect the momentum drop in the near wake and in the far wake beyond 7-10 diameters this effect is seen to dissipate and wake breakdown is governed by ambient turbulence mixing. This effect of ambient turbulence is further reinforced by Burton et al. (2001) where the breakdown of momentum theory in the far wake is discussed, without this factor there would be insufficent kinetic energy to rasie the static pressure to that of ambient pressure that must exisit in the far wake region. Actuator disks are now widely implemented for simplifying and modelling a MCEC at small scale. Experimental wake investigations are becoming more widespread and in Computational Fluid Dynamics (CFD) simulating the MCEC as a simple porous disk is common practice (Sun et al., 2008, Harrison et al., 2010).

Computational Fluid Dynamics (CFD) has been used by MacLeod et al. (2002), Batten and Bahaj (2006), Harrison et al. (2008), Sun et al. (2008) and McCombes et al. (2009) to visualise the wake behind individual turbines, fences and arrays, but many of these models have not been experimentally validated. Harrison et al. (2009) present initial work where wake structures produced by an actuator disk CFD model are validated by experimental testing. The model contains some inconsistencies with the experimental results but is under development. The main sources of discrepancy were the lower ambient and wake turbulence intensities in the model, in part because the modelled turbine disk was not a turbulence source. The author concludes that future CFD models should place emphasis on matching inflow turbulence intensities and more realistic approximations of the wake structure. For reliable CFD results good experimental validation is required because analysis inherently involves a range of user defined parameters that must be fixed to represent the "real" flow scenario. Without the back-up of experimental data the value of CFD reduces considerably, but with a good validation range CFD can be used to generate a large number of test cases with acceptable accuracy.

The act of energy extraction will cause a reduction in the static head of water downstream of the turbine which will affect the wake development by creating additional flow constriction between the surface and MCEC (Sun et al., 2008). Again the effects of the bounding surfaces and the added vertical constraint from any MCEC head drops will become even more significant in shallow tidal flows. Myers and Bahaj (2007) tested a 0.4m diameter horizontal axis turbine and a significant head drop from energy extraction was seen at 3-6 rotor diameters downstream. The drop was exaggerated compared with a full scale site because of high Froude numbers. The paper also highlights how the surface drop from energy extraction is much greater than that from a stationary rotor and substructure. This will be particularly important when considering actuator disk experiments where no surface drop will occur from device energy extraction. In a later series of tests Myers and Bahaj (2009) investigate the characteristics of the near wake and the effects of support structures using a 1:20th scale horizontal axis turbine. It is concluded that support structure design will have a significant effect on the near wake field, again an important consideration for interpretation of actuator disk results where the support structure is not modelled.

The effects of the bounding surfaces on the wake structure, including the free-surface, channel bed and lateral channel boundaries, are increasingly becoming an important area of research (Myers et al., 2008, Stallard et al., 2011). Myers et al. (2008) look at the effects of marine current turbines operating in constrained and un-constrained flow channels. It is concluded that the downstream wake length is shorter in vertically confined flows because streamlines are constrained around the turbine increasing the surrounding velocities and increasing the shear forces at the edge of the wake. The wake can thus be re-energised more rapidly and broken down in a shorter distance. This work forms a preliminary study, further work could be conducted to evaluate the wake characteristics for a range of shallow flow depths as it is postulated that in very heavily constrained flows where the MCEC occupies the majority of the water depth, the wake length will increase. This is because the expanding wake restricts flow above and below the MCEC, reducing the available wake area for turbulent dissipation. Later work by Myers and Bahaj (2010) supports earlier findings and the stated postulations, concluding that reducing the distance between the MCEC and seabed acts to increase wake length because of a restriction in the mass-flow rate beneath the MCEC. The work does not consider the combined effect of the proximity of the free-surface, but it seems clear that in shallow flows the downstream spacing of MCECs may need to be increased.

Almost all research conducted to date has predominantly focused on horizontal axis marine current turbines. For developers of other convertors such as vertical axis and oscillating hydrofoils it will be important to visualise their downstream wake structure development.

2.1.4.2 Array and farm layout

Array optimisation and research has become highly significant because early farms are now planned or on the verge of deployment. This section follows on from 2.1.4.1 as downstream wake structures will have a heavy influence on the tidal farm layout. Understanding MCEC interaction effects and global flow modification within the array is critical for understanding the power potential of different tidal stream sites. To reap the full power benefit from tidal arrays it is critical that their layout is geometrically optimised (Myers and Bahaj, 2012) and this optimisation is likely to be a compromise between maximising power generation, economics, environmental impact, geometric channel constraints and providing access for navigation including installation/maintenance vessels. Long single row arrays would be the most efficient in terms of maximising energy yield but real world site constraints such as bathymetry are likely to require multi-row layouts where downstream wake interactions become critical array design parameters (Bahaj and Myers, 2013). Adams et al. (2011) write from an industrial perspective and emphasise that the best tidal arrays will be ones that are economically attractive, hence the cost of energy will be a key design driver. The cost of energy will itself be a compromise, a developer will wish to maximise the farm's power output but in parallel have the objective to minimise structural loading and reduce the MCEC and substructure capital cost. Understanding the environmental impacts of large-scale arrays will be required and arrays may need to be located strategically and/or reduced in size to prevent large-scale environmental impacts and changes to sediment-dynamics (Neill et al., 2012). In shallow flows it is anticipated that the downstream array spacing could be heavily driven by longer wakes resulting from high device height to flow depth ratios (see section 2.1.4.1).

Myers and Bahaj (2012) present an experimental investigation into geometric array optimisation using porous actuator disks. Although actuator disks do not fully replicate a bladed turbine and substructure, it is a good approach for fundamentally investigating array layouts in an embryonic area of research. The lateral MCEC spacing can be adjusted to constrain the flow streamlines between devices and create an accelerated flow jet. This higher velocity jet can then be exploited to increase the power potential of a downstream turbine. The experimental work concluded that in a two row array, the downstream MCEC deployed in the jet did not influence the power potential of the upstream row. Turnock et al. (2011) also suggest that a staggered MCEC arrangement would be beneficial. Malki et al. (2011) and Garrett and Cummins (2007) describe how MCECs have a strong influence on the tidal channel flow field and show how geometric optimisation can magnify energy yield through careful MCEC positioning in augmented flow regions around and between devices. O'Doherty et al. (2011) also describes the advantages of an accelerated flow jet between devices spaced two diameters apart in the first row of the array. Malki et al. model staggered 3 turbine arrays using Blade Element

Momentum–CFD and conclusions broadly agree with Myers and Bahaj's experimental results. A third row of devices could be installed but because the wakes from the first two rows expand and merge in the far wake region there is little ambient flow passing through in which a third-row device could be placed. Thus the power potential would be reduced unless a large downstream spacing was employed. Early tidal stream farms are unlikely to contain more than two rows but as farm size increases layout optimisation will become even more complex and critical. Further papers, by Myers et al. (2011b) involving experimental work and O'Doherty et al. (2009) using CFD analysis, describe observations of increased flow velocities around arrays. This occurs from the global flow resistance presented by the farm and hence global flow modification must be carefully examined, especially when deploying first generation arrays.

Turnock et al. (2011) agree with Myers' conclusions for geometric array optimisation, stating that ideally farms should have relatively small lateral gaps between MCECs and downstream spacing should be large to allow for wake dissipation. Although Myers (2012) shows that there will be a compromise when turbines are placed in very close lateral proximity, because the wakes will combine and form one large wake that persists much further downstream affecting the optimum device spacing.

Roc et al. (2013) echo the importance for second row turbines to exploit accelerated flow jets. The authors then proceed to take this concept a stage further and apply the same principle to the global array layout. The same staggered device solution could be applied to groups of MCECs deployed in larger arrays to exploit regions of accelerated flow, for example three separate small two row arrays could be positioned in a triangular formation so that the third group is located in the accelerated flow jet between the two upstream array groups. The authors suggest that this "flow-optimised" approach would produce superior array power outputs compared with implementing traditional wind farm layout methodologies. However this work would benefit from further experimental validation and could be difficult to implement at geometrically constrained sites.

In farms both the lateral device spacing and downstream row spacing will become increasingly important factors as array size develops. A key development decision will be the resultant total array power that manifests from adding additional devices and/or multiple rows, considering the large downstream distances that are required to minimise wake effects when rows exceed two in number. MCEC impedance effects are likely to be even more critical in heavily constrained shallow flows due to the high MCEC area to channel ratio. Vennell (2011a) presents an improved 1D method for calculating the power potential of a tidal channel. Although better suited to tidal fence applications, Vennell introduces two important channel concepts, namely a

large inertia dominated channel (e.g. a very deep channel such as the Pentland Firth) and conversely a shallow bottom friction dominated channel (e.g. a shallow channel). In a large cross-sectional area inertia channel, adding more turbines is unlikely to affect overall energy yield as the percentage area occupied by turbines is still low. In a shallow bottom friction dominated channel, adding more turbines would significantly affect the channel's dynamic balance and hence the overall energy potential. In a shallow friction dominated channel there will be an optimum number of MCECs to attain maximum energy yield. In a later paper, Vennell (2013) develops previous blockage theory work (discussed in section 2.1.2) to consider the importance of tuning tidal arrays to their local site conditions to achieve maximum farm power. Providing individual MCECs with the maximum possible power coefficient will not necessarily yield the optimum power output from the farm as a whole because the high blockage may considerably reduce the inter-array flow velocities. Hence whilst the power yield from individual MCECs should be maximised this should not be done at the expense of the global array energy yield. For maximum farm power output the array must be tuned as a whole and it could well be the case that less energy should be extracted from individual turbines to reduce flow impedance elsewhere. Maximum array power will be a balance to ensure a sufficient level of blockage to divert flow into the swept areas of individual MCECs rather than having very high blockage where the array flow velocity and hence power is reduced considerably. MCEC tuning in this sense could be achieved by changing the Tip Speed Ratio (TSR) of individual turbine rotors, perhaps using re-designed MCEC blades. This methodology could be taken a step further by designing turbines with "intelligent" blade pitch actuators where individual MCECs could then be used to tune blockage and maximise farm energy yield during different states of the tide. As the size of tidal stream arrays increase in the future it is predicted that tuning MCECs will become even more critical, particularly as the requirement for optimisation and reduced cost of energy increases. In recent work a number of additional authors have considered individual device tuning as a fundamental parameter for array optimisation that could be implemented by varying MCEC designs and using control strategies. Myers and Bahaj (2013) and Funke et al. (2014) in particular state that because the energy production from individual devices will vary across the array tuning device designs might be warranted, especially with devices in the centre of the array. The effect of varying device performance within an array was illustrated during 1:100-350 scale experiments conducted by Draper et al. (2013) where tidal fences of varying lateral channel blockage were modelled in a 9m wide test basin. It was shown that MCECs located close to the fence ends would experience larger forces compared with those in the centre because of flow acceleration around the array. It is postulated that for arrays larger than 10MW these tuning parameters will increase in importance due to effects of array scale blockage (Bahaj and Myers, 2013).

The influence of ambient and wake flow turbulence must be considered when optimising arrays. O'Doherty et al. (2011) demonstrate how increasing ambient turbulence intensity levels to 20% would result in greatly fluctuating MCEC loads and power outputs. This situation of high turbulence could cause complications with both structural fatigue design and electrical grid integration. Mycek et al. (2013) experimentally investigate the effects of ambient flow turbulence on array layouts. The authors replicate two ambient turbulence intensity scenarios of 3 and 15%. With the higher 15% turbulence intensity the wake is broken down in a considerably shorter downstream distance, which results from greater turbulent mixing between the wake and the surrounding flow. At higher turbulence intensities the MCEC efficiency would also reduce somewhat due to increased lateral flow components. Considering these factors, as with wind turbine array design, ambient flow turbulence will be a critical optimisation parameter for tidal arrays.

O'Doherty et al. (2011) consider a further method for tuning turbines by equipping neighbouring devices with counter rotating rotors. As the fluid between devices is then moving in the same relative direction, the shear stresses are shown to decrease. The authors state that this would reduce downstream turbulence and enable more compact array configurations. However Bai et al. (2013) have also investigated counter rotating turbines and the approach appears to have little impact on turbine power. Rotor swirl flow effects are said to be confined almost entirely to the near wake. Nevertheless counter rotating turbines, with further investigation, could prove to be an applicable constraint for tidal array layout design and energy prediction.

When optimising full-scale tidal farms consideration for the design and streamlining of support structures will be important. Mason-Jones et al. (2013) calculated, by modelling the support structure, that reduced MCEC power output could be in the region of 13%. Additionally as farm size increases the added global blockage will create a larger head difference across the farm and MCECs will be required to resist an additional component of potential energy in the form of increased blade pressure loads. While this means MCECs can theoretically exceed the traditional Betz criterion and generate more energy it will also mean increased loads and perhaps re-consideration of traditional MCEC design approaches (Vennell, 2013).

Other work involving CFD and computer modelling of arrays has been conducted by Myers and Bahaj (2005), Batten and Bahaj (2006) and Bai et al. (2009). Myers and Bahaj (2005) analysed several array configurations of varying size, spacing and velocity distributions. Conclusions include that the main factor governing array energy output is not the number of rows but the lateral coverage of the array, agreeing with published work discussing blockage effects (section

2.1.2). High device blockage is highlighted as an area of concern for power production in small farms as flow may be diverted around the array. Bai et al. (2009) look at optimising array layouts through CFD analysis. Different configurations, latitudinal spacing and longitudinal spacing are considered but the work is not validated with experimental data. Blunden (2009) develops an analytical model to characterise the effects of deploying a large array of tidal turbines at Portland Bill, UK. It was concluded that the presence of the array will have a significant effect on local tidal parameters highlighting the fact that the power potential of arrays cannot be gained from the local free-stream velocities. The importance of optimal energy extraction from arrays to prevent degradation of the natural environment and power delivery is discussed.

Summary

With various full scale tidal stream farms being planned or on the verge of deployment, it seems that optimising MCEC arrays will be an important on-going and forthcoming research topic and the current gap in knowledge is rapidly being filled with experimental and validated CFD results. Key areas of research include local MCEC scale flow interaction effects, global basin scale flow modification, wake development and layout optimisation of larger arrays. It seems clear that initial research looking at the un-disturbed kinetic energy could be used for large cross-sectional area inertia channels, but for the majority of $1^{st}/2^{nd}$ generation tidal stream farms undisturbed kinetic energy is almost irrelevant for power prediction because bottom friction and turbine drag will dominate in these shallow channels and to maximise energy yield arrays must be geometrically optimised. As the tidal industry develops it is anticipated that array size will increase dramatically which will make understanding the influence of arrays on global channel flow even more critical.

Arrays will require geometric optimisation laterally and in the stream-wise direction. Lateral spacing is likely to involve a compromise, having MCECs close together would allow the second row to exploit the accelerated flow jets that would form between devices in the upstream row. However, very closely spaced MCECs could have a negative effect by forcing more global flow around the array and also the optimum downstream row spacing could be affected because wakes can combine into a single larger wake that persists further downstream. Downstream spacing will predominantly be determined by wake length of the upstream row although as stated more compact arrays could be achieved by utilising staggered layouts. Initial observations have been made investigating the effects of boundary proximity on the wake development behind MCECs. It seems clear that wake length will be heavily influenced by the proximity of the seabed/free-surface and to a lesser extent the lateral device to channel width effects, but this requires further validation and characterisation. Understanding this effect will be vital for

optimising device spacing in tidal arrays/farms, particularly in $1^{st}/2^{nd}$ generation sites which are anticipated to be in shallow and intermediate-depth locations. A great deal of recent research has focused on tuning individual MCECs to increase the total array performance. This tuning could be achieved by varying MCEC designs and control strategies across the farm. Ambient flow turbulence intensity and its effect on wake length have been highlighted as an additional array layout optimisation parameter. Furthermore high turbulence would reduce device efficiency and magnify fatigue loading on the MCECs and their substructures.

As stated array optimisation has become a large focus for research and development. Designers must consider two conflicting factors, firstly the goal to maximise the power from individual devices considering the relationship that power is proportional to flow velocity cubed. This fact encourages designers to increase inter-array spacing and move devices away from the high wake velocity deficits created by the upstream row. Secondly this must be considered in parallel with the maximum energy yield per unit area of the tidal array, given that the array must fit within the geometric boundaries of the specific site (Bahaj and Myers, 2013). These two key parameters combined with an abundance of other factors have led to the development of algorithm based optimisation methodologies for tidal array layouts. Sullivan and McCombie (2013) discuss the importance of a parameterised energy yield and cost optimised approaches to layout design. Algorithm based approaches, similar to those used within the wind energy industry, are now being developed for tidal array optimisation. As the industry starts to commercialise the need for cost reduction will naturally intensify, hence so will the importance of cost-based layout design tools. These modelling tools should consider capital costs (CAPEX) and ideally operational costs (OPEX) and will require numerous site-specific parameters, including bathymetry data, foundation type, cable length, distance from shore and seabed geology. Automated multi-parameter tidal array optimisation tools should be considered a key development in this field (Funke et al. 2014).

2.1.6 Vertical velocity profile

Obtaining field measurements or having an accurate prediction of the vertical velocity profile is imperative for determining site suitability, device selection and calculating the accurate magnitude of device loading/power potential. The velocity profile will influence the power output, structural loading and wake characteristics of MCECs (Myers, 2005). For efficient energy capture the profile ideally needs a vertically uniform upper section to reduce cyclic loading upon the blades as they rotate (Myers, 2005). This is because a non-uniform velocity profile will cause disparate loading resulting in higher structural fatigue damage from the larger

range of applied stress. Myers also states the importance of considering the effects of wave and current interactions for offshore structures.

The nature of the velocity profile can be influenced to varying degrees by the combined interaction effects of wind generated waves, ocean swell and tidal currents. Myers (2005) describes how simply adding the velocity vectors of waves and current is inaccurate in terms of calculating resultant forces. Velocity vector superposition is the traditional method for calculating structural loading offshore but given the large magnitude of tidal flows at potential deployment sites an integrated wave-current analysis could be more appropriate. Srokosz (1987) provides a general review of wave-current interaction analysis methods and concludes simple superposition could under predict velocities by up to 22-30% when waves and currents are aligned. When travelling in opposing directions a 10% under prediction could occur. It is postulated that these effects would have a significant impact on unsteady MCEC blade loads and resulting blade fatigue damage (Milne et al., 2010). Milne also states how wave-current effects can be heavily influenced by flow depth. In a shallow flow waves of a relatively long period can affect the majority of the water column. Prandle (1997) states that this feature is likely to affect tidal currents of depths less than 50m. Following on from this Wolf and Prandle (1999) concluded that wave and current effects will be significant in shallow tidal flows of less than 20m. Wave and current interactions have been investigated by a number of authors including Srokosz (1987), Wolf and Prandle (1999), Swan and James (2000), Smith (2006) and Milne (2010) but it appears a clear method to address its influence on tidal energy is yet to be found.

Velocity profiles have been measured at a few locations around the UK and their shape has been shown to vary with flow velocity during a tidal cycle (Rippeth et al., 2002, DTI, 2005, Mason-Jones et al., 2013). The DTI's study involved measurements of the inflow velocity profile at a tidal stream turbine deployment site in North Devon. It is common place to assume that velocity profiles can be approximated by a $1/7^{th}$ power law running from seabed to surface (Bryden et al., 1998) and one published velocity profile taken at a surface flow speed of just over 2m/s showed a very close resemblance to the modified $1/7^{th}$ power law (European Commission, 1996). HSE (2002) describes the significance of depth-averaged tidal velocities and states that over most of the water depth the speed of the current will vary by up to ±25% from the depth-averaged value and the current direction will be within ±10%. This large variation in velocity through the water depth highlights the importance of considering the entire velocity profile. The European Commission (1996) recommended that the top 8m and bottom 25% of the vertical velocity profile might be avoided due to surface wave effects and the sheared region of the boundary layer respectively. HSE (2002) recommended the use of a modified $1/7^{th}$ power law,

which assumes a constant upper section to the profile, but concludes that this method is less accurate very near the seabed, in deep water and in areas of weak tidal currents. More accurate logarithmic equations are given and are considered to give better accuracy near the seabed. Bryden et al. (1998) also state that the $1/7^{th}$ power law is too simplistic for many locations and in particular, estuarial environments will require a more complex parametric description. This indicates that the use of power laws in shallow tidal flows could provide limited accuracy. A $1/7^{th}$ power law may be appropriate for an intermediate-depth site but in a shallow flow the extent of the sheared boundary layer region will occupy a greater percentage of the overall channel depth and an alternative profile could be more accurate. The book by Dyer (1986) describes boundary layers and velocity profiles related to the marine environment in some detail. The use of power laws is discussed and exponents range from 1/10 at low flow rates to 1/5 for higher flow rates. Hence the $1/7^{th}$ power law as an average approximation is reinforced by this work. Dyer (1986) also discusses logarithmic laws for velocity profile curve fitting but the $1/7^{th}$ power law still remains the most widely used profile approximation for tidal energy.

The change in profile shear with varying velocity throughout a tidal cycle is shown from measured ADCP profiles in work by both Mason-Jones et al. (2013) and Rippeth et al. (2002). Both studies show during high spring tidal flow velocities the rate of shear in the velocity profile is greatest and can extend towards the free-surface compared with more linear profiles during periods of lower flow velocities (particularly around slack water). Mason-Jones et al. (2013) conclude that the profile will change considerably during the cycle and hence the $1/7^{th}$ power law may not be an accurate representation, and during high flows the power law is shown to underestimate the rate of shear close to the seabed. These observations of variation in velocity profile shape between low and high tidal flow rates is perhaps not unexpected when one considers the key factors affecting velocity profile development in viscous fluids. In turbulent open channel flows the boundary layer will typically extent to the free-surface and because in this situation bed roughness will influence the velocity profile throughout its depth the gradient of the lower sheared region in faster flows will be steeper with increased shear stresses. This slight profile shape change, between higher and lower flows, must occur to account for the transition from "no-slip or zero velocity" at the channel bed to the maximum velocity in the upper regions of the flow and because shear stress is proportional to flow velocity when studying fundamental theory. Additionally in high flow scenarios the turbulence or vorticity from the wake of bed roughness elements will be larger and hence the mean flow in the lower region close to the bed will also reduce. This will effectively increase the boundary layer's influence on the upper flow regions.

The deployment of Acoustic Doppler Current Profilers (ADCPs) to measure speed and direction of tidal flows is now common place (Myers and Bahaj, 2010). Devices have been used at the European Marine Energy Centre (EMEC), Orkney (Norris and Droniou, 2007). Results indicate that turbulence generated by surface waves and bed effects leaves only the central third of the water column with moderately tranquil conditions, which agrees with the European Commission's (1996) recommendation. Rippeth et al. (2002) used a high frequency ADCP moored on the seabed and measured velocity over six spring/neap tidal cycles. Shear stress was generally greater during spring ebb flow and increased towards the bed. As might be anticipated the generation of turbulent kinetic energy was lowermost during slack tides because turbulence generation increases with the flow velocity. This work highlights the importance of considering a number of velocity profiles across a tidal cycle. Surveying tidal flows using ADCPs at potential MCEC deployment sites will be required to understand energy potential and for array layout optimisation. In addition due care should be taken when estimating vertical velocity profiles from single point mean-depth data as the profile shape can vary throughout a tidal cycle. Full ADCP profiles are hence desirable.

There is an abundance of work on velocity profiles and boundary layers specifically related to open channel hydraulics. The open channel hydraulics text by Chow (1959) discusses the velocity distributions across channel sections, which is important for optimum MCEC location as not only will velocities vary vertically but also laterally across the channel. Theoretical and experimental work on velocity profiles and boundary layers is presented by Bonakdari et al. (2008), Ferro and Baiamonte (1994), Song and Graf (1996), Kirkgoz and Ardichoglu (1997) and Raupach et al. (1991). Both Ferro and Baiamonte (1994) and Bonakdari et al. (2008) provide evidence that flow velocity reduces slightly towards the free surface in narrow channels because low momentum fluid near the side walls is transported to the central section. In wider aspect channels this effect will be less prevalent and velocity profiles become logarithmic. This effect could require consideration when interpreting results from scaled testing in narrow channels. Although related more to rivers than tidal flows Song and Graf (1996) use flow measurement data from an acoustic Doppler velocity profiler and Fourier components to obtain velocity, turbulence intensity and Reynolds-stress profiles. This is significant for analysing higher order flow effects such as turbulence which are important when examining MCEC wakes. Kirkgoz and Ardichoglu (1997) describe boundary layer development and conclude that the boundary layer extends to the free surface for flow aspect ratios greater than 3, which will always be the case for tidal flows. This is of course true but in the upper flow region the velocity gradient will often be close to vertically uniform and best suited for energy extraction.

Work related specifically to shallow tidal flows is sparse but Kawanisi (2004), Andersen et al. (2006) and Dworak and Gomez-Valdes (2005) provide some insight. An understanding of the characteristics of shallow flows is of paramount importance to this project. Unfortunately when many authors refer to shallow water tides they are referring to tides occurring in deep ocean waters of depths less than 100m and not shallow tides of less than 30m as defined in this project. Both Kawanisi (2004) and Andersen et al. (2006) describe the complex nature of shallow tidal flows and their many constituents, which makes accurate prediction difficult. Work by Kawanisi (2004) is useful; however it considers data from a very shallow estuary with a maximum depth of less than 4m which is too shallow for energy exploitation. Useful conclusions are that the vertical velocity profile shape showed variation during the flood and ebb tides. Again highlighting the importance of assessing the flow profile at different states of the tide. The maximum suspended sediment is stated as being two to four times greater during flood tides which could be significant in terms of MCEC operation as particle ingress into components of the drive train could cause severe damage. These results have only been validated for very shallow flows and further work is required to fully understand their applicability to flows of greater depth.

Summary

The velocity profile will influence the power output, structural loading and wake characteristics of MCECs. For efficient energy capture the vertical velocity profile ideally needs a vertically uniform upper section to reduce cyclic loading and resulting fatigue damage. The shape of the velocity profile will be influenced by a number of site specific parameters including; seabed roughness, tidal flow velocity (varying throughout the tidal cycle), water depth and wave-current interaction. The profile at tidal sites is typically approximated by a power or logarithmic law, most commonly the $1/7^{th}$ power law. Although this may be a good assumption for intermediate-depth tidal sites during peak flow velocity conditions, for deep and shallow flows different profile approximations may be better suited due to variations in the bed shear flow. The variation in flow velocity throughout a tidal cycle will also have a significant bearing on profile shape. Research surrounding shallow flows is limited and because these flows are influenced by many local tidal constituents their prediction is complex. To gain a better understanding of vertical velocity profiles particularly in shallow tidal flows additional field measurements would be beneficial. This could be done by deploying ADCPs to measure velocities throughout the tidal cycle.

2.1.7 Tidal Fences

The concept of using a fence of tidal turbines spanning the width of a channel is a relatively new idea, with a limited amount of specific research. A key issue with tidal fences is the optimum lateral spacing and impedance of MCECs. The downstream spacing is also important if multiple fences are to be deployed. Draper et al. (2011) describe the concept of "Tidal Piers" where a tidal fence essentially juts out as a continuous row of MCECs from a headland. In this form the power potential is limited because of the bypass flow around the end of the pier/fence. This is also significant in terms of developing a tidal fence with a navigation gap and the importance of including flow modification from the structure in power potential calculations. Draper states that the undisturbed kinetic flux can only be used to optimise the fence location and it cannot be used to estimate the power potential of a tidal fence. This is because tidal fences are high blockage deployments that will significantly modify the free-flow conditions.

Garrett and Cummins (2005, 2008) indicate that tidal fences are more efficient when they extend across a full tidal channel and turbine efficiency would reduce for partial fences because high proportions of the channel flow will be attracted around MCECs and through bypass channels. An equation for maximum power is presented and in theory maximum power should be independent of fence location along a channel, although fewer turbines would be required in constricted sections where flow velocity is increased. Turbines are unlikely to be deployed in continuous uniform fences because of the need for foundations, gaps for navigation and passage for marine life (Garrett and Cummins, 2008). Garrett and Cummins (2008) also conclude that the optimum device blockage for a partial fence would be 46% of the tidal channel and increasing this would simply retard the through-fence flow and increase the by-pass flow, reducing power generation. Draper et al. (2011) and Vennell (2010) agree with this work and also conclude that a continuous tidal fence will produce maximum power when devices occupy large proportions of the channel cross-section. Vennell discusses how tidal turbine blockage in a fence could be "tuned" to maximise power potential. Tidal fences unlike barrages could be deployed across a bay or estuary with less significant modification of the natural flows (Garrett and Cummins, 2008).

Harrison et al. (2008) and Blunden et al. (2009) look at the effects of multiple row tidal fences, of up to ten rows, through experimental and computational modelling. Harrison et al. (2008) present some interesting findings including the variation in fence thrust coefficient. The thrust coefficient is seen to increase for the downstream fences compared with the second row fence because of increased ambient turbulence which leads to faster wake dissipation. It must be

highlighted that these tests were modelled using continuous mesh fences so lateral flow effects were disregarded.

Lalander and Leijon (2009) indicate through numerical modelling that placing a row of ten turbines across a river will cause a water surface elevation upstream, which would be expected from the high flow obstruction caused by a continuous tidal fence, the magnitude of which will depend on the degree of energy extraction and structural blockage. This would not be so significant in a tidal estuary because of the large temporal variation in water elevation, but if the upstream free board (the difference between water depth and channel depth) is limited, flooding could be a concern. High blockage fences could be developed with extensive substructures to channel the flow; these would result in an upstream surface elevation which could be extracted as potential energy using low head turbines. Essentially a fence could be tuned in terms of impedance to exploit a proportion of both kinetic and potential energy, increasing the fence's total power output (see section 1.3.4). The deployment of high energy and high blockage tidal fences would be well suited to shallow tidal flows as less physical structure would be required to create an exploitable upstream potential energy head.

Research into tidal fences is limited and could become a key area of future work particularly as tidal barrages are now considered to cause a significant environmental impact (Pelc and Fujita, 2002). Frid et al. (2012) describe the environmental benefits that tidal fences provide over barrage structures and how fences are becoming a favoured barrage alternative. These benefits include minimising amplitude/timing changes of the tide, reduced marine life passage effects due to lower physical blockage and lower interference with bird feeding grounds. Giles et al. (2010) present the case for a tidal fence in the Severn Estuary, in terms of mitigation of environmental impacts, reduced disruption to navigation, lower capital costs compared with a barrage and the ability to be constructed in a progressive manner from shore. The Severn Estuary fence concept only considered a highly porous kinetic energy fence. By designing a fence with more substructure and provided it was a continuous fence with navigation locks it is postulated that considerably more energy could be extracted in the form of both kinetic and potential energy. The Severn Estuary with its shallow mean water depths of approximately 25m and relatively low tidal velocities would be well suited to a high blockage fence that can exploit a proportion of both kinetic and potential energy.

Summary

Tidal fences are a relatively new concept and could be highly suitable for deployment in shallow tidal flows. There is potential for further research into aspects such as lateral spacing and impedance effects. The concept would provide a less environmentally damaging alternative

to an impermeable barrage in shallow flow regions such as the Severn Estuary. Of particular interest would be to investigate high blockage fences that extract a proportion of both kinetic and potential energy.

2.2 Flow measurement

2.2.1 Types of flow measurement

There exist a number of devices for measuring flow velocities at a point, both in the laboratory and the field. These devices can broadly be grouped into point measurement and remote sampling methods. Generally point measurement devices have the advantage of giving almost instantaneous readings although at reduced accuracy. However they often only measure flow in one dimension and can cause flow disturbance through their intrusive nature. Remote sampling methods eliminate flow disturbance errors found with point measurement flow meters. There exist remote sampling methods that are capable of measurements in three dimensions, at high sampling frequencies and capable of estimating higher order flow effects such as turbulence intensity and shear stress.

Pitot tubes and propeller meters are examples of point measurement devices. They are appropriate where instantaneous velocity readings in one dimension are required and where higher order effects such as turbulence intensity are less critical. The Pitot tube typically consists of a right-angled pipe which utilises Bernoulli's energy equation. An inner pipe measures the total pressure head and an outer pipe measures the static pressure head and then by subtracting the static from the total pressure the velocity head is arrived at (Hamill, 2001). Propeller devices come in a variety of sizes ranging from miniature laboratory meters to larger river flood flow meters. Every rotation of the propeller is converted into an electrical pulse and each meter requires a calibration graph which converts these rotation counts per unit time into flow velocity. Disadvantages of propellers include, intrusive sampling, frequency is too low for higher order flow effects and miniature probes are prone to clogging from suspended flow material.

Hot-wire velocimeters use a very fine wire placed in the flow, which is heated up to a temperature above ambient. The flowing water will cool the wire and hence change the resistance, thus a relationship between flow velocity and wire resistance is established. Unfortunately the relationship is non-linear which can make analysis difficult (Lange et al., 1999). Hot-wire velocimeters have the resolution to characterise more complex flow patterns and in the past have been very popular in fluid mechanics research because they can be used to generate some turbulence parameters (Lohrmann et al., 1994). They can also provide a virtually

continuous measurement of local velocity (Yue and Malmstrom, 1998, Poggi et al., 2002, Lange et al., 1999). However their spatial resolution is not as good as Laser Doppler Velocimeters, which limits their ability to resolve high velocity gradients (Ramasamy and Leishman, 2007, Lange et al., 1999). Other limitations include intrusive sampling which disturbs the flow, their high susceptibility to flow temperature fluctuations and their limited speed of response (Lange et al., 1999). Lange et al. (1999) also stated that the accuracy of hot-wire results close to solid boundaries was hindered by additional boundary heat losses. Hotwires have problems with directional flow ambiguity meaning they are not well suited for three dimensional flow characterisation or producing accurate turbulence parameters (Ramasamy and Leishman, 2007).

Laser Doppler Velocimeters (LDV) and Acoustic Doppler Velocimeters (ADV) are the two main techniques for non-intrusive high frequency flow measurement. They are appropriate where the flow effects are not rapidly varying with time, and data can be sampled over a time period. High frequency measurement is essential for recording the varying components of flow velocity and hence investigating high order flow effects such as turbulence intensity and shear stress (Voulgaris and Trowbridge, 1998, Lohrmann et al., 1995). For experimental investigations into tidal flows, high order flow effects are very important as sizable turbulence intensities and shear stress can be problematic for device fatigue loading.

LDVs measure the velocity of particles or solid surfaces contained within a fluid by creating a sampling volume from a number of crossed and focused laser beams. Particles that pass through the sampling volume scatter the light, which is detected by a photo-detector that makes use of the principle of a laser light Doppler shift (Le Duff et al., 2002, Buchhave and George, 1979). They are non-intrusive and hence do not interfere with the fluid flow (Poindexter et al., 2011), have a very high spatial resolution due to their compact sampling volume and can measure velocity in three dimensions at very high sampling rates (Le Duff et al., 2002, Poggi et al., 2002, Ramasamy and Leishman, 2007, Buchhave and George, 1979, Voulgaris and Trowbridge, 1998). However despite giving a high degree of accuracy, they require considerable operational experience, the technology is very costly and is only really suitable for laboratory applications (Le Duff et al., 2002). As LDVs are a point by point measurement device, mapping an entire flow field can take a considerable time (Ramasamy and Leishman, 2007). LDVs have the advantage of low instrument noise at small flow velocities and Domaratskii et al. (1972) state this turbulence to be in the region of 1% within the measured frequency range. Some channels may require seeding to improve instrument accuracy. The most important characteristic for seeding material is that it has suitable buoyancy that allows the individual particles to follow the fluid motion (Buchhave and George, 1979).

ADVs were initially developed in 1992 by the U.S. Army Engineer Waterways Experiment Station and the objective was to produce an accurate three dimensional current meter at a reasonable cost (Lohrmann et al., 1994, Rusello et al., 2006). These devices are based on the Doppler shift principle and velocity measurements are achieved by measuring the suspended particle velocities within a remote sampling volume (Voulgaris and Trowbridge, 1998, McLelland and Nicholas, 2000). Some consider this to be a non-intrusive technique (Voulgaris and Trowbridge, 1998, Precht et al., 2006) with the sampling volume located 50 or 100mm from the probe head. However the probe has to be located within the fluid flow and will slightly impact on the accuracy of the results depending on the flow direction and probe head size (Rusello et al., 2006, Snyder and Castro, 1999). Cea et al. (2007) state that given the distance between the sample volume and probe head is reasonably large the influence of the probe on the flow should be negligible. The probe head contains one central transmitter and three or four receivers (Chanson et al., 2005, Nortek, 2004). Chanson et al. (2005) specifically remark that ADVs are well suited for measuring velocities in shallow-water systems, which is important when investigating shallow tidal flows in scaled experimental facilities. Lohrmann et al. (1994) state that ADVs are suitable for low flow velocity measurements, which is also important because scaled velocities will be small. ADVs produce three dimensional velocity measurements at high sampling rates (typically up to 50 Hz) with no regular calibration requirements. The sampling volume is reasonably small allowing a good spatial resolution and ADVs do not suffer from water turbidity problems like LDVs (Voulgaris and Trowbridge, 1998, Lohrmann et al., 1994). It is a highly accurate technique that can be used both in the laboratory and the field at a reasonable cost compared with other technologies such as LDVs (Precht et al., 2006, Rusello et al., 2006, Lohrmann et al., 1994, Kraus et al., 1993). Compared with the LDV, ADVs are known to give a lower temporal and spatial resolution but produce comparable accuracy with significant benefits in terms of simplicity and versatility of operation at about one-tenth of the price (Lohrmann et al., 1994). ADVs may be described as a point by point device and hence can be deployed quickly in different measurement locations unlike devices that profile through the vertical water column (Kraus et al., 1993). ADVs have been shown to accurately measure intermediate length scales of turbulence and since their early development have been used to measure turbulence intensity and shear stress within the fluid flow (Rusello and Cowen, 2011). Measurement of turbulence intensity and shear stress will be important for tidal flows as these parameters will impact device loading, MCEC power output, site selection and downstream wake length.

2.2.2 ADV Operation

Generally ADVs are much simpler to use, are more cost effective and are more robust than other technologies and can be easily adapted for field work as well as laboratory use (Precht et al., 2006, Lohrmann et al., 1994, Rusello et al., 2006). ADVs are a Doppler technology where the probe is submerged within the flow and the transmitting transducer and receiver arms are focused on a sampling volume located a fixed distance from the probe head. A short acoustic pulse is transmitted from the transducer and these beams encounter suspended particles within the sampling volume which scatter back a fraction of the acoustic energy (McLelland and Nicholas, 2000). The reflected signals are then collected by the receiver arms and the shift in frequency or Doppler effect is utilised to estimate the particle velocity in three dimensions (Voulgaris and Trowbridge, 1998, Nikora and Goring, 1998, Precht et al., 2006). Particles are considered to follow the flow path and hence particle velocity is considered equal to the fluid flow velocity. A transformation matrix is used to convert measurements along the bistatic angles into the orthogonal coordinate system. The values of the transformation matrix are unique for each ADV and remain constant unless the probe head is damaged. Matrix parameters are determined by calibrating the device at a constant flow and at different angles of attack (Lohrmann et al., 1994). ADVs are ideal for laboratory situations investigating multi-directional flows which will be important for investigating lateral and vertical flow effects in tidal channels and around structures (Nikora and Goring, 1998). Rusello et al. (2006) describe a comparison study between first generation ADVs and the now common place second generation devices, such as the Nortek Vectrino ADV (Nortek, 2004). In general the new ADV designs give better performance at lower signal to noise ratios (SNR), have reduced system noise and require a lower density of back-scattering material in the water. The SNR is calculated using the signal amplitude and the background electrical and disturbance noise levels (McLelland and Nicholas, 2000). The SNR needs to be as high as possible to improve data quality. As it is not really possible to measure the signal without noise, the SNR is essentially the ratio of the combined signal/noise amplitude to the noise amplitude.

One problem that may be encountered particularly with clean laboratories in soft water areas is the need to seed the water with scattering particles. Seeding with materials such as hollow glass spheres is required to achieve a sufficient acoustic scattering and SNR for accurate operation (Snyder and Castro, 1999, Meile et al., 2008). Seeding is not always desirable due to contamination and the high expense of constant seeding (Rusello et al., 2006). In large channels or towing tanks seeding particles can quickly settle out. An alternative seeding technique to reduce the quantity of material is to inject seeding material into the flow region of interest rather than seeding the entire channel (Snyder and Castro, 1999). Generally ADVs require less particle

seeding compared with LDVs because the lower frequency acoustic pulses emitted by ADVs do not attenuate as rapidly.

During the set up procedure a velocity range must be selected and it is important that this is the smallest possible range that encompasses the velocity range of the flow in question. Although the velocity can be recorded beyond this range, the degree of accuracy will be sacrificed (Snyder and Castro, 1999).

Occasionally ADVs will show increased energy in a sample volume which is referred to as a "weak spot". There are a number of factors that govern the propensity for such erroneous readings including probe sampling configuration and the material composition of any solid surface ahead of the probe. Snyder and Castro (1999) describes this phenomenon and states that these small regions of resonance are mainly dependent on the material of the channel bed and can be avoided by covering the bed with rubber matting or simply moving the probe position slightly.

2.2.3 Accuracy and instrument setup

It is well known that there are inherent errors when using raw data from ADVs. Particularly with turbulent flow measurements the velocity components can contain high levels of noise and spiking (Chanson et al., 2005, McLelland and Nicholas, 2000). Spikes are random outlying data points that are discontinuous with the surrounding data time series. Measurement errors tend to stem from instrument velocity range, sampling frequency, probe orientation and local flow effects (McLelland and Nicholas, 2000). The effects of noise can be minimised by increasing the time period of a sample (Lohrmann et al., 1995) and sample quality can be enhanced through filtering out noise and removing spikes from the data (Cea et al., 2007). These velocity fluctuations are usually a combination of Doppler noise effects, velocity fluctuations within the channel, instrument vibration and signal aliasing (Cea et al., 2007, Chanson et al., 2005). In particular spikes are commonly caused by signal aliasing where different signals from the ADV become indistinguishable when sampled. Doppler noise means that the turbulent kinetic energy given from ADV measurements will be larger than the real turbulent kinetic energy within the flow (Cea et al., 2007). This is not a major concern because Doppler noise is white and the "noise floor" can be readily identified and the instrument noise removed from the sample (Lohrmann et al., 1995, McLelland and Nicholas, 2000). Cea et al. (2007) conclude that the main sources of error in ADV samples are Doppler noise and signal aliasing which have been investigated by Lane et al. (1998), Nikora and Goring (1998), Garcia et al. (2004) and Goring and Nikora (2002). Nikora and Goring (1998) concluded that when measuring turbulent flows

the noise in the horizontal plane could be up to 30 times greater than in the longitudinal or downstream plane and due to its chaotic nature noise increases considerably with turbulence. Increasing the aeration of a flow has been shown to increase the errors from ADVs (Cea et al., 2007) hence great care must be taken when measuring turbulent flows with high aeration and the increased turbulence will intensify the requirement for data filtering. Snyder and Castro (1999) conclude that ADV errors are independent of Froude number indicating that the same prevention measures can be used for all flow regimes.

Early comparison studies such as Lohrmann et al. (1994) directly compared the results from an ADV and LDV. Although these results were not considered conclusive they showed good concurrence between mean values. However Reynolds stress contained errors at low shear but showed good agreement at higher shear stress values. A later study by Voulgaris and Trowbridge (1998) used more rigorous comparison methods with two independent measures of turbulence. Results conclude that mean velocities recorded using ADVs were within 1% of LDV measurements. Reynolds stress was only underestimated by 1% using an ADV and turbulence intensity in the vertical plane was accurate but the downstream plane suffered from noise as a result of probe geometry. Voulgaris and Trowbridge (1998) conclude that the high accuracy and zero-drift measurements allow the ADV to produce precise results even close to boundaries. However Finelli et al. (1999) showed that although the ADV will still record data close to boundaries, these results are often underestimated. Finelli et al. (1999) compared ADV velocities near boundaries with measurements taken using a Hot Film Velocimeter (HFV) and concluded for heights greater than 10mm above the bed both devices gave similar results but for readings taken near the bed the ADV gave readings of 60-80% less than the HFV. The reason for this was stated as being because the sample volume was intercepting the boundary and if this were avoided these incorrect measurements would be circumvented. Following on from this work Precht et al. (2006) studied the near bed performance of two different ADV systems and compared them with results from an LDV. It was concluded that measurements taken close to boundaries must be treated with care. It is recommended that sampling at a level below 2.5 times the nominal sample volume height should be avoided. Snyder and Castro (1999) conclude that ADVs are ±0.25% accurate in the horizontal plane but in the vertical plane a velocity component error of 2% of the horizontal was induced from the presence of the probe head. In terms of turbulence the lowest observation level is limited due to the inherent Doppler noise of the ADV system. McLelland and Nicholas (2000) conclude that the analysis of turbulence statistics indicates that errors with Reynolds shear stress are small and ADVs are capable of accurately visualising velocity fluctuations at high sampling rates.

Voulgaris and Trowbridge (1998) describe the total velocity error as being the sum of, sampling errors due to phase shift resolution, random scattering within the sample volume and errors resulting from mean velocity shear within the sample volume. This is the reason for keeping the vertical extent of the sampling volume as small as possible to eliminate effects from shear. Nortek (2004) recommended for accurate measurements of turbulence parameters the minimum correlation coefficient should be 0.7 and the SNR for mean flow measurements should be greater than 5dB and for instantaneous measurements greater than 15dB. Hence it is important that these parameters are monitored throughout experimentation. An unpublished report form the National Sedimentation Laboratory, Mississippi (Gordon, 2000), provides some significant recommendations for ADV operational parameters. For velocimeters to collect samples without impairing data quality the sampling rate should be kept below 50Hz. If very small sampling volumes are used the noise level increases considerably. Using a higher velocity range will also increase instrumental noise levels and data spiking appears not to be related to current speed but rather to the turbulence intensity.

It is important to ensure the ADV probe head orientation is kept vertical because Snyder and Castro (1999) established that errors can be as high as 10% for high pitch angles of 30-50 degrees.

2.2.4 Data post processing

Data requires post processing to remove noise and spurious points. Filtering is essential to improve measurements of higher order flow effects, such as turbulence intensity and shear stresses, because any spikes in the data will give a false impression of the flow. Unfiltered data often gives the illusion of a more energetic flow and a data filter must be implemented to remove the non-flow effects and leave a more realistic data sample.

Chanson et al. (2005) state that post-processing of ADV data will affect all turbulent velocity parameters. However ADV data accuracy is severely reduced without suitable filtering techniques. Filtering generally has a much smaller effect on mean flow velocities as spikes tend to be equally negative and positive but Chanson et al. (2005) state that unfiltered results should not be used even for studies of mean-temporal velocity components (Chanson et al., 2005). Filtering is particularly important when investigating highly turbulent free surface flows with high aeration as it is virtually impossible to obtain spike-free samples (Cea et al., 2007).

Cea et al. (2007) present the following characteristics for high-quality ADV data filters:

1. Filtered data should have similar statistical properties to the unfiltered sample.
2. Filters should use iteration to ensure results have converged to an accurate solution.
3. There must be no parameters fixed by the user.
4. Filters should be independent of the measuring frequency.
5. Replacement of data should be avoided but when required should be conducted after filtering.
6. Filtering criteria should depend on the entire sample and not neighbouring data.

Cea et al. (2007) present a filter called the "velocity correlation filter". It is considered an improvement on the maximum/minimum threshold filter, acceleration threshold filter (Nikora and Goring, 2000) and the phase-space threshold filter (Goring and Nikora, 2002). Filtering is usually conducted in two stages; the first involves removal of spikes and solution iteration and the second stage involves replacement of data through interpolation (Cea et al., 2007). It is possible to filter with or without data replacement, but for investigating temporal based parameters data replacement will be necessary.

The maximum/minimum threshold filter simply establishes an upper-bound and lower-bound threshold and any data lying outside this range are deemed inaccurate and excluded. It is common for the maximum/minimum thresholds to be fixed through visual inspection which is of course dependent on an individual's perception (Cea et al., 2007). The acceleration threshold filter (Nikora and Goring, 2000) establishes a threshold based on the acceleration of a particle within the flow. However this method is limited by the fact that two constraints are required that are based on the authors' experience. The phase-space threshold filter (Goring and Nikora, 2002) constructs an ellipse based on derivations of the ADV signal and all the data contained within the ellipse are considered valid. The velocity correlation filter proposed by Cea et al. (2007) is based around the concept of the phase-space filter but it plots all three velocity components against each other and no data replacement is conducted during the filtering process. The filter constructs an ellipsoid and all data outside are excluded and considered to be erroneous. As velocity parameters are considered together the efficiency of the filter is improved considerably.

Chanson et al. (2005) present a three stage data post-processing method. Stage one involves an initial velocity signal check, stage two is known as "pre-filtering", with the effects of major flow disturbances being removed, and stage three removes data spikes using a phase-space threshold filter which is iterated until the number of errors are close to zero, as described by Cea

et al. (2007). Chanson et al. (2005) also thoroughly tested an acceleration threshold filter and determined that the phase-space filter was more reliable.

Cea et al. (2007) conclude that although all the investigated filters identify varying numbers of spikes, all the methods produce reasonable results. This perhaps indicates the importance of testing different filters with sampled data to ensure adequate filter performance. Cea et al. (2007) also highlight the importance of using visual inspection of the data before and after filtering to check for any filtering errors. It seems reasonable however to assume from Chanson et al. (2005) and Cea et al. (2007) that either a phase-space filter or the velocity correlation filter will offer the best performance.

2.3 Literature review conclusions

Following the literature review a number of recommendations and avenues for further investigation have been identified:

- Assessments of the UK, European and global tidal resources are still surrounded with a high degree of uncertainty and offer a key area for future research. It is anticipated that localised resource assessments for MCEC deployment sites will drive future research.
- Previous resource assessments appear to have neglected a large proportion of the shallow tidal resource by excluding flow depths of less than 20m. This perhaps occurred due to a lack of suitable technology to exploit such resources. However with the development of shallow water MCECs it could be crucial to establish the energy potential of shallow tidal sites.
- Given the significance of many shallow tidal resources for first generation tidal stream farms, further research and development into efficient shallow water MCECs could be important.
- Flow blockage research to date has been dominated by area blockage techniques and has neglected the de-coupled lateral and vertical blockage effects. These are foreseen to be of paramount importance for future research, particularly with the first commercial arrays on the threshold of deployment.
- Understanding lateral flow constriction effects is fundamental as these will have a strong influence on the global flow around and through tidal arrays, hence affecting device performance and also wake dissipation. Many first generation sites are likely to involve high vertical blockage in terms of seabed/free-surface proximity but relatively low lateral blockage; hence these effects will require independent investigation.
- Initial observations have been made investigating the effects of seabed and free-surface proximity on the wake development behind MCECs. Understanding this area will be particularly important for shallow tidal flows where MCECs are expected to occupy large proportions of the vertical water column. Wake length characterisation for different MCEC height to flow depth ratios will be vital for optimising device spacing in tidal arrays/farms.
- It may be possible to locally constrain tidal flows to magnify the velocity resulting in an increased number of sites suitable for economic energy extraction. This could be done by artificially raising the sea bed through gravity ramp-foundations, installing flow concentrators or manufacturing a duct to surround the turbine.

- The added non-energy drag from ducts around shrouded turbines could make this approach unsuitable to shallow drag dominated channels. A better approach in shallow flows could be to deploy seabed ramp-foundations that magnify velocities using principles of cross-section continuity. Ramps may only be applicable in shallow flows due to the large ramp heights that would be required in deeper flows to yield sizable MCEC power benefits. Ramp length would also need to be tuned to allow for a well-developed energy extraction flow profile to occur across the ramp.
- There appears to be a limited amount of experimental and theoretical understanding related to turbine arrays. Including local MCEC scale flow interaction effects, global basin scale flow modification and layout optimisation of larger arrays. This is very important given the next stage of development will be the deployment of small tidal stream farms.
- The velocity profile will influence the power output, structural loading and wake characteristics of MCECs. To gain a better understanding of vertical velocity profiles in tidal flows additional field measurements would be beneficial. This could be done by deploying ADCPs to measure velocities throughout the tidal cycle.
- Tidal fences are a relatively new concept and could be highly suitable for deployment in shallow tidal flows. There is potential for further research into aspects such as lateral spacing and impedance effects. Of particular interest would be investigating the increased power available from high blockage fences that extract a proportion of both kinetic and potential energy.
- Acoustic Doppler Velocimeters are now well accepted for accurate measurement of the flow velocity and higher order flow parameters. The importance of filtering data is highlighted, particularly for turbulent flow characteristics.

Chapter 3

3 Theory

3.1 Flow characterisation

3.1.1 Tides

Tidal theory has developed over the centuries from many early works, such as those by Galileo, Newton, Euler, Bernoulli, Airy and Harris. Summaries of the development of tidal theory can be found in many modern texts including Brown et al. (1999), Reeve (2004), Hardisty (2009) and Woodroffe (2002). Myers (2005) also provides background theory and Blunden (2009) presents a detailed review of tidal theory. A short potted description of tidal theory will be presented here and further detail can be found in the stated publications.

Tides are long water waves and result from the gravitational forces from the moon and sun and the centrifugal force from the Earth's rotation. The resultant of these forces acts on the oceans that cover the Earth to create tides and the magnitude of the tides vary with time as the resultant force depends on the relative position of the Earth, sun and moon. The starting point for all tidal theory is Newton's force equation for gravitational attraction (equation 3.1).

$$F = G\frac{m_1 m_2}{r^2} \tag{3.1}$$

Although the sun has a much greater mass than the moon, its vast distance from Earth offsets this. Hence the magnitude of lunar tides is approximately twice that of solar tides. Doodson (1921) explains that there are approximately 400 tidal components that influence sea level around the World. It is the interaction of these components that influences the tidal height at a specific location on the Earth. Tidal heights can be predicted over a long period of time. However because of the complex interactions of the tidal components it is preferable to obtain tidal measurements. Two key tidal events, termed spring and neap tides, both occur twice in a lunar month. Spring tides are high in magnitude and occur when the sun, moon and Earth are all aligned (at full and new moon). The weaker neap tides occur when the sun and moon are at 90° to each other. Tidal currents in the open sea have small velocities but are magnified in shallow coastal regions and where there is constraining topography such as in estuaries, around headlands and through tidal straits. It is these flows that become exploitable for energy extraction.

The simplest method for calculating gravity waves is linear or Airy wave theory which applies reasonably well in the open sea but not in estuaries and shallow water regions which are of key interest to this project. In these locations it is necessary to utilise a tidal harmonic prediction using the various local tidal components. Tides in the deep ocean are progressive waves with peak flood and ebb tides in phase with high and low water respectively. In shallower water and estuaries the tidal wave resembles a standing wave with the peak flows and water depths out of phase with each other. In estuaries and restricted channels tides tend to be bi-directional, whereas in the open sea environmental directionality varies because of other factors such as the Coriolis force (Hardisty, 2009).

A common formula for approximating a semi-diurnal tidal velocity profile (such as those found around the UK) is given by the European Commission (1996) in equation 3.2.

$$U_{(t)} = \left[B + C\cos\left(\frac{2\pi t}{T_1} \right) \right] \cos\left(\frac{2\pi t}{T_0} \right) R \qquad (3.2)$$

Constants B and C are found from the mean spring peak current and the ratio between the mean spring peak and the mean neap peak current. T_1 is the spring-neap period in hours, T_0 is the diurnal period (12.417 hours) and *t* is the time.

If: $\cos\left(\frac{2\pi t}{T_0} \right) \geq 0$ then R is equal to 1 (often the case and thus R is omitted from equation 3.2).

If: $\cos\left(\frac{2\pi t}{T_0} \right) < 0$ then R is the ratio of flood to the ebb tide.

The equation can therefore be used to estimate the mean spring and neap flow velocities for any site. It must be assumed that the tidal velocities follow the tidal range of a nearby site. A large amount of tidal data can be gleaned from Admiralty charts but in the majority of cases is of insufficient resolution for assessing the exploitability of tidal sites.

3.1.2 Vertical velocity profile

There is no substitute for measuring vertical velocity profiles in the field using devices such as Acoustic Doppler Current Profilers (ADCPs). However from fitting curves to site data, power laws or logarithmic laws can provide an approximation given the depth averaged velocity and flow depth at a particular site. For MCECs in particular it is important to consider the non-uniformity of a velocity profile. For example the region of sheared flow near the bed should be avoided due to effects of disparate loading on the device (Myers, 2005). For many locations a

simple 1/7th power law can be used as a good fit to a tidal flow velocity profile (HSE, 2002), equations 3.3 and 3.4.

$$U_{t(z)} = \left(\frac{z}{0.32d}\right)^{\frac{1}{7}} \overline{U_t} \qquad for\ 0 \le z \le 0.5d \qquad (3.3)$$

$$U_{t(z)} = 1.07\overline{U_t} \qquad for\ 0.5d \le z \le d \qquad (3.4)$$

HSE (2002) states that equations 3.3 and 3.4 are accurate to within ±15% but are less accurate very near the seabed, in deep water and in weak tidal currents. For a more accurate estimation of the profile, in particular the region of flow near the seabed, a logarithmic law is proposed (HSE, 2002), equations 3.5 and 3.6.

$$U_{t(z)} = \frac{\overline{U_t}\ln(z/k)}{\ln(\delta/2k) - \delta/2d} \qquad for\ k \le z \le 0.5\delta \qquad (3.5)$$

$$U_{t(z)} = \frac{\overline{U_t}\ln(\delta/2k)}{\ln(\delta/2k) - \delta/2d} \qquad for\ 0.5\delta \le z \le d \qquad (3.6)$$

The lower sheared region of the velocity profile ultimately results from bed surface roughness, which is discussed in boundary layer theory first developed and published by Prandtl (1904). Detailed descriptions of boundary layer theory can be found in Vallentine (1969) and Chow (1959). If the channel cross-section or bed roughness changes, the vertical velocity profile will re-develop and change shape. The thickness of the boundary layer is denoted by the term δ and is often defined as "the magnitude of the normal distance from the boundary surface at which the velocity is equal to 99% of the limiting velocity". In a turbulent tidal flow the boundary layer will extend through to the free-surface and can be approximated by either a logarithmic or power law. If the bed roughness is small and does not project into the laminar sub-layer, flow is termed as "smooth-wall turbulent". For larger bed roughness (such as in a typical tidal channel) the roughness elements project beyond the laminar sub-layer and flow is termed "rough-wall turbulent". These velocity distributions were developed as the Kármán-Prandtl equations (3.7 and 3.8). For large scale tidal flows, it has been shown that the velocity profile can be approximated by equations 3.3-3.6.

$$\frac{U}{u_*} = 5.75log\frac{u_* z}{\nu} + 5.5 \qquad smooth\ wall\ turbulent\ flow \qquad (3.7)$$

$$\frac{U}{u_*} = 5.75log\frac{z}{k} + 8.5 \qquad rough\ wall\ turbulent\ flow \qquad (3.8)$$

$$u_* = \sqrt{\tau/\rho} \qquad shear\ velocity \qquad (3.9)$$

The upper 25% of the water column is generally avoided due to wave effects that would result in device cyclic loading leading to fatigue of the blades and rotor (European Commission, 1996). This assumption is confirmed by studying the influence of wave and current interactions on MCECs. In a shallow flow with the turbine hub height located close to the free-surface, surface waves will have a significant contribution to unsteady blade loading for MCECs (Milne et al., 2010). There are three main contributors to unsteady tidal flows, which are shear flow, turbulence and waves.

3.1.3 Higher order flow effects

Tidal flows are almost always characterised by turbulent flow, where motions are rotational and exhibit rapid mixing. With turbulent flow, the internal destabilising inertial forces dominate the stabilising viscous forces (Reynolds, 1883) . Higher order flow effects such as turbulence and shear stress are highly significant for MCECs in terms of device loading, wake recovery and locating devices away from regions of high flow instability. Despite turbulent flow being rapid and fluctuating, a good understanding of the flow pattern can be developed by evaluating the temporal mean velocity over a short period at each sample point (Vallentine, 1969). This section presents equations for calculating important higher order flow effects including turbulence intensity and shear stress.

Turbulence Intensity:

Turbulence intensity (equation 3.10) is discussed in Burton et al. (2001). Turbulence intensity is a measure of the overall turbulence level. Equation 3.10 must be used with caution close to boundaries where velocities become very small and therefore Turbulence Intensity (I) would tend to infinity. Regarding its application in this project these effects should be minimised because the main region of interest is the central flow area located away from the boundaries. Hence the zone where the MCEC would be located.

$$I = \frac{\sigma}{\overline{u}} = \frac{\sqrt{\frac{1}{N}\sum_{i=1}^{N}(u_i - \overline{u})^2}}{\frac{1}{N}\sum_{i=1}^{N} u_i} \tag{3.10}$$

σ = the standard deviation of the sample

$\overline{U}$ = the mean velocity of the sample

Shear Stress:

Shear stress was first defined by Newton's Law of Viscosity (Newton, 1687). Within the thin viscous sublayer shear stress is given by equation 3.11 (Newton's Law of Viscosity).

$$\tau = \mu \frac{du}{dy} \tag{3.11}$$

However outside the vicious sublayer the flow is turbulent hence a completely different flow regime occurs and equation 3.11 cannot be applied. In this outer region of turbulent flow, which is particularly relevant to tidal flows, the stresses become what are termed apparent shear stresses or Reynolds stresses. The turbulence causes mixing which means at a specific location within the flow the velocity will fluctuate with time. This results in higher apparent shear stresses in the turbulent region which can be defined as "eddy viscosity" which is several orders larger than molecular viscosity. Eddy viscosity was first postulated by Boussinesq (1877) and further developed by Prandtl's Mixing Length Theory (Prandtl, 1925) . Velocity can be thought of as having two components - a mean component ($\bar{u}, \bar{v}, \bar{w}$) and a fluctuating component (u', v', w'); this is commonly called a Reynolds' decomposition. Horizontal, longitudinal (e.g. downstream) and vertical shear stress may be defined by equations 3.12, 3.13 and 3.14.

$$Horizontal\ Shear\ Stress \quad = \overline{u'v'}\rho \tag{3.12}$$

$$Longitudinal\ Shear\ Stress \quad = \overline{u'w'}\rho \tag{3.13}$$

$$Vertical\ Shear\ Stress \quad = \overline{v'w'}\rho \tag{3.14}$$

Where: $u' = u - \bar{u} \quad v' = v - \bar{v} \quad w' = w - \bar{w}$

3.1.4 Characterisation of flows in open channels

The hydraulics texts by Chow (1959), Chadwick et al. (2004), Hamill (2001) and Douglas et al. (2005) provide good background open channel theory. Of particular interest are concepts of continuity and specific energy.

There are four main classifications for open channel flow:

1. ***Uniform flow:*** this is flow where all flow parameters remain constant, including depth, channel cross section, discharge and mean velocity.
2. ***Non-uniform flow:*** this is common for natural flows such as tidal streams, where the discharge remains constant but other parameters such as the depth, cross-section and mean velocity vary along the channel.

3. ***Steady flow:*** flow that remains constant with time. Tidal flows can be presumed to be steady state, assuming an instantaneous point in the tidal cycle is examined. A full tidal cycle could be examined in a number of steady state time steps.
4. ***Unsteady flow:*** typical of the natural environment where flow parameters vary with time. For example river discharge will vary according to the local hydrograph.

In reality the type of tidal flow will be site dependent but will always be unsteady. Locations with near uniform depth will exhibit uniform type flow whereas other sites with varied bathymetry will display non-uniform flow. The velocity will always be unsteady but it is driven by predictable forces (in the most part) and some local effects, hence at any point in space and time the velocity should be quite predictable. Tidal flows can be simplified to steady state by assuming a series of time steps.

Of particular importance are the Froude (equation 3.15) and Reynolds numbers (equation 3.16), which are dimensionless parameters related to gravity and viscous drag respectively.

$$Fd = \frac{U}{\sqrt{gd}} \tag{3.15}$$

$$\mathrm{Re} = \frac{\rho dU}{\mu} = \frac{dU}{\nu} \tag{3.16}$$

These dimensionless numbers can be used for scaling experiments from full scale parameters. In the case of open channel flow and tidal flows, a Froude model is used because gravitational forces are dominant. Given that the density and viscosity of water are constant at model and full scale by selecting Froude number parity, Reynolds number equality will not be achievable. However because tidal flows are turbulent, a model can be designed so that the Reynolds number is in the turbulent range.

Re < 500	***Laminar flow***
Re = 500 to 2000	***Transitional flow***
Re > 2000	***Turbulent flow***

The Froude number may also be used to determine the flow regime in a channel:

$Fd < 1.00$	***Subcritical flow***, a relatively deep, slow flow (common in a tidal flow)
$Fd = 1.00$	***Critical flow***, transitional flow
$Fd > 1.00$	***Supercritical flow***, a shallow, fast flow

When the Froude number is unity the corresponding flow depth is known as critical depth which is defined as the state of flow at which specific energy is minimum for a constant discharge. In tidal streams the flow region will almost always be subcritical with corresponding Froude

numbers of less than 0.2. For example for flow depths in the range of 10-30m unrealistic accompanying tidal flow velocities of 10 to 17m/s would be required to induce critical depth conditions. However in some very shallow and fast flows critical depth may be approached especially if it is constrained between closely-spaced MCECs. As the Froude number approaches unity the depth becomes increasingly sensitive to changes in specific energy. Undular waves and other flow instabilities will have a significant impact upon power production and device structural loading so the design of farms or arrays should be mindful to avoid over constraining the flow.

It is convenient to use specific energy principles for open channel flows rather than total energy (the Bernoulli equation). Specific Energy is the energy calculated above the channel bed, given by equation 3.17.

$$E = d + \frac{U^2}{2g} \tag{3.17}$$

Specific energy at a known channel section and flow rate is a function of the flow depth only, thus the conservation of energy principles can be utilised to solve many flow problems. For example the specific energy equation can be used to solve the problem for flow over a raised hump (Figure 3-1). For a constant total head (H) the specific energy decreases when the elevation of the channel bed is raised. In tidal energy the flow will almost always be subcritical (Fd<1) and an associated surface drop would be observed over the raised bed. Hence for a change in channel bed elevation the downstream flow conditions (E_2, d_2) can be deduced directly from the specific energy curve (Figure 3-1).

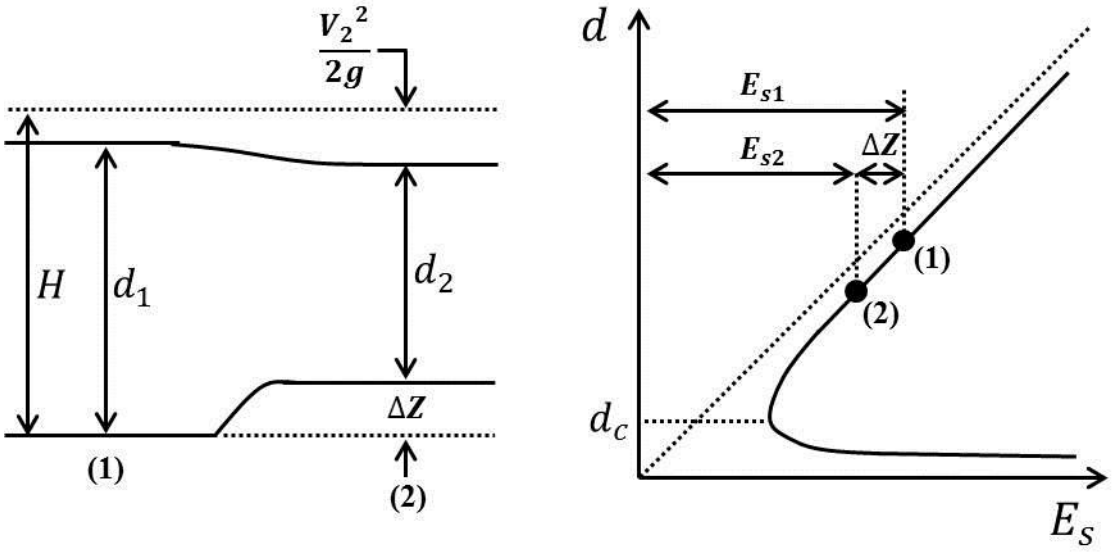

Figure 3-1: Specific Energy Diagram and flow over a raised hump (Subcritical)

3.2 Axial Momentum Theory

Axial momentum theory originally developed by Froude in 1889 can be implemented to estimate the thrust load and resulting turbine power for a given free-stream flow velocity. In recent history it has been developed specifically for wind turbines (Burton et al., 2001) but can be applied to any rotor extracting kinetic energy from a moving fluid; hence tidal turbines extracting kinetic flow energy, operating in flows with low rotor to channel area ratios. The concept represents the turbine as an "actuator disk" and assumes no fluid interaction between the flow through the rotor and that which surrounds it. All turbines of this type extract energy by creating a step change in pressure across the device. A detailed explanation of axial momentum theory related to wind turbines or actuator disk theory can be found in Burton et al. (2001). Sharpe (2004) includes the effects of wake rotation and concludes that there is no associated loss of turbine efficiency. These effects result from the fact that turbine blades rotate with an angular velocity and it is this rotation that creates the "actuator disk" and associated pressure difference. Actuator disk theory is directly related to tidal turbines by Myers (2005). When applying actuator disk theory to tidal turbines it must be recalled that the theory was derived for a turbine operating in an un-constrained flow domain. Directly applying it to a marine turbine operating in a highly constrained or blocked flow without suitable correction will lead to errors in device efficiency prediction. When turbines operate in blocked channels with boundaries in close proximity, the modified surrounding flow will interact with the rotor's streamtube. Essentially the shape of the streamtube will deform compared with the predicted tube shape for a MCEC deployed in an un-blocked channel. Hence the velocities and the pressure change across the rotor, and resulting MCEC performance will be altered.

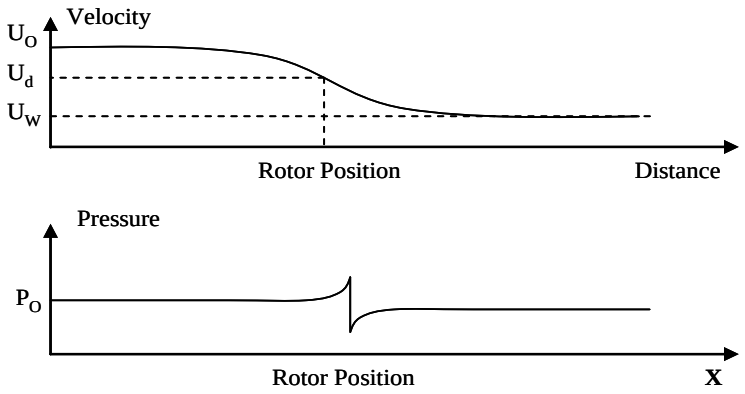

Figure 3-2: Stream velocity and pressure distribution across the rotor disk

As stated and shown in Figure 3-2, marine current turbines extract energy from a moving fluid by creating a step change in pressure across its swept area. The solidity of the rotor causes the flow from the upstream direction to slow down, hence the pressure increases and as the fluid

flows through the rotor the pressure reduces to below the free stream pressure. Downstream the pressure increases again, the velocity reduces forming a region of slow moving flow commonly referred to as a wake. At some point downstream the static pressure must return to its normal value for equilibrium to be satisfied. Therefore no change in static pressure between the upstream and downstream locations occurs but there is a reduction in the kinetic energy of the fluid. A marine current turbine converts some of this kinetic energy into mechanical and then electrical energy. In the following derivation the subscript 'o' represents the upstream position, 'd' is the position at the rotor disk and 'w' is a position far downstream. To derive the power and thrust equations axial momentum theory is used which considers the energy extraction process with an 'actuator disk' located in a stream tube. Due to continuity and to conserve the mass flow rate, the upstream cross-section of the stream tube is smaller than the disk and downstream cross-sections.

Power equation

The flow velocity at the rotor disk U_d is related to the upstream velocity U_O by equation 3.18.

$$U_d = U_o(1-a) \tag{3.18}$$

Flow velocity is reduced towards and across the rotor (because static pressure increases upstream due to the impedance associated with the disk) and an axial induction factor is defined (a) to take account of this. For example if a = 0.5, the flow velocity is reduced by 50% of its upstream value. As the fluid travels through the rotor disk there is a change in velocity of $U_O - U_W$ and a rate of change of momentum equal to equation 3.19.

$$\text{Rate of change of momentum} = (U_O - U_W)\rho A_d U_d = (U_O - U_W)\rho A_d (1-a) U_O \tag{3.19}$$

By applying Bernoulli theorem to equation 3.19, equation 3.20 is derived. The full derivation can be found in Burton et al. (2001).

$$U_W = U_O(1-2a) \tag{3.20}$$

The force on the fluid is given by equation 3.21.

$$F = 2\rho A_d {U_O}^2 a(1-a) \tag{3.21}$$

The force is concentrated at the disk, therefore the rate of work by the force is $F \times U_d$ and the power extracted from the fluid is therefore given by equation 3.22.

$$\text{Power} = 2\rho A_d {U_O}^3 a(1-a)^2 \tag{3.22}$$

A power coefficient is then defined, equation 3.23.

$$C_P = \frac{power}{\frac{1}{2}\rho U_O{}^3 A_d} \tag{3.23}$$

The denominator represents the power available to the turbine from the fluid in the absence of the actuator disk. Therefore, equation 3.24.

$$C_P = \frac{2\rho A_d U_O{}^3 a(1-a)^2}{\frac{1}{2}\rho U_O{}^3 A_d} = 4a(1-a)^2 \tag{3.24}$$

Thrust equation

A thrust coefficient can be defined in a similar manner. The thrust on the rotor disk is caused by the change in momentum of the fluid flow through the rotor disk. A thrust coefficient C_t can be derived by presenting the equation in non-dimensional form (equation 3.25).

$$C_t = \frac{thrust}{\frac{1}{2}\rho U_O{}^2 A_d} = 4a(1-a) \tag{3.25}$$

Betz limit

The Betz limit (Betz, 1920) is the maximum value of power coefficient that can theoretically be obtained. It represents the maximum proportion of energy that may be extracted by a turbine placed in an unconstrained flow.

The maximum value of C_P occurs when: $\frac{dC_P}{da} = 4(1-a)(1-3a) = 0$

Which gives a value of $a = 1/3$ and results in equation 3.26.

$$C_{P\max} = \frac{16}{27} = 0.593 \tag{3.26}$$

For marine current turbines values of C_P are usually a combination of the maximum theoretical C_P limit minus any other losses in the turbine, such as transmission losses. A good value for C_P would approach 0.4 (Myers, 2005). Marine Current Turbines' SeaGen device has been reported to have reached peak C_P values of 0.48 (Fraenkel, 2010). Hardisty (2009) defines the overall efficiency factor for a MCEC to be made up of the hydraulic efficiency (ratio of hydraulic power at the turbine to the incident power in the flow), rotor efficiency (ratio of shaft power to hydraulic power at the rotor) and electrical efficiency (ratio of electrical power output to shaft power). In highly constrained flows, the C_p value could exceed the Betz limit; this could be applied to highly constrained shallow channels or tidal fences where a high proportion of the flow is diverted through the MCEC devices (Vennell, 2010). This increase in C_p can result from either an element of potential energy being introduced into the flow or more flow being

entrained through the MCEC rotor. Both these cases could occur in highly constrained shallow flows.

3.3 Potential Flow Theory

Potential flow theory can be employed to theoretically model fluid flow in two or three dimensions. Background theory is presented in the fluid mechanics texts Douglas et al. (2005) and Massey (2006) and a further in-depth presentation can be found in the hydrodynamics text by Vallentine (1969). Potential flow theory assumes flow to be non-viscous and irrotational (zero vorticity). This provides a direct and manageable solution for complex flow patterns that otherwise could only be realistically solved using Computational Fluid Dynamics software that approximate solutions to the non-linear Navier-Stokes flow equations. Removing the viscous term from the Navier Stokes equations yields the Euler equations and with a further assumption of irrotational flow the readily solvable potential flow theory is arrived at. However, because of the assumptions associated with potential flow, the limitations to its applicability must be well understood before applying the theory to a particular flow scenario. Potential flow theory uses the entirely theoretical concept of an "ideal fluid" by using the following assumptions:

1. Zero viscosity, hence zero shear stress (no non-slip boundary conditions)
2. Irrotational flow (zero vorticity)
3. Incompressible fluid
4. No surface tension
5. No vaporisation pressure limit

The theory can be utilised to solve a range of practical flow scenarios with reasonable accuracy (Vallentine, 1969) including flow around streamlined objects, converging passages and jet flows. Assuming a small free-surface drop, flow over a ramp-foundation can be likened to a converging passage and potential flow techniques can be used to solve the inflow and across ramp flow field. Douglas et al. (2005) emphasise the fact that potential flow cannot be used to solve viscous boundary layer flows but can be applied to the region of flow outside the boundary layer provided the flow is of high Reynolds number with small viscosity and high flow velocity.

The flow field for a potential flow model is made up of a mesh of streamlines and velocity potential lines that can be defined by a stream function and a velocity potential function respectively. Streamlines can be defined as "lines where all points are tangential to the flow's velocity vectors". Flow patterns can be made up of any number of streamlines depending on the precision required and they divide the flow up into channels of equal flow rate (q). Equation 3.27 describes the flow rate in each channel.

$$q = \frac{Q}{n} \tag{3.27}$$

Where: Q = total flow rate n = number of streamlines

The mean velocity (V) at any point along a particular channel can be found using equation 3.28.

$$V = \frac{q}{b} \tag{3.28}$$

Where: b = distance between streamlines

Stream functions (Ψ) and velocity potential functions (Φ) are mathematical functions that describe in a concise manner the flow pattern for a particular irrotational flow scenario (potential flow solution) and are both a function of the x and y coordinates in two-dimensional space. The velocity components u and v (when considering two-dimensions) are the partial derivatives of the stream and velocity potential functions (equations 3.29 and 3.30). Velocity potential lines always cross the streamlines at right angles and form a mesh of curvi-linear squares. The relationship between stream and velocity potential functions can be developed through the Cauchy-Riemann equations. Thus if a stream function is known, the velocity potential can be calculated and vice versa, provided flow is irrotational.

$$u = \frac{\partial \phi}{\partial x} = \frac{\partial \Psi}{\partial y} \tag{3.29}$$

$$v = \frac{\partial \phi}{\partial y} = -\frac{\partial \Psi}{\partial x} \tag{3.30}$$

A fundamental condition for potential flow is that both the stream and velocity potential functions must satisfy the Laplace equations 3.31 and 3.32 by applying zero vorticity and continuity conditions respectively.

$$\frac{\partial^2 \Psi}{\partial x^2} + \frac{\partial^2 \Psi}{\partial y^2} = 0 \quad \text{(zero vorticity condition)} \tag{3.31}$$

$$\frac{\partial^2 \phi}{\partial x^2} + \frac{\partial^2 \phi}{\partial y^2} = 0 \quad \text{(continuity condition)} \tag{3.32}$$

Despite being relatively straight forward to implement for very simple flow problems, potential flow theory it is still very challenging, in some cases impossible, to solve for complex problems involving intricate boundary conditions. Over the years a number of analytical, numerical and graphical techniques have been developed and are described as follows:

- ***Direct mathematical solution:*** direct application of the potential flow equations such as equations 3.28 to 3.31. Only applicable to very simple flows; including rectilinear flow and source/sink flows.
- ***Superposition:*** this involves combining simple flow patterns to produce more complex flow scenarios, such as combining linear flow with a source to yield flow around a half body (Rankine body). Doublet flow is developed by combining a sink and source of equal strength. Flow around a cylinder can be created by combining rectilinear flow with a doublet.
- ***Conformal Transformations:*** the use of complex variable theory and the Schwarz-Christoffel transformation to analytically generate more complex flow patterns. Examples include flow past an ellipse, an aerofoil/hydrofoil. The method can be used to solve complex patterns of flow but in return the mathematics also becomes complex and requires very elegant solutions. The Schwarz-Christoffel transformation could be utilised to calculate flow across a ramp-foundation.
- ***Graphical flow net:*** for more complex flow scenarios and boundary conditions a graphical approach for solving the Laplace equation can be used by drawing a family of streamlines and velocity potential lines with known boundary conditions. Mathematical approaches have the advantage of generality but in all but very simple cases the mathematics is highly complex. For individual cases a trial-and-error graphical approach is a good alternative allowing difficult flows and boundaries to be solved with reasonable accuracy.
- ***Numerical analysis:*** this is a method based on the calculus of finite differences and can be readily used to solve complex flow scenarios that are too difficult to solve analytically. In the past this method would have been solved by hand iteration but it is perfect for computational analysis. This makes it very suitable for solving the flow across ramp-foundations for a variety of ramp profiles. The approach is to assume a network of stream and velocity potential function values for a particular set of boundary conditions and to adjust (or relax) these values systematically to satisfy the Laplace equation and boundary conditions.

The described numerical analysis approach can be implemented to solve the Laplace equation by successively applying a relaxation method on a square mesh. As stated this could be applied to flow over a raised bed-form by applying the following set of boundary conditions:

- Inflow: uniform vertical inflow velocity or variable velocity profile;
- Outflow: free flow condition;
- Bed and ramp: free-slip (with or without post boundary layer correction);
- Free-surface: free-slip, assuming the surface drop is small.

3.4 Acoustic Doppler Velocimeter

3.4.1 Theory of operation

An Acoustic Doppler Velocimeter (ADV) measures water velocity in three dimensions. Utilising the Doppler effect it measures the flow velocity by transmitting a short pulse of sound from a central transmitter, receiving its echo and measuring the change in pitch or frequency of the echo. As sound cannot be reflected by the water itself, the meter uses particles suspended in the water instead. These particles consist of suspended sediment or zooplankton; it is assumed that these particles travel at the same velocity as the water and the measured particle velocity is equivalent to the velocity of the flow. The pulse of sound from the central transducer strikes the particles in a sample volume and these particles reflect back the sound. The Doppler shift introduced by the sound pulse reflections is received by the four receivers that surround the central transducer. The instantaneous 3D velocity is then recorded for each pulse and the average velocity for a sample of defined time period is calculated.

3.4.2 Filtering methods

Data is filtered to remove noise and spurious points (Figure 3-3, shows data spikes) although the large quantity of suspended particles in both the circulating channels used during this project has been shown to minimise sample error. Filtering is required to improve measurements of higher order flow effects, such as turbulence intensity and shear stresses, because spikes in the data give the impression of increased energy within the flow. However filtering has a very small effect upon mean flow velocities as spikes are generally equally positive and negative.

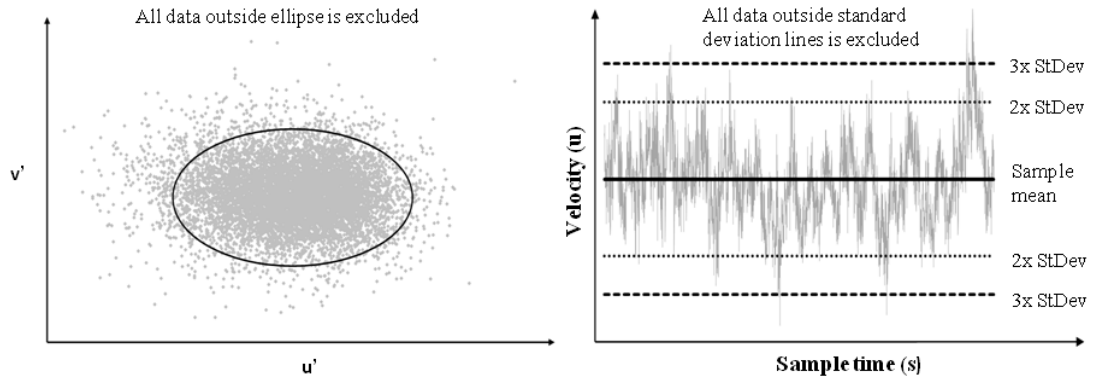

Figure 3-3: Velocity correlation filtering method (left) and minimum/maximum filter (right)

The importance of filtering and methods were discussed and reviewed in chapter 2. Based on this review and performance testing of a range of different filters, the velocity correlation filter developed by Cea et al. (2007) was chosen. The velocity cross-correlation filter was ultimately

chosen due to its ease of use and effectiveness after a single pass (Cea et al., 2007). This method plots the varying components of velocity against each other and constructs an ellipse in three-dimensional space to exclude any data points that deviate significantly from the sample mean (Figure 3-3, left). Similar filters can be set up to remove statistically or physically improbable values. The former can be based upon the removal of data points more than 3 sample standard deviations from the mean sample value assuming that the dataset is normally distributed; this type of simple filter is commonly referred to as a minimum/maximum filter (Figure 3-3, right). Physically improbable criteria include techniques such as removing data points where the varying velocity component exceeds the acceleration due to gravity (highly improbable in a tidal flow given the viscosity of water, however accelerations can exceed gravity in other flow situations such as breaking waves). The importance of filtering for higher order flow effects is illustrated by Table 3-1. It can be seen that the percentage change from the raw data values to the filtered values (velocity correlation filter) is much higher for the turbulence intensity compared with the mean velocity. Hence as stated by Cea et al. (2007) filtering is required to compute the correct turbulence parameters.

Sample	**u-plane velocity (m/s)**				**u-plane turbulence intensity (%)**			
	Raw	**Min/max**	**Vel. Cor.**	**% Change from raw**	**Raw**	**Min/max**	**Vel. Cor.**	**% Change from raw**
1	0.2446	0.2448	0.2459	0.54	9.56	9.56	7.43	-22.24
2	0.2949	0.2949	0.2911	-1.29	18.86	18.86	15.17	-19.54
3	0.2863	0.2863	0.2860	-0.11	10.59	10.59	8.91	-15.83
4	0.2869	0.2863	0.2843	-0.93	11.55	11.55	10.05	-12.94
5	0.2456	0.2457	0.2470	0.56	9.26	9.26	7.31	-20.99

Table 3-1: Minimum/maximum and velocity correlation filter comparison

A numerical routine was developed to implement the velocity cross-correlation filter. The theory developed by Cea et al. (2007) is described from this point forward.

Firstly the constant $\lambda = \sqrt{2\ln N}$ is defined where N = total number of data points in the sample.

Linear regression of the data is performed to compute the centre of the data exclusion ellipse and the rotation angle of its principal axis. Varying velocity components are represented by the parameters x', y' and z', which are the actual velocities minus the mean value of the sample, e.g. $x' = x - \bar{x}$. The least squared method is applied to $x' - y'$ and gives:

$$m = \frac{N\sum x'_i\, y'_i - \sum x'_i \sum y'_i}{N\sum x'^{\,2}_i - \left(\sum x'_i\right)^2} \tag{3.36}$$

$$c\sum x'_i = \sum x'_i\, y'_i - m\sum x'^{\,2}_i \tag{3.37}$$

Parameters m and c are linear fit coefficients $y' = mx' + c$ that create a linear line, which orientates the ellipse to the data cluster. If the mean of the fluctuating velocities is considered to be zero the coefficients of linear fit simply become:

$$c = 0 \tag{3.38}$$

$$m = \tan\theta = \frac{\sum x'_i \, y'_i}{\sum x'^{\,2}_i} \tag{3.39}$$

Where $\tan\theta$ is the rotation angle of the principal axis.

The axis x_o and y_o of the data exclusion ellipsoid are given by:

$$x_o^2 = \frac{(\lambda\sigma_x \cos\theta)^2 - (\lambda\sigma_y \sin\theta)^2}{\cos^2\theta - \sin^2\theta} \tag{3.40}$$

$$y_o^2 = \frac{(\lambda\sigma_y \cos\theta)^2 - (\lambda\sigma_x \sin\theta)^2}{\cos^2\theta - \sin^2\theta} \tag{3.41}$$

Expressions for $x' - z'$ and $y' - z'$ can be derived in a similar manner.

Chapter 4

4 Introduction to Constraining Tidal Flow

4.1 Introduction

A critical limiting factor for the commercialisation and deployment of large-scale tidal energy is the availability of suitable sites. Suitable locations need to be easily accessible for device installation and maintenance, close to grid connections and most importantly have sufficient tidal flow velocities. Power from a tidal turbine is proportional to the cube of the flow velocity, hence any small increase in velocity will result in considerable power benefits (Fraenkel, 2002). Power output from a free-stream tidal turbine is defined by rearranging equation 3.23.

$$power = \frac{1}{2} C_p \rho U_o^{\,3} A_d \tag{4.1}$$

Where C_p is the fraction of the kinetic energy captured across the swept area of the turbine rotor. It has a maximum (limiting) value of 0.593 for an un-constrained rotor as defined by Betz (Betz, 1920). In practice it also includes blade, drivetrain and other losses. Peak C_p values for MW-class wind turbines are now approaching 0.5. Many suitable sites for marine current energy converters (MCECs) are located in shallow tidal flows such as those found close to the shore and in estuaries. Shallow flows have a reduced cross-sectional area suitable for energy extraction compared with deeper channels, but they have other benefits including close proximity to the shore with many sites situated away from shipping channels. This could make construction and grid connection both easier and economically feasible. Regions of flow that presently have insufficient velocities for economic power generation could also be made economically viable with the use of artificial flow constraint structures.

Two methods of flow augmentation have been identified. Flow concentrators that surround tidal turbines could be used to locally magnify the flow velocities, such as the shrouded Rotech turbine designed by Lunar Energy (Lunar Energy, 2011, Thorpe, 2005) and the two-way diffuser detailed by Setoguchi et al. (2004). Klaptocz et al. (2007) and Roddier et al. (2007) present studies of vertical side wall concentrators for tidal stream turbines and both conclude that these structures are beneficial in terms of power generation. An alternative concept which is proposed and developed as part of this project is a seabed mounted tidal flow constraint structure.

4.2 Fundamental concept

Ramp or apron structures placed on the seabed could be used to locally increase the flow velocity whilst also offering scour protection and an increased foundation footprint (Figure 4-1). Enlarging the footprint area and foundation mass would increase the downforce created by the foundation and hence increase the bed shear capacity. With careful design of the leading edge it may also be possible to smooth the vertical velocity profile that will serve to reduce rotor loading. These structures would form an integral part of the MCEC foundation and would be most applicable to shallow tidal flows with depths ranging from 10 to 30m. Foundations could be a gravity base and constructed using reinforced concrete or steel caissons which are floated out from shore and sunk in the required position. The concept could be used for deeper flows but ramp height would need to be considerably greater to magnify the flow velocity, leading to increased construction cost.

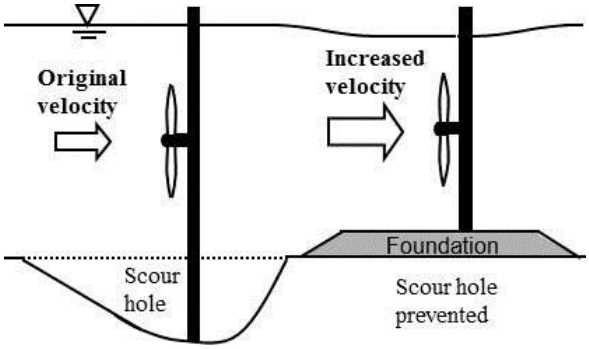

Figure 4-1: Proposed ramp-foundation benefits

The anticipated benefits of ramp foundations are reinforced by considering the fundamental laws of flow continuity, where a local flow velocity increase would occur for any reduction in tidal channel width or depth. Using fundamental one-dimensional flow theory these flow parameters across the ramp can be directly estimated by applying the principles of specific energy (see section 3.1.4, Figure 3-1).

Although there is a lack of work directly related to marine energy extraction, open channel hydraulics, channel bed obstructions and possibly submerged weirs could be applied. Starting with simple open channel hydraulics texts (Chow, 1959, Chadwick et al., 2004), which describe principles of specific energy and continuity, it is evident that in a laterally constrained channel the introduction of a ramp-foundation occupying a large proportion of the width will magnify the flow velocity and cause a small surface drop in the case of subcritical flows. This theory cannot be directly applied to tidal flows, except perhaps in narrow channels or a tidal fence application, because flows such as those in open sea locations are generally laterally unconstrained. A number of authors (Lyn, 1993, Shen et al., 1990, Fadda and Raad, 1997,

Dyer, 1986, Dewey et al., 2005) specifically address open channel bedforms and describe velocity profile development, turbulence characteristics, the importance of avoiding critical depth conditions and flow separation. Weir flow theory can be found in the text Chow (1959). Furthermore, Wu and Rajaratnam (1996) present an experimental study into submerged weir flow, however the study focuses on sharp-crested weirs which bare few similarities to a long submerged ramp-foundation. A submerged bed obstruction has a clearer resemblance to a ramp-foundation structure than a submerged weir mainly due to the ratio of flow depth to ramp height.

For efficient energy capture and reduced rotor loading the vertical velocity profile ideally needs to be relatively constant with depth, certainly in the region of flow swept by the rotor (Myers, 2005). Vertical velocity profiles have been measured at a few locations in UK waters (Rippeth et al., 2002, DTI, 2005). One of these shows a very close resemblance to the modified $1/7^{th}$ power law (European Commission, 1996), with a sheared boundary layer region near the bed and an approximately uniform upper section. When the flow encounters the upstream edge of a ramp structure the lower sheared section of the vertical velocity profile will effectively be removed (Lyn, 1993) and the profile will start to re-develop across the ramp. Figure 4-2 shows some measured vertical velocity profiles across a scaled ramp in a water channel facility. Ideally the MCEC would be located at the optimum location along the ramp where the maximum velocity increase occurs coupled with a more uniform vertical profile.

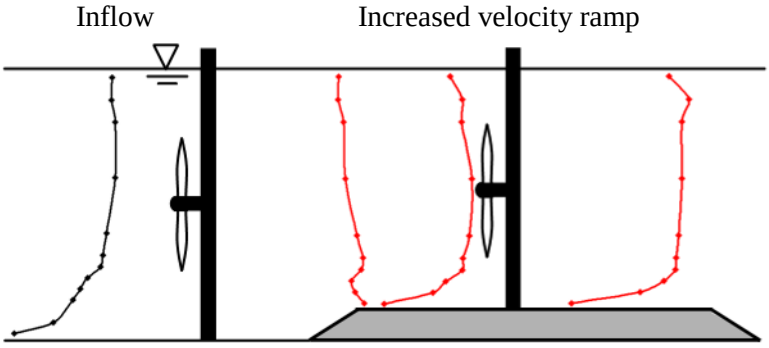

Figure 4-2: Boundary layer re-development

It is preferable to avoid the sheared region of flow near the sea bed as the differing mass flow rates will cause disparate rotor loadings. It has been estimated that the top 8m and bottom 25% of the depth might be avoided due to surface wave effects and the steeper section of the boundary layer respectively (European Commission, 1996). It is also important to ensure the ramp will not induce more turbulence which could have a negative effect on MCEC loading and performance.

Section 4.3 describes a simple one dimensional theoretical model that investigates the fundamental flow augmentation potential of ramp-foundations. By simple analysis of the cubic tidal flow velocity and MCEC power relationship it is clear that any small degree of flow amplification would result in considerable device power benefits across a tidal cycle. Figure 4-3 shows how sensitive the power output of a small 10m diameter tidal turbine is to the tidal flow velocity.

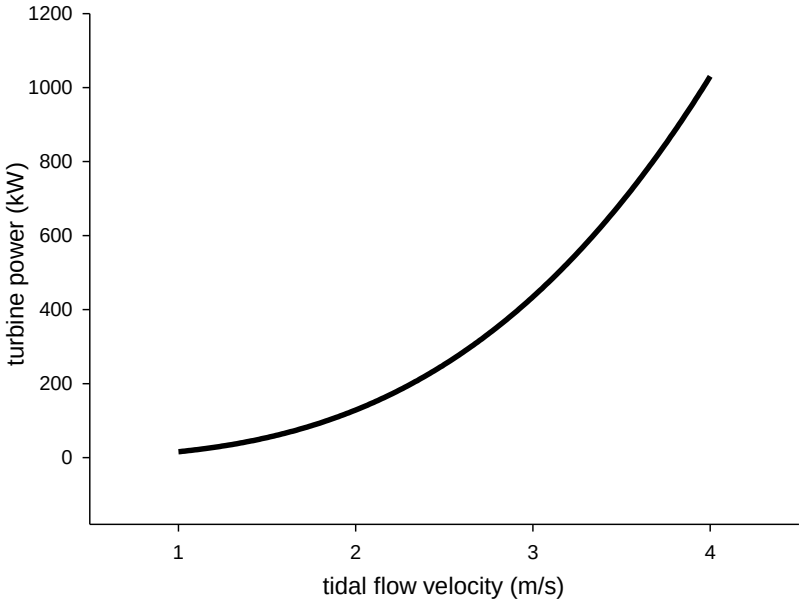

Figure 4-3: turbine power and flow velocity relationship

A concern when installing a ramp-foundation is the free-surface drop that would occur across it, assuming subcritical flow. As stated in section 3.1.4 tidal flows for energy extraction will almost always be subcritical because of the huge flow velocities that would be required to induce critical depth conditions. If the surface drop was large it could result in a restriction of device size or ventilation of the turbine blades at some states of the tide. However, when applying the specific energy concept derived from Bernoulli's principle of energy conservation, it can be estimated that this surface drop resulting from the ramp alone would be small. Applying equation 4.2 to a typical ramp height to flow depth ratio (ramp occupying 10% of the flow depth) a small surface drop of approximately 0.5% of the flow depth would occur. The location of points 1 and 2 described in equation 4.2 can be visualised in Figure 4-4.

$$surface\,drop = d_1 - d_2 - Z_2 = \frac{U_2^{\,2}}{2g} - \frac{U_1^{\,2}}{2g} \tag{4.2}$$

For the ramp concept to be commercially viable it must primarily be technically feasible, but of equal importance is its necessity to be economically attractive. The presence of the ramp will

increase the device power output across the tidal cycle and hence increase the revenue generated from the exported energy. But despite the ramp-foundation being of multi-use, such as acting as an integral foundation, there will be an increased capital cost involved compared with a conventional MCEC. Techno-economic analysis will be required to investigate both the ramp's technical and financial performance.

In summary the overarching objective of this ramp-foundation concept is to increase the available power per unit channel cross section by physically constraining the tidal flow. Low velocity shallow currents can thus be constrained and the velocity increased to an exploitable level.

4.3 Fundamental model

A one-dimensional model was developed from fundamental fluid flow theory, such as those presented in the texts by Chow (1959), Chadwick et al. (2004) and chapter 3. Theories include: continuity, specific energy for open channel flow, axial momentum theory, $1/7^{th}$ power law and semi-diurnal tidal theory.

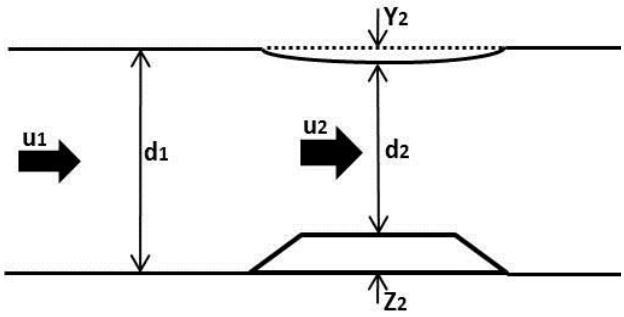

Figure 4-4: one-dimensional model key parameters

Specific energy principles were used to calculate the resulting flow depth across the ramp (d_2) given the initial upstream depth (d_1) and velocity (u_1). Continuity was used to simplify the cubic specific energy equation from an equation with two unknowns to one unknown (equation 4.3). Once the depth across the ramp was calculated, continuity (equation 4.4) was used again to find the velocity across the ramp (u_2) from the discharge per unit width (q) and the across-ramp depth (d_2).

$$d_2{}^3 - d_2{}^2\left(d_1 + \frac{u_1{}^2}{2g} - Z_2\right) + \frac{q^2}{2g} = 0 \tag{4.3}$$

$$q = d_1 u_1 = d_2 u_2 \tag{4.4}$$

A check was made to ensure flow was in the subcritical range as supercritical flows are not suitable for energy extraction because of their torrential and shallow nature. This was done by ensuring both depths d_1 and d_2 were greater than critical depth (d_c) using equation 4.5.

$$d_c = \left(\frac{q^2}{g}\right)^{1/3} \tag{4.5}$$

The free-surface drop was calculated directly from equation 4.6.

$$\text{Surface Drop (m)} = d_1 - d_2 - Z_2 \tag{4.6}$$

To estimate the power gain potential of the ramp-foundation, the theoretical power from a horizontal axis MCEC was estimated (equation 4.7) for the situations with and without a ramp-foundation. A power conversion coefficient (C_p) of 0.4 was used. Previous work has recommended that a MCEC might have a rotor diameter of 50% of the flow depth and should be located in the centre of the vertical water column (European Commission, 1996). When a MCEC is deployed with a ramp-foundation its maximum diameter may be reduced. The magnitude of this depends on the relative ramp height and associated free-surface drop. The power output is very sensitive to the swept area of a MCEC and hence it is important that this reduction in area is investigated during power gain calculations if the rotor is prevented from encroaching into the upper and lower restricted flow depth zones. However if the flow depth above the ramp permits, it may be possible to keep the rotor diameter equal to the diameter of a device operating without a ramp. Both these cases are investigated.

$$Power = C_p \frac{1}{2} \rho {U_0}^3 A_d \tag{4.7}$$

In addition to the instantaneous power gain estimate, the potential power gain across a tidal cycle was estimated using a semi-diurnal tidal velocity profile approximation (equation 4.8). For each case the calculated velocities u_1 and u_2 were assumed as the maximum spring peak flow velocities for both with and without ramp cases.

$$U_{(t)} = \left[B + C cos\left(\frac{2\pi t}{T_1}\right)\right] cos\left(\frac{2\pi t}{T_0}\right) R \tag{4.8}$$

From the single one-dimensional velocities at each location, the velocity profile was extrapolated using the 1/7th power law (equations 4.9 and 4.10).

$$U_{t(z)} = \left(\frac{z}{0.32d}\right)^{1/7} \overline{U_t} \qquad for\ 0 \le z \le 0.5d \tag{4.9}$$

$$U_{t(z)} = 1.07\overline{U_t} \qquad for\ 0.5d \le z \le d \tag{4.10}$$

The calculation process is illustrated using a flow logic diagram (Figure 4-5).

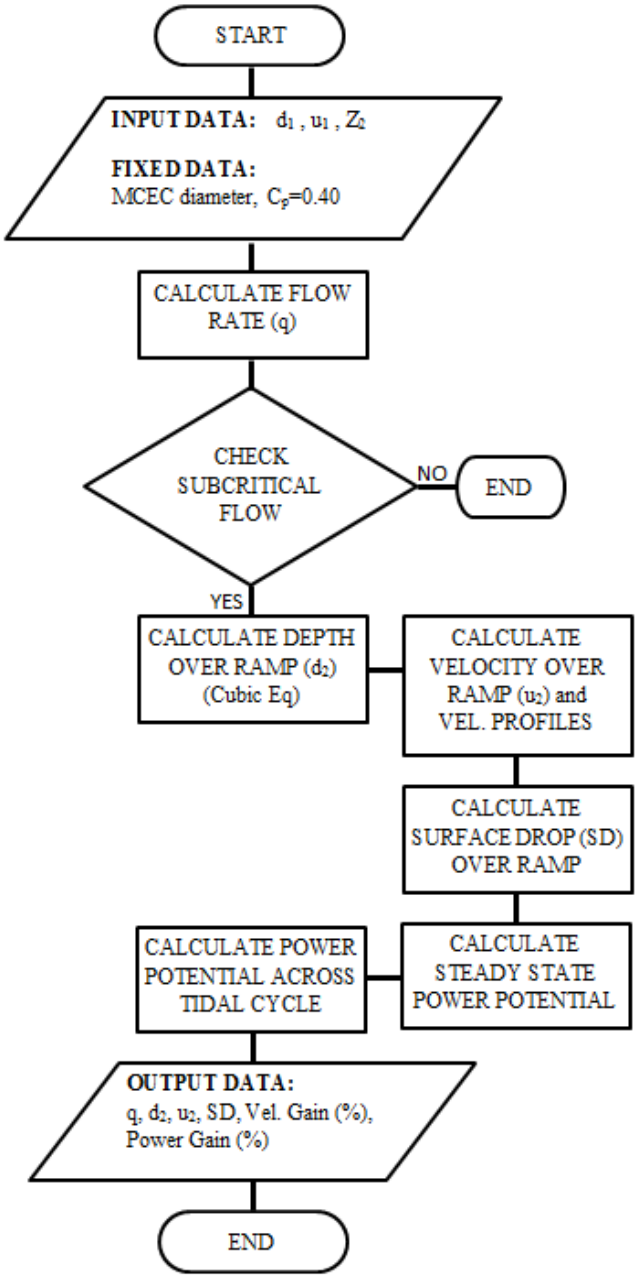

Figure 4-5: flow logic diagram for one-dimensional ramp model

This simplified one-dimensional model gives a good impression of the global flow scenario with ramp-foundations, but due to its simple nature it comes with a number of limitations. These include:

- One-dimension means no estimate of the velocity distribution or lateral flow effects. The model therefore only considers a ramp spanning the whole channel width.
- No account for bed friction.

- No account for vorticity/turbulence.
- The velocity profile can only be generated indirectly by extrapolating a 1/7th power law approximation.
- The free-surface drop only considers the presence of the ramp and does not included the head loss from MCEC energy extraction.
- Flow modifying effects from the physical presence of a MCEC are not considered.

Despite these limitations, as a proof of concept method the model gives a good first approximation of the potential of ramp-foundations in terms of velocity and power gain in an un-constrained channel.

4.4 Model predictions

Using equations 4.3, 4.4, 4.7 and a trigonometric method for solving the cubic equation 4.3 some fundamental equations for velocity gain and power gain potential of ramp-foundations were developed. The input parameters for these equations are: the free-stream flow depth (d_1), the free-stream velocity (u_1) and the ramp height (Z_2). Equation 4.11 provides a direct estimate of the potential velocity gain across a ramp-foundation of height Z_2.

$$V_{GAIN} = 100 \times \left[\frac{3d_1}{a}\left[2cos\left(\frac{cos^{-1}\left(1-\frac{27q^2}{4ga^3}\right)}{3}\right)+1\right]^{-1}\right] - 100 \quad (4.11)$$

$$Where: a = d_1 + \frac{{u_1}^2}{2g} - Z_2$$

As stated previously two cases for power gain are investigated. The first given by equation 4.12 is the case where there is no reduction in rotor diameter when a MCEC is deployed with a ramp-foundation. This would be the situation where depth permits and the deployed turbine diameter is small enough.

$$P_{GAIN} = 100 \times \left[\frac{3d_1}{a}\left[2cos\left(\frac{cos^{-1}\left(1-\frac{27q^2}{4ga^3}\right)}{3}\right)+1\right]^{-1}\right]^3 - 100 \quad (4.12)$$

Equation 4.13 describes the case where the rotor diameter is restricted to 50% of the above-ramp depth (d_2) as recommended by the European Commission (1996). The permissible rotor diameter is restricted by the addition of the ramp height/associated free-surface drop and the recommendation to avoid the top and bottom 25% of the flow depth for wave and bed shear effects respectively. With this scenario it can be theoretically shown that the potential power gain is reduced and is exactly equal to the potential velocity gain. This yields a reduction in

power potential compared with the constant MCEC diameter case because of the decrease in turbine energy extraction area. This fundamentally results because in the restricted scenario both the power gain and velocity gain are proportional to the reduced depth across the ramp (d_2). If there is no ramp depth restriction the power gain is proportional to the larger un-obstructed channel depth (d_1).

$$P_{GAIN} = 100 \times \left[\frac{3d_1}{a}\left[2cos\left(\frac{cos^{-1}\left(1-\frac{27q^2}{4ga^3}\right)}{3}\right)+1\right]^{-1}\right] - 100 \tag{4.13}$$

A number of flow case scenarios were run through the model and the results are presented in Table 4-1. The variables for each case are the Froude number and the ramp height/flow depth ratio. The objective here was to illustrate the influence of the ramp height/flow depth ratio, Froude number (flow velocity) and the significance of restricting the rotor to 50% of the depth above the ramp.

$$\frac{ramp\ height\ (Z_2)}{flow\ depth\ (d_1)} = R_V \tag{4.14}$$

TEST	Flow depth (d_1) m	Ramp height (Z_2) m	R_V	Froude number	Velocity (u_1) m/s
1	10	0	0	0.15	1.5
2	10	0.5	0.05	0.15	1.5
3	10	1	0.1	0.15	1.5
4	10	2	0.2	0.15	1.5
5	20	1	0.05	0.15	2.1
6	20	2	0.1	0.15	2.1
7	20	4	0.2	0.15	2.1
8	30	1.5	0.05	0.15	2.6
9	30	3	0.1	0.15	2.6
10	30	6	0.2	0.15	2.6
11	10	1	0.1	0.20	2.0
12	20	2	0.1	0.20	2.8
13	30	3	0.1	0.20	3.4
14	10	1	0.1	0.25	2.5
15	20	2	0.1	0.25	3.5
16	30	3	0.1	0.25	4.3

Table 4-1: one-dimensional model flow scenarios

Figure 4-6 shows how varying the ramp height / flow depth ratio (R_V) affects the velocity and power gain potential across a ramp-foundation for constant Froude number. It is clear that restricting the MCEC diameter to 50% of the above-ramp flow depth considerably reduces power potential compared with using the same sized device that would be deployed in the no-ramp scenario. It is postulated that an R_V ratio in the region of 0.1 would be optimum in terms of providing appreciable power gains from an economically constructible ramp. Increasing R_V and hence ramp height would have significant cost implications. Even when restricting the turbine diameter across the ramp, power gains in the region of 12% are possible. If the turbine diameter was kept constant with the diameter possible without a ramp-foundation (e.g. the turbine was allowed to encroach into the lower sheared region and/or the upper wave-affected region) power gains could be as high as 38%.

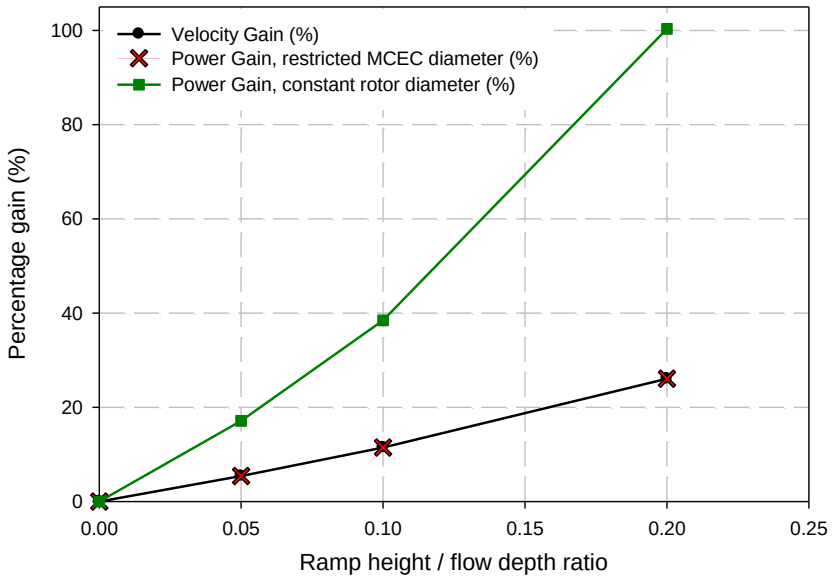

Figure 4-6: velocity and power gains for varying ramp height / flow depth ratio

From these results it is clear that by mitigating the negative disparate turbine loading effects, which would result from a larger turbine encroaching into the sheared boundary layer and wave influence regions, could result in very significant power improvements. It could be prudent to design MCEC blades with higher in-built blade strength to resist the higher disparate loading and access these increased power gains. Of course for R_V ratios of greater than 0.1 there will be a stricter limit on the device diameter due to the increased vertical blockage from the ramp-foundation height. Figure 4-7 shows potential velocity and power gains for varying Froude number at a constant R_V ratio of 0.1. The general trend is for a slight increase in the percentage gain for all cases. This results from a higher free-surface drop at larger Froude numbers (Figure 4-9), which restricts the flow vertically and, by continuity it results in an increased across ramp

velocity. Although these magnifications are small for the restricted diameter turbine case, for the unrestricted case they are significant and Froude variation must be considered.

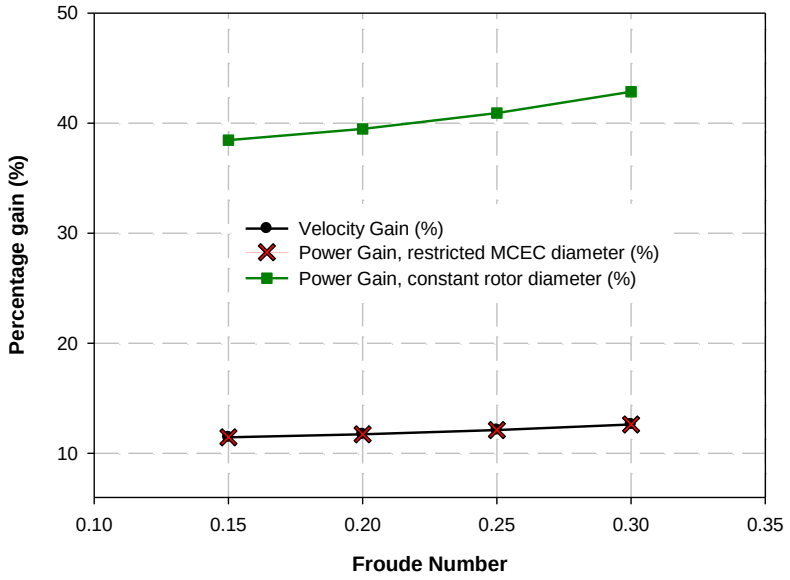

Figure 4-7: velocity and power gains for varying Froude number

Figure 4-8 and Figure 4-9 display the results for across-ramp free-surface drop for varying R_V and varying Froude number respectively. It must be reiterated that this head drop results only from the ramp-foundation. Head drops resulting from MCEC energy extraction are not included in this model. It is clear that the free-surface drop resulting from the ramp is very small for all cases considered (less than 1% for Fd < 0.25). Thus it will be assumed negligible during the course of further work.

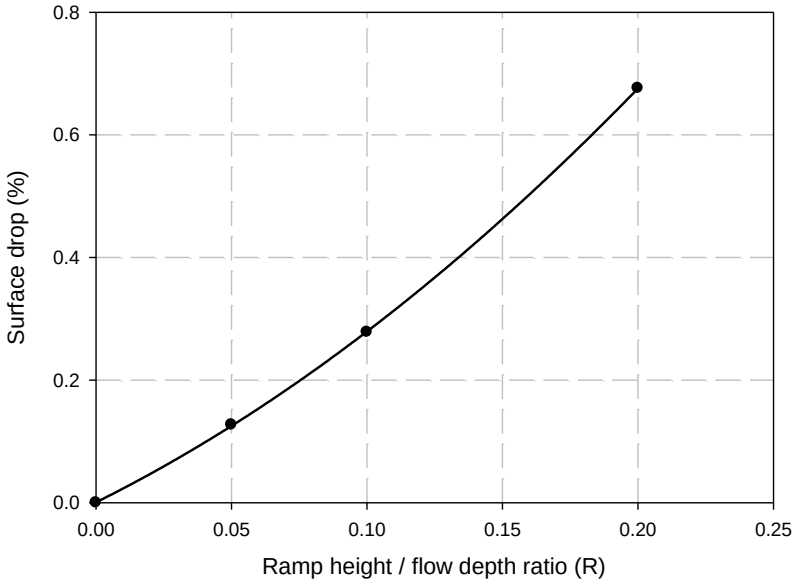

Figure 4-8: surface drop across ramp for varying ramp height / flow depth ratio

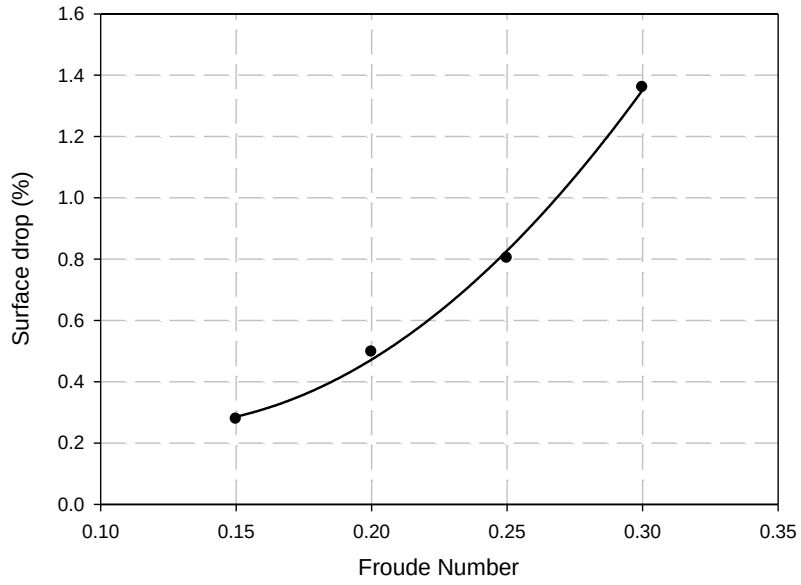

Figure 4-9: surface drop across ramp for varying Froude number

The extrapolated velocity profiles using the 1/7th power law can be seen in Figure 4-10. With increasing R_V ratio the effects of the lower bed sheared region occupying a larger proportion of the flow depth is illustrated. This emphasises the difficulties in terms of disparate MCEC loading that may result when deploying larger height ramp-foundations. This extrapolated data must be treated with caution and will be better validated with experimental data.

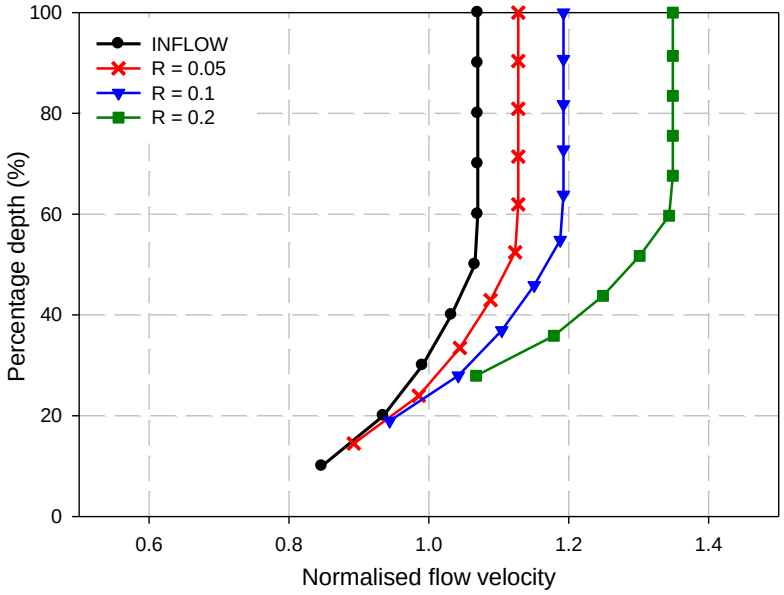

Figure 4-10: vertical velocity profile approximation using 1/7th power law

The ramp height to flow depth ratio of 0.1 was selected as a focus for further theoretical modelling and experimental testing. This value was selected based on preliminary stability calculations, practical construction limits, theoretical power gain, minimising restrictions for MCEC rotor height and commercial factors from Pulse Tidal Ltd. A key requirement of the ramp concept was for it to be multi-purpose, including having the ability to act as a gravity base for the MCEC. The ramp mass in tonnes would increase dramatically with increased ramp height therefore a compromise must be made between maximising the power gain potential, reducing the ramp's capital cost and maintaining its ability to operate as a gravity-based structure. The selection of the 0.1 ratio was further reinforced following a sensitivity analysis looking into structural stability with increasing ramp height and discussions with the industrial sponsor Pulse Tidal Ltd. Figure 4-11 shows the results of some preliminary structural stability calculations for a concrete foundation (details presented in Chapter 8, Section 8.8) giving the minimum factor of safety (FoS) against an overturning or bed-shear sliding failure. For this analysis a feasible fixed ramp length of 10m was selected and to achieve a minimum 1.35 factor of safety a ramp height to flow depth ratio of 0.1 was required.

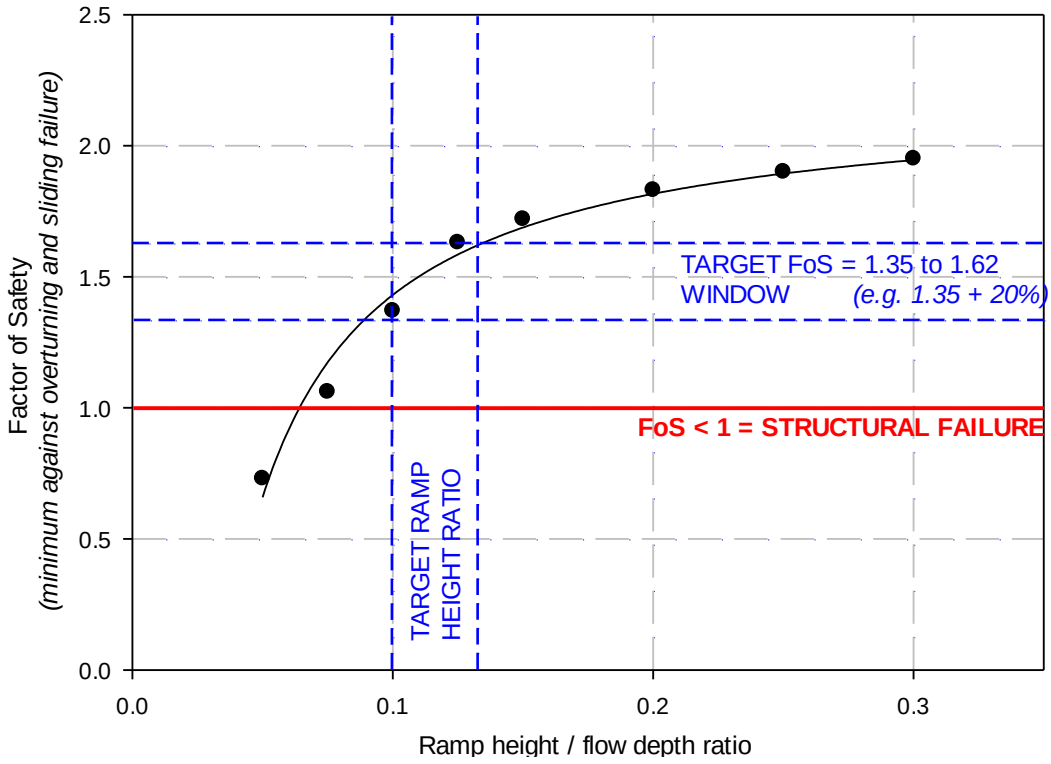

Figure 4-11: ramp height to flow depth ratio selection

4.5 Summary

To provide an approximation of the potential velocity and power gains available from a ramp-foundation for a given free-stream depth, velocity and ramp height/depth ratio the direct equations 4.11, 4.12 and 4.13 can be used. In using these equations the limitations described in section 4.3 must be considered.

It is important to consider the recommendation from the European Commission (1996) to restrict MCEC diameter to the central 50% of the flow depth. Above the ramp this would mean a reduced device diameter compared with one deployed in the free-stream scenario. If this approach was adopted then power gains would equal the velocity gains in the region of 12%. Maintaining the free-stream device diameter, by allowing the MCEC sweep to encroach into the lower sheared flow and upper wave affected region, would permit power gains to be as high as 38%. Thus it could be prudent to design MCEC blades with higher in-built blade strength to operate in these upper and lower 25% depth regions, accessing the increased power gains. Despite the European Commission's recommendations and because this study will focus on small vertical ramp blockages of 10% of the flow depth, further work will not allow for a reduction in turbine diameter when a ramp is deployed and reduces the effective channel depth. Hence across the ramp-foundation the MCEC will be allowed to occupy slightly more than the central 50% of the water column and therefore the rotor might protrude slightly into the lower sheared flow and upper wave-affected regions. This will enable the much higher one-dimensional power gain potential of 38% to be accessed. As a key recommendation, a ramp occupying 10% of the flow depth was selected as a focus for further theoretical modelling and experimental testing. This was selected following discussions with Pulse Tidal Ltd. as a compromise between maximising the power gain potential, minimising restrictions for MCEC rotor height, reducing the ramp's capital cost and maintaining its ability to operate as a gravity-based structure with an acceptable factor of safety against a global overturning or bed-shear sliding failure.

There is a small variation in power gain with varying Froude number. As the Froude number increases so will the associated small free-surface drop across the ramp and this will cause a velocity increase from continuity and principles of specific energy (Figure 3-1). However it is clear that the physical free-surface drop resulting from the ramp is very small for all cases considered (less than 1% for $Fd<0.25$) and thus will be assumed negligible in terms of the available vertical depth across a ramp-foundation.

Following on from this simplified model many of the limitations described in section 4.3 will be mitigated partly through further theoretical potential flow modelling and more significantly through physical modelling in circulating water channels. The fundamental limitation of this model is its 1D nature, meaning lateral flow effects across the channel and the vertical velocity profile are neglected.

Chapter 5

5 Experimental Analysis of Ramp-foundations

5.1 Introduction

In this chapter the concept of ramp-foundations presented in chapter 4 is investigated experimentally using water channel facilities for small-medium scale testing. The limiting factor for the theoretical model presented in chapter 4 is its one-dimensional nature. Here the full-scale tidal flow scenario is represented three-dimensionally through 1:100 scale experiments. Initially the ramp-foundation is geometrically optimised (section 5.2) without the interaction of a MCEC. The second phase of experimental testing (section 5.3) investigates the interaction of a MCEC operating with a ramp-foundation. Experimental results are then scaled up to the full-scale tidal flow domain and potential power benefits are investigated.

It may seem intuitive, by principles of continuity and specific energy (Figure 3-1), that a ramp spanning the full channel width will increase the velocity, as shown in chapter 4. However, in reality it would not be feasible to construct and install such a vast structure. The ramp-foundation would only occupy a small lateral (cross flow) proportion of the channel and hence the interaction effects of the bounding flows are critical. In addition, minimising the ramp's dimensions will reduce the construction costs and improve concept viability. These factors are the basis for the geometric optimisation in section 5.2.

The combined effect of a MCEC and a ramp-foundation on the flow field is of paramount importance. The benefits of the ramp-foundation may be reduced if the MCEC has a high coefficient of thrust, meaning higher device solidity and a resulting higher flow impedance. This flow impedance will force more flow around the sides of the device and therefore a higher solidity MCEC will reduce the velocity increase across the ramp. This needs to be quantified but the ramp is still expected to provide considerable flow enhancement and hence power benefits compared with a MCEC operating in free-flow conditions, because the bulk flow will be across the ramp in the downstream direction. These factors are the basis of the interaction tests presented in section 5.3.

5.2 Ramp-foundation optimisation

5.2.1 Experimental approach

5.2.1.1 General

In order to test the concept at a manageable scale, ramps were constructed and tested in a circulating water channel at the University of Southampton (Figure 5-1). The majority of the testing was conducted in a channel with a working section of 21m in length, 1.37m wide and a maximum 0.4m flow depth for steady operation with a maximum flow rate of $0.2m^3/s$. The velocity profile in the flume is well developed and closely resembles the modified $1/7^{th}$ power law (Myers and Bahaj, 2012).

Figure 5-1: Full channel width ramp (left), half channel width ramp (right)

Using Froude scaling, the experimental flow domain was scaled from a prototype MCEC deployment site with an average full-scale depth of 10-30m. Spring peak and neap peak tidal flow velocities are in the range of 0–3m/s. Initially it was assumed that a feasible full-scale ramp-foundation height would be 10% of the average flow depth (see chapter 4), but the effect of ramp height was investigated by adjusting the ramp height to flow depth ratio. For good quality scaled experiments the full-scale environment must be accurately replicated (Myers et al., 2008). Of particular importance is:

1. Accurate linear scaling of ramp dimensions.
2. Ramp height to flow depth ratio (R_V).
3. Replication of ambient flow field conditions, including: Froude number, vertical velocity profile (approximately $1/7^{th}$ power law) and turbulence intensity.

When conducting small-scale tests in a circulating water channel, there will be limitations. These include replicating full-scale channel bathymetry, the temporal dynamics of a tidal cycle (such as varying depth, flow velocity and direction), lateral ramp width to channel width ratio and Reynolds and Froude number parity. These parameters must be considered when interpreting results but should not affect the general conclusions presented in this chapter and it

would be virtually impossible to fully represent all the features found in a natural tidal channel at this scale. It will not be possible to achieve Reynolds number parity between model and full scale, although for the experimental tests presented here the model Reynolds numbers were all fully turbulent as demonstrated by the shape of the measured vertical velocity profile. The lateral ramp span to channel width ratio is of concern but the channel is significantly wider than it is deep so effects are minimised (lateral ramp blockage is investigated in section 5.2.8).

A range of different flow parameters and ramp dimensions were investigated for the ramp only tests. These included varying the following: Froude number, ramp height to flow depth ratio, ramp width and length. The angled sections at the upstream and downstream ramp ends are termed "leading and trailing edge profiles" and were initially angled at 30 degrees to the horizontal. Different leading/trailing edge profiles are investigated in section 5.2.6. Dimensions of key ramps are shown schematically in Figure 5-2 and tests are detailed in Table 5-1 (the ramp letters A-C relate to the ramp sketches shown in Figure 5-2, further ramp dimensions that were used during testing but not illustrated in Figure 5-2 are denoted by "-" in Table 5-1).

Test	**Froude**	**Experimental scale**					**Ramp**	**Full scale**			
		Depth [mm]	**Mean Vel. (m/s)**	Ramp size (mm)				**Mean Vel. (m/s)**	Ramp size (m)		
				L	W	H			L	W	H
1	0.25	300	0.43	500	1200	30	**A**	2.48	16.5	39.6	1
2	0.35	300	0.60	500	1200	30	**A**	3.47	16.5	39.6	1
3	0.15	300	0.26	500	1200	30	**A**	1.49	16.5	39.6	1
4	0.15	300	0.26	500	1200	30	**A**	1.49	16.5	39.6	1
5	0.2	300	0.34	500	1200	30	**A**	1.98	16.5	39.6	1
6	0.3	300	0.50	500	1200	30	**A**	2.97	16.5	39.6	1
7	0.15	400	0.30	500	1200	30	**A**	1.49	16.5	39.6	1
8	0.15	200	0.21	500	1200	30	**A**	1.49	16.5	39.6	1
9	0.25	200	0.35	500	1200	30	**A**	2.48	16.5	39.6	1
10	0.2	400	0.40	500	1200	30	**A**	1.98	16.5	39.6	1
11	0.2	200	0.28	500	1200	30	**A**	1.98	16.5	39.6	1
12	0.2	300	0.34	500	600	30	**-**	1.98	16.5	19.8	1
13	0.2	300	0.34	500	450	30	**B**	1.98	16.5	14.9	1
14	0.2	300	0.34	300	450	30	**-**	1.98	9.9	14.9	1
15	0.15	300	0.26	300	450	30	**-**	1.49	9.9	14.9	1
16	0.2	300	0.34	200	450	30	**-**	1.98	6.6	14.9	1
17	0.2	300	0.34	200	300	30	**C**	1.98	6.6	9.9	1

Table 5-1: Experimental parameters and full-scale dimensions for ramp only testing

To determine the potential benefits of the ramp-foundation, velocity profiles were measured upstream of the ramp and at various locations along the ramp's length, numbered in Figure 5-2.

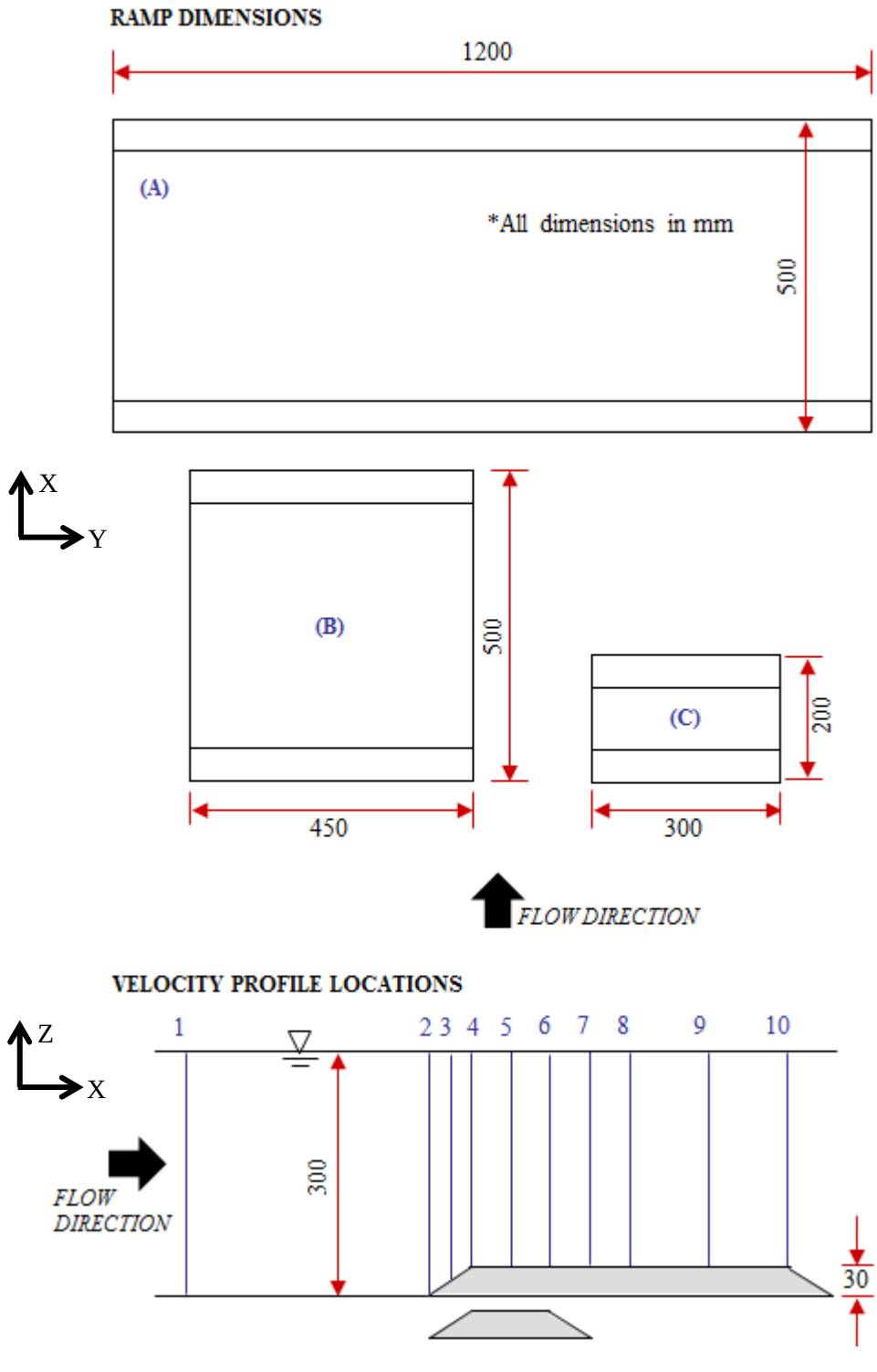

Figure 5-2: Ramp dimensions (top) and centreline velocity profile locations for ramp only testing (bottom)

Characterisation of ambient turbulence levels is important as long length-scale turbulence may lead to increases in dynamic rotor and structure loading. The ambient turbulence intensities in the circulating channels used during this study were approximately 6-8% and were calculated in all three planes (x,y,z). Turbulence intensity is defined in chapter 3 by equation 3.10.

High shear stress can be detrimental to MCEC survival. Horizontal shear stress should be approximately zero throughout the channel depth as lateral velocity components are small. Longitudinal shear stress will increase towards the channel bed due to increased shear in the boundary layer. Horizontal and longitudinal shear stresses are defined in chapter 3 by equations 3.12 and 3.13.An 'xyz' coordinate system was adopted throughout testing (Figure 5-2), with 'x' representing the downstream direction, 'y' the lateral cross-channel direction and 'z' the height above the channel bed. The velocities are 'u,v,w' respectively for the 'xyz' coordinate directions. Non-dimensional results for velocity measurements and turbulence intensity are presented by normalising ramp profiles with the depth averaged values from the upstream profile 1.

5.2.1.2 Flow measurement

In order to measure the velocity profiles and visualise the flow field around the ramps, samples were taken using a high frequency ADV. Operational issues and the accuracy of ADVs have been addressed in section 3.4 and at length in many publications (Lohrmann et al., 1994, Voulgaris and Trowbridge, 1998, Rusello et al., 2006, Blanckaert and Lemmin, 2006). A Vectrino ADV was used throughout testing and for each data point 7500 discrete velocity samples were acquired over a 150-second period at a frequency of 50Hz. This value was reached through a compromise between sample time and percentage velocity variation from a larger 600 second sample. Figure 5-3 shows that samples in the range of 150 to 240 seconds vary by less than 1% compared with the 600 second sample. Samples of 7500 readings (2.5 minutes) recorded variations of less than 0.3%. Turbulence intensity is affected more dramatically by reducing the sampling period (Figure 5-3). Short sampling periods exhibited variation of up to 15% whereas at the 150 second sampling period used herein (7500 readings) showed variations of less than 2%.

There are a range of user specified ADV parameters that can be adjusted to improve instrument accuracy:

- **Sample rate:** this can be set in the range of 0-200Hz but the noise floor of the Vectrino ADV is slightly above 50Hz so this is generally taken as the practical maximum value for the sampling rate (Gordon, 2000) and is used throughout testing. If a higher sampling frequency was used it is probable that the recorded turbulent energy would have a component of electrical noise and would not represent the true flow turbulence.
- **Velocity range:** the lowest velocity range that encompasses the majority of the tested flow regime should be chosen.

- **Sampling volume height:** the diameter of the sampling volume is fixed at 6mm as this corresponds to the diameter of the cylindrical ceramic emitter of the Vectrino. The height of the sample volume is chosen by the user and is a compromise between maximising the size to intercept more water and ensuring the height is not too large to interfere with other sampling heights or indeed incur a non-uniform velocity profile (velocity shear) across the sample. A larger sample size is beneficial for the signal to noise ratio (SNR) because a larger sample volume can intercept more flow particles. In this testing the flow depth was small, generally in the range of 200-400mm, hence a corresponding small sample volume height of 2.5mm (approximately 1% of total depth) was chosen.

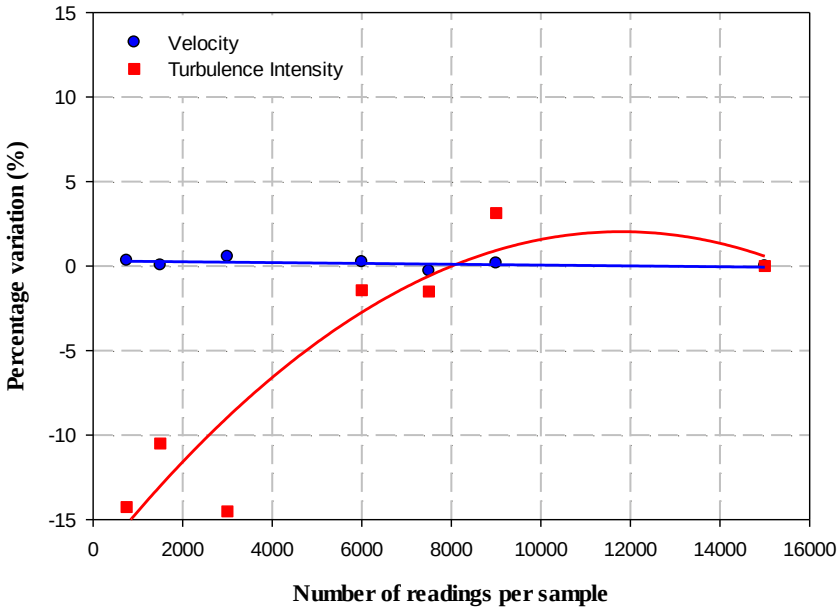

Figure 5-3: ADV velocity and turbulence intensity percentage variation with decreasing sample readings

For ADVs to operate efficiently a high level of water turbidity is required as discussed in chapter 2. Higher turbidity will be reflected in the SNR which is recommended to be above 15 (McLelland and Nicholas, 2000). The channels used for the majority of this testing are located in hard water regions meaning the water contains large volumes of suspended particles, thus the ADV data is of high quality. This was reflected in the SNR, which was constantly around 20-25, considerably higher than the proposed threshold of 15 for accurate readings. Another indicator of accuracy is the correlation coefficient, which is a measure of the variance between consecutive instrument signals, and is recommended to be greater than 70%. It was also monitored during testing and for all work presented herein it was generally greater than 90%. Figure 5-4 shows a typical ADV sample velocity trace with the probe head located at the channel centre-line. In this case the channel was running empty without any obstructions. Hence

the lateral and vertical velocities in the y and z planes are minimal. The variation in the flow's primary x direction represents the channels ambient turbulence. At approximately 2 seconds into the sample a flow irregularity spike can be seen, which would be removed during the data filtering process.

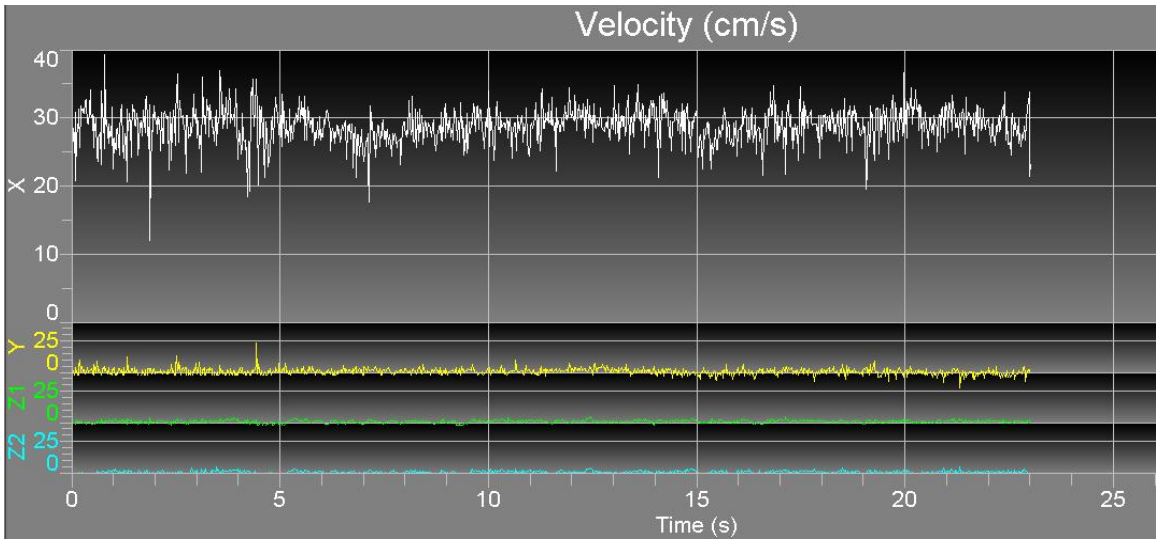

Figure 5-4: Typical ADV velocity sample trace

Probe heads:

The Vectrino can be used with two different probe heads - a downward-looking probe or a side-looking probe (Figure 5-5).

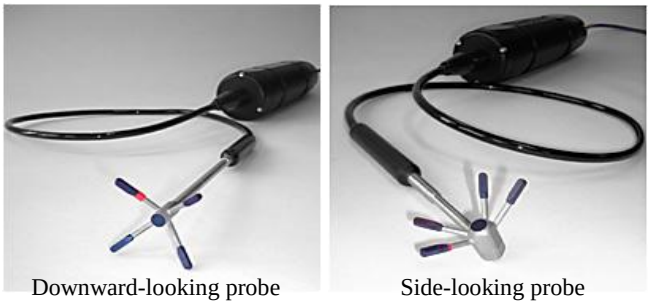

Downward-looking probe Side-looking probe

Figure 5-5: Vectrino probe heads

The downward-looking probe is better suited to deeper flows and sampling close to the channel bed. As the probe head must be submerged and the measurement volume is centred 50mm from the vertical emitter, the top 60mm of water cannot be characterised. The side-looking probe is more capable in this region (can sample up to 10mm below the water surface) and also close to lateral flow boundaries such as the side walls of flumes and channels. Due to the geometry of the receiver arms (Figure 5-5) the side-looking probe tends to suffer from higher levels of instrument noise in the vertical plane and has a very bad response to flow coming from behind the probe head which should be avoided.

5.2.2 Full width ramp

The initial set of tests involved a ramp spanning the full channel width. A range of Froude numbers with a fixed flow depth of 300mm were investigated. Velocity profiles were taken at the locations detailed in Figure 5-2.

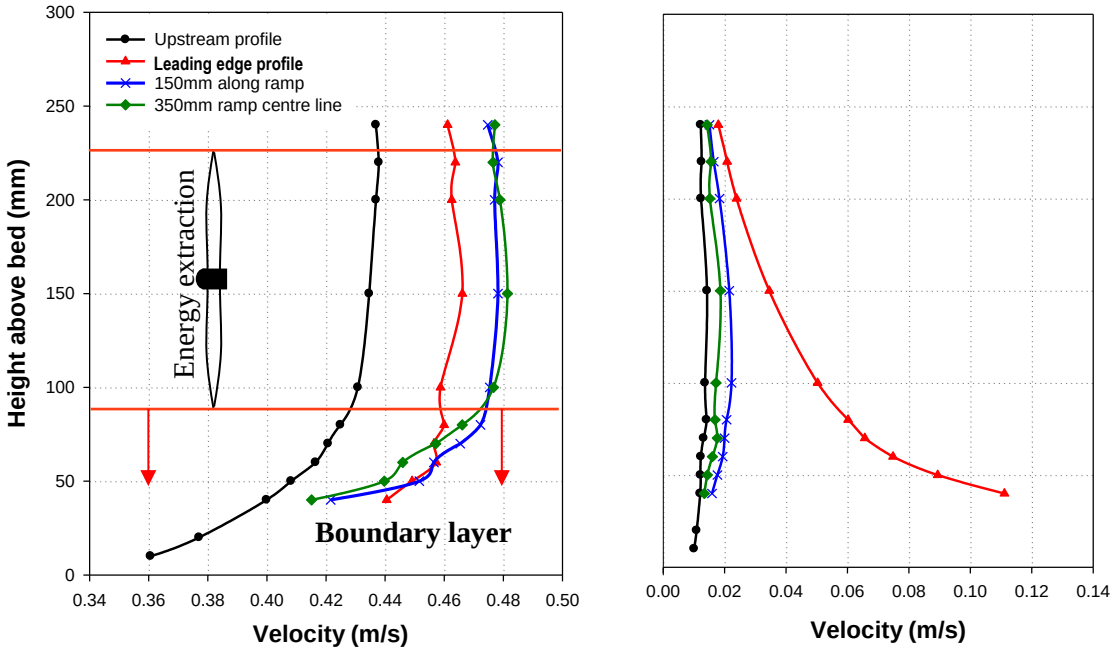

Figure 5-6: u-plane (left) and w-plane (right) velocity profiles:
Full channel width ramp, Fr = 0.25, d = 300mm

Figure 5-6 shows how the u-plane and w-plane velocity profiles developed across the ramp-foundation for a flow depth of 300mm and a Froude number of 0.25. The ramp leading edge initially disrupts the u-plane vertical velocity profile by essentially interrupting the sheared boundary layer, leaving a more uniform velocity profile that re-develops across the ramp top surface. The profile taken 150mm (or 5 ramp heights) downstream of the ramp leading edge shows the best profile for energy extraction, in terms of velocity increase and a uniform upper section. The optimum profile location is selected as a compromise between maximising the velocity in the uniform upper profile section and selecting a point where the sheared boundary layer development is minimised. The boundary layer thickens across the ramp, shown clearly by the 150mm and 350mm u-plane velocity profiles in Figure 5-6. The sheared boundary layer region does not increase considerably with the presence of the ramp due to conservation of the mass flow. Hence the increased velocities in the uniform upper section of the flow profile are accompanied by a more compact sheared boundary layer. In general these conclusions are true for all tests conducted with the full-width ramp-foundations at a flow depth of 300mm. The u-plane velocity was increased by approximately 11-12% in all cases. Fundamentally the velocity

increase across the ramp can be explained by principles of continuity and specific energy (see section 3.1.4 and Figure 3-1).

Velocities in the v-plane (lateral) and w-plane (vertical) were found to be approximately equal to zero throughout the flow depth, which is expected as the bulk flow is in the downstream (u-plane) direction. With the exception of profiles 2-4 (Figure 5-2) taken across the leading edge ramp where small w-plane velocity components were introduced near the ramp (Figure 5-6). This results because the ramp causes the flow just upstream to slow and change direction close to the bed, introducing larger regional vertical velocity components.

Turbulence intensities reduced slightly across the ramp for all planes (u,v,w). This is significant as it was previously stated that turbulence can have negative effects on MCEC performance. It is postulated that the increase in flow speed and the associated increase in shear stress close to the ramp-foundation may have reduced some of the smaller length-scale turbulent motion.

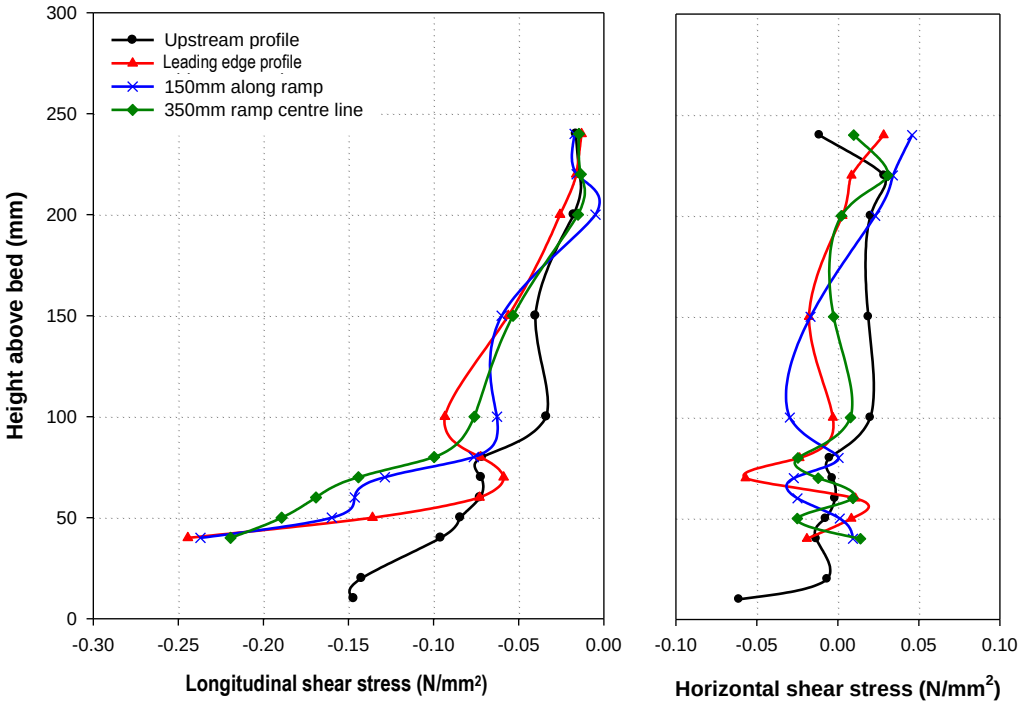

Figure 5-7: Longitudinal and horizontal shear stress profiles: Full channel width ramp, Fr =0.25, d =300mm

The horizontal and longitudinal shear stresses were calculated throughout the water depth. Horizontal shear stress was found to be approximately zero throughout the depth (Figure 5-7). This was expected as there are no significant lateral components of velocity to cause shear in this direction, both for the ambient upstream flow and that across the ramp structure. The

longitudinal shear stress increased significantly close to the ramp as would be anticipated as the faster overlying flow will cause more shearing in the lower boundary layer. The vertical extent of this increase was limited to the lower part of the water column and it did not seem to adversely influence the shape of the vertical velocity profile in the region where a tidal turbine rotor might be located (Figure 5-6).

A series of tests were conducted to investigate the effects of changing the ramp height/flow depth ratio. Here the ramp height was kept constant, but the flow depth in the channel was varied. The results are illustrated in the normalised graphs (Figures 5.9-5.11, presented in section 5.2.4). It can be seen that if the ratio is increased (i.e. flow depth reduced) the benefits of the ramp-foundation are greater in terms of velocity gain. If the ratio is reduced the velocity gain depreciates because the relative flow cross-sectional area reduction across the ramp is reduced. This highlights the underlying principles of flow area continuity and the fact that this technology might be difficult to implement in deep tidal flows because the ramp height would need to be considerable. In addition this effect can again be explained in terms of specific energy (see section 3.1.4 and Figure 3-1), essentially when the bed is raised the kinetic energy within the flow must increase at the expense of potential energy. This is characterised by a reduction in specific energy. If the ramp height was increased dramatically of course unstable critical depth conditions could develop but given the feasible ramp height to flow depth rations involved with this project the situation is unlikely to occur (assuming typical tidal flow velocities of 2-3m/s critical flow conditions would need unrealistic corresponding water depths of 0.5 to 1m).

These ramp height/depth ratio experiments were conducted with ramps effectively spanning the whole width of the channel but in reality this is unlikely to occur. Further experiments were conducted to understand the significance of varying the ramp width and length (section 5.2.3).

5.2.3 Varying ramp geometry

Ramp lengths and widths were progressively reduced to establish an optimum ramp size and to understand the effects of the ramp side edges on the flow.

In general the conclusions from the full width tests held but with the benefits reduced, explained in part by the principles of flow cross-sectional area continuity. Figure 5-8 shows the u-plane velocity profiles from two of the reduced width/length ramps. For this configuration velocity still increased but by only 5-6%.

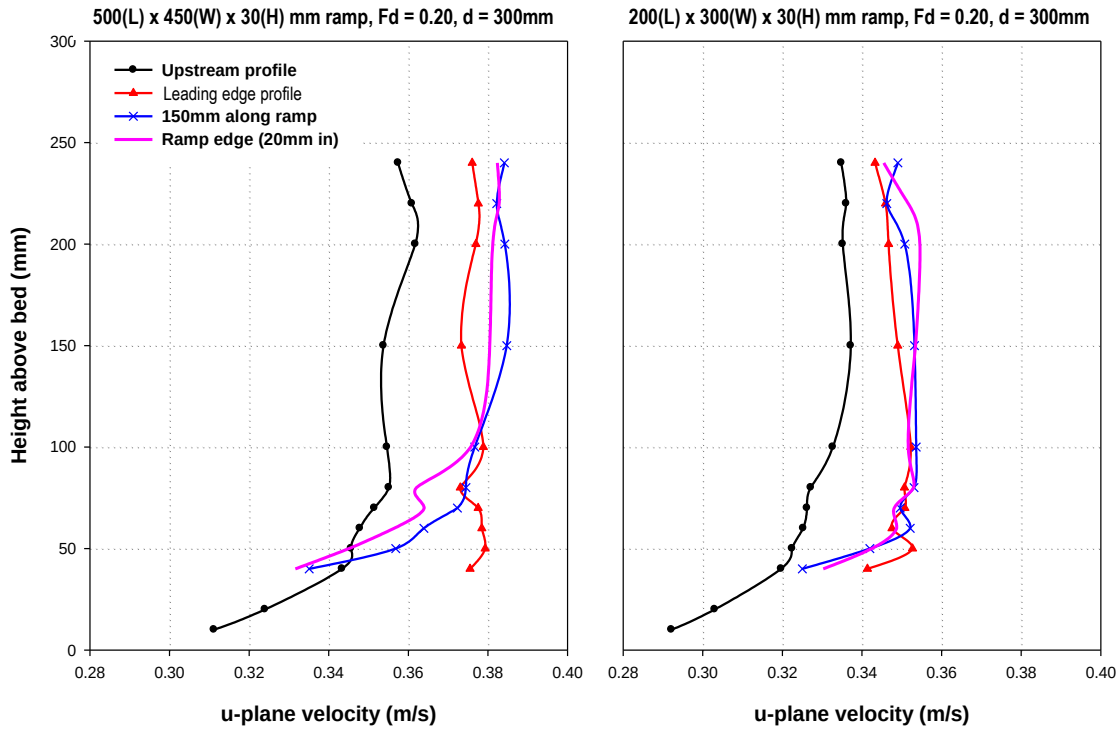

Figure 5-8: u-plane velocity profiles (tests 13 & 17)

For all the tested ramp-foundations at a flow depth of 300mm the optimum vertical velocity profile remained at 150mm downstream (or 5 ramp heights) from the leading edge of the ramp. However for the smallest ramp this point is at the very end of the ramp, so it can be concluded that this ramp-foundation was insufficient in length to allow formation of a fully developed velocity profile at the ramp centre-line. The optimum ramp length would thus be 300mm so that the optimum profile will occur at the ramp centre line allowing a device to benefit from the increased energy flux from both directions in a bi-directional tidal flow. This would equate to a ramp length equal to the flow depth (for example, a 10m long ramp in a 10m deep tidal flow).

There were no significant reductions in velocity observed near the side edges of the ramp, as shown by the vertical profiles measured 20mm from the side of the ramp-foundation in Figure 5-8. This would mean full scale ramp-foundations would not need to exceed much beyond the device width, reducing construction costs. Lateral flow components are minimal as the bulk flow and the ramp are both orientated in the stream-wise direction which means for the ramp only tests, the flow across the ramp can be approximated to a two-dimensional flow problem.

At Froude numbers of approximately 0.2 there were no observed changes in water surface elevation over the ramp structure. It is anticipated that Froude numbers approaching 1 (or critical condition) may be required in order to observe and quantify any reduction in water

surface elevation over ramp structures. This could be achieved by increased flow speed or a reduction in total water depth (investigated in section 5.2.7).

5.2.4 Optimal downstream distance for energy extraction

Figure 5-9 shows a normalised comparison between point 4 located at the top of the leading edge profile for different flow cases. It shows how the sheared boundary layer is initially removed by the ramp to give an almost completely vertical velocity profile. This would be an ideal profile for energy extraction. However, the velocity profile is not yet fully developed and power gains would be lower.

Figure 5-10 shows velocity profiles taken at the optimum energy extraction location. It highlights how increasing the ramp height/flow depth ratio increases the velocity gain and how reduced ramp size reduces the velocity magnification. Profiles exhibit compressed sheared boundary regions and good vertical profiles for energy extraction.

Turbulence intensities showed similar trends for all tests (Figure 5-11). Both the u and v-plane profiles were an inverse of the u-plane velocity profile showing a constant upper section equal to 6-7%. The w-plane turbulence intensity was generally constant with depth, displaying slightly lower values of approximately 5%. Figure 5-11 shows how the turbulence intensity was slightly reduced across the ramp compared with the average upstream values. It is postulated that the increase in flow speed and the associated increase in shear stress close to the ramp-foundation may have reduced some of the smaller length-scale turbulent motion.

In essence the lower section of the flow depth should be avoided for energy extraction for both increased shear stress and turbulence intensity.

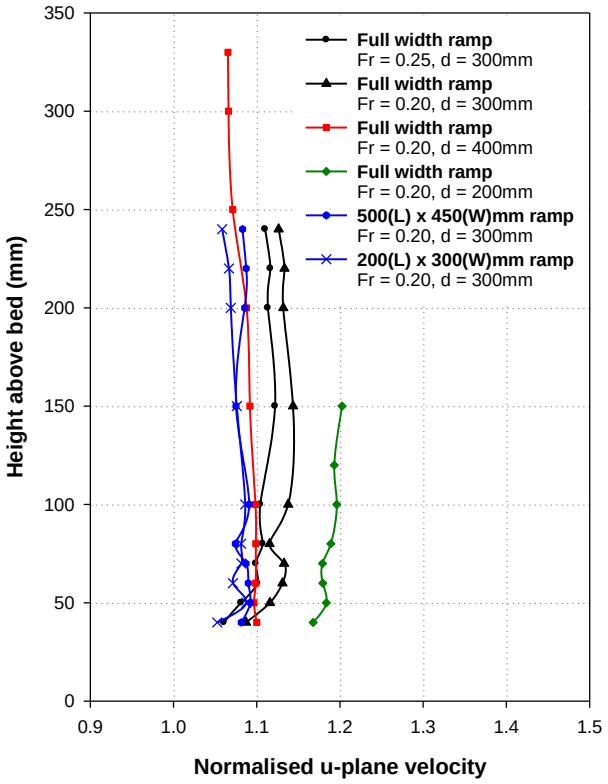

Figure 5-9: Normalised u-plane, point 4, velocity profiles: top of leading edge profile.

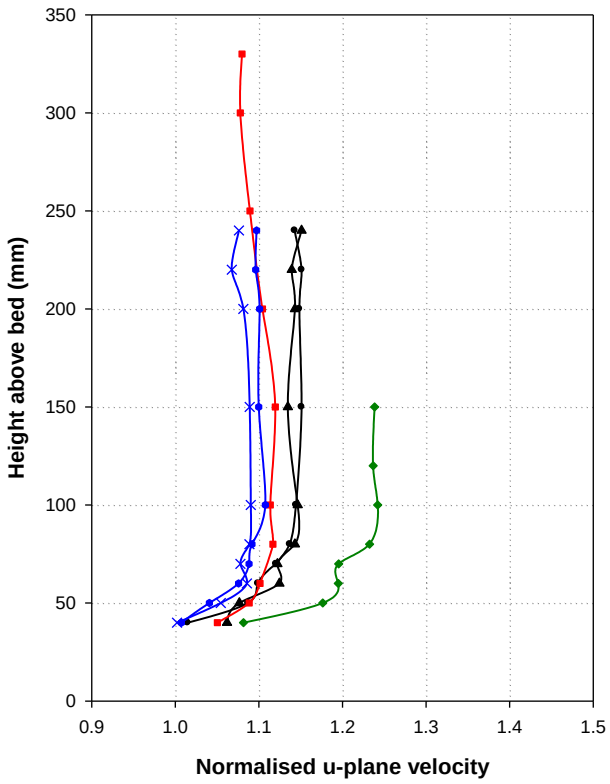

Figure 5-10: Normalised u-plane, point 6, velocity profiles: 150mm along ramp.

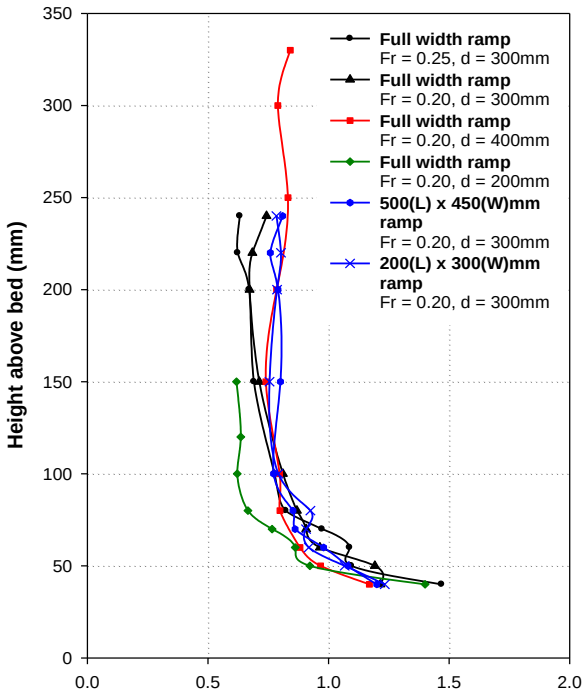

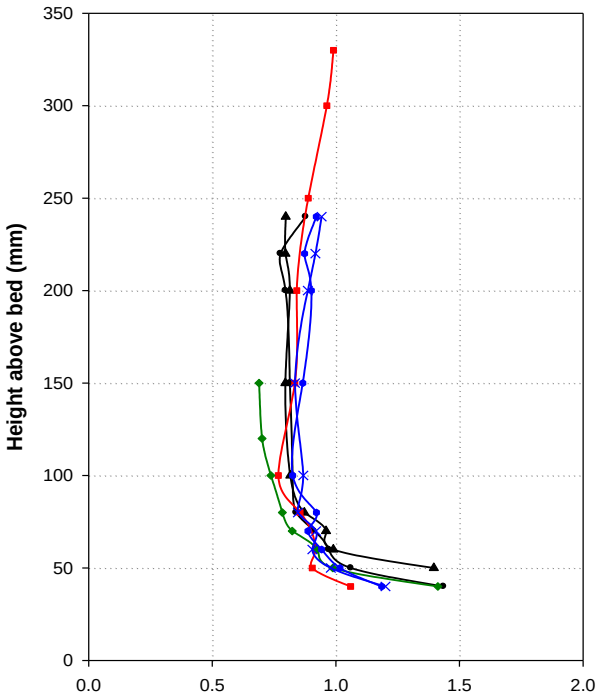

Figure 5-11: Normalised turbulence intensity profiles (optimum profile location): (a) u-plane (left) & (b) v-plane (right)

5.2.5 Velocity, turbulence and shear stress intensity visualisation

The 2-Dimensional graphical contour plots shown in Figure 5-12 illustrate how the centreline velocity intensity increases across the ramp-foundation and how the turbulence intensity and shear stress develops. The plots consist of 102 ADV measurement points which are interpolated into multi-colour contour plots. The uppermost plot of Figure 5-12 illustrates well the optimum energy extraction point and boundary layer redevelopment, with a constant uniform velocity profile at approximately 100mm downstream and the ongoing formation and thickening of a boundary layer beyond this point. The lower plot of longitudinal shear stress illustrates the boundary layer thickening and mirrors the velocity plot with highest shear stresses occurring near the bed. These high shear stresses occur close to solid boundaries due to a no-slip condition at the surface of the solid boundary (water in direct contact with the boundary has zero velocity) and the gradual transfer of momentum between water particles in this region and the undisturbed free stream. The sheared profile persists from the solid boundary until a distance is reached where the influence of the boundary has no effect upon the transfer of momentum between adjacent water particles.

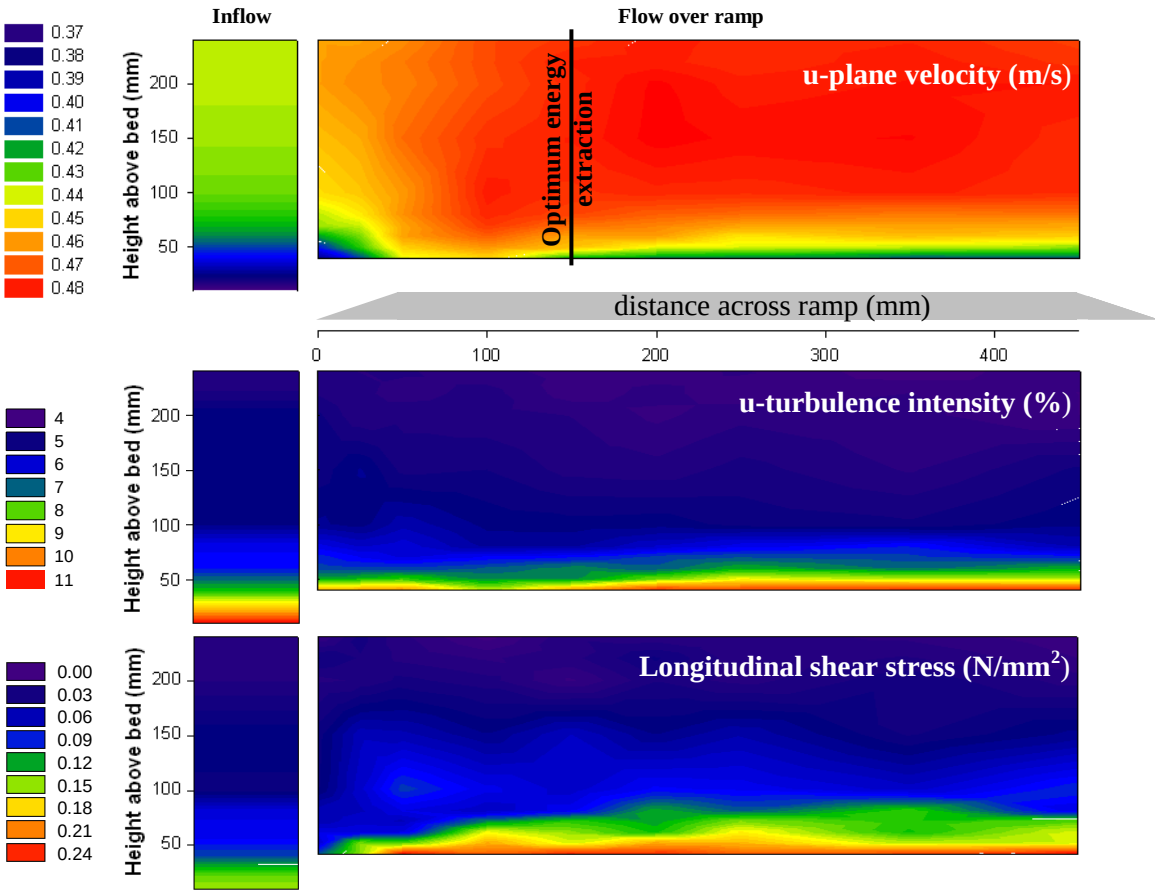

Figure 5-12: Contour plots of u-plane velocity, u-plane turbulence intensity and longitudinal shear stress. Full channel width ramp, Fr = 0.25, d = 300mm (Test 1)

Observing the turbulence intensity in the middle plot of Figure 5-12 it can be seen that it remains relatively constant along the ramp with turbulence increasing in the boundary layer. This is because the ramp and leading edge profile are relatively smooth and hence do not generate large turbulent structures. Again in general the turbulence intensity reduces slightly across the ramp which could also in part be due to the lower surface roughness of the ramp compared to the channel bed.

5.2.6 Leading edge profile

For the initial tests detailed in sections 5.2.2-5.2.5 the leading edge profile was 30 degrees to the horizontal. In order to fully optimise the ramp-foundation an investigation into different leading edge profiles was conducted and is presented here. The objectives were to:

- Ensure stable flow onto the ramp
- Maximise flow velocity
- Reduce construction complexity

There is likely to be a compromise between optimising the velocity profile and minimising the construction complexity to create a feasible full-scale solution. In total six different profiles (Figure 5-13) were tested for Froude numbers of 0.15 and 0.2 with a constant flow depth of 300mm. As no significant lateral flow components occur across the ramp it was decided to conduct these tests in a narrow 300mm wide flume.

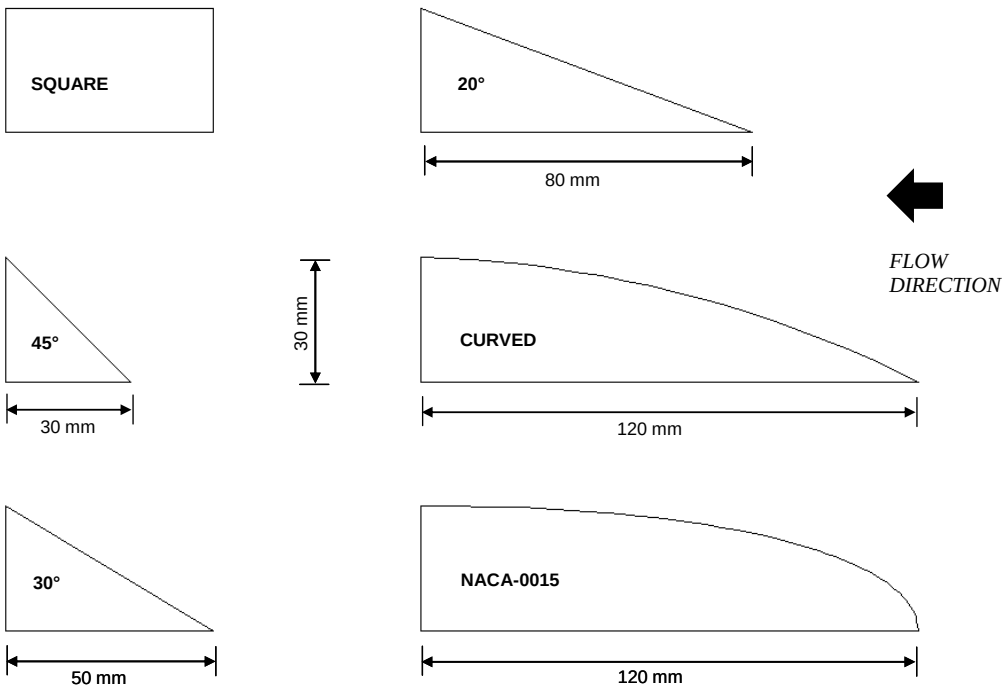

Figure 5-13: Leading edge profiles

The height of the ramp was maintained at 30mm as with previous testing (10% of the flow depth) and the length was taken as the optimum length of 300mm for a flow depth of 300mm.

- **Square profile:** this establishes a control profile to help ascertain the benefits of having a profiled leading edge. In addition it might be of benefit for developing a vertical velocity profile where the sheared boundary layer is effectively removed by the sharp leading edge (Lyn, 1993).
- **Angled profiles:** these profiles would be simple to construct at full scale and, provided a shallow angle is avoided, the amount of construction material required would be less than with a more complex curved ramp. These profiles were machined from hardwood.
- **NACA-0015 profile:** this was chosen as a known aerodynamic profile. For this profile to be feasible it would have to offer considerable velocity increase benefits as the construction complexity would be high. The profile shape was established using equation 5.1 and was machined from high-density foam using a CNC hotwire cutter.

$$y = c\frac{t}{0.20}\left[0.2969\sqrt{\frac{x}{c}} - 0.1260\left(\frac{x}{c}\right) - 0.3516\left(\frac{x}{c}\right)^2 + 0.2843\left(\frac{x}{c}\right)^3 - 0.1015\left(\frac{x}{c}\right)^4\right] \quad (5.1)$$

- **Curved profile:** this profile had a "less bluff" leading edge and was tested as a comparison for the NACA profile. It was also machined from high density foam.

Velocity profiles were recorded along the channel centre line using the ADV with the same setup and procedure as in 5.2.1.2. A profile was taken at four flow depths upstream of the ramp and four profiles were recorded across the ramp each spaced at 0.25d, with point 4 being located at the ramp centre-line (Figure 5-14).

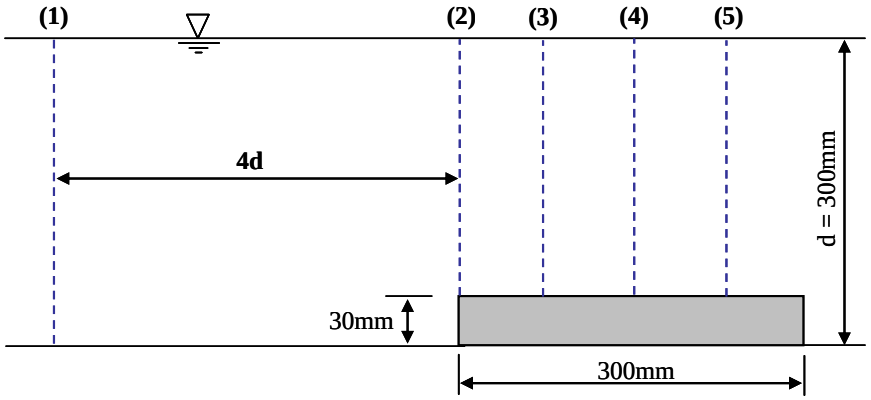

Figure 5-14: Velocity profile sampling locations

As projected from previous work, the optimum velocity profiles tended to occur at point 4 at the ramp centre line (Figure 5-14). The v-plane velocity and horizontal shear stress was approximately equal to zero throughout as would be expected with the 2D experimental domain.

The results presented in Figure 5-16 and Figure 5-17 are the velocity, turbulence and shear stress profiles measured at point 4 - the optimum energy extraction location across the ramp. These profiles were normalised with profile 1 located four flow depths upstream. At this distance upstream the ramp has negligible influence on the profile shape and thus point 1 is approximately equal to a free-stream profile (with no ramp present).

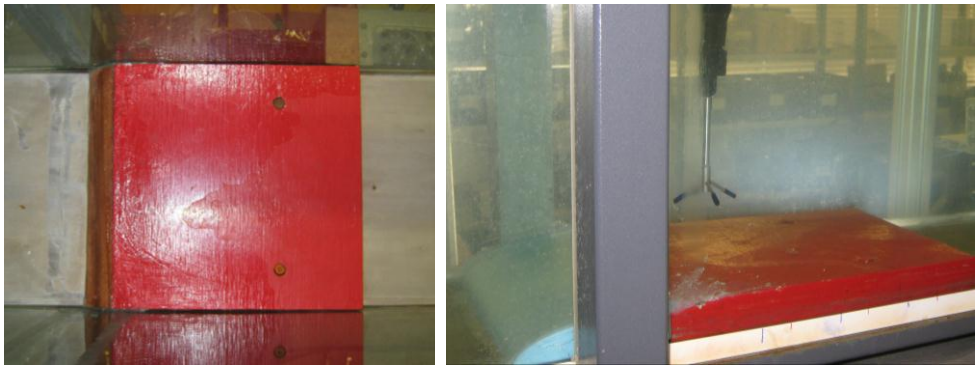

Figure 5-15: Leading edge profile testing

The square ramp-foundation offers the greatest benefit in terms of velocity increase (≈2.5% increase above a 30° ramp). However the drawback with the square ramp is high turbulence intensity and shear stress close to the ramp (the lower 25% of the flow depth). This would primarily be a concern for foundation design because this lower region is unlikely to be used for energy extraction. The bed shear capacity of the foundation would need to be higher to resist the resultant shear force. For the square ramp, turbulence intensity near the bed was approximately 55% higher than other profiles. The reason behind the square ramp's higher flow velocity in the upper flow region results from continuity of the mass flow rate. The aggressive removal of the boundary layer by the sharp leading edge yields a lower mass flow rate in the boundary layer and hence a higher mass flow in the upper flow region. Essentially a stagnation point is created by the ramp's vertical leading edge causing a turbulent eddy to develop downstream. This region of separated turbulence reduces the mass flow close to the ramp.

With the angled profiles the flow is smoothed and heavy flow separation is prevented, which reduces the turbulence and shear stress close to the ramp (Figure 5-17). Increasing the ramp angle reduces the levels of turbulence and shear stress due to less aggressive boundary layer modification near to the ramp. However the 45° wedge appears to considerably reduce the near ramp turbulence and shear stress without significantly reducing the velocity gains seen with the

square edge ramp. Although the turbulence intensity and shear stress near the bed are not reduced as much as with shallower angled or curved ramp profiles, the increase is minimal considering the improved velocity gain. The curved ramps did not offer any significant benefits over the angled profiles.

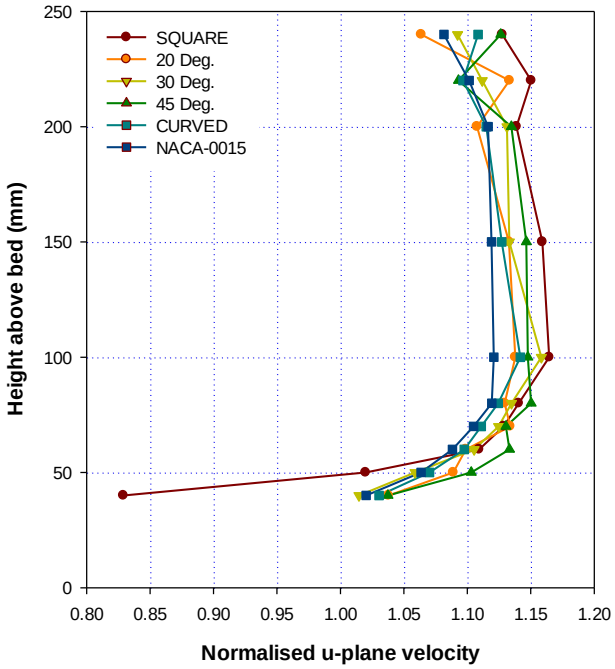

Figure 5-16: Normalised v-plane velocity profile comparison (point 4)

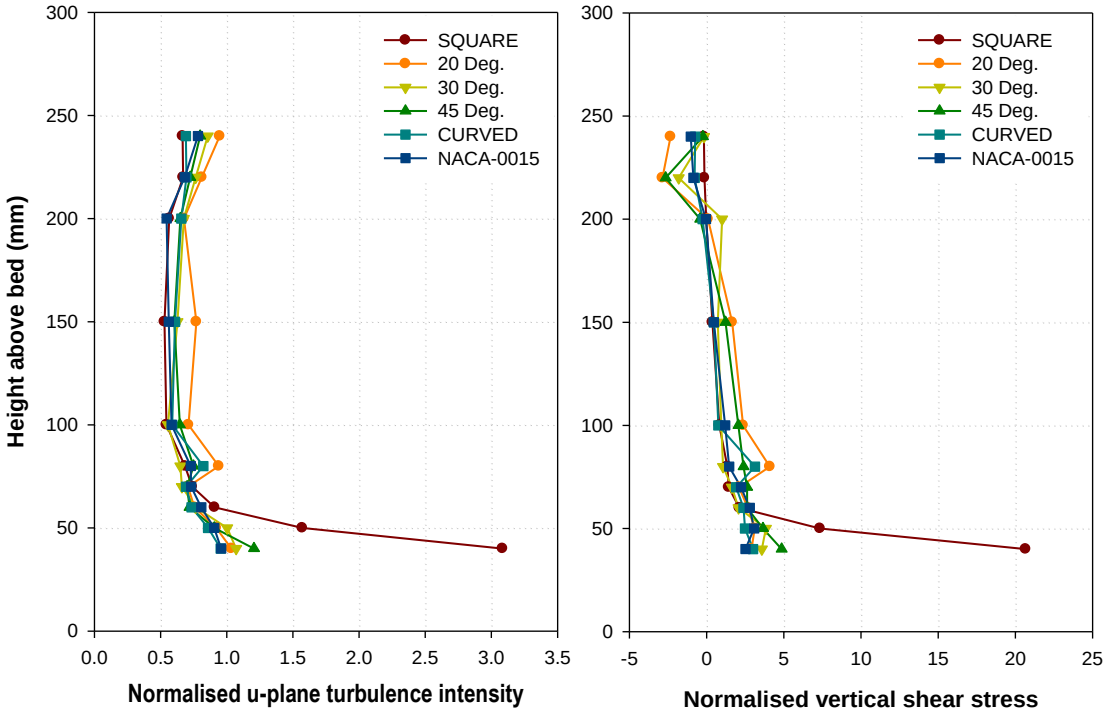

Figure 5-17: Normalised u-plane turbulence intensity and shear stress comparison (point 4)

Recommendation:

Based on these tests a 45° leading and trailing edge profile at both ends of the foundation to exploit bi-directional flows would be recommended. It is a good compromise between increased velocity and minimising turbulence/shear stress near the foundation. A 45° profile would require less material for construction than shallower angled ramp-foundations and the construction method would be much simpler compared with curved profiles.

5.2.7 Water surface profiles

When using the specific energy method (see section 3.1.4 and Figure 3-1) and flow is subcritical (equation 5.2) a surface drop is estimated. Throughout testing at Froude numbers of less than 0.3 there have been no significant signs of measurable surface drops and this corresponds with previous experiments conducted in circulating water channels (Bahaj et al., 2007b).

$$surface\,drop = d_1 - d_2 - \Delta Z = \frac{U_2^{\,2}}{2g} - \frac{U_1^{\,2}}{2g} \tag{5.2}$$

Using the same 2D flume as the leading edge profile tests (section 5.2.6) a series of tests were undertaken to establish the point where the surface drop (or Froude number threshold) might become significant in terms of MCEC operation. This was done by progressively increasing the Froude number (Table 5-2) and measuring the surface water profile upstream, across the ramp and downstream of the structure using a point gauge.

Test	Froude	Depth (mm)	Upstream mean velocity (m/s)	Ramp centreline mean velocity (m/s)	Maximum measured surface drop (mm)	Theoretical surface drop (mm)
1	0.15	300	0.26	0.28	1.5	0.6
2	0.20	300	0.34	0.38	1.0	1.5
3	0.30	200	0.40	0.47	6.5	3.1
4	0.40	200	0.56	0.65	9	5.6
5	0.45	200	0.63	0.75	11	8.4
6	0.50	200	0.70	0.85	15	11.9

Table 5-2: Leading edge profile tests and general results

The results are presented in Table 5-2 and Figure 5-18. Error bars (of ±2mm) have been added to Figure 5-19 because measurements taken with point gauges are subject to both human error and flow discrepancies. Unfortunately for the higher Froude numbers the flow depth had to be reduced because of flume pump capacity. This is not a concern as the head drop should be Froude number dependent not depth dependent and the ratio between velocity and depth can

simply be adjusted to achieve the required Froude. It can be seen from Figure 5-19 that there is a trend for the surface level to increase slightly as you move downstream. This is expected as the water depth in the flume is controlled using a weir at the downstream end of the channel and therefore an "M1" backwater surface profile was formed leading to this measured increase in depth.

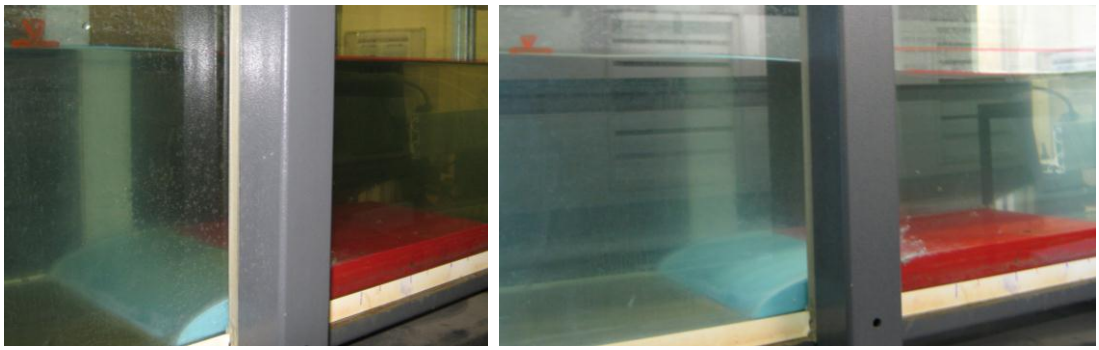

Figure 5-18: Water surface profiles (left) Froude = 0.15 and (right) Froude = 0.50

As can be seen from Figure 5-18 and Figure 5-19 for Froude numbers of less than 0.45 there is a very small reduction in depth over the ramp, but as the Froude number increases above 0.45 such reductions were clearly observed and measureable. For a Froude number of 0.5 a 5% head drop was observed, which at full scale would equate to a 0.5m reduction in depth in a 10m-deep flow. The error bars clearly show that the result is outside the region of experimental error. However the channel is narrow and surface drops would be expected to be less in a wider channel or the open sea, due to the interaction of the augmented across ramp flow with the surrounding free-stream flow.

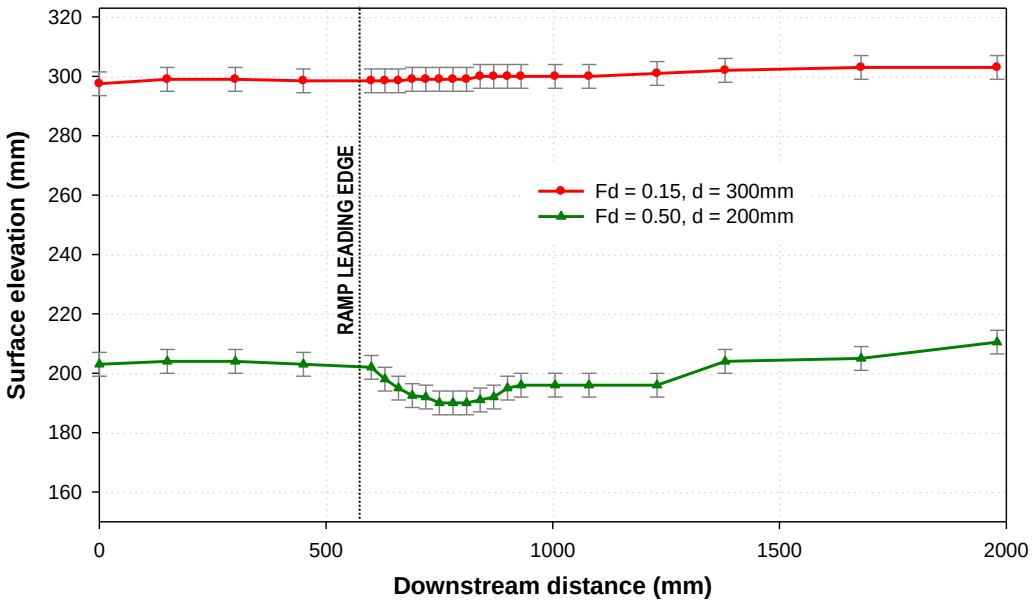

Figure 5-19: Water surface profiles across ramp for varying Froude

In reality the Froude number of a tidal flow would be in the lower range (Fd < 0.45) and the flow would be laterally unconstrained. So a significant surface drop resulting from the ramp-foundation would not be anticipated at full scale. Flows will be in the upper subcritical range away from critical depth conditions and realistic ramp height to flow depth ratios will be small. However, there would be an additional surface head drop across a MCEC resulting from energy extraction from the flow.

5.2.8 Lateral ramp blockage

This set of tests investigates the effects of reducing the ramp width (or span) with respect to the channel width, e.g. the lateral ramp blockage ratio, equation 5.3.

$$Lateral\ Ramp\ Blockage\ Ratio\ (R_L) = \frac{ramp\ width}{channel\ width} = \frac{y_{ramp}}{W} \qquad (5.3)$$

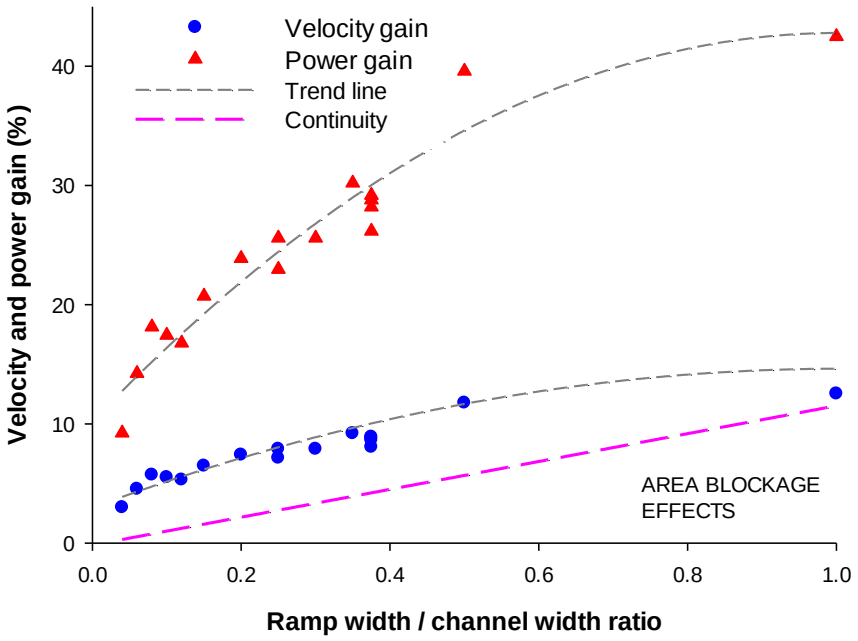

Figure 5-20: Potential velocity and power gain - preliminary testing without MCECs presence

As concluded from previous sections, the ratio of ramp width to channel width has a very significant effect on the power potential of ramp-foundations. Here the velocity and power gains from the ramps tested in Table 5-1 and further ramp width/channel width ratios are displayed in Figure 5-20. The additional tests were conducted by systematically reducing the ramp width and taking a vertical velocity profile at the ramp's centre. The velocity gain potential and power gain potential (momentum theory) was calculated. These ramp only tests clearly show that the degree of flow velocity increase, and thus power gain, is dependent on the lateral channel blockage of the ramp-foundation.

By simply applying the theory of one-dimensional flow area continuity, the velocity increase was calculated by considering the reduction in channel cross-section from the ramp's physical presence. Considering these laws of continuity; by reducing the physical area of the channel with the ramp's cross-section, the flow velocity must increase to some extent. The "continuity" line on Figure 5-20 illustrates the predicted velocity increase from only considering flow area reduction across the ramp and it is clear at low ramp width to channel width ratios the predicted velocity increase would be almost insignificant. However when studying the experimental results in Figure 5-20 ("velocity gain" line) more significant velocity increases are found when considering low ramp width to channel width ratios. This is critical for the application of ramp-foundations and it can be concluded that the reduction in u-velocity gain with lateral ramp blockage ratio is a combined function of channel cross-sectional area continuity and some localised flow effects.

It is postulated that these localised effects result from compression of the vertical extent of the boundary layer across the ramp and flow streaming occurring from the fact that the bulk flow is in the downstream direction. This local "flow streaming" occurs because flow above the ramp's boundary layer possesses significant momentum and hence has a resistance to directional change. This resulting downstream flow momentum therefore prevents large proportions of lateral cross-channel flow and the reported velocity increases are larger than simply considering one-dimensional area continuity. The region between the continuity and velocity gain line in Figure 5-20 represents these localised effects and as lateral ramp blockage increases these localised flow effects become less dominant because the situation approaches that of one-dimensional flow continuity where the ramp spans the entire channel width.

Clearly a ramp-foundation occupying the entire width of the channel would not be feasible except perhaps in a tidal fence application (Giles et al., 2010). As velocity benefits decrease with lateral ramp blockage ratio, ramp-foundations would be better suited to fences or wider arrays deployed in constrained tidal channels or straits between islands. In channels with very low ramp width to channel width ratios, foundation flow augmentation may not be economically viable. Thus when considering the use of ramp-foundations the ramp or overall array width must be tuned to the local channel width to maximise the power benefit.

It is important to remember at this stage that the interaction and flow impedance effects of the MCEC are not included. The presence of the MCEC would reduce the velocity and power gain potential making lateral ramp blockage even more critical in terms of concept viability. MCEC interaction effects are investigated in section 5.3.

5.2.9 Full scale velocity and power benefits

The experimental findings from these ramp only tests were scaled to a full scale tidal site. The benefits of an integral ramp-foundation are illustrated by calculating potential power gains obtainable from an example scenario with a 5m diameter horizontal axis marine current turbine operating in a 10m deep flow. It was taken into account that the top and bottom 25% of the flow depth are recommended to be avoided, due to wave effects and the sheared boundary layer respectively but as explained in chapter 4 the rotor diameter was assumed to be 50% of the free-stream depth. Power was calculated using equation 3.23 where a power conversion efficiency factor of 0.4 was assumed. Results are illustrated in Figure 5-21.

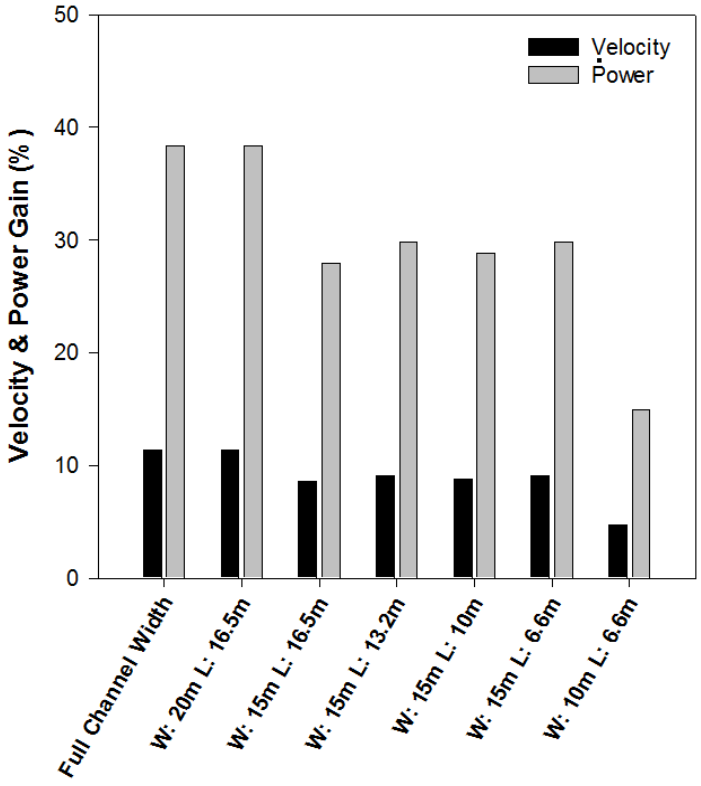

Figure 5-21: Potential velocity and power percentage gain

Interpretation of the results clearly shows that for a small velocity increase the resulting power gains are considerable. Even for the small ramp-foundation, 15% power gains could be obtained (disregarding MCEC interaction effects).

Figure 5-22 presents an estimate of the potential area increase of exploitable 10 to 30m depth shallow tidal flow sites around the UK with the addition of ramp-foundations. Bathymetry data and mean spring peak velocities were obtained from BWEA "Marine Energy Resource Atlas" (ABP, 2008, Cooper et al., 2005) and the layers were manipulated using geographic information system (GIS) software. Results must be treated with caution due to the limited data resolution,

but an exploitable sea area increase of 72% appears very promising. However this figure does not take into account the suitability of sites for ramp-foundation deployment. Constrained flow sites such as tidal channels between land masses (e.g. Bristol Channel) and straits between islands (e.g. Orkney and Channel Islands) will be most suitable. Un-constrained open sea locations would be less effective.

Increasing flow speeds at sites already with suitable velocities would allow developers to either increase the rated power of turbines (to increase annual energy yield) or increase the plant load factor to provide steady power production over a greater range of flow speeds. The choice made would depend upon any financial premium associated with either strategy.

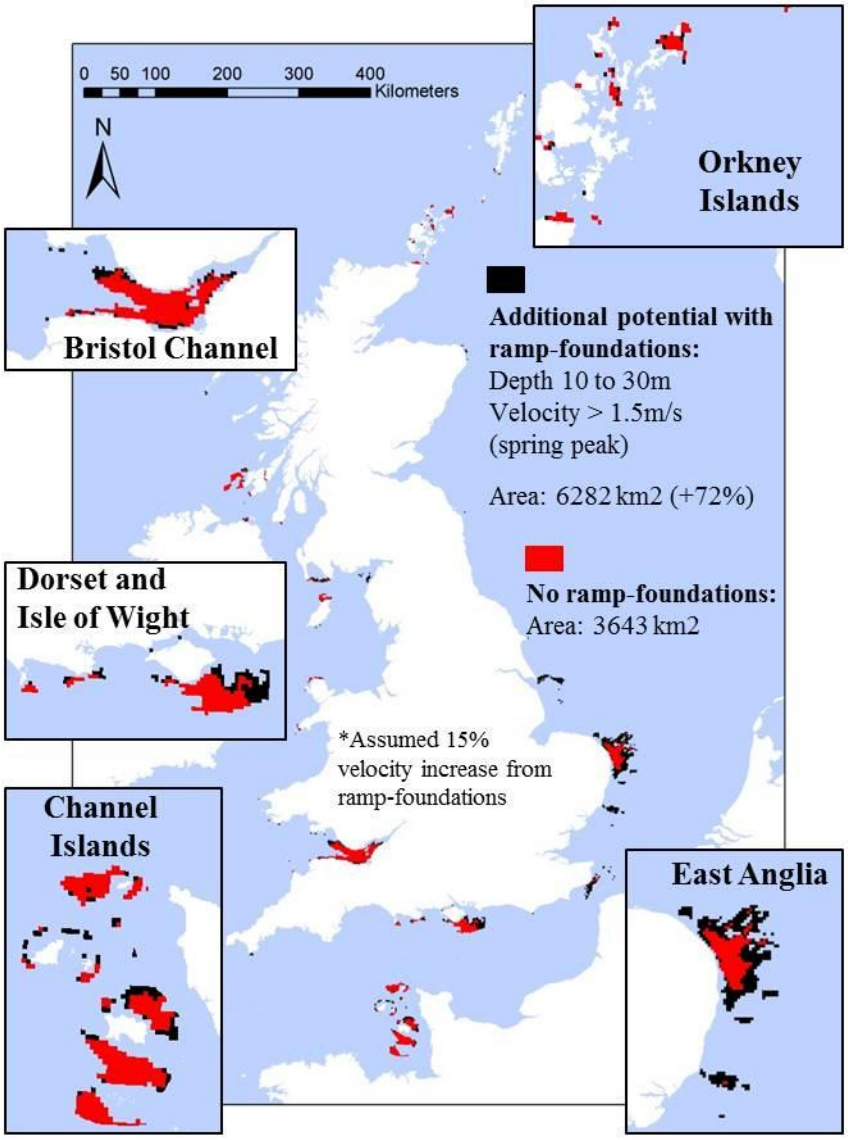

Figure 5-22: Potential shallow flow resource with ramp-foundations

5.2.10 Summary

Ramp-foundation structures could be utilised to locally magnify tidal flow velocities and increase MCEC power output. This initial phase of testing with ramp-foundations showed that the increase in available power was in the region of 15-38%, depending on the ramp size and ramp height/flow depth ratio (the potential will see a reduction once MCEC interaction effects are included). Data from the BWEA "Marine Energy Resource Atlas" was utilised in a GIS model and it was concluded that with the addition of ramp-foundation structures the potential UK shallow tidal resource with depths of 10-30m could be increased by approximately 72%. Further work investigating the suitability of sites based on their lateral ramp span to channel width ratio and the use of higher-resolution data would seek to advance this figure.

This increased velocity and power potential across the ramp results because of two key factors. Firstly continuity and localised flow streaming forces the flow velocity to increase with the flow area reduction across the ramp. Secondly the optimum energy extraction region occurs because of boundary layer redevelopment over the ramp surface. The optimum location is near to the early part of this redevelopment; moving further upstream the profile will not have redeveloped sufficiently and further downstream the growing shear flow region would be undesirable for energy extraction.

It was established that there is an optimum ramp length depending on the ramp height/flow depth ratio. For a ramp height of 1m and a 10m tidal flow depth this would be approximately 10m (e.g. optimum ramp length equals flow depth). In terms of the influence that the ramp side edges have on the across ramp flow it can be concluded that the width of the ramp would not need to considerably exceed the width of the MCEC, as the bulk flow is in the downstream (u-plane) direction and no significant velocity reductions were measured near the ramp side edges.

The extent of the sheared boundary layer region does not significantly increase with the presence of a ramp-foundation; due to mass flow continuity it is effectively compressed by the increased flow velocity in the upper region of the profile. Turbulence intensities were slightly reduced in the flow across the ramp, which would be beneficial to device operation and survival. It is postulated that the increase in flow speed and the associated increase in shear stress close to the ramp-foundation may have reduced some of the smaller length-scale turbulent motion. Additionally the lower surface roughness of the ramp compared with the channel bed could be supporting this effect.

Based on the leading edge tests presented in section 5.2.6, a 45° leading and trailing edge profile to exploit bi-directional flows would be recommended. This provides a good compromise between increased velocity and minimising turbulence/shear stress near the foundation. A 45° profile would require less material for construction than shallower angled ramps and the construction method would be simpler compared with a curved profile.

Section 5.2.7 investigated the surface drop across the structure resulting from the ramp's presence. In reality a tidal flow's Froude number would be in the lower range (Fd < 0.45) and the flow would be laterally unconstrained. So a significant surface drop resulting from the ramp-foundation would not be anticipated at full scale. Flows will be in the upper subcritical range away from critical depth conditions and realistic ramp height to flow depth ratios will be small. However there would be a surface head drop across a MCEC resulting from the fact that it would be extracting energy from the flow.

These ramp only tests show that the degree of flow velocity increase and hence power gain is dependent on the lateral channel span of the ramp-foundation. Clearly a ramp occupying the entire width of the channel would not be feasible except perhaps in a tidal fence application (Giles et al., 2010). Thus when considering the use of ramp-foundations the ramp width or overall array width must be tuned to the local channel width to maximise the power benefits.

This concept would perhaps only be commercially viable for shallow tidal flows with lateral ramp blockage ratios greater than 0.1. Hence at full-scale the concept would be better suited to wider arrays deployed in laterally constrained tidal flows, such as channels between landmasses and straits between islands. The ramp-foundation would also need to be of multi-use. This means in addition to increasing device power output, it would also need to act as an integral foundation and aid scour protection. These initial results are promising for concept development but it must be stressed that the flow interaction and impedance effects of the MCEC are not included and will be investigated in section 5.3.

5.3 Ramp-foundation and device interaction

5.3.1 Experimental approach

Here the effects of MCEC flow interaction and impedance on ramp velocity and power gain are investigated. Again testing is at 1:100 scale and the MCEC is modelled using a porous actuator disk.

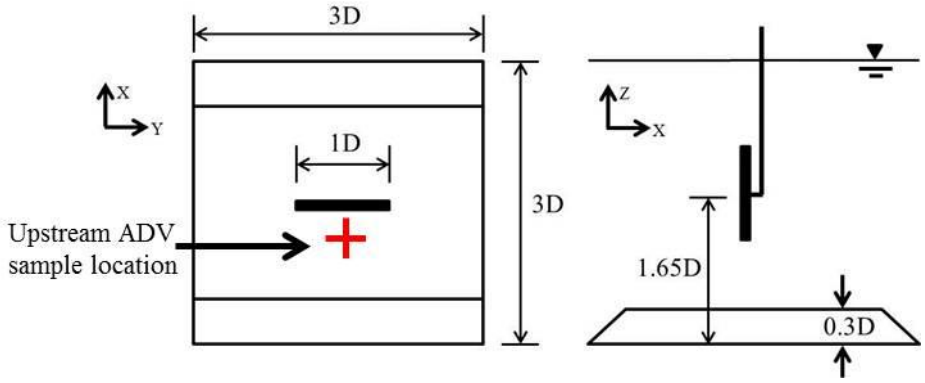

Figure 5-23: MCEC flow interaction and impedance experimental setup. Dimensions given in disk diameters (D)

The ramp only tests (section 5.2) were used to geometrically optimise the ramp-foundation for these interaction tests (Figure 5-23).

Actuator disks are used due to the scaling constraints. Myers and Bahaj (2012) state that with rotor diameters of less than 0.8m problems are associated with the lack of incident energy flux at representative Froude Numbers resulting in power take-off compromises and a reduced range of turbine control (e.g. a narrow range of operational TSR). Hence actuator disks are better suited as an experimental model. For example, if a bladed rotor was modelled at 1:100 scale it would require a rate of rotation in excess of 1500 rpm in order to achieve typical full scale blade tip speeds of 10 m/s. This is clearly not possible and large components of swirl would be induced in the wake. The key limitation of actuator disks is modelling the near wake. But it has been shown in a number of studies that actuators model well the global wake structure and the far wake of horizontal axis turbines, where wake break down is dominated by turbulent mixing induced by the flow surrounding the wake (Myers and Bahaj, 2010, Builtjes, 1978, Sforza et al., 1981, Giles et al., 2011). Near wake differences are generally known to dissipate in fewer than four rotor diameters downstream (Connel and George, 1982, Vermuelen, 1979, Vermeer et al., 2003) for horizontal axis wind turbines. The actuator disk porosity was kept constant throughout testing at 0.48 (ratio of open to closed area). The peak axial induction factor for an actuator disk is 1/3, which equates to an optimum C_t value of 0.9. The chosen porosity gives a C_t value of approximately 0.8 and was calculated from a combination of experimental testing and the

empirical relationship developed by Whelan (2009). The porous disk is pictured in Figure 5-24 (left).

The 100mm diameter actuator disk was positioned in the flow according to Figure 5-23. This was achieved using a lever arm rig that measures the disk thrust (Figure 5-24 (right)). The lever arm was used to mechanically amplify the low thrust forces on the disk and enable thrust to be measured above the water line using a load cell. Thrust was measured by recording the change in voltage across the calibrated load cell and from this the actual disk thrust in Newtons was calculated. The measurement of actuator disk thrust will be used as a direct measure for the increase in performance from a MCEC operating with and without a ramp-foundation.

Figure 5-24: Actuator disk (left). Lever arm rig (right)

The flow field around the actuator disk was characterised using an ADV in the same manner as in the previous ramp only tests (section 5.2). With the physical presence of the disk, it is not possible to take a velocity profile in the precise region of the actuator, but a profile was taken just upstream to map the actuator disk inflow (see Figure 5-23). This is important as the blockage or axial induction effects must be considered as they will directly influence MCEC power potential.

The geometric setup gives a lateral ramp span to channel width ratio of 0.22 for all tests. From the lateral blockage ramp only tests, this ramp blockage ratio gave a velocity gain of 7% and a power gain of 23%.

MCEC thrust comparisons (tests 1-6) and flow contour plots (tests 1,2 & 4) were conducted for the tests detailed in Table 5-3.

Test	Fd	Depth (m)	Average Vel. (m/s)
1	0.15	0.3	0.26
2	0.20	0.3	0.34
3	0.22	0.3	0.38
4	0.25	0.3	0.43
5	0.20	0.2	0.28
6	0.2	0.4	0.41

Table 5-3: MCEC/ramp interaction tests

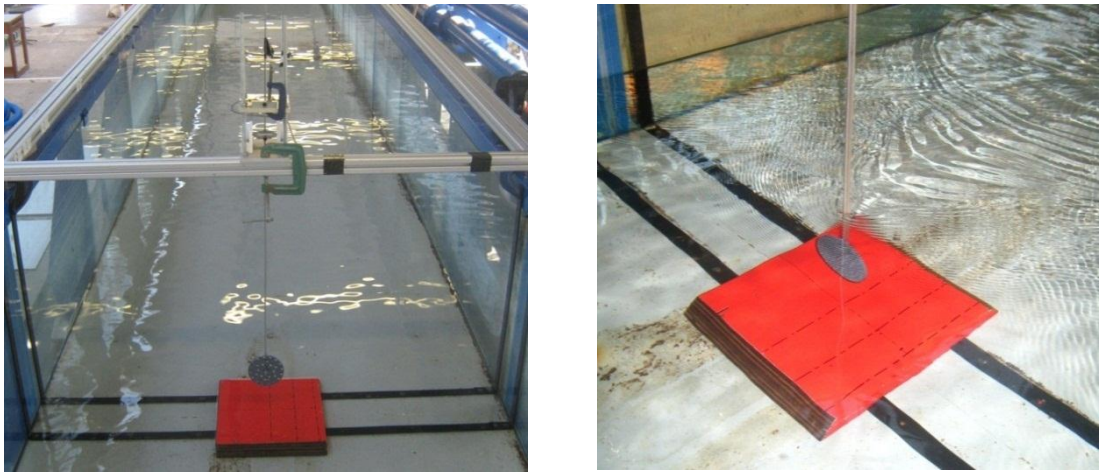

Figure 5-25: MCEC/ramp interaction test photographs

5.3.2 Results

5.3.2.1 Centre-line velocity

Figure 5-26 shows the variation of the horizontal velocity component, u, with height above the bed, h, for the free-stream flow profile and the across ramp profile with and without a MCEC present. At first glance it may appear that the ramp-foundation is providing little flow velocity increase benefit for the MCEC because the free-stream and across ramp profiles are similar, but this is not the case. As would be anticipated from momentum theory, flow velocity at the MCEC is reduced because the static pressure increases upsteam due to the disk's impedence. Energy is then extracted by the MCEC (or in the case of an actuator disk, converted into smaller scale turbulence) and pressure drops downstream of the MCEC. Without the ramp-foundation's presence the magnitude of the velocities would be lower and less energy would be avaiable for extraction (this is confirmed when comparing the thrust in section 5.3.2.3).

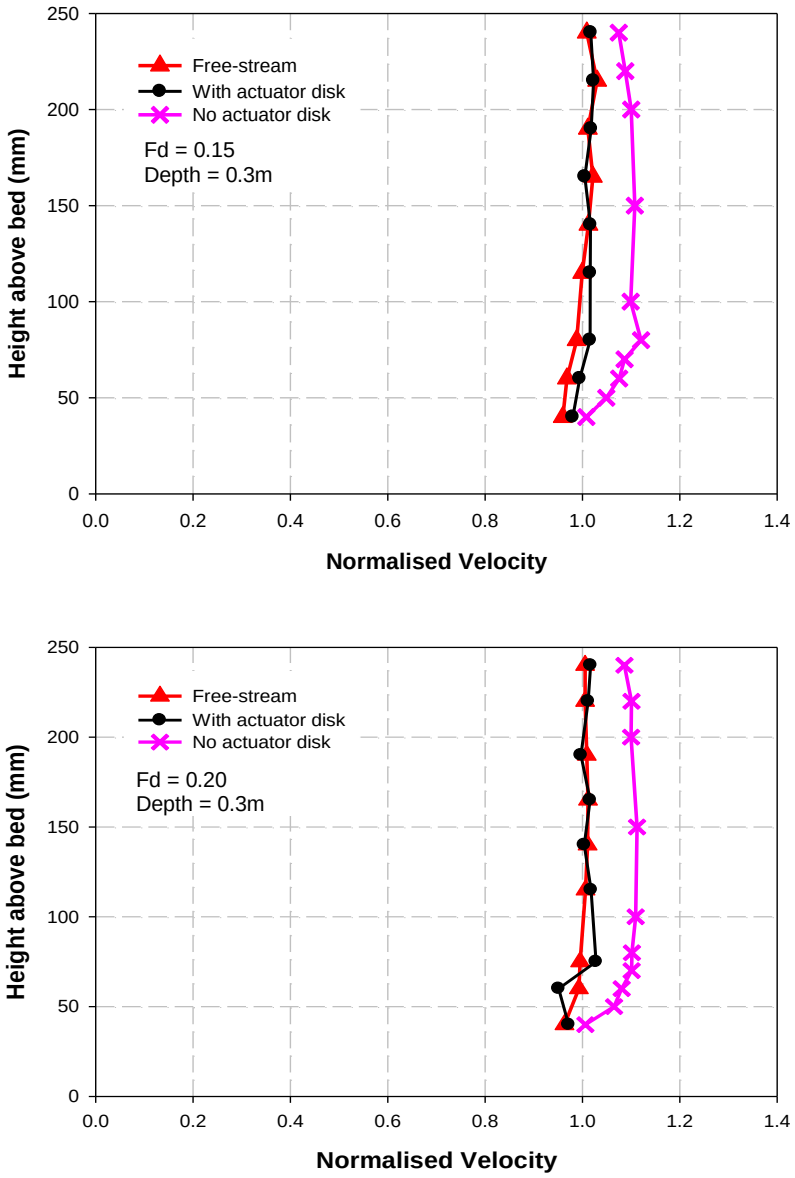

Figure 5-26: Typical vertical velocity profiles across a ramp-foundation with and without actuator disks present. Test 1 (top) and Test 2 (bottom)

A general rule can thus be established; the free-stream velocity profile and across ramp profiles are approximately equal in magnitude (for vertical and lateral ramp blockage ratios of 0.1 and 0.22). One could perhaps say in these cases that the ramp-foundation is effectively removing the flow retardation from axial induction. Figure 5-27 shows the centre-line normalised velocity for test 1 and 2. From this graph and examining other results it can be concluded that wake recovery is independent of the Froude number at constant depth because the flow behaviour and mechanisms are primarily driven by the geometric channel properties, the induction factor of the disk causing the initial reduction in velocity in the near wake and the ambient turbulence that serves to re-energise the wake flow. A similar result was observed during experimental work

presented by Myers et al. (2008). This also means that the axial induction factor is constant for constant flow depths and hence the C_t value can also be assumed to be constant. For the C_t values calculated from the experimental thrust results (section 5.3.2.3) the axial induction factor was found to be 0.26. From Figure 5-27 the axial induction factor is approximately 0.26-0.30, very similar to the 0.26 value calculated from thrust. It is approximate because it is not possible in reality to measure the velocity at the disk due to its physical presence. Figure 5-27 also shows that at 20 disk diameters downstream all but 10% of the free-stream velocity has been recovered. For MCT's SeaGen device the peak C_p = 0.52, hence the peak axial induction factor is 0.21. As C_t and C_p are directly related to actuator disk porosity, the actuator disk used during the tests has a theoretical C_p value of 0.57. At first sight this appears slightly high but this value does not consider any turbine and power train losses. If these were included the value would be close to that of MCT's figure.

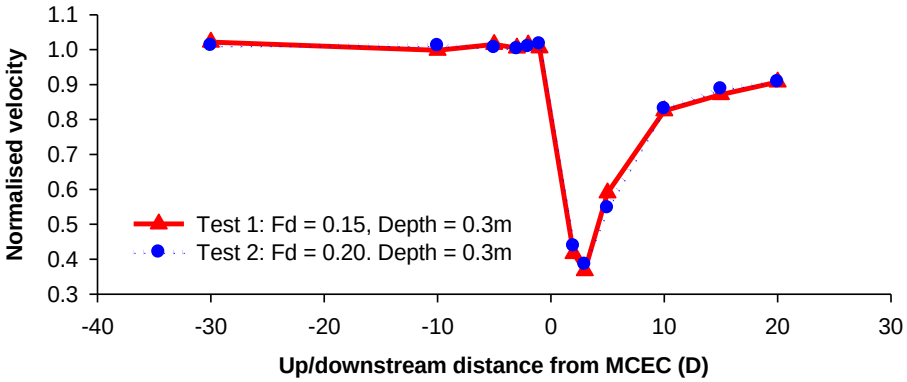

Figure 5-27: Upstream/downstream centre-line velocity

Figure 5-28 shows the lateral cross-channel wake recovery for tests 1 and 2. The very similar trend for wake recovery between the different Froude numbers can again be visualised and reinforces the fact that wake recovery is independent of velocity at a constant flow depth (and channel width). The velocity profiles (-1D and 2D) close to the actuator disk show some signs of increase in lateral velocity around the sides of the disk, with values in the region of a 6-8% increase on the free-stream value. These values are slightly higher than those found in chapter 7 (wake structures resulting from vertically constrained tidal flows) but this is expected because of the increased vertical flow constraint from the ramp's presence. Chapter 7 shows that for increased vertical constraint the velocity of the lateral flows on either side of the MCEC will increase. As vertical channel blockage increases the flow above and below the device is restricted and in order to maintain flow continuity the lateral side-channel flow must increase.

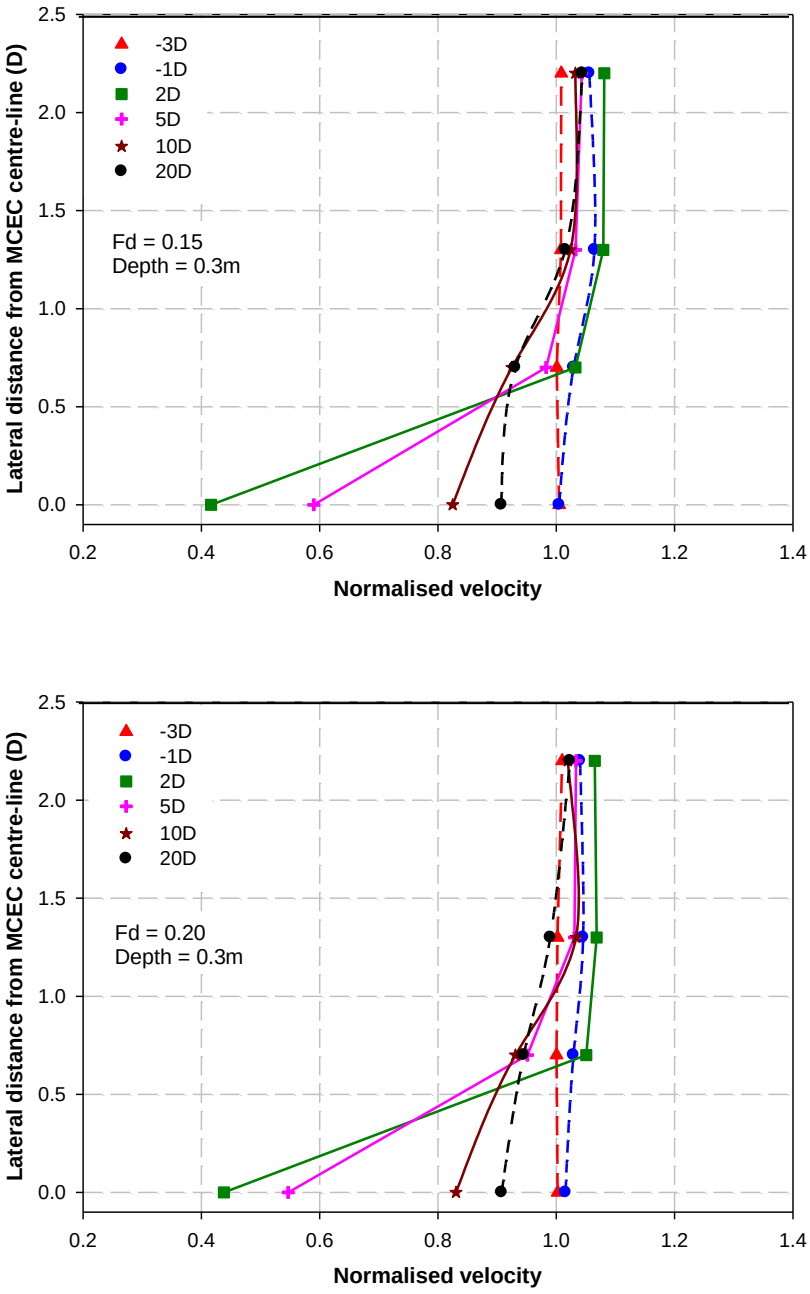

Figure 5-28: Lateral (cross-channel) hub-height velocity. Test 1 (top), test 2 (bottom)

5.3.2.2 Velocity and turbulence intensity visualisation

Figure 5-29 shows typical downstream vertical (xz-plane) plane flow fields around a horizontal axis MCEC (with 108 ADV data sample points). The plot clearly shows the reduced velocity flow immediately upstream of the device, the increase in flow velocity above/below the MCEC and the downstream wake development. In both tests the region of increased velocity flow below the MCEC is caused by the presence of both the ramp and MCEC. Just downstream of

the ramp, a region of boundary layer re-development can be identified. This boundary layer re-develop occurs in a similar manner to the across ramp profile, due to the abrupt change in channel bed elevation (ramp height) and continuity as flow leaves the ramp's trailing edge. It seems that the majority of the downstream wake is dissipated within 20 disk diameters. This agrees with work presented by Myers and Bahaj (2010) which showed significant velocity recovery (up to 95%) at 20-diameters downstream, for a turbulence intensity of ≈8%, suggesting faster recovery if ambient turbulence intensity is higher at a full-scale site. The wake length is slightly longer (+1-1.5D) but in general is very similar to that of a MCEC operating in the same flow depth without a ramp-foundation because as Figure 5-29 shows the ramp's downstream influence on the wake is small (see chapter 7). It is therefore encouraging in terms of farm spacing that the addition of a ramp-foundation does not appear to significantly increase the wake length.

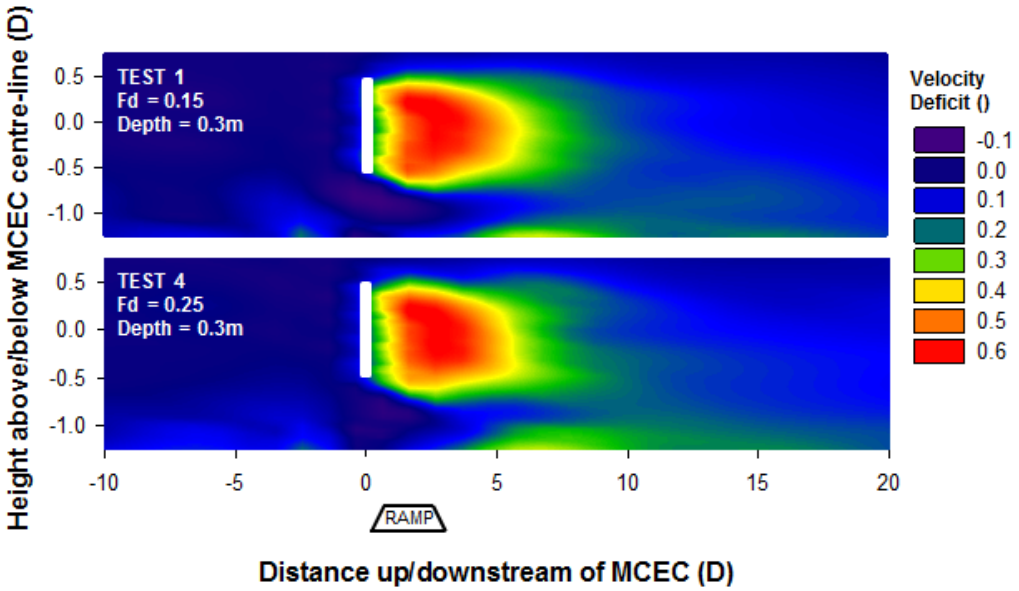

Figure 5-29: xz plane, u-velocity, contour plots. Test 1 (top), test 4 (bottom)

Figure 5-30 shows the u-plane Turbulence Intensity (xz-plane). The wake region behind the MCEC is clear, depicted by the higher turbulence levels. Again the wake structure similarities between the two different Froude number tests can be seen with similar turbulent intensity profiles. The lower section of the plots shows the area of higher turbulence intensity generated downstream of the ramp-foundation which corresponds to the previously described region of boundary layer re-development. This region does not seem to interfere directly with the wake structure, but as discussed in Chapter 7 if the flow depth was reduced further, given its similar properties to the wake, the boundary layer could combine with the wake. This could result in a longer wake structure due to the reduction in velocity gradient between the wake and bounding flow.

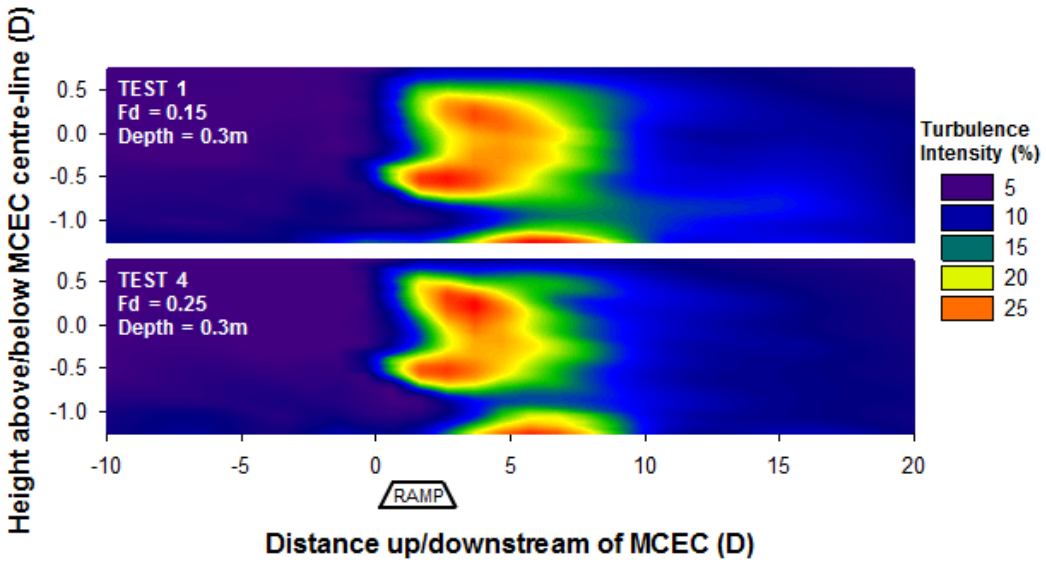

Figure 5-30: xz plane, u-turbulence intensity, contour plots. Test 1 (top), test 4 (bottom)

Figure 5-31 confirms that the lateral extent of the wake does not expand, with significant velocity deficits, beyond 2 times the MCEC diameter. This results from the fact that the bulk flow is in the stream-wise direction. Longitudinal downstream spacing is the key driver for array design rather than these small lateral wake expansions.

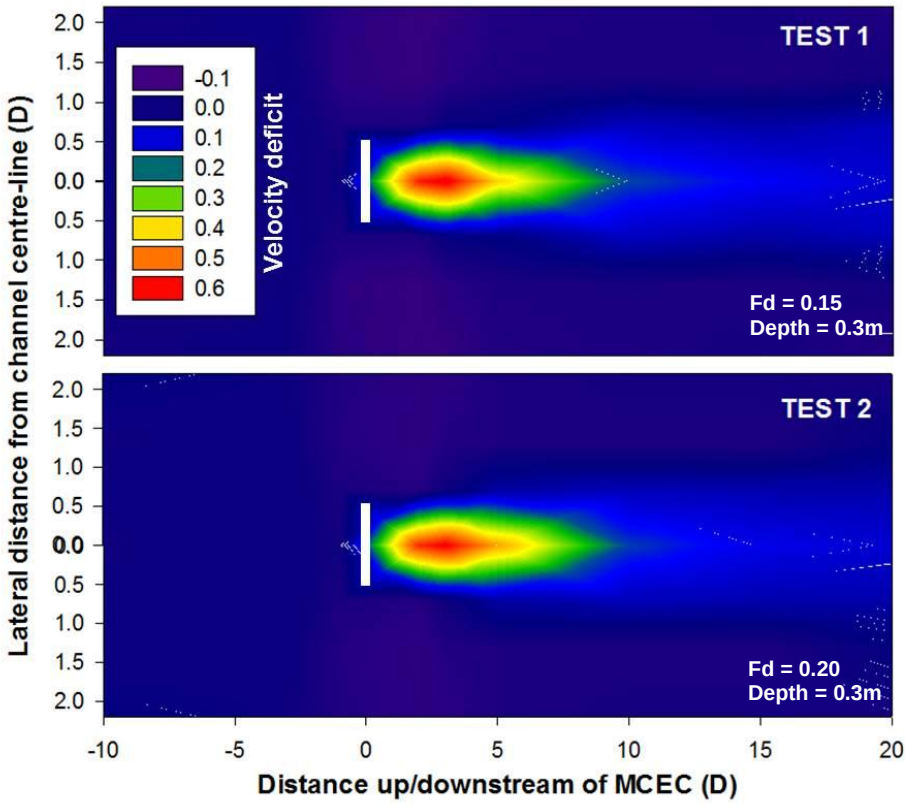

Figure 5-31: XY plane, u-velocity, contour plots. Test 1 (top), test 2 (bottom)

5.3.2.3 Thrust measurements

In order to measure the device thrust and power gains these combined ramp and actuator disk tests were conducted. Some key thrust measurement results are presented in Table 5-4. Thrust was measured directly using the load cell and power gain was calculated using momentum theory (section 3.2). An allowance for the small amount of thrust loading on the lever was calculated and subtracted from the total recorded thrust. During the testing no significant support arm vibrations were observed. The lever arm's natural frequency was calculated as approximately 12.8 Hz in the downstream direction and 5.1 Hz in the lateral cross-channel direction.

Test	Fd	Depth (m)	Thrust no ramp (N)	Thrust with ramp (N)	Thrust gain (%)	Power gain (%)
1	0.15	0.3	0.20	0.22	**6.64**	**10.12**
2	0.20	0.3	0.31	0.34	**9.62**	**14.76**
3	0.22	0.3	0.39	0.43	**9.78**	**15.02**
4	0.25	0.3	0.48	0.52	**8.83**	**13.53**
5	0.20	0.2	0.21	0.25	**18.76**	**29.42**
6	0.20	0.4	0.44	0.48	**7.04**	**10.74**

Table 5-4: MCEC/ramp interaction thrust results

It can be concluded from these tests that when modelling ramp-foundations with the presence of a MCEC the thrust and power benefits will be reduced compared with the gain inferred by the increase in flow velocity alone. Average power benefits for different tested Froude numbers are in the region of 12-15% for the lateral ramp blockage ratio (R_L) of 0.22 and a vertical ramp blockage ratio of 0.1 (a ramp occupying 10% of the flow depth). These power gains are approximately 40% less than those presented in section 5.2. The justification for this reduction in potential is that the combined flow impedance effect of the MCEC device and ramp-foundation is forcing a proportion of the flow around and away from the influence of the ramp (see lateral flow velocity increases around the MCEC in Figure 5-28).

Figure 5-32 shows the increase in thrust with lateral ramp span to channel width ratio for the two experimental methods, the combined experimental velocity gain/axial momentum theory and the direct measurement of actuator disk thrust. Figure 5-33 shows the MCEC power gains predicted using thrust results and momentum theory; and again highlights the importance of the ramp's lateral channel span. The lateral ramp blockage results from section 5.2.8 were factored using the average thrust and power gains from Table 5-4 for a ramp interacting with an actuator disk (MCEC) and a vertical ramp height to flow depth ratio of 0.1. With increased lateral ramp span (e.g. a wider ramp/device width or a wider array) the power gain potential of ramp-foundations increases significantly. The optimum lateral ramp blockage ratio for a device or

array appears to be 0.5 because a full channel width ramp only increases power gain by a further 1%. It is postulated that this optimum ratio occurs because localised flow streaming effects are more significant than the flow continuity effects at ratios of less than 0.5. At the larger ramp blockage ratios velocity increase is dominated by flow continuity effects and the localised flow component is less substantial. Hence due to the decreasing velocity component from localised flow-streaming power gain remains relatively constant for lateral ramp blockage ratios above 0.5. Until large arrays are deployed and occupy large widths of tidal channels, lateral ramp blockage ratios for initial tidal stream developments are likely to be at the lower end of the spectrum with power benefits of <10% across a tidal cycle. This is still a significant figure in terms of energy return but must be investigated in relation to the increased capital investment of the ramp-foundation itself (see chapter 8, section 8.9).

Although these results reveal that the potential for power/thrust amplification is less than previously calculated, it must be reiterated that ramp-foundations have multiple benefits in addition to increasing energy yield; they make up a large proportion of the foundation down-force, can offer scour protection and could provide an engine room for machinery.

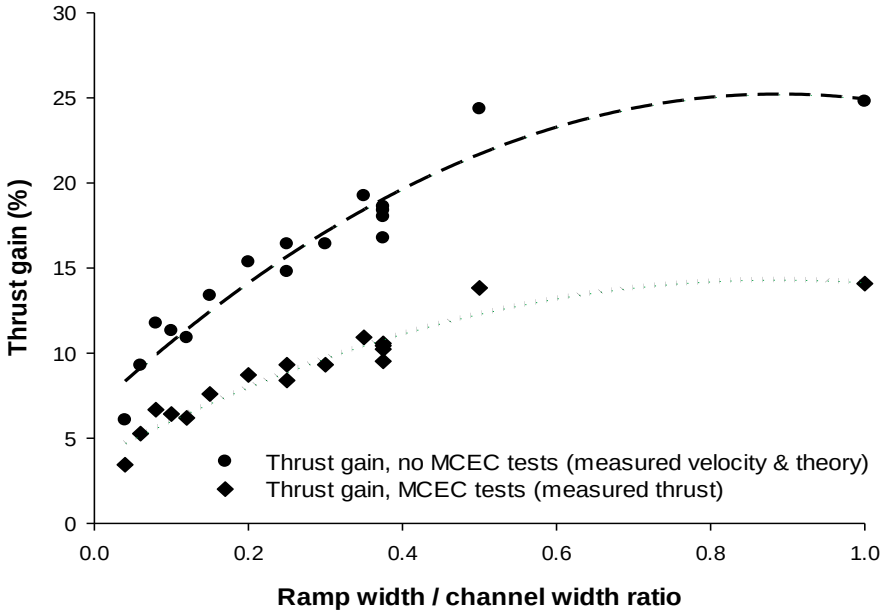

Figure 5-32: Comparison of expected thrust results for different lateral ramp blockage ratios, from theory and measured

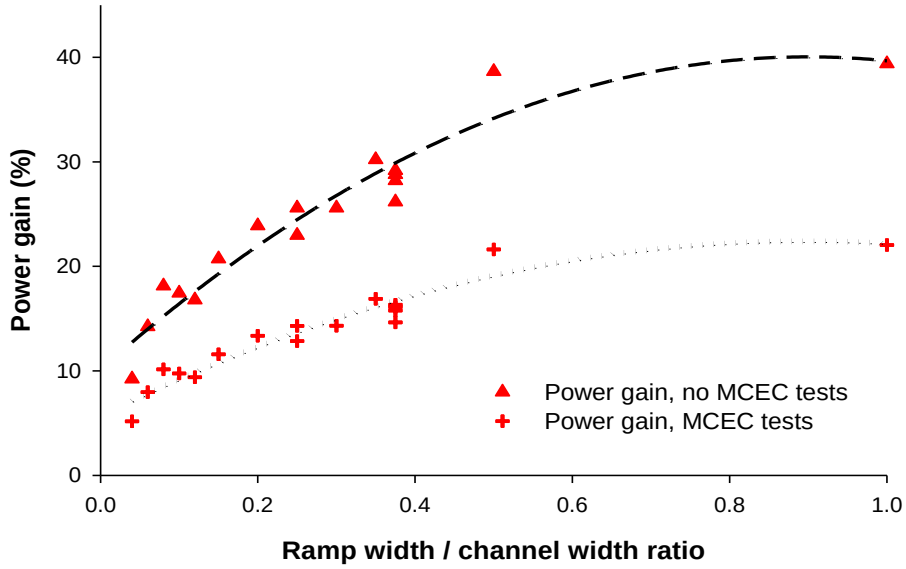

Figure 5-33: Comparison of expected ramp-foundation power gains for different lateral ramp blockage ratios

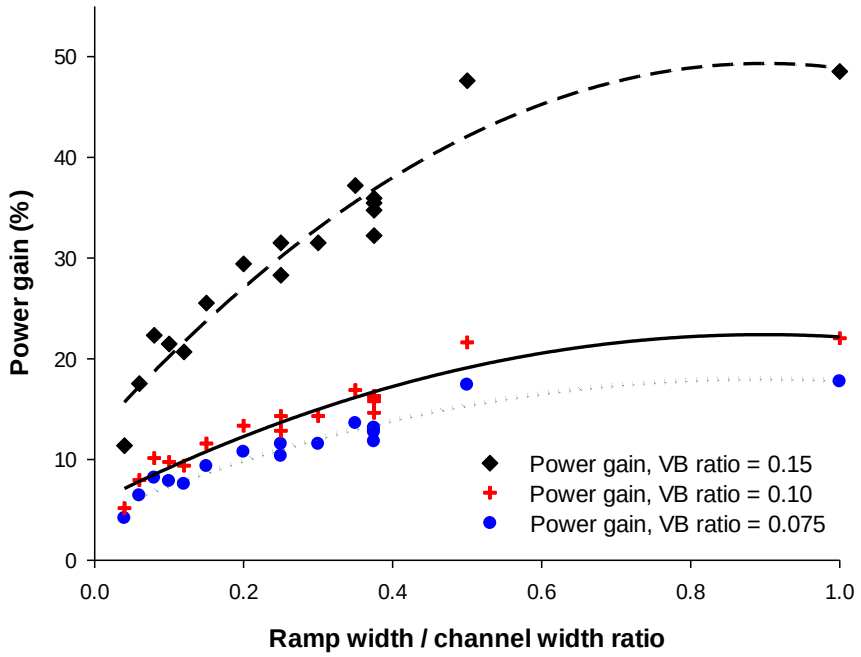

Figure 5-34: Comparison of expected ramp-foundation power gains for different vertical (VB) and lateral ramp blockage ratios

Figure 5-34 shows results for vertical ramp blockage ratios (ramp height/flow depth) of 0.075, 0.1 and 0.15. The results in ratio terms are in keeping with the vertical ramp blockage velocity results presented in section 5.2. When the ramp height to flow depth ratio is high (e.g. shallow depth and high ramp, VB = 0.15) the resulting power gains are considerably higher than with the 0.1 vertical ramp blockage ratio. Hence both lateral and vertical ramp dimensions are critical

factors when designing/optimising these foundations. As previously stated the reduction in power gain with decreasing lateral ramp span is a combined function of, flow cross-sectional area continuity and localised flow streaming effects due to vertical boundary layer modification and the fact that the bulk flow has momentum and hence a resistance to directional change in the downstream direction. If power gain was simply calculated from channel area reduction continuity of the mass flow the expected power gain would be almost insignificant at the low lateral ramp blockage ratios. This confirms the presence of localised flow effects and Figure 5-34 highlights the importance of decoupling vertical and lateral ramp flow blockage. The tests in this project have assumed a ramp occupying 10% of the water column to be optimum in terms of construction economics and energy gain (see chapter 4).

5.3.3 Summary

The combined ramp-foundation and MCEC experimental testing presented here in section 5.3 conclude that the thrust and hence power benefits of a ramp-foundation decrease from 9-38% to 5-22% when a MCEC is interacting with a ramp occupying 10% of the water column (varying with the ramp width to channel width ratio). Importantly this combination represents the full scenario and the reduction in benefit can be attributed to the increased channel flow impedance presented by the MCEC. The MCEC solidity is effectively forcing a proportion of flow away from the ramp/MCEC. Despite this reduction it must be reiterated that ramp-foundations offer multiple benefits besides increased energy yield. Such benefits include: added foundation down-force, scour protection and an engine room for machinery. In terms of calculating thrust and power benefits from ramp-foundations these interaction results from section 5.3 must be used. The ramp only results from section 5.2 can still be utilised for geometric optimisation of the foundation. Combining the findings from 5.2 and 5.3 it can be concluded that ramp power gain is a function of channel flow continuity from the ramp's physical presence, localised flow streaming effects and impedance effects from the MCEC's solidity.

It is interesting to compare the wake with the case from chapter 7 where the MCEC is characterised without a ramp-foundation. In general the results are similar, but the wake appears to be slightly longer (+1-1.5D). This is because the additional vertical obstruction from the ramp restricts further the flow above and below the MCEC and hence reducing the sheared flow between the wake and free-stream flow. This increase in length is not substantial and would not impact significantly with the applicability of ramp-foundations and downstream farm spacing.
The lateral extent of the wake does not expand with significant velocity deficits beyond 2 times the MCEC diameter. This results from the fact that the bulk flow is in the stream-wise direction.

Longitudinal downstream spacing is the key driver for array design rather than smaller lateral wake expansion.

The optimum lateral ramp blockage ratio for a device or array appears to be 0.5, as for a full channel width ramp-foundation there is only a further 1% increase in power gain. It is postulated that this optimum ratio occurs because localised flow streaming effects are still more significant than the flow continuity effects at ratios of less than 0.5. At the larger ramp blockage ratios velocity increase is dominated by flow continuity effects and the localised flow component is less substantial. Hence due to the decreasing velocity component from localised flow-streaming power gain remains relatively constant for lateral ramp blockage ratios above 0.5. Until large arrays are deployed and occupy large widths of tidal channels, lateral ramp span ratios for initial tidal stream developments are likely to be at the lower end of the spectrum with power benefits of <10% across a tidal cycle. This is still a significant figure in terms of energy return, but the concept must also be investigated in relation to the increased capital investment of the ramp-foundation (see chapter 8, section 8.9).

In terms of the ramp's vertical presence, when the ramp height to flow depth ratio is high (e.g. shallow depth and high ramp) the resulting power gains are considerably higher than with lower vertical ramp blockage ratios. Hence both lateral and vertical ramp dimensions are critical factors when designing/optimising ramp-foundations.

Table 5-5 highlights the variation in the three different power gain calculation methods used during this project for full channel width ramp-foundations. It is encouraging to see the similarities between the simple 1D model (chapter 4) and the ramp only tests (section 5.2). The reduction in potential found during the MCEC/ramp interaction tests can be attributed to the flow impedance effects from the MCEC, which diverts a proportion of the flow away from the influence of the MCEC and ramp-foundation. This effect is confirmed by the increase in the lateral flow components found in section 5.3.

Calculation Method	**Power gain potential, full channel width ramp (%)**
1D theory (chapter 4)	**38**
Ramp only tests (chapter 5, section 5.2)	**38**
MCEC/ramp interaction (chapter 5, section 5.3)	**22**

Table 5-5: Power gain estimation method comparison

1.4 Empirical relationships

1.4.1 Introduction

Empirical relationships for both the velocity and power gain from a ramp-foundation are developed from theoretical relationships and compared with the experimental data. The relationships take into account both the vertical ramp blockage (ramp height to channel depth ratio) and lateral ramp blockage (ramp width to channel width ratio).

1.4.2 Empirical velocity gain

The velocity increase across a ramp-foundation for lateral ramp blockage ratios (equation 5.3) between 0 and 0.5 can be described as a function of the:

1. Ratio of the flow area above the ramp (A1) to the flow area in the 'bypass' channels either side of the ramp-foundation (A2).
2. Velocity gain from a full channel width ramp-foundation, (calculated form the 1D theory equation 4.11, developed in chapter 4). Referred to as $V_{\substack{max \\ gain}}$
3. "localised flow streaming factor" of 10/27 – this empirical modification factor represents the additional velocity increase from the localised flow effects across the ramp. If the factor was set to unity the empirical relationship would only represent the velocity increases due to consideration of the reduction in cross sectional area of the channel. This increase is averaged over the channel according to principles of one-dimensional continuity whereas in reality this is not the case due to more complex three-dimensional flow interaction effects. During the testing presented in section 5.2.8 it was found velocity increases exceed the values from area continuity. It is postulated that these localised effects result from compression of the vertical extent of the boundary layer across the ramp and flow streaming occurring from the fact that the bulk flow has momentum and hence a resistance to directional change in the downstream direction.

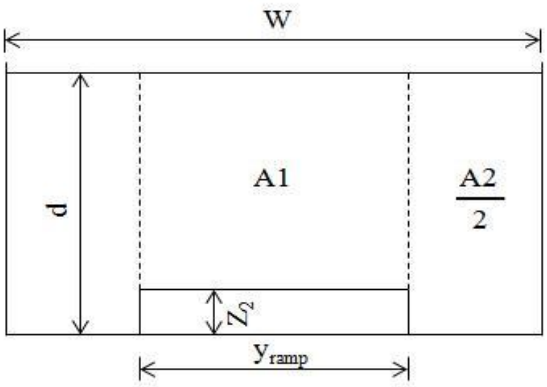

Figure 5-35: Empirical area relationship

The empirical relationship for ramp velocity gain with varying vertical and lateral ramp blockage ratios (between 0 and 0.5) can be described by equation 5.4.

$$V_{gain} = \underset{gain}{V_{max}} \left(\frac{A1}{A2}\right)^{\frac{10}{27}} = \underset{gain}{V_{max}} \left(\frac{y_{ramp}(d-Z_2)}{d(W-y_{ramp})}\right)^{\frac{10}{27}} \quad (5.4)$$

where:

$$\frac{(d-Z_2)}{d} = \frac{Ramp\ Height}{Channel\ Depth} = VB\ ratio \quad (5.5)$$

$$\frac{y_{ramp}}{(B-y_{ramp})} = \frac{Ramp\ Width}{Bypass\ Channel\ Width} \quad (5.6)$$

$$\underset{gain}{V_{max}} = 100 \times \left[\frac{3d_1}{a}\left[2cos\left(\frac{cos^{-1}\left(1-\frac{27q^2}{4ga^3}\right)}{3}\right)+1\right]^{-1}\right] - 100 \quad (5.7)$$

$where: a = d_1 + \frac{{u_1}^2}{2g} - Z_2$

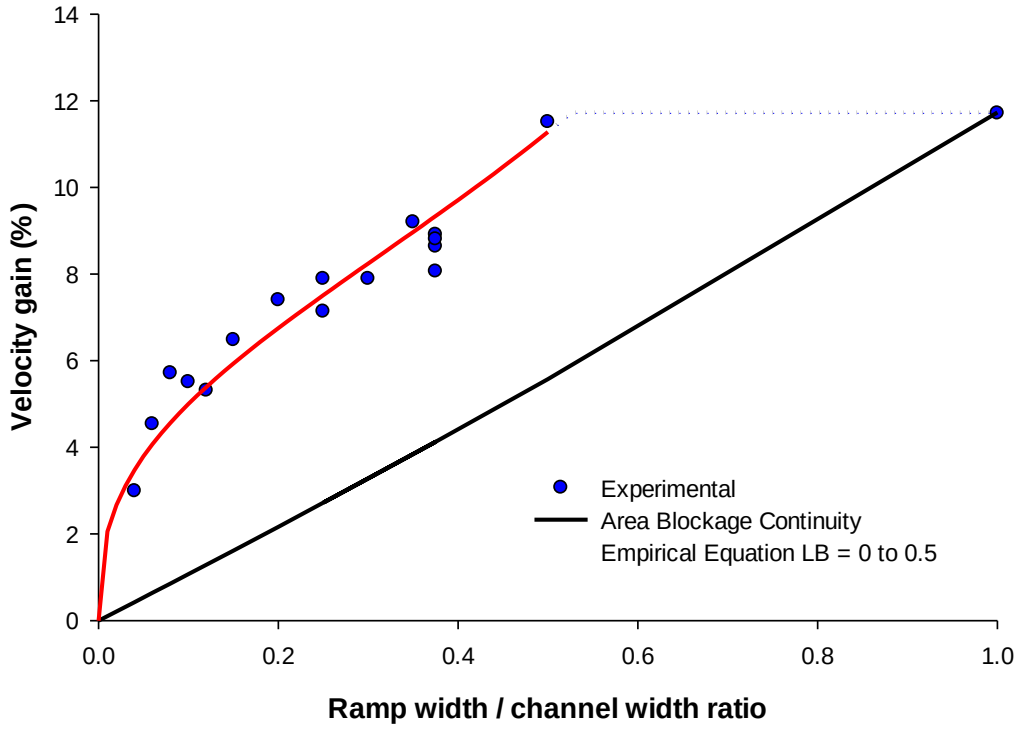

Figure 5-36: Empirical velocity gain relationship vs. experimental data

Figure 5-36 shows a comparison of the empirical relationship from equation 5.4 with lateral ramp blockage experimental data from section 5.2.8 for a vertical ramp blockage ratio of 0.1 (ramp occupying 10% of the flow depth). Visually in Figure 5-36 the empirical relationship

represents the experimental results with good agreement for lateral ramp blockage ratios from 0 to 0.5 and the average overall error from experimental data points was calculated at approximately 8%.

Figure 5-36 can be divided into two velocity increase regions, the lower triangular portion can be attributed to flow cross-sectional area continuity. The upper section above the continuity line can be attributed to localised flow streaming effects, that result from vertical boundary layer modification and flow streaming occurring from the fact that the bulk flow has significant momentum and hence a resistance to directional change in the downstream direction. This resulting downstream flow momentum therefore prevents large proportions of lateral cross-channel flow and the reported velocity gains are larger than simply considering one-dimensional area continuity. Without these localised effects velocity gains would be almost insignificant when deploying smaller ramps in large cross-section channels. For lateral ramp span to channel width ratios greater than 0.5 the empirical fit breaks down and it appears that velocity gain does not increase dramatically above that of a full channel width ramp, illustrated by the dotted line in Figure 5-36. These effects were discussed further in section 5.2.8.

1.4.3 Empirical power gain

The overarching objective of the ramp-foundation is to increase the available power per unit channel cross sectional area by physically constraining the tidal flow. Low velocity shallow currents can thus be constrained and the velocity increased to an exploitable level. Using the same approach as in section 5.4.2 a similar empirical relationship for the power gain potential of ramp-foundations for varying vertical ramp blockage, and lateral ramp blockage ratios between 0 and 0.5 can be developed. Instead of using the maximum velocity gain, now the maximum power gain for a full channel width ramp-foundation is substituted into equation 5.4 to yield equation 5.8.

$$P_{gain} = P_{\substack{max \\ gain}} \left(\frac{A1}{A2}\right)^{\frac{10}{27}} = P_{\substack{max \\ gain}} \left(\frac{y_{ramp}(d-Z_2)}{d(W-y_{ramp})}\right)^{\frac{10}{27}} \quad (5.8)$$

$P_{max\ gain}$ comes from the maximum power gains calculated from the MCEC thrust results for full channel width ramps presented in section 5.3. Figure 5-37 shows the close correlation between the empirical fit and the experimental estimate of power gain for lateral ramp blockage ratios from 0 to 0.5. The error between empirical and experimental was again approximately 8%.

Based on these results it appears reasonable to use the empirical relationship to estimate the full-scale power gain potential of ramp-foundations deployed in tidal channels with lateral ramp span to channel width ratios in the validated range of 0.04 to 0.5. For ratios greater than 0.5 the empirical fit breaks down and it appears power gain tends towards the full channel width power gain, illustrated by the dotted lines in Figure 5-37. As with velocity gain, power gain can be described as a function of channel cross-section continuity and localised flow streaming effects. The empirical relationship could be applied to single devices deployed in narrow channels or could be expanded to estimate the potential of wider arrays or tidal fences. Section 5.5 applies the empirical relationship to potential full-scale MCEC deployment sites.

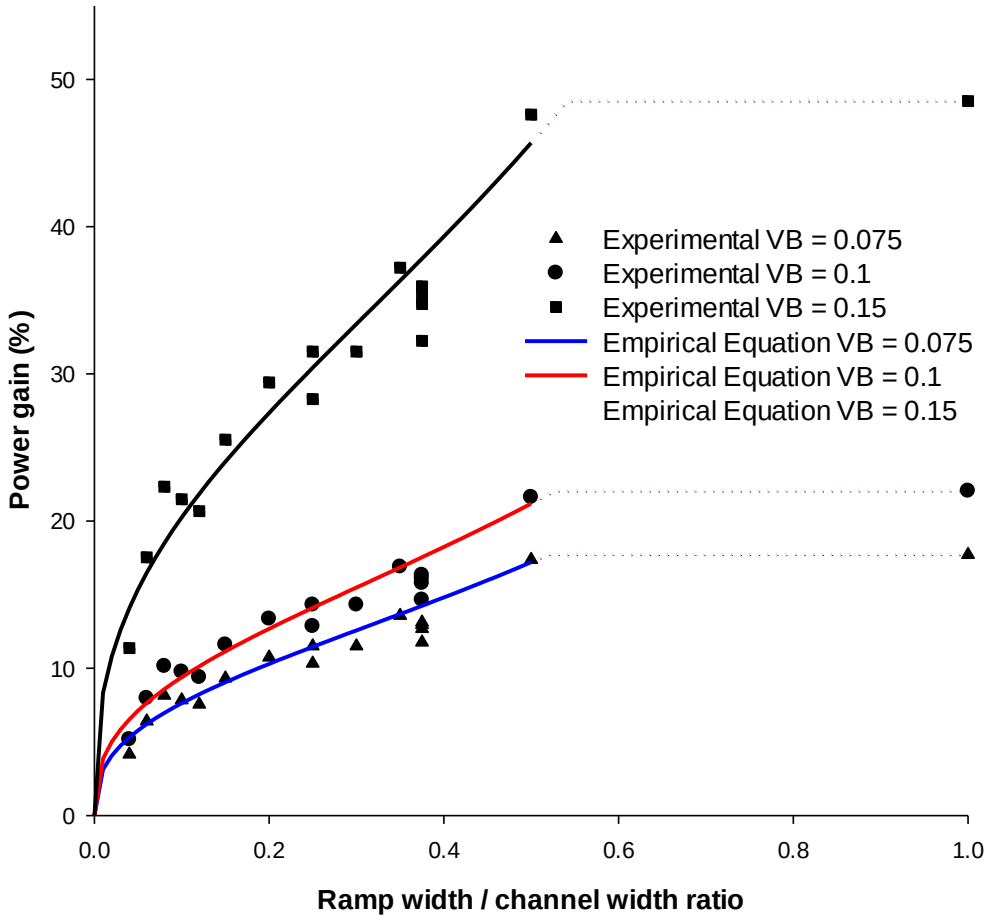

Figure 5-37: Empirical power relationship vs. experimental estimate

5.5 Full-scale performance

In this section the power benefits of ramp-foundations across a full tidal cycle are investigated for four different shallow tidal case study sites (Figure 5-38 and Table 5-6). Average free stream spring and neap peak velocities are taken from tidal diamonds on Admiralty charts (Table 5-6) and the corresponding tidal flow heights are found from commercial chart plotting software. A standard tidal sine wave is fitted to these average tidal diamond values to give an estimated average 14 day tidal cycle for the maximum mean spring and neap tidal velocities (Figure 5-40). Using the 14 day peak sine wave a full hour-by-hour tidal velocity profile is estimated by factoring the daily ebb and flood tides according to the ratios of the tidal diamond (Figure 5-40). A full corresponding tidal height profile is developed in a similar manner. Maximum velocity tides are assumed to occur at mid-tide height for both spring and neap tides due to their phase difference in shallow tidal waters.

Figure 5-38: Example full-scale tidal deployment site map

Site	**LAT m**	**Msp** (ebb) **m/s**	**Msp** (flood) **m/s**	**Mnp** (ebb) **m/s**	**Mnp** (flood) **m/s**	**Range m**
Strangford Narrows	20	4.01	3.70	2.01	1.85	5.41
Kyle Rhea	20	3.03	1.46	1.46	0.70	5.28
Menai Strait	15	1.70	1.44	0.87	0.77	4.51
Bristol Channel	20	1.65	1.65	0.77	0.77	11.67

LAT = Lowest Astronomical Tide Msp = Mean spring tide peak velocity
Mnp = Mean neap tide peak velocity

Table 5-6: Example full-scale tidal deployment sites

The sites were chosen because of their significance for current and future deployments of MCECs. Strangford Narrows is the location for MCT's SeaGen turbine, Kyle Rhea is a potential deployment location for Pulse Tidal's 1.2MW commercial demonstration device, the Menai Strait was chosen as a suitably narrow channel to maximise ramp-foundation efficiency and the Bristol Channel is a wider channel example, which was the proposed location for a full channel width tidal fence scheme (Giles et al., 2010). All locations, except the Bristol Channel, are relatively narrow (Table 5-7) and hence assumed most suitable for ramp-foundation deployment. Figure 5-39 clearly shows that Strangford Narrows has the greatest potential in terms of velocity. Both the Menai Strait and the Bristol Channel have much lower peak velocities which may be uneconomical for pure tidal stream technology.

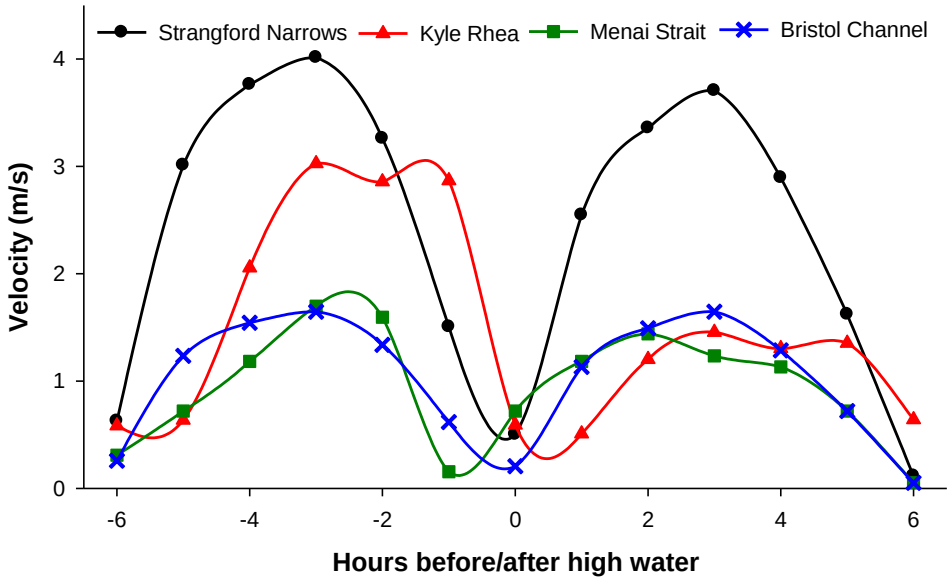

Figure 5-39: Average ebb and flood spring tide velocities (from tidal diamonds)

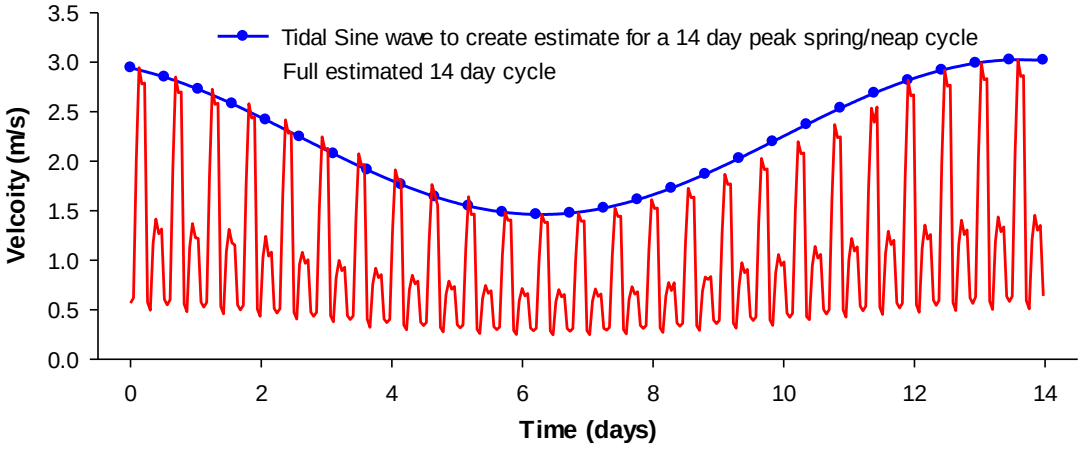

Figure 5-40: Estimated full 14 day tidal cycle for Kyle Rhea

For each site the ramp-foundation height is assumed to be 10% of the average flow depth, informed from chapter 4. The rotor diameter (Table 5-7) is taken as half of the average flow depth to avoid the sheared lower 25% of the flow depth and the wave effects in the upper 25% region (European Commission, 1996). It is also assumed that when a device is operating above a ramp-foundation, the rotor diameter can be kept equal in size to a MCEC operating without a ramp-foundation (see chapter 4, section 4.5).

Site	Ramp height m	Turbine diameter m	Channel width m	Average Ramp height/flow depth ratio
Strangford Narrows	2.3	11.44	650	0.1
Kyle Rhea	2.3	11.50	400	0.1
Menai Strait	1.8	8.87	315	0.1
Bristol Channel	2.6	12.77	16500	0.1

Table 5-7: Further channel parameters

The power potential from a MCEC without a ramp-foundation is calculated from momentum theory. The following turbine parameters are assumed: a C_p value of 0.4, a turbine cut-in velocity of 0.4m/s and a rated velocity of 3m/s. The power generated for each time step in the tidal cycle is calculated and an annual energy yield in MW-hours is calculated for each location.

For each site (Figure 5-38) four different MCEC/ramp deployment scenarios are considered. Here it is assumed that the power from the increased number of turbines is independent of MCEC channel blockage, which would of course not be the case for a large array. However the method provides a baseline comparison. The four scenarios under consideration are:

1. A single device
2. A twin rotor "SeaGen" type device
3. A small 10 turbine array deployed in a single cross channel row.
4. A full channel width row of tidal stream devices (tidal fence) with a full channel width ramp-foundation.

As concluded from the empirical relationships in section 5.4 the lateral ramp blockage for a tidal device or farm has a significant effect on the power gain potential of ramp-foundations. The subsequent power gain potential is calculated across the tidal cycle for each of the locations and for the different deployment scenarios detailed in points 1-4 above. Each scenario has a very different lateral ramp blockage ratio (Table 5-8). The vertical ramp height to channel depth ratio at each site does not vary significantly from 0.1, hence the 0.1 empirical curve was used from Figure 5-37 throughout the analysis.

Site	**Single turbine**	**Twin rotor ("SeaGen")**	**10x turbine row**	**Full channel fence**
Strangford Narrows	0.02	0.04	0.21	1.00
Kyle Rhea	0.03	0.06	0.35	1.00
Menai Strait	0.03	0.06	0.34	1.00
Bristol Channel	0.0008	0.0015	0.01	1.00

Table 5-8: Lateral ramp blockage ratios for the four deployment scenarios

Figure 5-41 shows the annual energy yield for each of the tidal sites and the four different lateral ramp blockage deployment scenarios. In general it is clear that Strangford Narrows and Kyle Rhea are the better sites for deploying small MCEC arrays due to their higher free-stream tidal currents and narrow channel dimensions. The Bristol Channel works with a tidal fence application but requires nearly 1000 turbines to achieve a significant energy yield. Figure 5-41 also shows how the power potential from ramp-foundations increases dramatically with higher lateral ramp span ratios, such as with a 10 turbine row or a tidal fence.

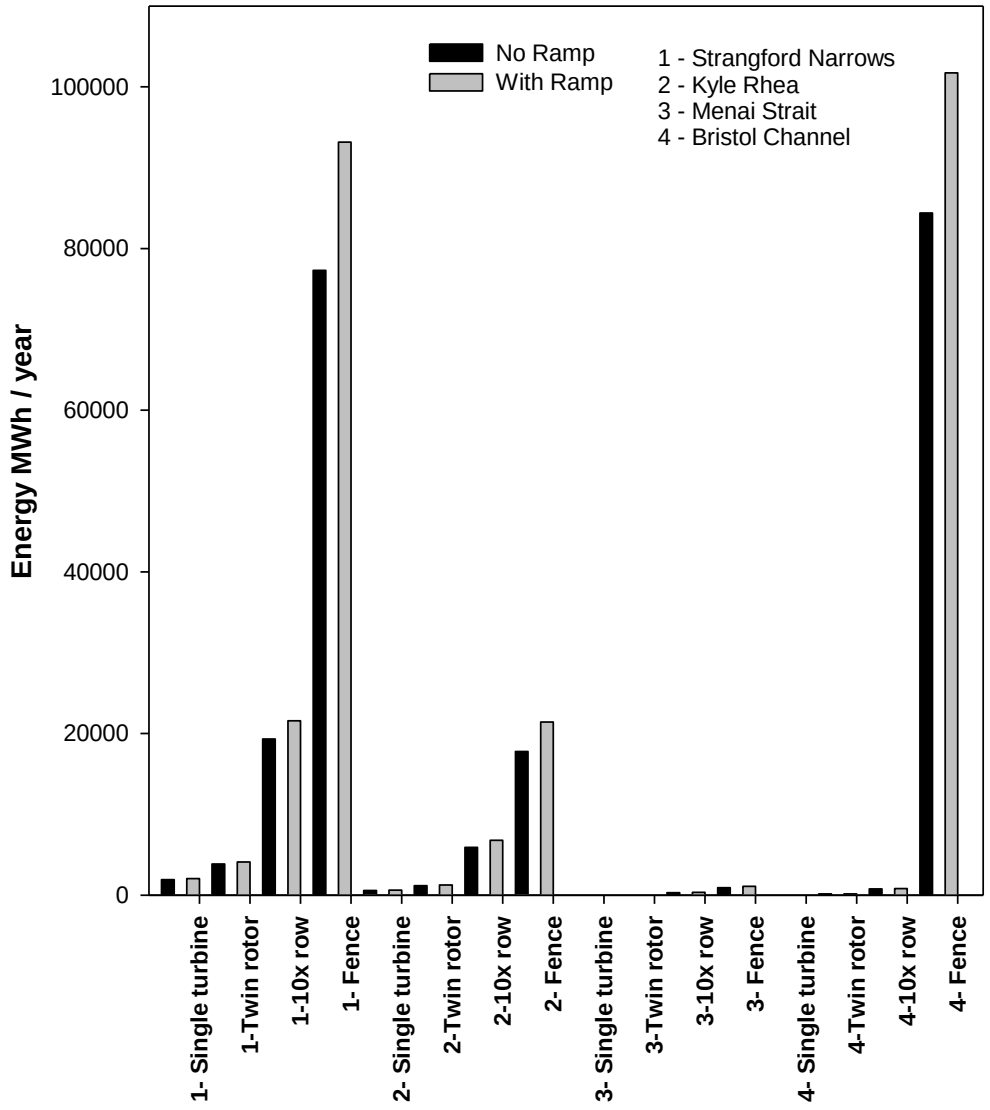

Figure 5-41: Estimated annual energy yield

Table 5-9 displays the potential power gain across a spring/neap tidal cycle for each site and deployment scenario. It is evident that single or dual rotor devices deployed in the relatively narrow channels might achieve power gains in the region of 6-8%. Increasing the lateral ramp width and introducing more devices in a row would significantly increase the potential of ramp-foundations. For a 10 turbine row deployed in the narrow channels (excluding the Bristol Channel) power gains could be in the region of 13-16%. Obviously the optimum solution would be a tidal fence and in this case it is anticipated that these benefits would be even greater because of the opportunity to deploy densely packed turbines and support-structures creating an additional energy in the form of a potential energy head across the fence. For the Bristol Channel, power gain figures are unavailable for the single and twin rotor turbines because the

small lateral ramp blockage ratios are too far outside the tested data range and cannot be validated.

Site	Single turbine	Twin rotor	10x turbine row	Full channel fence
	Power gain %	Power gain %	Power gain %	Power gain %
Strangford Narrows	6.31	6.95	12.61	22.18
Kyle Rhea	6.72	7.74	16.05	22.18
Menai Strait	6.70	7.70	15.89	22.18
Bristol Channel	#	#	6.01	22.18

lateral ramp blockage ratio too small for validation.

Table 5-9: Potential power gain with the addition of ramp-foundations across a 14 day tidal cycle

In summary, when applying the empirical results presented in section 5.4 to full-scale tidal stream deployment sites, it seems clear that ramp-foundations will only be technically viable in relatively narrow channels or ideally in arrays or tidal fences. Ramp-foundations appear viable in Strangford Narrows, Kyle Rhea and the Menai Strait provided a row of 10 or more turbines are installed. The concept could also be viable with a single MCEC on condition that smaller returns of power were accepted and the ramp-foundation did not add significant capital cost to the device. The large width of the Bristol Channel means that ramps could only be viable in a very long row of MCECs or a tidal fence. The Bristol Channel has the second highest tidal range in the world and ignoring this vast potential energy resource and only exploiting the relatively low quantities of kinetic energy could be imprudent.

Chapter 6

6 Theoretical Analysis of Ramp-foundations

6.1 Introduction

This chapter reports the development of a two-dimensional potential flow model for the flow over a ramp-foundation. It uses the numerical theory from chapter 3, section 3.3, which is explained in greater detail by Vallentine (1969). Vallentine describes how an irrotational potential flow analysis can be applied to develop a turbulent flow pattern, provided the flow is converging and temporal mean velocities are assumed. This means that the method can be used to model the inflow and across ramp flow. For a diverging flow, such as flow directly downstream of the ramp, potential flow cannot be employed due to the unknown nature of flow separation.

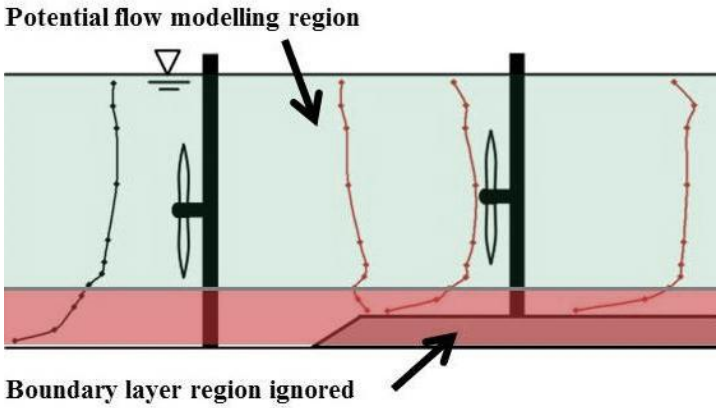

Figure 6-1: Potential flow modelling regions

It is critical to understand the limitations of the potential flow solution, when applied to the ramp problem. Potential flow assumes the concept of an "ideal fluid" rather than a "real fluid" and it is this fact that causes the deviation of a potential flow model from the real fluid behaviour. The key limitations of an ideal fluid and the implications to the potential flow model are discussed below:

- **Irrotational flow:** potential flow assumes the flow to be irrotational and hence vorticity equals zero. This means the effects of turbulence are ignored, but it can be assumed that potential flow represents the temporal mean velocities of a flow with sufficient accuracy.

- **Inviscid fluid:** the principal deviation from real fluid behaviour arises from neglecting viscous effects. This means shear forces cannot be transmitted through the fluid, which indicates potential flow models are inaccurate close to boundaries. Turbulent flows that would occur in tidal streams are approximated well by potential flow because viscous effects are low (except close to solid boundaries - see Figure 6-1). In laminar flows, the flow is dominated by viscous forces and hence potential flow provides a less satisfactory solution.
- **Boundary layer:** this limitation follows on from ignoring viscosity. Indeed ignoring the boundary layer development in a tidal flow is a very significant assumption. Potential flow assumes a free-slip boundary condition. Across the ramp-foundation the assumption is reasonable because the boundary layer is vertically compressed (Figure 6-1). Although the model breaks down in the boundary layer, the more imperative energy extraction region is well represented. There are a number of methods for adjusting the potential flow model using a "coupled boundary layer". This will be discussed later.
- **Surface deformation:** the potential flow model ignores the surface drop across the ramp. This assumption is justified by the results from the one-dimensional model presented in chapter 4, where surface drops are calculated to be minimal for Froude numbers encountered in typical tidal flows.
- **Modelling MCEC:** as potential flow does not model the turbulent effects and MCEC wake breakdown is driven by turbulent mixing it was decided to model the ramp-only flow scenario (investigated experimentally in chapter 5, section 5.2).
- **Lateral flow effects:** being a 2D model the flow effects from reducing the ramp's lateral span to channel width ratio are not modelled. This can in part be justified because experimental results from section 5.2 showed that the ramp flow is essentially 2D because lateral flow components are small. The model will be used to validate the full channel width ramps and the vertical ramp height to flow depth tests presented in section 5.2.

Despite these limitations, the potential flow model has a number of advantages that make it readily applicable as an approximate ramp flow solution. The most accurate modelling solution would be a Computational Fluid Dynamics (CFD) model, which iteratively solves the complex Reynolds-Averaged Navier-Stokes (RANS) flow equations. The disadvantages of this approach include complex solutions and a large computing time. Furthermore CFD requires a large degree of tuning, extensive validation and many commercial codes have numerous user defined parameters. RANS models also struggle when representing diverging flows with separation. In contrast potential flow can be developed from fundamental principles using simplified numerical solutions and can be arrived at with modest computing power and low numbers of iterations. Additionally the method does not require extensive validation or large numbers of

user input parameters. The technique yields results for 2D velocity and pressure distribution with acceptable accuracy (Vallentine, 1969), providing a good compromise between complex RANS solutions and simplistic one-dimensional theory. The potential flow numerical approach is described in chapter 3, section 3.3.

If the ramp potential flow model is run without any boundary layer modification, it will underestimate the flow velocity in the upper section of the velocity profile (Figure 6-2). This occurs because the model does not take into account the lower velocity sheared region of the boundary layer. If the average for the velocities in the true (experimental) velocity profile is taken, this average value is equal to the velocity of the potential flow prediction. This effect can be corrected so that the potential flow model velocities are equal to those of a real fluid (experimental results) in the upper energy extraction region above the ramp-foundation. This adjustment can be achieved using a "coupled boundary layer" (Molland and Turnock, 2007). Molland and Turnock propose a method of increasing the size of the geometry (the ramp in this case) by an amount equal to the displacement thickness of the local boundary layer. The results of this correction can be seen in Figure 6-2 and the correction is applied as follows:

1. Calculate the average velocity in the energy extraction region from the potential flow model.
2. Calculate 99% of the average velocity, the definition of where the boundary layer ends above the bed/ramp.
3. Calculate the thickness of the boundary layer using experimental data (or $1/7^{th}$ power law), e.g. the point at which the velocity profile has a value of 99% of the average velocity.
4. For turbulent flows the displacement thickness is approximately $1/8^{th}$ of the boundary layer thickness (Vallentine, 1969).
5. Increase the ramp height by the displacement thickness.
6. Re-run the model and the uniform upper section of the flow profile should now show better agreement with the experimental results (Figure 6-2).

The boundary layer adjustment means that the upper energy extraction region of the flow profile agrees with the behaviour of a "real fluid". Although the lower compressed boundary layer is still not modelled (Figure 6-2), the velocity in the important energy extraction region is well represented.

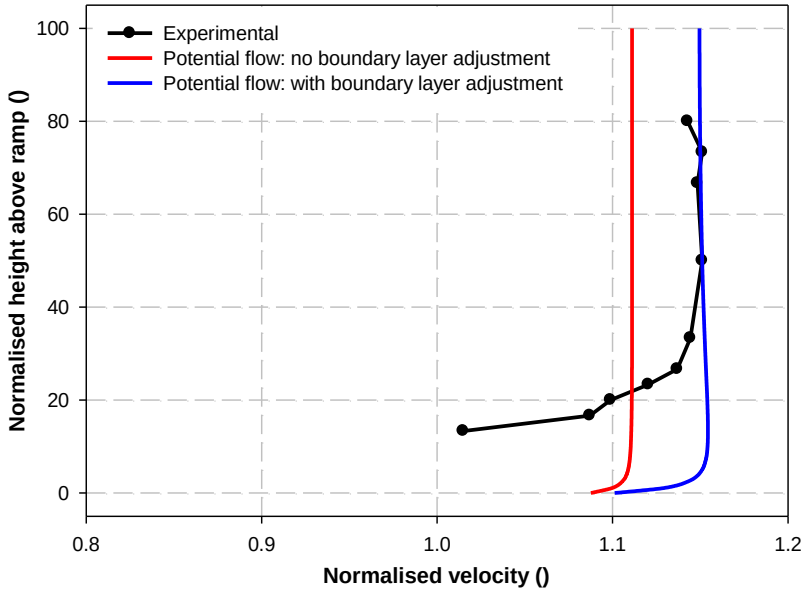

Figure 6-2: Potential flow boundary layer adjustment

6.2 Modelling objectives

The aim of the potential flow model was to provide a further validation tool for the experimental testing conducted in chapter 5. The model was used to validate the full channel width ramps and the variable ramp height to flow depth ratio tests in section 5.2. The 2D model provides an improved validation for the experimental results compared with the 1D model presented in chapter 4. The results presented in sections 6.3 to 6.6 were obtained using the numerical method described in Chapter 3, section 3.3.

6.4 2D ramp-foundation model

This section presents the normalised "base case" results for a ramp-foundation occupying 10% of the vertical water column with a leading edge profile angle of 30°. Results are normalised, hence a velocity of unity represents the free-stream velocity without a ramp-foundation. The model was run with boundary layer correction defined in section 6.1.

Figure 6-2 shows the results from the boundary layer correction model. Normalised vertical velocity profiles from the experimental testing (alternatively the $1/7^{th}$ power law profile could be used) were used to calculate the approximate boundary layer thickness and from this the boundary layer displacement thickness was calculated. For this "base case" the flow depth is 100 units (normalised) and the ramp height is therefore 10 units. When the boundary layer correction is applied, the ramp height must be increased by 3.13 units to a height of 13.13 units.

By re-running the model with this correction, the corrected upper section of the flow profile is calculated (Figure 6-2). It must be noted that before boundary layer correction, the average value of the whole experimental velocity profile is equal to the average of the uniform un-corrected potential flow profile (with variation of <1%). Correction simply adjusts the model so that the upper region of the u(x) velocity profiles are equal for both the "real fluid" (experimental) and the "ideal fluid" (potential flow).

Figure 6-3 shows the normalised contour plots for the "base case" scenario. The flow velocity increase across the ramp can be clearly seen in the top u(x) velocity plot with velocity increases of approximately 15% in the uniform upper profile section. This figure agrees with experimental results presented in chapter 5, section 5.2 and will be discussed further in section 6.5. Figure 6-3 and Figure 6-4 clearly show how the presence of the ramp causes the flow velocity directly upstream and close to the leading edge to reduce and at the top of the leading edge profile there appears to be a local flow velocity increase. The lower plot of Figure 6-3 shows the vertical velocity components v(y). As might be anticipated these are highest across the leading edge profile, where the flow is forced to change direction.

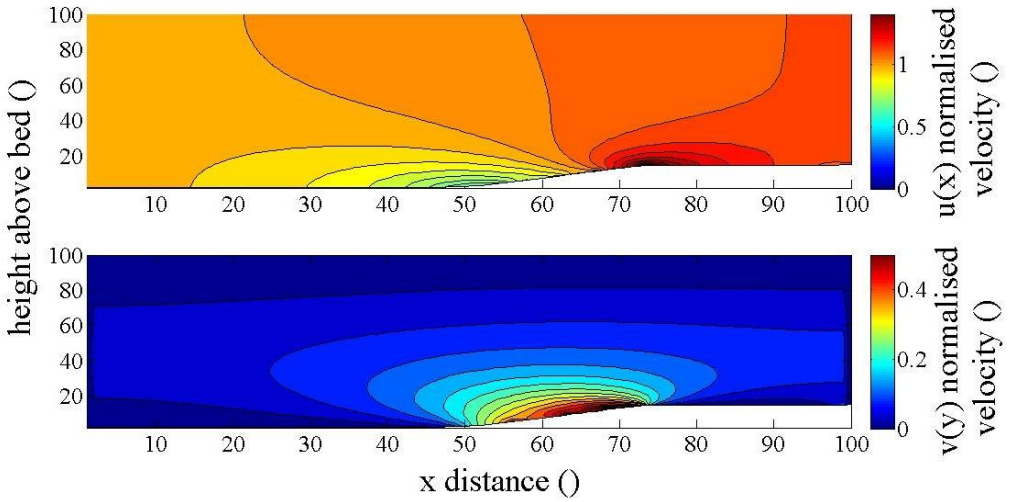

Figure 6-3: Base case normalised contour plots, u(x) velocity (top), v(y) velocity (bottom)

Figure 6-4 shows the normalised across ramp centre-line profiles. The velocity profile development is clear. Starting from a uniform velocity inflow, initially the flow velocities in the lower regions upstream of the ramp are reduced (profile 50). Above the ramp and beyond the top of the leading edge profile local flow velocity increase occurs close to the ramp surface (profile 70). Finally the vertical velocity profile stabilises into a globally augmented profile downstream of the leading edge profile (profile 100). At full scale the stabilised profile (profile 100) would be used for energy extraction and in a 10m deep flow, would be located 5m downstream of the leading edge profile.

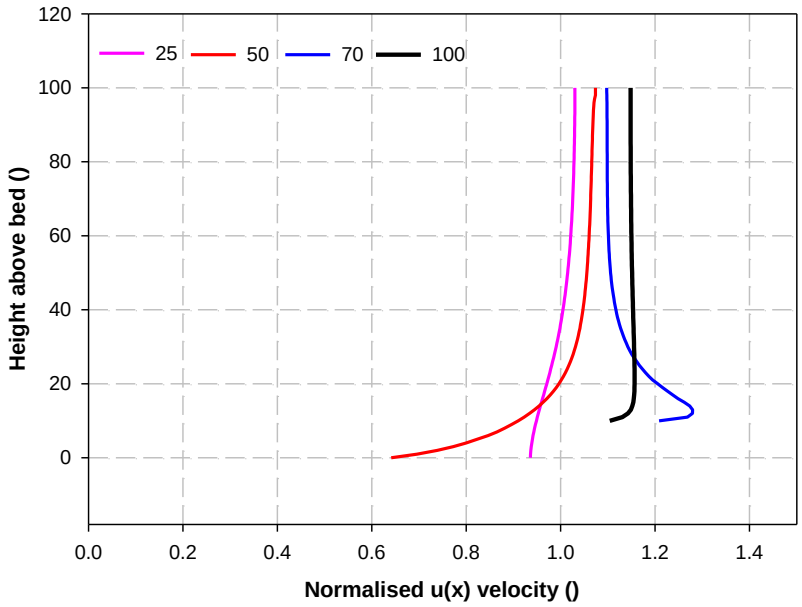

Figure 6-4: Centre-line velocity profiles normalised across the ramp

6.5 Experimental comparison

In this section the non-dimensional results from the experimental testing (chapter 5) and the results from the 2D potential ramp flow model are compared and examined. Both cases of the potential flow model are examined, the case without boundary layer correction and the scenario with boundary layer modification. Experimental and potential flow results are analysed for the three instances of vertical blockage (ramp height to flow depth ratio).

Vertical ramp blockage ratio	**Experimental**		**Potential Flow**		**1D Model**	
	Average velocity gain (%)	Energy extraction region velocity gain (%)	No boundary layer correction velocity gain (%)	With boundary layer correction velocity gain (%)	Average velocity gain (%)	$1/7^{th}$ Power Law energy extraction region velocity gain (%)
0.15	18.9	23.3	18.0	23.4	18.6	26.9
0.1	11.1	14.6	11.2	15.1	11.6	19.4
0.075	8.6	10.7	7.9	10.4	8.4	16.0

Table 6-1: Experimental vs. potential flow model velocity gain at the ramp centreline comparison

Table 6-1, Figure 6-2 and Figure 6-5 show results for u(x) velocity gain for the different vertical ramp blockage ratios tested. It is clear from the results that a potential flow model with boundary layer correction represents the u(x) velocity with the highest degree of accuracy in the middle 50% of the water depth, or the energy extraction region. In terms of calculating the power gain from a MCEC, this set-up with boundary layer correction must be used. Table 6-1 shows how the average u(x) velocity from the experimental velocity profiles including the reduced velocity shear region is approximately equal to the average velocity in the potential flow model without boundary layer correction. This indicates that in terms of the 1D u(x) average velocity, or for mass flow rate continuity, the potential flow model without boundary layer modification is required. Table 6-1 also shows how the 1D ramp flow model agrees well with the average velocity in the vertical water column, however when you apply the $1/7^{th}$ Power Law correction (presented in Chapter 3) to estimate the vertical profile from the average 1D value, the estimated velocity increase in the energy extraction region is over predicted. In fact for the vertical ramp blockage ratios from 0.15 to 0.75 presented, power law exponents ranging from $1/10^{th}$ to $1/20^{th}$ would be required. This results from findings already presented in Chapter 5 where at greater ramp heights the boundary layer becomes increasingly compressed. In summary it appears that the traditional $1/7^{th}$ power law correction is not suitable for modelling the flow in the upper energy extraction region above the ramp foundation. Thus it seems clear, unless the correct power law exponent can be predicted, the 2D flow model provides a better flow approximation than the simple 1D model presented in chapter 4.

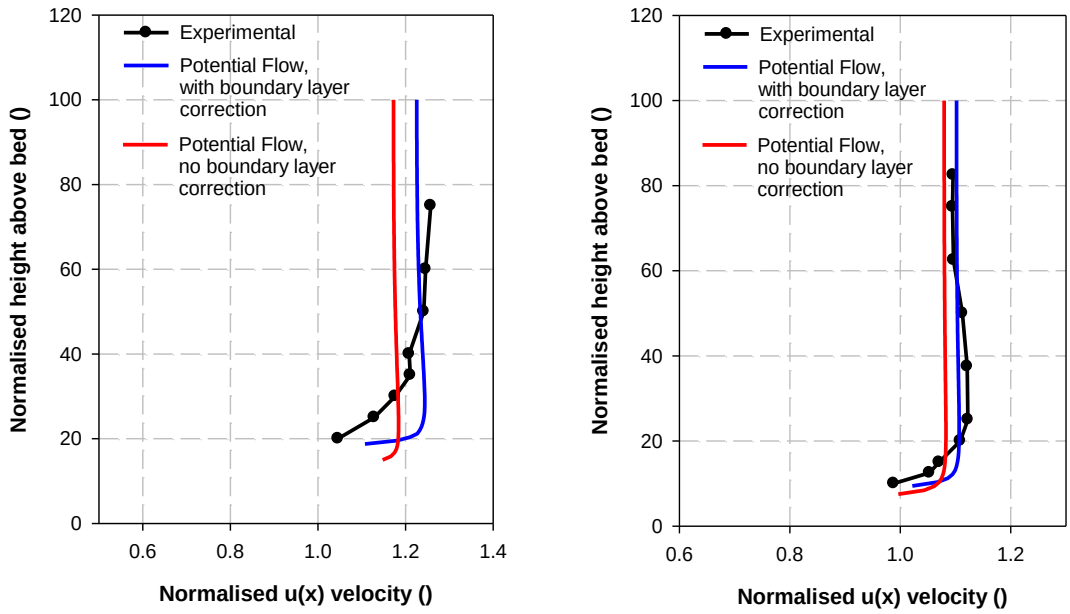

Figure 6-5: Normalised centre-line u(x) velocity profiles at ramp centre line (point 100). Vertical ramp blockage = 0.15 (left) and vertical ramp blockage = 0.075 (right).

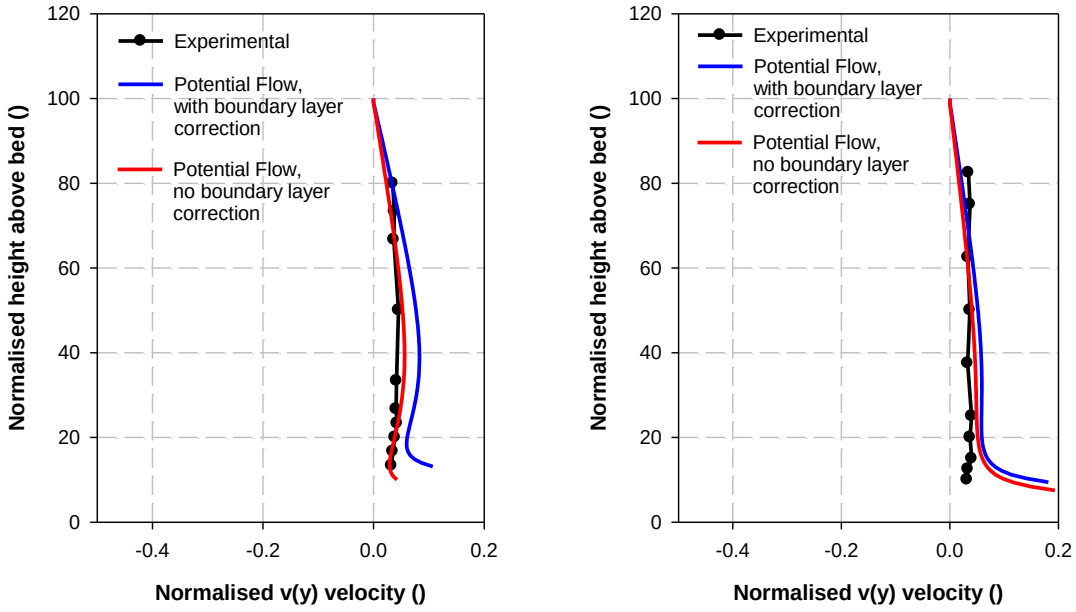

Figure 6-6: Normalised centre-line v(y) velocity profiles at ramp centre line (point 100). Vertical ramp blockage = 0.1 (left) and vertical ramp blockage = 0.075 (right).

Figure 6-6 shows the velocity profiles for the vertical velocity components, v(y). It is clear from these graphs that the potential flow model without boundary layer correction is more accurate. Results from the corrected boundary layer model tend to overestimate the vertical velocity components, v(y), in the flow. This is because the artificially increased ramp height with the coupled boundary layer model magnifies vertical velocity components. It is therefore recommended that the coupled boundary layer ramp model is used for estimating the u(x) velocity components for the energy extraction region (for velocity and power gain estimations) and the un-corrected potential flow model is used for calculating the vertical velocity components, v(y).

Figure 6-7 shows the downstream u(x) velocity development across the leading edge profile and main ramp structure for experimental and potential flow model results. It is clear that across the leading edge profile (points 50 and 60) and at the ramp centre-line (point 100) the potential flow models the vertical u(x) velocity profiles well. In the region between the top of the leading edge profile and the ramp centre-line (points 70-93) the lower 25% of the vertical flow profile is not modelled well by the potential flow model. This is not unexpected as it has already been stated that potential flow does not model regions where viscous forces are significant and such flow close to solid boundaries. It is important to note that the velocity is well represented above the sheared boundary layer region and it is this region that would be used for a MCEC in most deployments.

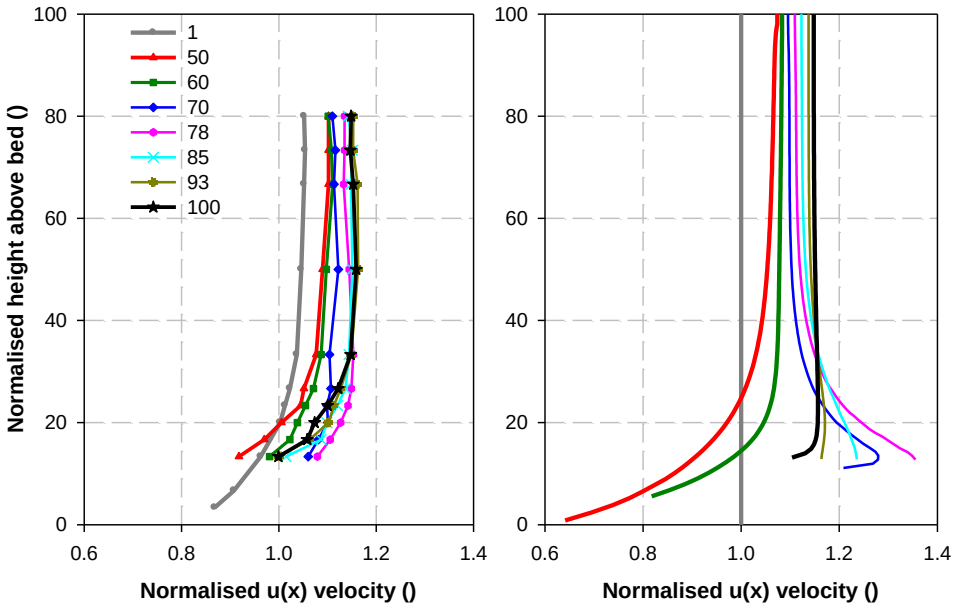

Figure 6-7: Normalised centre-line u(x) velocity inflow and across ramp profiles, vertical ramp blockage = 0.1. Experimental (left) and Potential flow with boundary layer correction (right)

The contour plots for the u(x) velocity development across a ramp-foundation (Figure 6-8) give a good overview and comparison for the experimental and potential flow results. The close similarities between the experimental results and the potential flow model can be seen. Of particular note is the improvement in accuracy from using the coupled boundary layer model compared with the no boundary layer correction model. Although there are clear discrepancies between the theory and experimental results, the general flow domain trends are very similar. Results are positive given the assumptions involved with potential flow analysis.

A good measure of model accuracy is the percentage error between experimental and potential flow results. Figure 6-9 shows the percentage u(x) velocity variation between experimental results and both the corrected and un-corrected boundary layer potential flow models. It can be seen with boundary layer correction, for the bulk of the flow domain, that velocity variation is less than 2% except in the boundary layer region (lower 25% of the flow depth). Looking at the model without boundary layer correction, velocity variation is greater in the critical energy extraction region (2-6%). However the region close to the ramp-foundation is more accurate without boundary layer correction because of the exaggerated presence of the ramp in the corrected model.

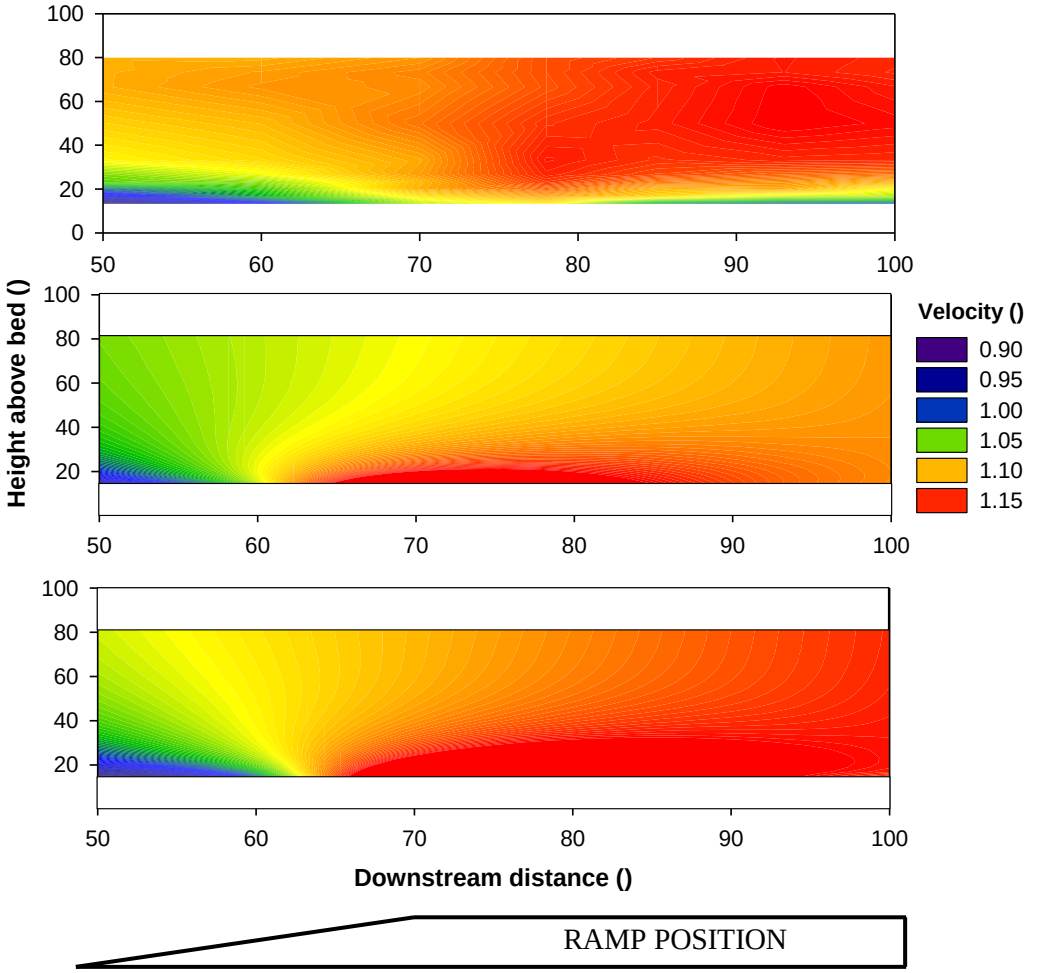

Figure 6-8: Normalised u(x) velocity contour plots, vertical ramp blockage = 0.1. Experimental (top) and Potential flow no boundary layer correction (middle) and Potential flow with boundary layer correction (bottom)

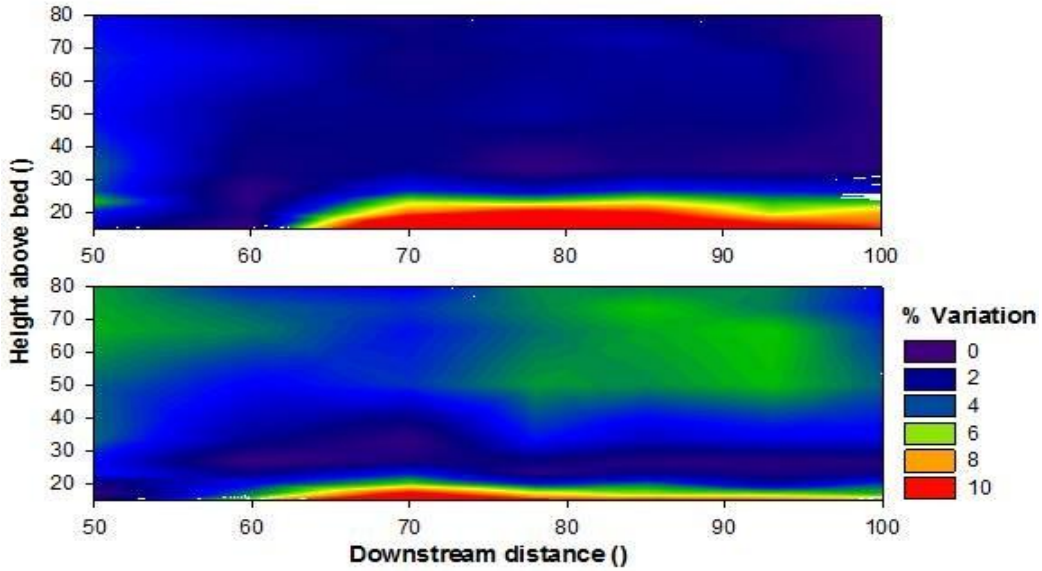

Figure 6-9: Percentage variation between experimental and potential flow u(x) velocities, vertical ramp blockage = 0.1. With boundary layer modification (top) and without modification (bottom)

6.6 Full scale analysis

In this section it is shown how the 2D potential flow model can be used to estimate velocity and pressure distributions across a ramp-foundation installed in a real tidal energy deployment location. Velocity and pressure magnitudes across the ramp are calculated by entering the average depth and free-stream velocity from a particular site into the 2D ramp-foundation model.

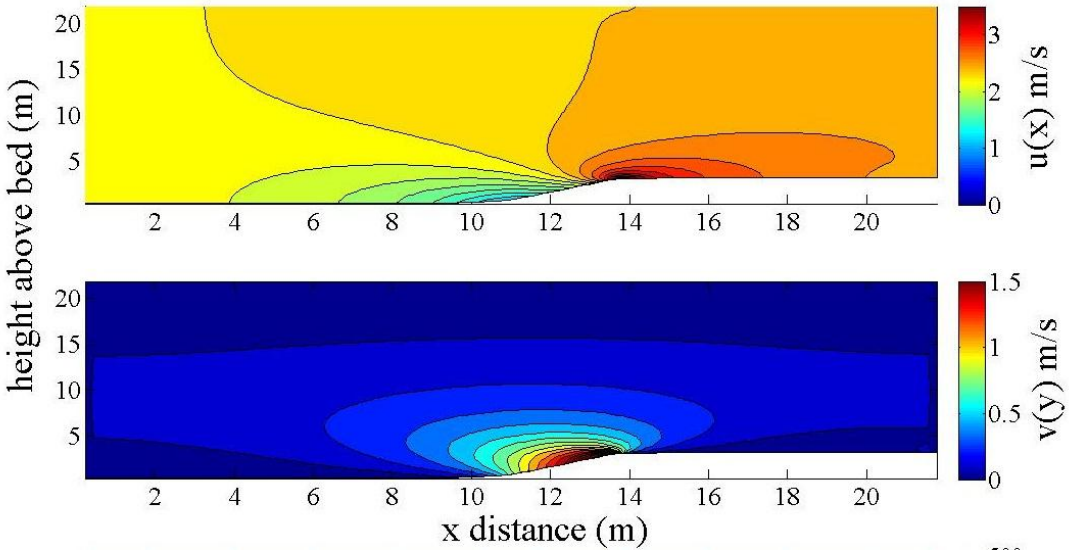

Figure 6-10: Kyle Rhea contour plots, u(x) velocity (top), v(y) velocity (bottom)

Kyle Rhea discussed in chapter 5, section 5.5, is used with its average depth of 20m, average spring velocity of 2.25m/s and a 2m high ramp occupying 10% of the flow depth. Given the 2D nature of the model, the velocity increases would represent those for a full channel width tidal fence deployment (discounting MCEC flow impedance effects).

Figure 6-10 shows the u(x) and v(y) velocity contour plots for the Kyle Rhea input data. In essence the results are the same as the "base case" but with the actual magnitude of velocity rather than normalised results. The effects of flow velocity increase across the ramp and increased vertical v(y) velocity components above the leading edge profile are clear. The average u(x) velocity increase in the energy extraction region is approximately 15%, as found in the non-dimensional base case.

Figure 6-11 shows the u(x) and v(y) vertical velocity profiles for the free-stream flow and across ramp flow in the energy extraction region. The augmented u(x) flow profile with a velocity increase of 15% in the energy extraction region is shown and the increased vertical velocity (v(y)) components can be observed near to the ramp surface (Figure 6-11, right).

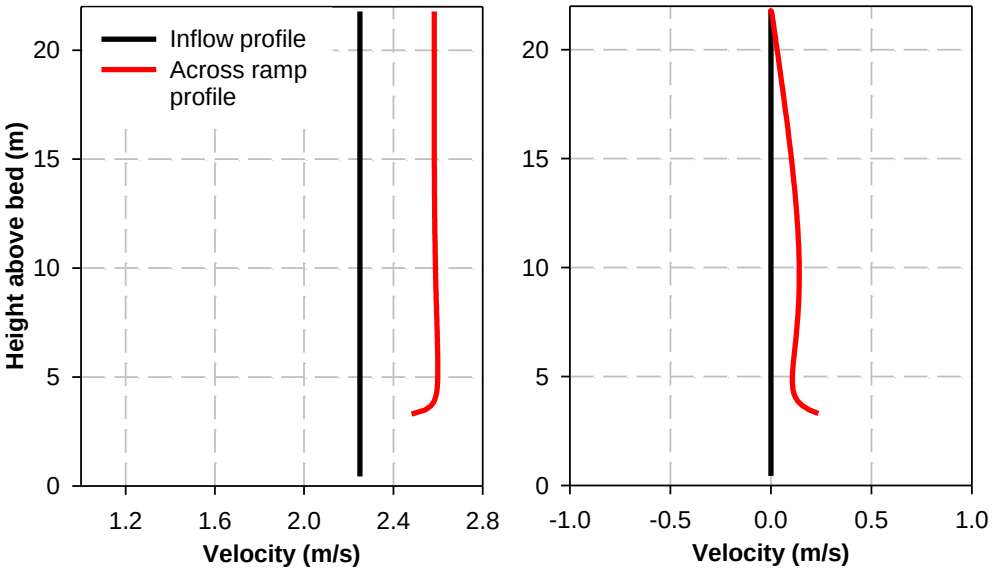

Figure 6-11: Kyle Rhea inflow and across ramp velocity profiles, u(x) velocity (left), v(y) velocity (right)

Looking at the vertical pressure distributions in Figure 6-12 for the free-stream and across ramp locations it can be identified that the increased velocity across the ramp is accompanied by a pressure drop as would be anticipated from the laws of conservation of fluid energy. With development of a third dimension this model could be used to represent the case with a single MCEC ramp-foundation deployed in the centre of a tidal channel. This is beyond the scope of this project; this 2D potential flow model was intended to validate the experimental full channel width ramp-foundation results presented in chapter 5, section 5.2.2.

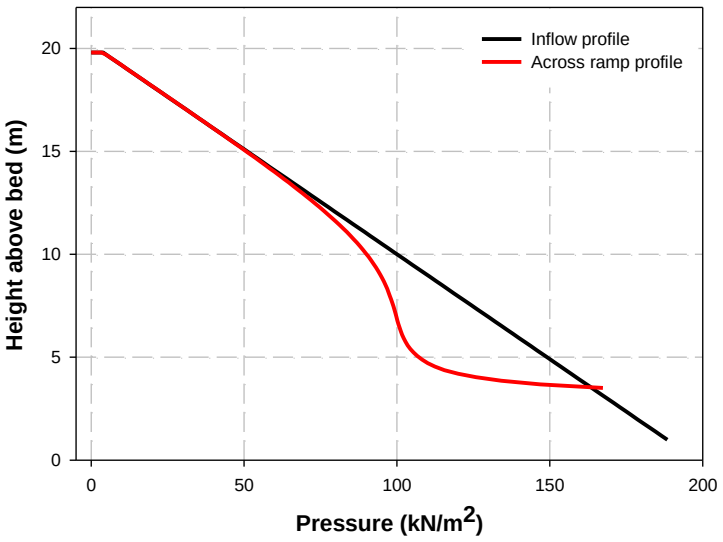

Figure 6-12: Kyle Rhea inflow and across ramp pressure profiles

6.7 Summary

The potential flow model acts as a validation tool for the experimental modelling presented in chapter 5. Good agreement for the u(x) and v(y) velocity distributions has been shown for the full channel width ramp-foundations and vertical ramp blockage experiments. In the critical energy extraction region above the boundary layer, variation between experimental and potential flow is less than 1% for much of the profile when a coupled boundary layer model is used for the u(x) velocity. Given the potential flow model limitations, including zero vorticity and inviscid fluid, the accuracy of the results are very positive and it can be concluded that the model acts as a good validation tool for the full channel width ramp-foundations. Potential flow provides a valuable compromise between the complex Navier-Stokes equations and simplistic 1D flow theory (e.g. 1D theory using the principles of specific energy for flow over a raised bed, section 3.1.4 and Figure 3-1).

If the model is run without boundary layer correction, the average u(x) velocities in the energy extraction region (centre of ramp) are equal to the average velocity value of the whole experimental velocity profile or similar to the 1D model average velocity estimation. In terms of the 1D u(x) average velocity or for mass flow rate continuity, this means that the potential flow model without boundary layer modification is required. When the model is run with boundary layer correction (coupled boundary layer) the u(x) velocities represent well the velocities in the upper energy extraction region of the vertical velocity profile (middle 50%). In terms of calculating the power gain from a MCEC, this set-up with boundary layer correction must be implemented. Thus it seems clear, unless the correct velocity profile power law exponent can be predicted, the 2D flow model provides a better flow approximation than the simple 1D model presented in chapter 4.

For the vertical velocity components v(y) the model without boundary layer correction is more accurate. Results from the corrected boundary layer model tend to overestimate the vertical velocity components in the flow. This is because of the artificially increased ramp height with the coupled boundary layer model, which causes increased vertical velocity components across the ramp.

It is possible to apply the model to full scale tidal sites, in terms of predicting the velocity gain for a full channel width ramp-foundation in a tidal fence type application. With the development of a third dimension and replication of a MCEC (by using further iteration and a source term) the model could be applied to narrow MCEC rows or single devices deployed in the centre of a channel, but this is beyond the experimental thrust of the project. Experimental results from

section 5.2 have already shown that lateral velocity components across ramp are small and the flow can be well approximated to 2D. The potential flow model could be validated with this experimental data and then used as an analysis tool for assessing any geometric ramp arrangement that falls within the validated range.

In summary it can be concluded that the coupled boundary layer ramp model should be used for estimating the u(x) velocity components for the energy extraction region (for velocity and power gain estimations) and the un-corrected potential flow model is used for calculating the vertical velocity components, v(y). Potential flow is a valuable flow estimation tool, but in its application the identified limitations must be considered at all times.

Chapter 7

7 Wake Structures Resulting from Vertically Constrained Tidal Flows

7.1 Introduction

When deploying a farm of MCECs, the nature of the downstream wake flow will be a critical factor for determining the farm layout and packing density. MCEC wake is dissipated through shear flow mixing between wake and surrounding flow and it is known that the wake length is heavily influenced by the flow depth or the degree of vertical flow constraint. Vertical flow constraint in this instance describes the ratio of the MCEC diameter to flow depth. This chapter presents experimental findings of the flow fields around scale MCEC simulators operating in circulating flumes at varying depths to represent the range of depths expected at MCEC deployment sites. Examples of shallow tidal sites include the Bristol Channel, the Humber Estuary and areas around the Channel Islands (see Figure 7-1). Deeper flows exist in the Pentland Firth and in various locations around the West of Scotland.

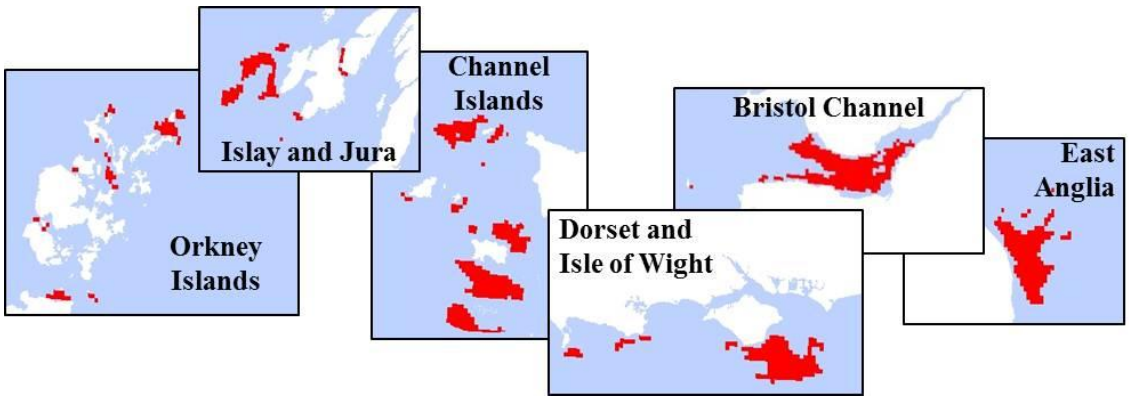

Figure 7-1: Potential UK first generation shallow tidal flow sites, not to scale

Previous work presented by Myers et al. (2008) concluded that MCECs operating in shallow fast-moving flow regimes will see a difference in the downstream flow field compared with devices installed in deeper water. It was stated that investigating the effects of sea bed proximity has shown that wake recovery is not as favourable when the total depth to MCEC diameter ratio is large. This is because in deep unconstrained flows, velocities around the MCEC are not augmented as much as in more constrained flows. Hence shear forces between the wake and surrounding flow are lower leading to a more persistent downstream wake. Conversely if the

vertical flow constraint increases, the downstream wake length reduces. This results from the augmented flow velocities that surround the wake which work to increase the shear forces at the wake boundary and drive wake dissipation. Previous experimental work did not investigate the full range of vertical blockage cases, such as highly constrained shallow flows. Myers and Bahaj (2010) state that further reducing the distance between the seabed and rotor disk will increase the wake length. In these very constrained flows where the MCEC occupies the bulk of the water column the wake is unable to expand fully. This is because the wake is met prematurely by the seabed and free-surface which restricts flow below and above the MCEC. Below the disk, the highly turbulent and slow-moving wake combines with the channel boundary layer which has similar properties. Differential shear is hence low and there is little mass flow between the disk and bed. This chapter presents work developed from the previous studies (Myers et al., 2008, Myers and Bahaj, 2010) to further investigate the effects of vertical flow confinement on the downstream wake development behind MCECs. A thorough understanding of wake development is critical for the optimisation of the downstream device spacing in tidal stream farms. Minimising the downstream spacing will enable a higher farm device density and hence higher yields from a specific site. The implications for the thrust coefficient and thus potential power yield will also be investigated.

For a multiple-row MCEC array, longitudinal spacing of devices is expected to be great enough to ensure that downstream devices have an incoming flow regime (and hence power output) that is comparable to devices located upstream. However, at spatially constrained sites this approach to spacing may be tightened in order to increase energy capture per surface area of the site and to reduce electrical connection costs. It is postulated that there will be an optimum device height to flow depth ratio that will minimise downstream wake length. For sites that are deeper or shallower than this optimum depth range, the downstream wake length is expected to increase. The term “wake length” in this chapter can be defined as the downstream distance behind the MCEC at which the centreline velocity has returned to 90% of the free-stream value. Although it must be noted that 90% velocity recovery would only result in approximately 70% of the maximum power for downstream devices compared with the upstream row.

In order to conduct the testing at a reasonable scale a porous mesh actuator disk was used to model a horizontal axis turbine (as used in chapter 5 and discussed in section 5.3.1).

For this work the principal parameters that require replication from large to small scale are (Myers et al., 2008):

a) Device thrust force controlled through the level of actuator disk porosity (ratio of open to closed area).
b) Linear scaling of length ratios such as disk diameter to water depth and channel width.
c) Replication of ambient flow field conditions such as Froude number, vertical velocity profile and turbulence intensities. Full-scale and model Reynolds numbers cannot achieve parity at small scale but should lie within the turbulent classification.

Testing was conducted at a scale of 1:100 using actuator disks of 0.1m diameter. The porous actuator's impedance was specified using an empirical relationship between thrust coefficient (C_t) and plate porosity. The actuator disk porosity used was 0.48 and was of the same value as that used in chapter 5 and by Myers et al. (2008). Myers and Bahaj (2010) state that varying the rotor disk thrust has little effect on the wake structure greater than seven diameters downstream and beyond this, in the far wake region, velocity deficits converge for all values of disk thrust. This reinforces the assumption that dissipation of the wake in this region is driven principally by turbulent mixing. It also justifies the use of one disk thrust coefficient for all the testing reported in this chapter and hence the results in the far wake region can be extended to different rotor thrust coefficient values.

The actuator disk was mounted on the same lever arm rig used in chapter 5. The rig can be seen in Figure 7-2. The same load cell was used to measure the total thrust force.

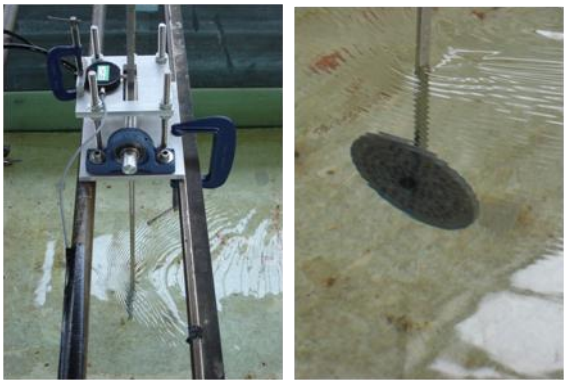

Figure 7-2: Actuator lever arm rig (left) and actuator disk mounted on lever arm (right)

The downstream wake was characterised using the high frequency ADV as described in chapter 5 section 5.2.1.2.

The recovery of the wake is defined in terms of velocity deficit; this is a non-dimensional number relative to the free-stream flow speed at hub height and the wake velocity, defined by equation 7.1.

$$U_{def} = 1 - U_w / U_o \tag{7.1}$$

The ambient turbulence intensities in the circulating channel used during this study were approximately 6-8% and were calculated in all three planes (u,v,w). Turbulence intensity is commonly defined as the root-mean-squared of the turbulent velocity fluctuations divided by the mean velocity of the sample (chapter 3, section 3.1.3).

Table 7-1 details the parameters of the constrained flow tests conducted as part of this work and the previously undertaken unconstrained flow tests at the Ifremer facility. Dimensions are detailed in disk diameters (D).

Test	Water depth (D)	Channel width (D)	Actuator centre from surface (D)	Depth-averaged Froude No.	Depth-averaged Reynolds No.	Disk height/depth ratio
1	4.0	13	2.00	0.15	$1.2x10^5$	0.25
2	3.0	13	1.50	0.15	$7.8x10^4$	0.33
3	2.5	13	1.25	0.15	$5.7x10^4$	0.40
4	2.0	13	1.00	0.15	$4.2x10^4$	0.50
5	1.5	13	0.75	0.15	$2.7x10^4$	0.66
6*	20	40	2.00	0.113	$9.9x10^5$	0.05

*unconstrained test conducted at Ifremer, France.

Table 7-1: Experimental test parameters

Myers et al. (2008) showed experimentally that for a constant depth the wake velocity deficit is independent of velocity (for a representative range of Froude numbers). This is the justification for using a constant Froude number throughout testing (Figure 7-3).

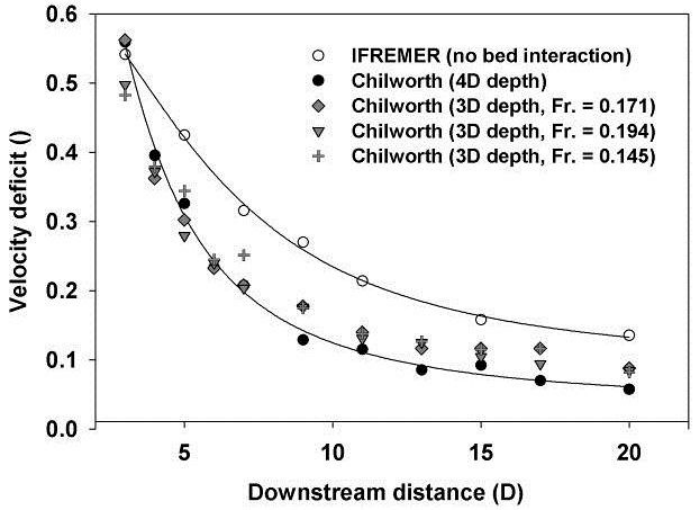

Figure 7-3: Froude number, centreline deficit comparison

Each test can be defined in terms of the disk height to flow depth ratio (or vertical blockage ratio, VB). For example test 6 could represent the deep/unconstrained flow scenario such as the Pentland Firth. Test 1 could represent the mid-constraint flow scenario such as areas around Orkney and MCT's deployment site in Strangford Lough, Northern Ireland. Test 4 could

represent the shallow-depth/constrained flow scenario such as sites in the Bristol Channel and Kyle Rhea, Scotland.

7.2 Testing facilities

7.2.1 Constrained

Shallow water experiments were conducted in the tilting flume at the Chilworth hydraulics laboratory, University of Southampton, UK (Figure 7-4). The working section of this flume is 21m in length, 1.37m wide and a maximum depth of 0.4m for steady operation. ADV data was filtered to remove noise and spurious points, although the large quantity of suspended particles in the Chilworth channel maximised returned signal strength.

Figure 7-4: Chilworth channel

7.2.2 Unconstrained

The vertically unconstrained/deep flow results used to compare with the constrained tests were presented by Myers et al. (2008) and were conducted in the Ifremer circulating channel, Boulogne-sur-Mer, France. The channel has a working section of 18m in length, 4m wide and 2m deep (Figure 7-5). In order to achieve sufficent signal to noise ratios with the ADV the channel required granular seeding due to the lack of suspended sediment.

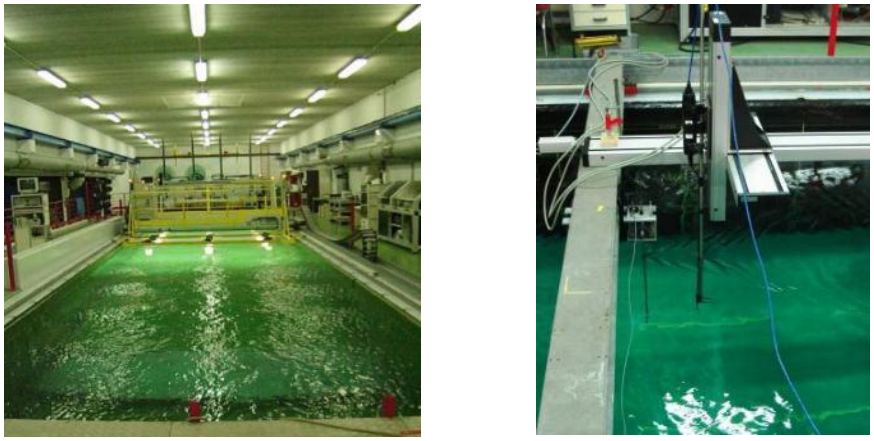

Figure 7-5: View downstream of the Ifremer water channel (left), installed mesh disk rig and ADV mounted on 3-dimensional axis (right)

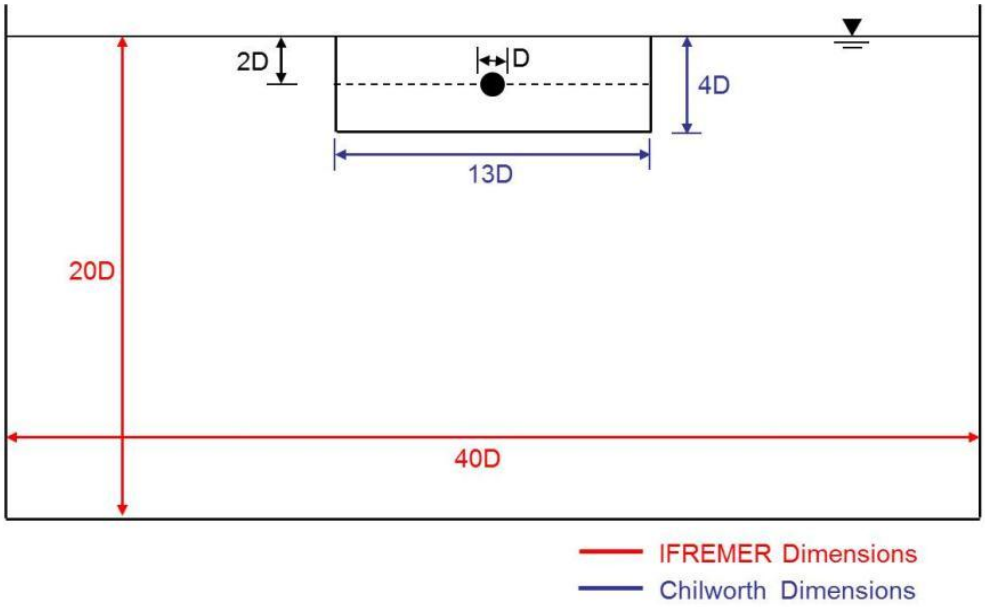

Figure 7-6: Constrained and unconstrained flow domain comparison

7.3 Free-stream results

Figure 7-7 (left) shows the normalised vertical velocity profiles for the three cases. These are the free-stream results from the Chilworth and Ifremer facilities. Depth is expressed in terms of disk (or rotor, full scale) diameters (D). The velocity profile at Chilworth is well-developed but the close proximity of the bed induces a more pronounced gradient that leads to disparate mass flow rates above and below the disk. This is most noticeable in the shallow vertically constrained scenario. Flow speed in the deep unconstrained case is similar above and below the disk.

Figure 7-7 (right) shows the ambient turbulence intensities in all three planes (u,v,w) for the unconstrained and mid-constraint scenarios (Ifremer and Chilworth channels, respectively). At the Chilworth facility the presence of the flume bed 2-diameters below the disk causes an increase in turbulence intensity immediately above the bed and hence close to the disk. The u and v components are of a similar magnitude at 6-7% whilst turbulence intensity in the vertical plane is slightly greater. The Ifremer channel turbulence intensity is more constant with depth close to the disk. The turbulence intensity in the vertical plane is much lower than at Chilworth. The difference occurs due to the nature with which water is delivered to the upstream end of the channel's working section.

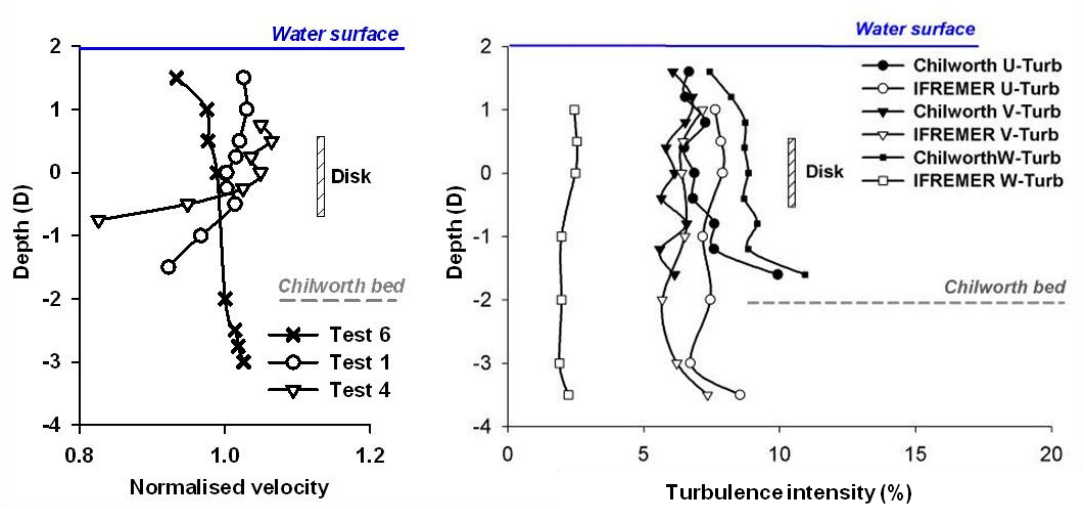

Figure 7-7: Normalised vertical velocity profiles at the Chilworth and Ifremer water channels (left) and turbulence intensities (right)

7.4 Horizontal axis turbine wake

7.4.1 Downstream wake length

Figure 7-8 shows the longitudinal centre plane velocity deficits for the six depth cases. It is clear that in the mid-constraint cases (tests 1&2) the wake is broken down in a significantly shorter downstream distance than in the unconstrained case (test 6) and high vertical constraint (or "heavy") cases (tests 4&5). In the mid-constraint case for test 1 the wake appears to be broken down in less than 10 disk diameters downstream. This results from flow velocity augmentation above and below the actuator disk that acts to break the wake down through greater lateral turbulent mixing and shear forces between the wake and surrounding flow. This effect was postulated by Myers et al. (2008) and is reinforced following analysis of these results.

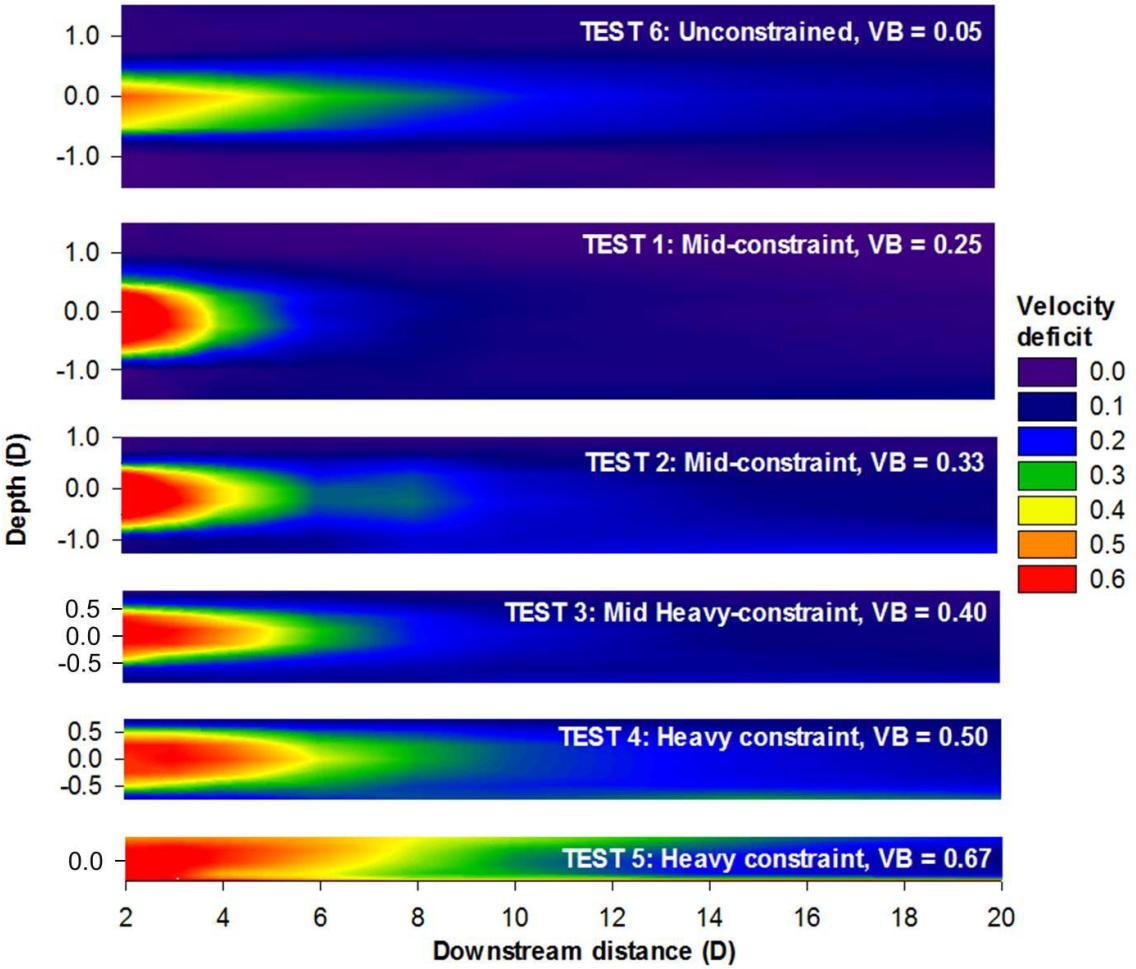

Figure 7-8: Centre plane velocity deficit profiles; unconstrained site, mid-constraint sites and heavily constrained sites

The wake persists much further downstream in the deep-unconstrained (test 6) and shallow constraint cases (tests 4&5). In these cases the wake persists downstream for approximately 18-20D; this occurs from restrictions in flow augmentation around the MCEC. In the deep-

unconstrained case (test 6) vertical device blockage is low and hence flow velocities surrounding the wake are reduced, thus lowering the degree of turbulent mixing between the wake and surrounding flow allowing the wake to persist further downstream. In the shallow heavily constrained flow scenario (tests 4&5) vertical blockage is high and again the wake persists further downstream. Local flow augmentation above and below the MCEC is restricted because the wake expands and intersects with the bounding surfaces, reducing the exploitable surface area of the wake for dissipation.

Figure 7-9 shows vertical line plots of centreline velocity deficit at two downstream locations for three depth cases. Looking at the 3D downstream graph it is clear that the initial velocity deficits directly behind a MCEC are similar irrespective of the vertical flow constraint; this is because wake is re-energised by turbulent mixing from the surrounding flow and in the near wake this effect is less pronounced because flow is diverted around the disk. Further downstream (e.g. 6D) the effects of varying degrees of vertical blockage can be seen. The vertically unconstrained and heavily constrained cases give similar profiles, whereas the velocity deficits for the mid-constraint case are reduced considerably because of increased turbulent mixing between the wake and the higher velocity surrounding flow. The effects of flow augmentation in the mid-constraint case can be observed.

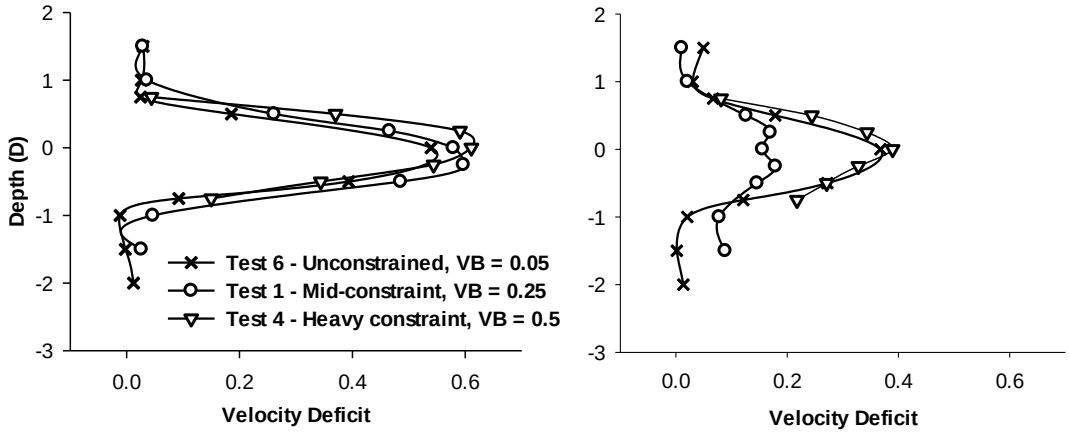

Figure 7-9: Centreline vertical velocity deficits at 3 diameters downstream (left) and 6 diameters (right)

Figure 7-10 shows the downstream centreline deficits. As suggested by Figure 7-8 the wake recovers much more quickly in the mid-constraint case. Again the principal mechanism for this is flow augmentation around the disk which serves to break up the wake more rapidly. In Figure 7-10 the similarities in terms of downstream velocity deficits between the shallow high constraint and deep unconstrained cases are clearly illustrated.

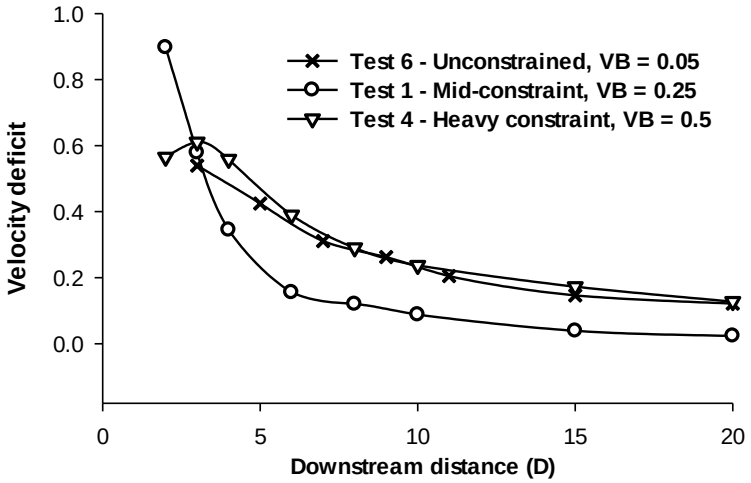

Figure 7-10: Disk centreline velocity deficit comparison

7.4.2 Lateral wake width

The lateral width of the wake is significantly less important than the wake length in terms of farm spacing. Although the wake must expand laterally for the conservation of momentum, in the far wake this width will be small compared with the downstream wake length (see Figure 7-11) and hence will have a much smaller resulting influence on farm spacing.

Figure 7-11 shows the lateral flow domains for the mid-constraint and high constraint cases. The reduction in wake length in the mid-constraint flow is clear. In terms of lateral wake spread, there are no significant variations in all the depth cases, which results because the bulk flow is in the downstream direction and restricts lateral wake expansion.

Throughout the testing at Chilworth, the lateral dimension of the flow domain was constant due to the fixed channel width. Hence any variation in wake dimensions must result from constraining the flow vertically. Figure 7-12 shows that with increasing vertical constraint, the lateral flow augmentation either side of the MCEC is enlarged. In very shallow flows, the lateral flow augmentation around the side of the MCEC increases because the device occupies a large percentage of the channel depth and flow is hence restricted above and below the MCEC. This means that augmented flow above/below a MCEC (as in mid-constraint flows) is more significant in terms of wake dissipation than lateral flow augmentation (in very shallow and wide flows). The flow is relatively un-constrained laterally and the velocity increase effects are dissipated over a wider area which again justifies the increase in downstream wake length associated with shallow flows.

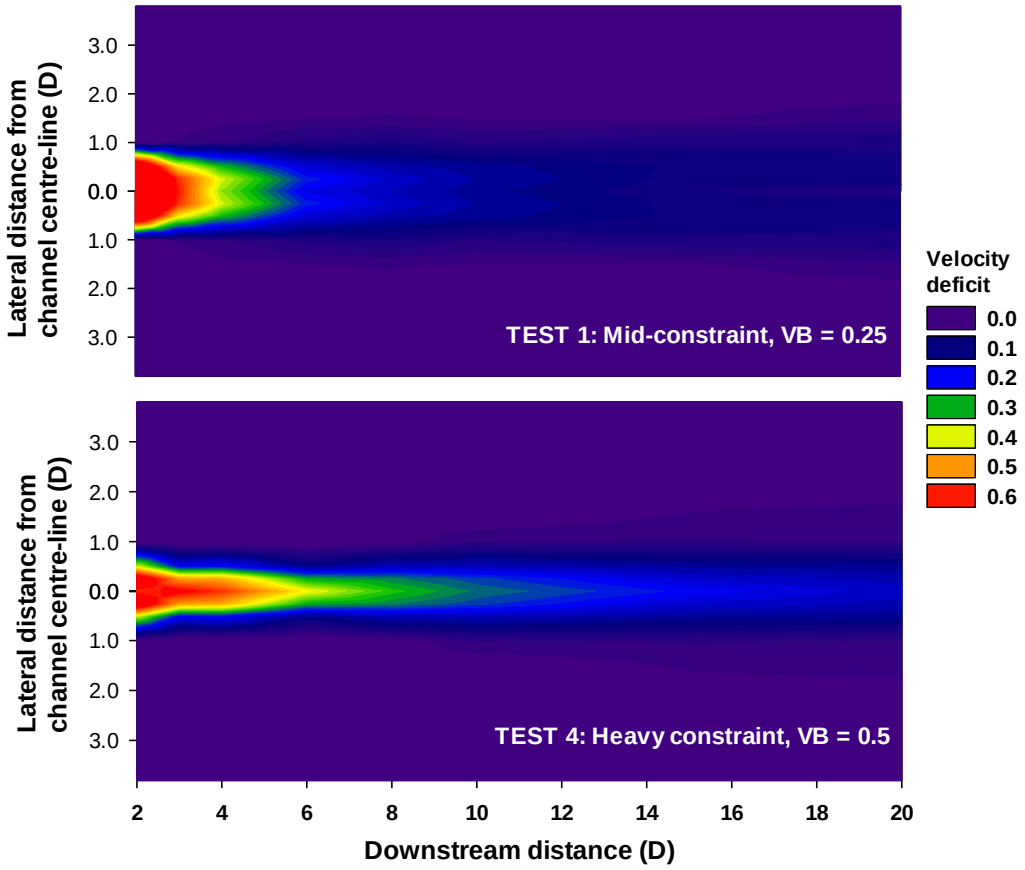

Figure 7-11: Lateral plane velocity deficit profiles; mid-constraint site and heavily constrained site

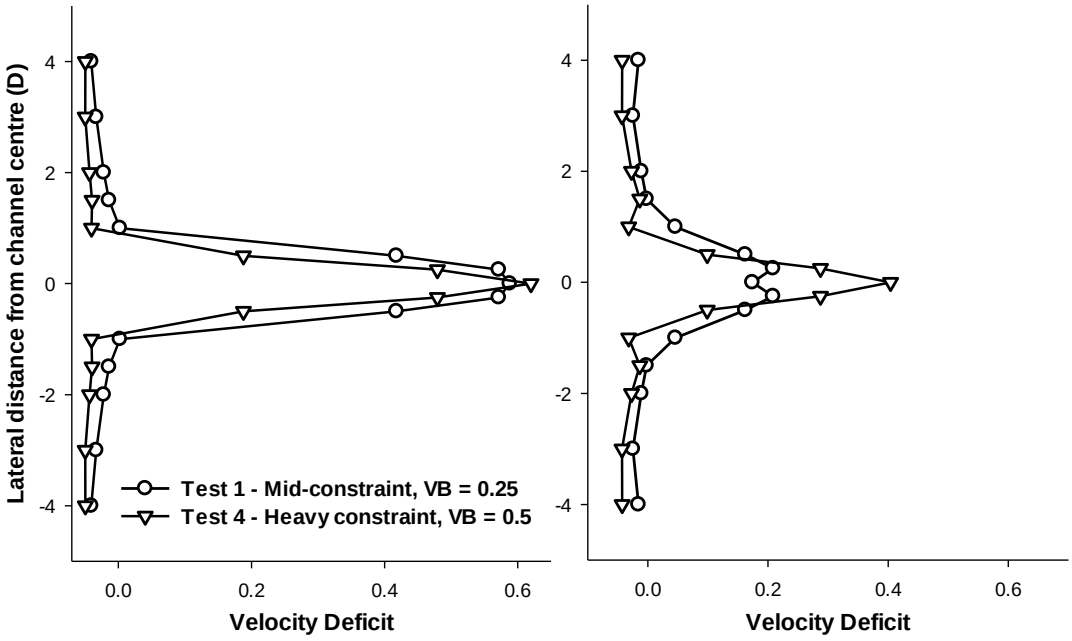

Figure 7-12: Lateral velocity deficits at 3 diameters downstream (left) and 6 diameters (right)

7.4.3 Thrust results

This section investigates the thrust coefficient (C_t) - a non-dimensional parameter that can be used to compare the effect that device height to flow depth ratio has on the MCEC thrust and hence power generation. Figure 7-13 shows how C_t varied throughout the vertically constrained tests. The C_t value remained constant for the deep unconstrained and mid-constraint flow cases, but there was a slight reduction in the two shallow highly constrained cases. This appears to contradict traditional blockage theory, where the C_t value might be expected to increase in heavily constrained flows (Whelan et al., 2009). This suggests that the effects of lateral flow around the sides of the MCEC in shallow and wide flows (Figure 7-12) are significant in terms of MCEC thrust and hence power coefficients. Essentially in shallow heavily constrained sites a greater proportion of the flow is forced around the sides of the MCEC but because the flow is laterally unconstrained it is diverted away from the influence of the MCEC. Thus simply applying one-dimensional area blockage correction methods is not suitable for very shallow and wide tidal flows. Whelan (2009) assumes no lateral flow effects in the one-dimensional model and it is anticipated that neglecting lateral flow may account for this discrepancy in C_t value.

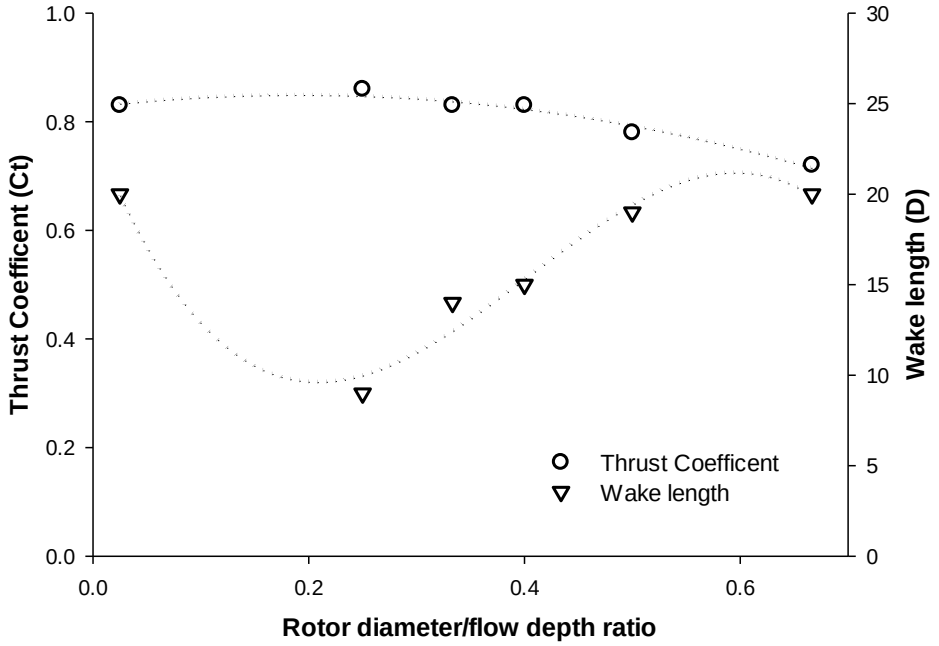

Figure 7-13: Thrust Coefficient (C_t) comparison

7.5 Farm row optimisation

This section highlights the significance and importance of this work for tidal stream farm design and optimisation. Figure 7-8 indicated that there would be an optimum rotor height to flow depth ratio in order to minimise MCEC wake length and furthermore Figure 7-14 shows the optimum rotor diameter/flow depth ratio in terms of wake recovery for the range of experimental tests. Three different downstream location cases are compared for all the tests detailed in Table 7-1. It appears that 0.25 is the optimum rotor diameter/flow depth ratio for maximising wake shear and hence minimising downstream MCEC spacing. At full scale this might equate to a site with a depth range of 30-50m depending on the rotor diameter. There could also be slight variations on this optimum ratio for different ambient turbulence levels but the general trends are anticipated to remain. For different lateral MCEC blockage ratios the magnitudes of the velocity deficits would change but it is projected that the optimum rotor diameter/flow depth ratio would be similar.

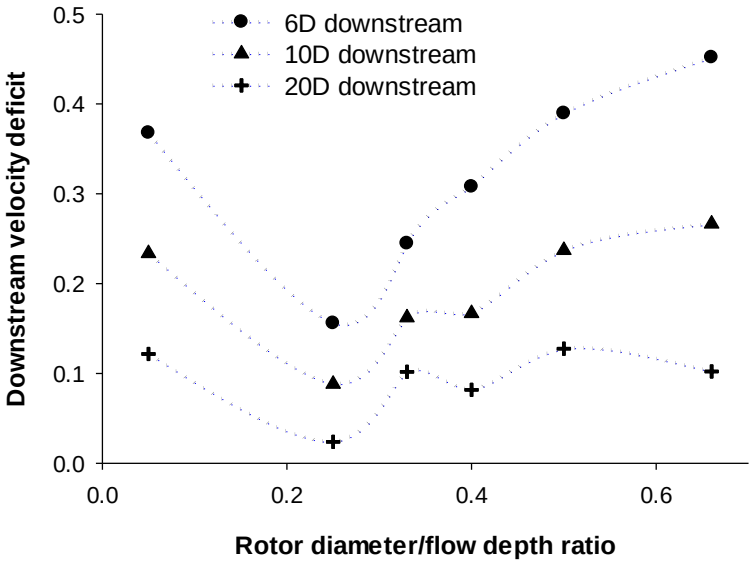

Figure 7-14: Optimum rotor diameter/flow depth ratio in terms of wake recovery

7.6 Summary

It is critical that tidal stream farms or arrays are optimised in terms of their downstream spacing and packing density. This chapter has shown the importance of tuning the downstream device spacing to the local flow depth. At spatially constrained sites inter-device spacing may be reduced in order to increase energy capture per surface area of the site. It is anticipated that many first generation sites will be located in shallow constrained tidal flows (Myers and Bahaj, 2010) and the longer wake lengths compared with intermediate-depth waters must be factored

into the design process. In terms of the full scale significance and to reduce wake length, the optimum rotor diameter/flow depth ratio is found to be 0.25.

The wake length is controlled by the amount of flow mixing between the slower-moving wake flow and the surrounding faster-moving free-stream flow. Increased wake length in unconstrained and heavily constrained flows result from vertical device blockage. In an unconstrained flow the MCEC occupies a small percentage of the water depth and hence local flow augmentation around the wake and thus shear forces at the wake boundary are reduced. In a very constrained shallow flow the MCEC occupies a large percentage of the water depth and flow above and below the MCEC is restricted. This is because the wake cannot expand fully and occupies the majority of the vertical water column. Furthermore, below the disk the highly turbulent and slow-moving wake combines with the channel boundary layer which has similar properties. Differential shear is hence low and there is little mass flow between the disk and bed. This means more flow is forced around the sides of the MCEC and because lateral channel blockage is low, enhancement is lower and the resulting turbulent wake dissipation is restricted. Both these shallow constrained and deep unconstrained flow scenarios result in less wake flow mixing and thus increased wake length. Mid-constraint tidal sites will offer the shortest wake lengths due to higher flow augmentation of the flow surrounding the wake. This flow serves to break down the wake in a shorter distance through higher turbulent mixing and boundary shear forces. Looking at the effects of vertical flow constraint on the lateral width of the wake, it is clear that this dimension will be almost insignificant when designing farm layouts because although the wake must expand laterally for the conservation of momentum, even in the far wake this width will be small compared with the downstream wake length. High lateral wake expansion is prevented by the constraining effects of the surrounding downstream bulk flow.

It is hoped that the relationship between vertical flow constraint and wake length will help with the layout design of future tidal stream farms. It is postulated that if the lateral blockage was increased (MCEC diameter/channel width), blockage effects would align themselves more closely with 1D blockage theory (such as Whelan et al.). Nevertheless this work highlights the importance of decoupling vertical and lateral blockage effects.

Chapter 8

8 Commercial Application of Ramp-foundations

8.1 Introduction

The overarching objective of this chapter is to investigate if ramp-foundations have the potential to be a commercial reality rather than just an academic concept. A commercial demonstrator device with an integral ramp-foundation is currently being developed by Pulse Tidal Ltd. (Paish et al., 2010).

The decision to include an integral ramp-foundation was supported by the fundamental work presented in chapters 4-6. Informing and optimising the design for Pulse Tidal's ramp-foundation has been a key focus of this project and shows a direct full scale commercial application. This work has involved experimental flow modelling, geometric optimisation, techno-economic analysis and advising the construction, deployment and recovery strategies.

8.2 Pulse Tidal

Pulse Tidal was founded independently in 2004 to develop the Pulse Stream tidal power concept of tandem oscillating hydrofoils. A DTI technology fund grant to build a 100kW demonstrator (the PS100) was secured in 2005. This was match-funded by investment from consortium partners and the project commenced in 2006. The grid-connected PS100 was commissioned in 2009 and operated in the Humber Estuary (Figure 8-1). During 2008, Pulse Tidal worked with IT Power to assemble the Pulse Stream Commercial Demonstrator (PSCD) consortium, to bid for FP7 funding. In 2009 the consortium secured an 8 million Euro grant to develop a full scale, 1.2 MW system. The design for this machine is now well advanced.

Figure 8-1: Pulse Stream 100 shallow flow prototype

8.3 Pulse Stream Commercial Demonstrator

The non-surface piercing PSCD will be a 1.2MW oscillating hydrofoil device with an integral ramp-foundation. One of its unique selling points is its specific development for shallow tidal flows (Figure 8-2).

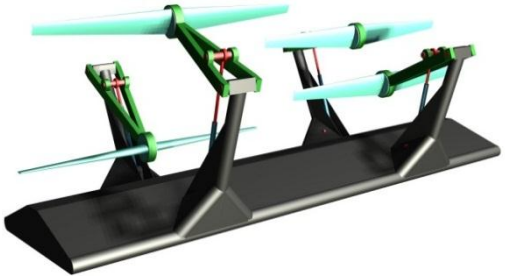

Figure 8-2: PSCD with a ramp-foundation

The outline design for the PSCD is illustrated in Figure 8-2. The system consists of two pairs of blades oscillating on levers which are pivotally connected to a base. The primary power take-off is through hydraulic cylinders acting between the levers and the base. They provide power to four closed loop hydraulic transmissions which drive a generator via a set of variable swash plate axial piston motors. The base is designed to provide several functions. It is the structural backbone of the system, the engine room, the buoyant hull for delivery/onsite maintenance/ deployment and recovery, and the augmenter to intensify the flow through the swept area.

8.4 Flow augmentation ramp

Pulse Tidal's initial decision to include a flow augmentation ramp-foundation was informed by preliminary work presented by Giles et al. (2009). The PSCD design with an integral ramp-foundation can be seen in Figure 8-3. The initial geometric design was established from previous generic ramp-foundation testing presented in chapter 5. From this an initial ramp height of 2.5m was chosen because it equates to 8.3-10% of the 25-30m proposed optimum deployment depth for the PSCD.

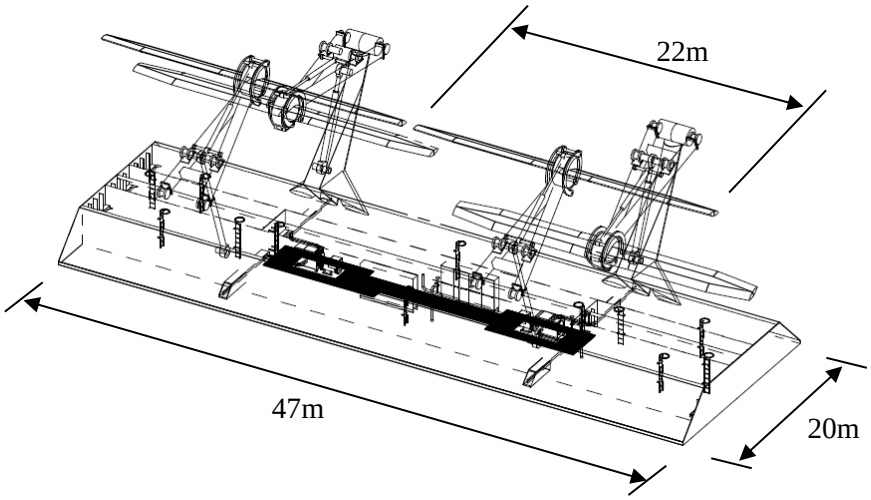

Figure 8-3: PSCD general arrangement

The base width of 47m was selected from the proposed width of the PSCD's hydrofoils. The ramp length was initially set at 20m but this decision was investigated through further optimisation testing. The ramp-foundation dimensions can be seen schematically in Figure 8-3. The 45° leading and trailing edge profile was chosen from the experimental results in chapter 5, section 5.2.6. This is a good compromise between velocity profile stabilisation, reducing turbulence intensity and minimising the ramp-foundation construction size.

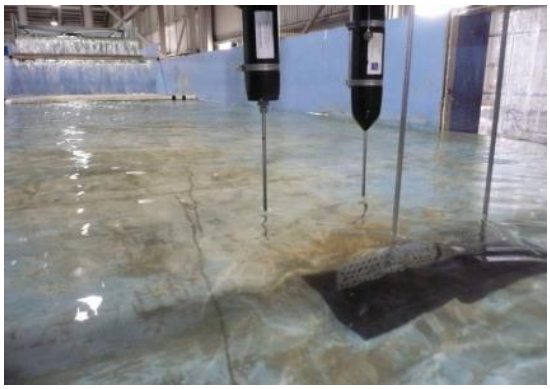

Figure 8-4: PSCD testing at HR Wallingford

To establish the flow field structure around the PSCD at different operational loads a PSCD specific experimental testing program was conducted in HR Wallingford Ltd.'s circulating flow channel (Figure 8-4). Following on from the initial testing at HR Wallingford and to help answer questions raised during the PSCD design process a further series of experimental tests were undertaken at the University of Southampton's Chilworth channel. The focus of this body of work was the geometric optimisation of the PSCD and the results are discussed in section 8.5.

8.5 PSCD Geometric optimisation testing

8.5.1 Introduction

This section presents the results and findings from the extensive PSCD tank testing, conducted in the University of Southampton's Chilworth circulating water channel. These 1:100 scale tests aimed to investigate device blockage effects and various device geometric parameters.

The PSCD was represented using porous actuator plates (the benefit and limitations surrounding mesh actuators were discussed in chapter 5). The impedance of the porous aluminium actuator plates were designed using an empirical relationship between thrust coefficient (C_t) and plate porosity. This relationship was developed from a combination of experimental findings from the University of Southampton and equations presented by Whelan et al. (2009). Four plates termed LOW, MID, HIGH and V.HIGH solidity were tested to represent the device at different operating conditions (Table 8-1).

Solidity	C_t	Porosity %
LOW	0.31	-
MID	0.44	79
HIGH	0.66	68
V.HIGH	0.95	-

Table 8-1: actuator plate parameters

The C_t for the PSCD is projected to be 0.70 at a rated flow velocity of 2.5m/s (provided by Pulse Tidal Ltd.) and dropping off above rated to approximately 0.3 C_t. Unfortunately it is not possible to tune actuator plates to high degrees of precision but it can be seen from Table 8-1 that the C_t range encompasses the calculated range for the full scale PSCD. The HIGH solidity plate therefore represents the PSCD under rated power operating conditions, and was used throughout this testing.

Using Froude scaling, the experimental flow domain (Figure 8-5) was scaled from a proposed PSCD deployment site with an average full scale depth of 20-30m. Spring peak and neap peak tidal flow velocities are in the range of 0-4m/s.

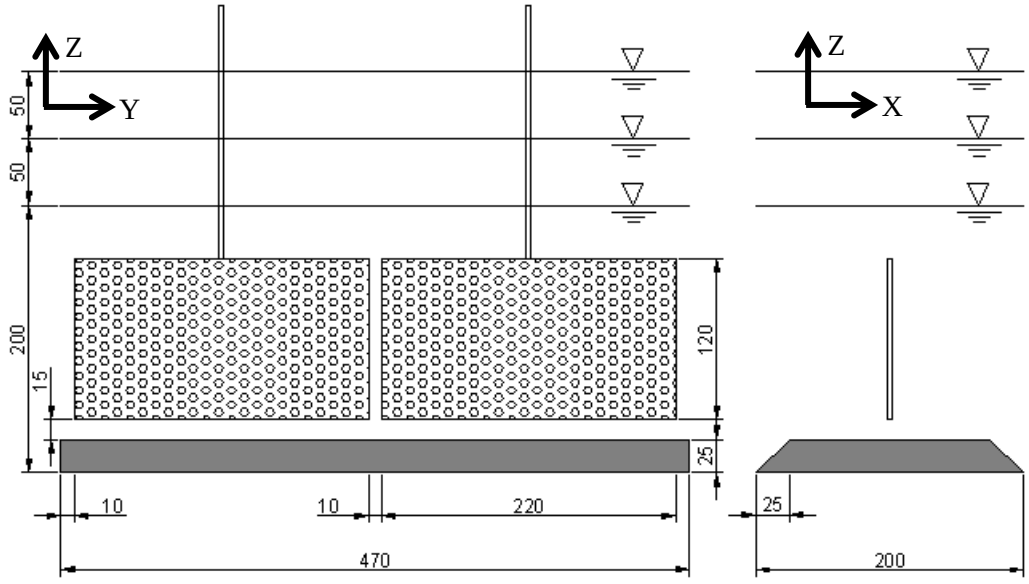

*not to scale, all dimensions in mm

Figure 8-5: PSCD experimental set-up

The ramp dimensions were scaled from the proposed full scale foundation dimensions for the PSCD. It was machined from HDPE plastic and located laterally in the centre of the channel. The key geometric and flow parameters are presented in Table 8-2. All tests were conducted at a Froude number of 0.2 and at two different model scale depths of 0.25m and 0.30m.

Geometric parameters	**Full Scale (m)**	**Model Scale (m)**
Hydrofoil width	22	0.22
Sweep height	12	0.12
Central gap	1	0.01
Ramp width	47	0.47
Ramp height	2.5	0.025
Ramp length (Phase I)	21	0.21
Ramp length (Phase II)	13	0.13
Lower gap	1.5	0.015
Side gaps	1	0.01
Channel width	137	1.37
Flow depth 1	25	0.25
Flow depth 2	30	0.3
Flow parameters	**Full Scale**	**Model Scale**
Flow velocity 1 (m/s)	3.13	0.31
Flow velocity 2 (m/s)	3.43	0.34
Froude Number	0.2	0.2

Table 8-2: PSCD testing, key parameters

Initially two tests with just the ramp-foundation and no actuators were conducted to ensure that the velocity benefits found with previous work (chapter 5) were still present. Following on from these tests the following geometric tests were carried out:

- Ramp augmentation
- Central gap width sensitivity
- Inward or outward facing hydrofoil investigation
- Hydrofoil vertical position
- Ramp length sensitivity

Velocities were measured using an ADV. Actuator plate thrust was measured using the lever arm rig and load cell discussed in chapter 5, section 5.3.1. Thrust coefficient (C_t) values of the mesh actuator were calculated for all tests. In principle, from actuator theory, the C_t value should remain constant for all flow conditions, but this only applies to a MCEC operating in a purely unconstrained flow. Any observed variation in C_t value during the tests can thus be attributed to other flow modifying effects, such as the ramp structure, device height to flow depth ratio or the actuator's proximity to bounding surfaces.

It must be stated that actuator plates model the global (or averaged) effects of the hydrofoils and highly localised effects, such as specific regions of high thrust, are not easily identifiable.

Figure 8-6: Actuators/ramp (left) and recording thrust (right)

8.5.2 Velocity check

Two different flow condition tests (Table 8-3) were undertaken to establish the degree of flow velocity increase from the PSCD ramp-foundation and to compare these results with previous work presented in chapter 5.

TEST	Froude	Depth (m)	Ave. Velocity (m/s)
A	0.2	0.25	0.31
B	0.2	0.30	0.34

Table 8-3: Tests A and B parameters

With the 25mm high ramp, flow velocity increases of 7.3% and 5.2% occurred with flow depths of 0.25m and 0.30m respectively (Figure 8-7). Applying axial momentum theory this gives potential power benefits of 23.4% and 16.3%.

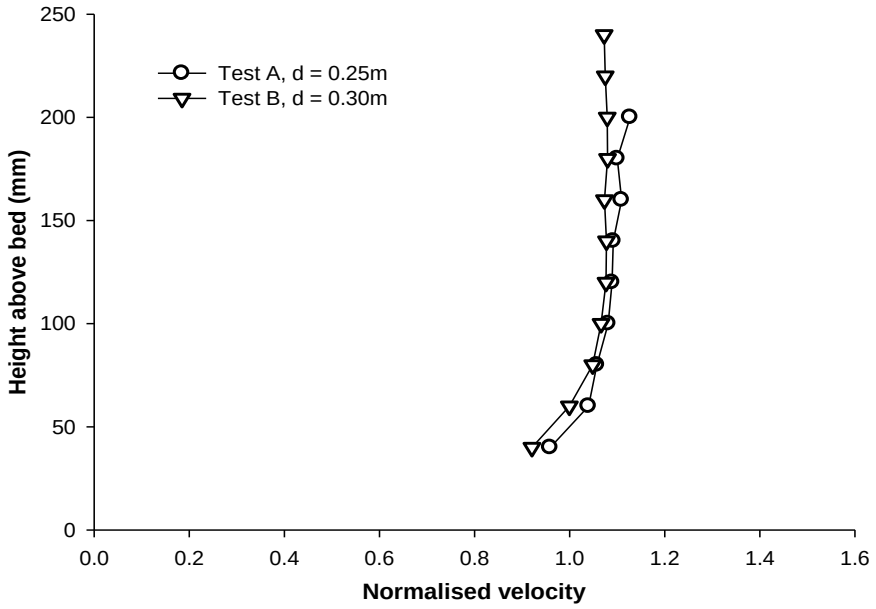

Figure 8-7: Tests A and B velocity profiles

These results correlate well with previous Chilworth testing presented in chapter 5, where velocity increases of between 5% and 10% occurred depending on ramp dimensions. With a ramp-foundation of similar proportions and lateral ramp blockage to the PSCD ramp, flow velocity increases were approximately 5-7%.

8.5.3 Ramp augmentation

It is essential to establish the importance of the ramp-foundation in terms of device thrust and power benefit. These tests were designed to investigate the benefits of the ramp-foundation in terms of thrust increase on the PSCD. A series of tests were conducted with the following combinations:

- Twin actuators with ramp
- Twin actuators without ramp
- Single actuator with ramp
- Single actuator without ramp

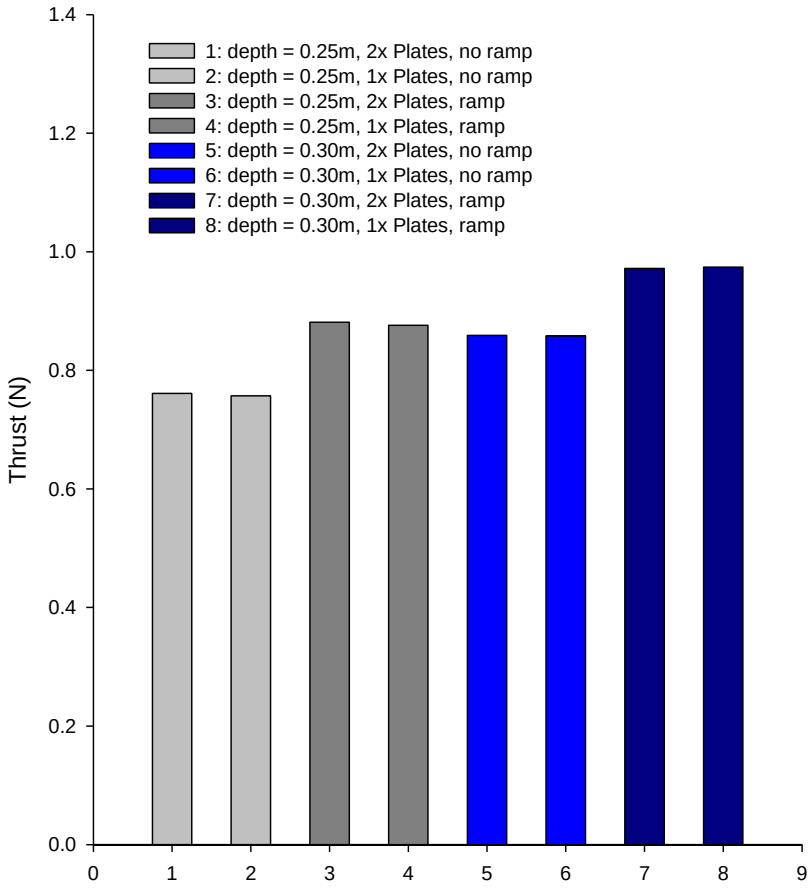

Figure 8-8: Global channel blockage vs. ramp augmentation thrust results

It is clear from the results that the ramp-foundation has a greater effect of increasing device thrust (average 14.54%) and hence power potential (22.59%) compared with the blockage effect of having the second set of hydrofoils located laterally close to the first set (Figure 8-8).

When comparing C_t in Figure 8-9, C_t values remain relatively constant across both the tested depths. This indicates that the results follow traditional momentum theory and the increase in thrust with a ramp-foundation occurs directly from the flow velocity augmentation across the ramp, rather than any other flow characteristic. Interestingly by looking at Figure 8-9 the C_t value of the actuator plate increases slightly in the deeper, less constrained tests. This effect is in keeping with the vertical flow constraint results presented in section 7.4.3.

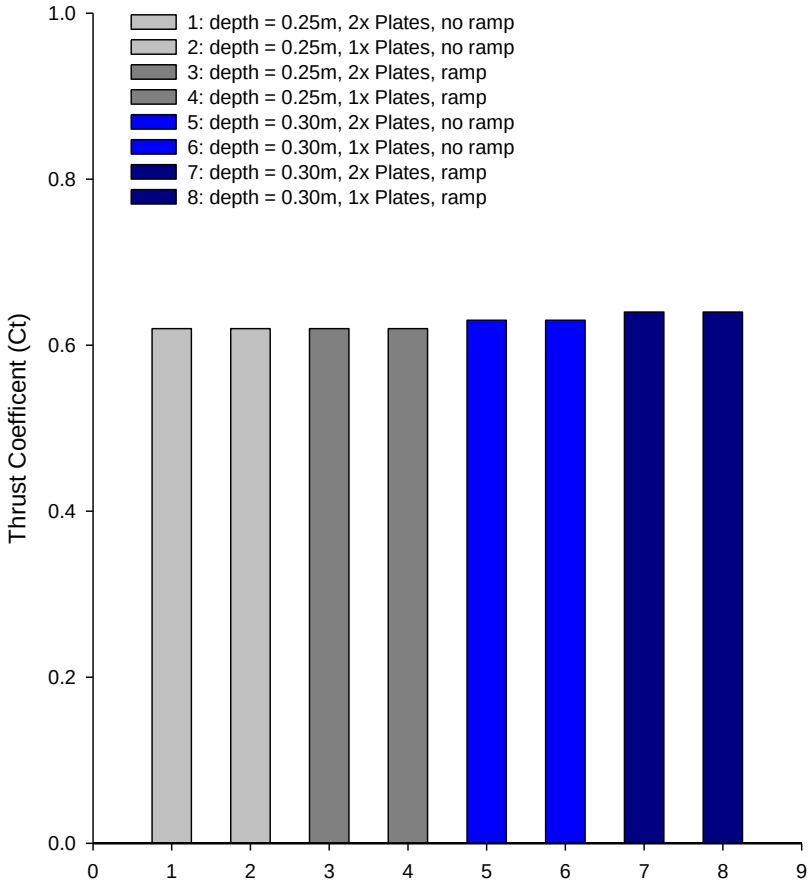

Figure 8-9: Global channel blockage vs. ramp augmentation thrust coefficient results

8.5.4 Central gap width

An important design consideration for the PSCD is the central gap between the two sets of hydrofoils (Figure 8-10). This was initially set at 1m, but this series of tests aimed to investigate the sensitivity of varying this width. During the initial HR Wallingford tests it was postulated that the narrow 10mm (1m full scale) central gap between the plates (hydrofoils) increases the thrust loading on the actuators compared with having a single actuator or a wider central gap.

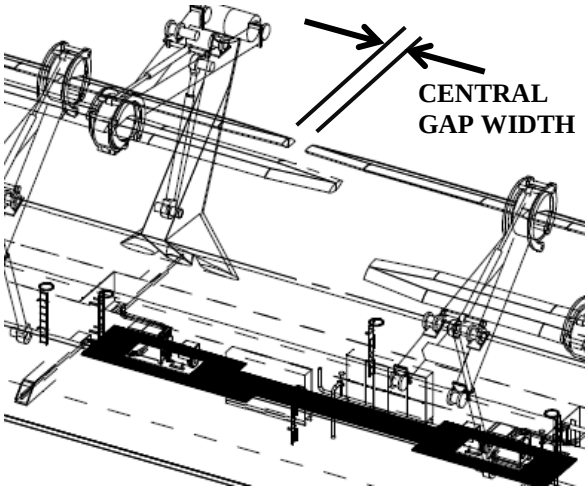

Figure 8-10: Central gap between hydrofoils

With gap widths of less than 20mm (2m full scale) the thrust can be seen to increase and by up to 6-7% at a gap width of 10mm (Figure 8-11). Between 20mm and 100mm the thrust is largely insensitive to gap size. For the full scale PSCD it is assumed from geometric and cost limitations that this gap cannot be less than 1m or greater than 5m.

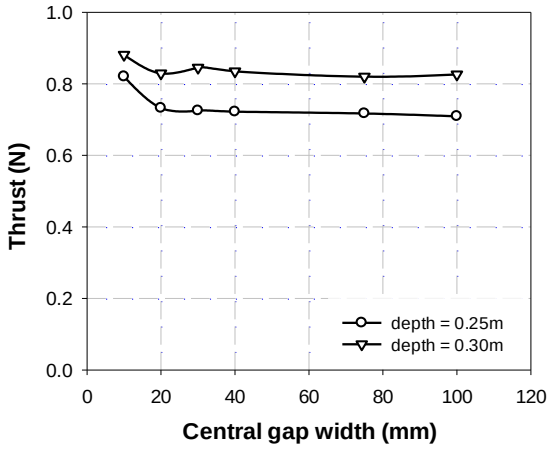

Figure 8-11: Central gap width thrust results

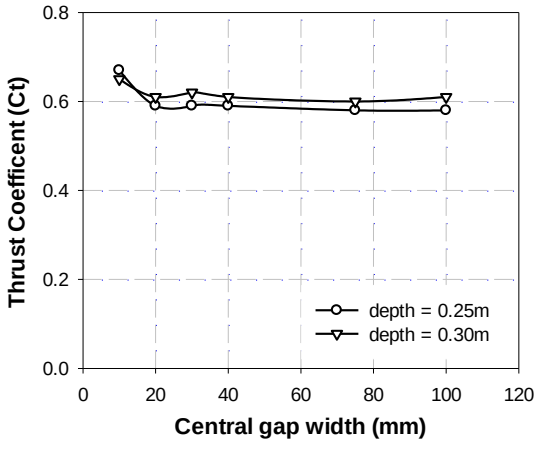

Figure 8-12: Central gap width thrust coefficient results

Looking at the C_t results (Figure 8-12) it can be observed that the C_t value increases with the narrow central gap. This increase in C_t with narrow gap width confirms that these thrust and potential power benefits can be attributed to flow impedance effects. This increase in thrust with

a narrow central gap occurs because the central streamlines cannot expand as they would in an unconstrained scenario (e.g. the outside edges of the plates) and hence more flow is forced through the device rather than around it. As the central separation distance increases the streamlines are free to expand and the flow takes its natural path around the edge of the mesh plates. Again analogous with chapter 7's results, the C_t values are slightly higher for the deeper 0.3m flow depth.

8.5.5 Inward or outward facing hydrofoils

The current design and the initial testing involved inward facing hydrofoils, where both hydrofoils are located above the ramp centreline. However there was also a proposal to have outward facing hydrofoils (Figure 8-13, right) where they would be located away from the ramp centre-line. A series of tests were conducted to establish the effect of separating the hydrofoils and moving them closer to the ramp edges. This was achieved by moving the actuator plates away from the ramp centreline (position 1, Figure 8-13, left) to a position half a sweep height upstream of the ramp (position 10). Eight additional locations were tested between position 1 and 10 (Table 8-4).

INWARD FACING OUTWARD FACING

Figure 8-13: Inward or outward facing hydrofoils

Position	Upstream distance from ramp centre
1	Ramp centreline
2	15mm
3	30mm
4	45mm
5	60mm
6	75mm
7	90mm (top of leading edge ramp)
8	120mm
9	150mm
10	180mm (1/2 plate height upstream of ramp)

Table 8-4: Actuator stream-wise location

These tests do not fully characterise the situation because the outward facing condition models only the upstream foil but not the downstream hydrofoil position, hence it assumes the thrust from the upstream and downstream foils occurs wholly at the upstream location. This is not

considered problematic because the experiments aim to model the relative effect of having a hydrofoil located over the leading edge of the ramp rather than the precise interaction effects of the downstream foil.

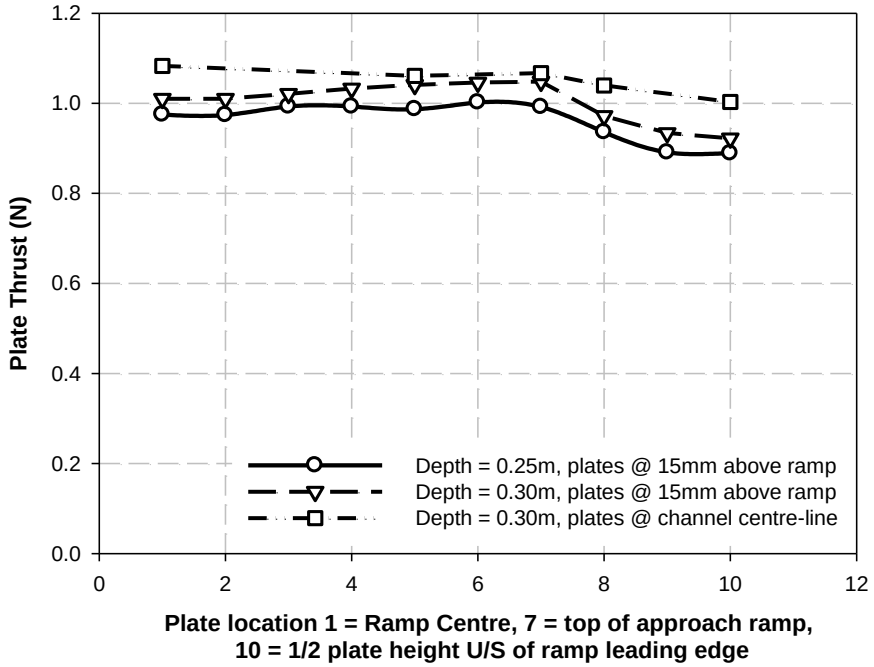

Figure 8-14: Inward or outward facing hydrofoils, thrust results

It appears that positioning hydrofoils at any location, provided they are directly above the ramp surface (Figure 8-14 & Figure 8-15) will not significantly affect thrust results as long as they are situated in close proximity to the ramp surface or channel bed. With a small 15mm gap between the ramp and the bottom edge of the actuator it appears that the thrust actually increases as the plate is moved towards the ramp leading edge. This can be explained by referring back to chapter 5, section 2.2.4. Here Figure 5-9 shows normalised velocity profiles near the ramp leading edge which are nearly uniform in velocity. Looking at Figure 5-10 showing velocity profiles at the ramp centreline - although in the upper region the profile has developed, close to the ramp the profile is heavily sheared and hence average velocities are reduced compared with the lower region of Figure 5-9. With the plates located higher up in the water column (e.g. centre height), as shown in Figure 8-14 the optimal location is the ramp centre-line because the velocity profile is well developed with larger fully augmented velocities. Thus although greater velocities will always occur higher in the water column, it would appear when hydrofoils are located close to the ramp (current design) that outward facing hydrofoils could be used provided they are not located beyond the top of the leading edge profile (location 7).

Figure 8-15: Optimum hydrofoil location

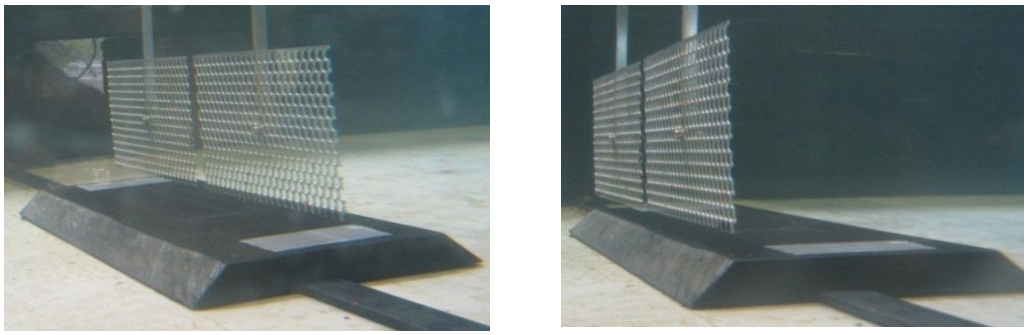

Figure 8-16: Inward facing foils (left) & outward facing foils (right)

8.5.6 Vertical position within water column

Here two tests were run using the PSCD actuator plates, which were moved incrementally through the height of the water column to find the optimum depth in terms of thrust load increase and hence potential energy yield. As discussed in section 8.5.5 the optimum location results from the shape of the vertical velocity profile, with the lower regions having a reduced bed sheared velocity.

These results (Figure 8-17) show that with the hydrofoils located close to the ramp/bed (as they are in the current PSCD design) there is a reduction in device thrust and hence efficiency. A loss of 12.5% thrust can be seen compared with having the hydrofoils located at intermediate-depth. It would be advisable based on these results to increase the level of the hydrofoil centre height or increase sweep height to improve device efficiency across a tidal cycle.

Figure 8-18 shows that the plate C_t remains relatively constant throughout the tested depths. This means that when the hydrofoils are located close to the bed/ramp the lower device thrust can be attributed to the reduced bed shear flow velocity. This is clear from Figure 8-7, which shows the free-stream velocity profiles.

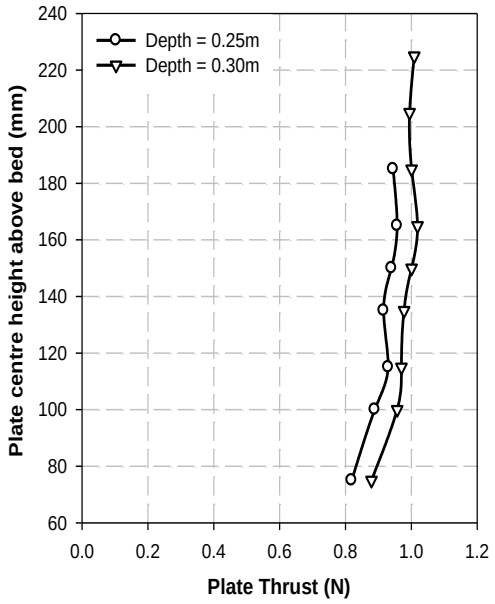

Figure 8-17: vertical hydrofoil position, thrust results

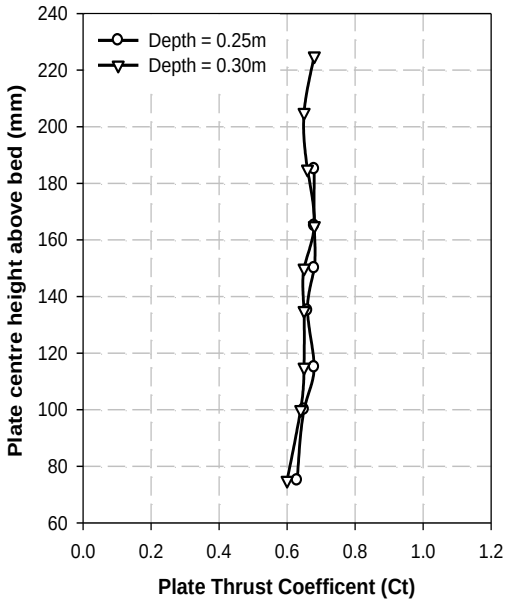

Figure 8-18: vertical hydrofoil position, C_t results

8.5.7 Ramp-foundation length sensitivity

Three tests were carried out to establish the effect of reduced ramp-foundation length on PSCD performance (Figure 8-19). During the initial design stages the proposed length of the PSCD ramp was reduced from 21m to 13m full scale. This was predicted to slightly reduce the flow augmentation benefits of the ramp-foundation. Here the ramp length was progressively reduced in three stages and the effect on actuator thrust was recorded. The results from the no ramp situation are included for comparison.

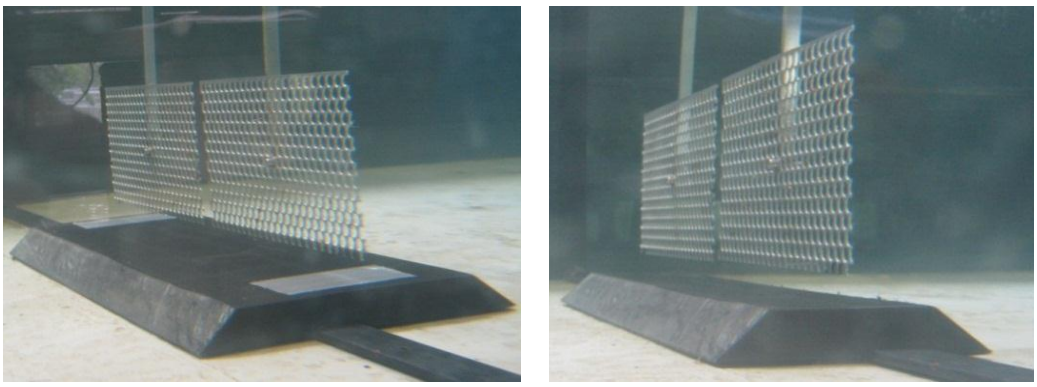

Figure 8-19: Ramp length, 210mm (left) & 130mm (right)

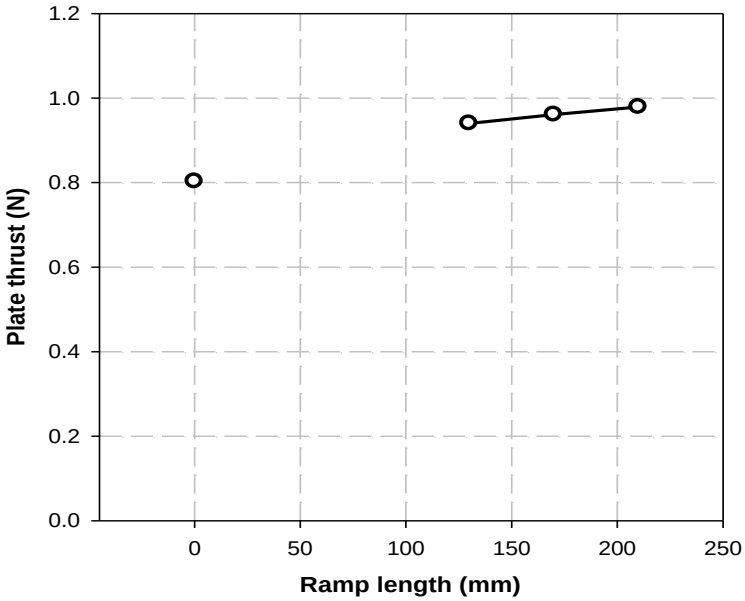

Figure 8-20: Ramp length sensitivity, plate thrust. Fd = 0.2, Depth = 0.25m

It can be seen in Figure 8-20 that there is a reduction in thrust when reducing the length of the ramp from 210mm (21m, full-scale) to 130mm (13m, as in the current full-scale PSCD design) because the velocity profile has less distance over which to develop. The reduction is in the region of 4-5%. Ramp length zero corresponds to the condition with no ramp-foundation and it can clearly be seen that there is a significant reduction in thrust compared with having a ramp-foundation (17-22%). This again highlights the prospect of considerable power benefits from ramp-foundations (27-35% from these results).

8.5.8 Summary

Following these experimental tests the following design recommendations and observations were presented to Pulse Tidal:

- **Ramp augmentation:** Ramp-foundations increase the flow velocity and hence during the testing they provided average device thrust benefits of 14.5%. From momentum theory this gives an average theoretical power benefit of 22.6% (for the lateral and vertical ramp blockage ratios tested).
- **Central gap:** The current design with a narrow central gap of 1m appears to increase device thrust by approximately 6-7% when compared with increasing the gap width up to 10m because the thin gap restricts expansion of the central streamlines. It must be reiterated here that this is a global thrust effect on the actuator plates and it does not characterise any locally high thrusts that could be occurring due to the narrow central gap.
- **Inward or outward facing foils:** It appears that locating hydrofoils at any location provided they are within the region directly above the horizontal ramp surface, will increase the thrust loads on the PSCD. This is on the condition that they are located in close proximity to the ramp surface (or channel bed). Hence outward facing foils could be used as long as their sweep does not extend beyond the geometric extent of the ramp's top surface. However locating the hydrofoils near the channel centre height still gives more thrust in all locations compared with having them located 15mm (1.5m full scale) above the ramp.
- **Vertical position:** With the hydrofoils located close to the ramp/bed (as they are in the current PSCD design) there is a reduction in device thrust and hence efficiency. A loss of 12.5% thrust can be seen compared with having the hydrofoils located near the channel centre depth. It would be advisable to increase the height of hydrofoil centre height or adjust sweep height with the state of the tide to improve device efficiency across a tidal cycle.
- **Ramp-foundation length:** There is a reduction in thrust when the ramp length is reduced from 210mm (21m, initial HR Wallingford tests) to 130mm (13m as in current PSCD design). The reduction is in the region of 4-5%. But thrust benefits are still considerable even with the shortened ramp. For the purpose of increasing thrust/power the ramp should be as long as possible, but other constraints are likely to determine the maximum stream-wise length.

It must be reiterated that the results for thrust and power benefit presented in these PSCD tests will only be correct in magnitude for the lateral ramp blockage ratio tested (0.34). The general trends (e.g. increased power from ramp-foundations) will be true for different lateral ramp span to channel width ratios but will need to be factored using empirical relationships developed in chapter 5, section 5.4.

8.6 PSCD wake

8.6.1 Introduction

This section follows on from the work presented in chapter 7 for horizontal axis turbines operating in vertically constrained flows. Here the free-surface and channel bed proximity effects on the downstream wake length are investigated in the same way for the PSCD. 1:100 scale tests were conducted using the actuator plate (220x120mm) to represent the PSCD swept area (the "High Solidity" plate from section 8.5 was used). To allow direct comparison between the results in chapter 7 it was decided to just model one set of PSCD hydrofoils using a single actuator plate. The downstream wake flow behind the PSCD was characterised using the ADV and the three tests are described in Table 8-5. At full scale this test range encompasses the anticipated initial operating depths of the PSCD which is in the range of 20-40m.

Test	Full-scale water depth (m)	Scale water depth (m)	Channel width (m)	Actuator centre from surface (m)	Depth-averaged Froude No.	Plate height/depth ratio
1	40	0.4	1.37	0.20	0.15	0.30
2	30	0.3	1.37	0.15	0.15	0.40
3	20	0.2	1.37	0.10	0.15	0.60

Table 8-5: PSCD wake tests

8.6.2 Downstream wake length

Figure 8-21 shows the centre plan wake deficits behind the PSCD for tests 1-3. The same trend can be seen as with the horizontal axis turbines, where the wake length is at a minimum for mid-constraint device height to flow depth ratios (e.g. intermediate-depth sites) and the wake length increases as the vertical flow constraint increases (e.g. shallow sites). It can be seen in a flow depth of 40m full-scale - the PSCD wake persists for approximately 15 PSCD sweep heights downstream. For a PSCD operating in a shallow 20m depth the wake will persist much further, in excess of 20 sweep heights downstream. This again highlights the importance of tuning downstream farm spacing with the local flow depth to maximise device efficiency.

As postulated in chapter 7, the reduced wake length in mid-constraint tidal sites occurs from increased flow velocities above and below the PSCD, which aids to break down the wake in a shorter distance through turbulent mixing and increased shear forces at the wake boundary. In a shallow depth site the increased wake length results from the close proximity of the bounding surfaces to the MCEC, which results in the wake prematurely intersecting with the free-surface and channel bed, restricting flow above and below the PSCD. This reduces the intensity of

turbulent mixing between the wake and surrounding free-stream flow, allowing the wake to persist further downstream.

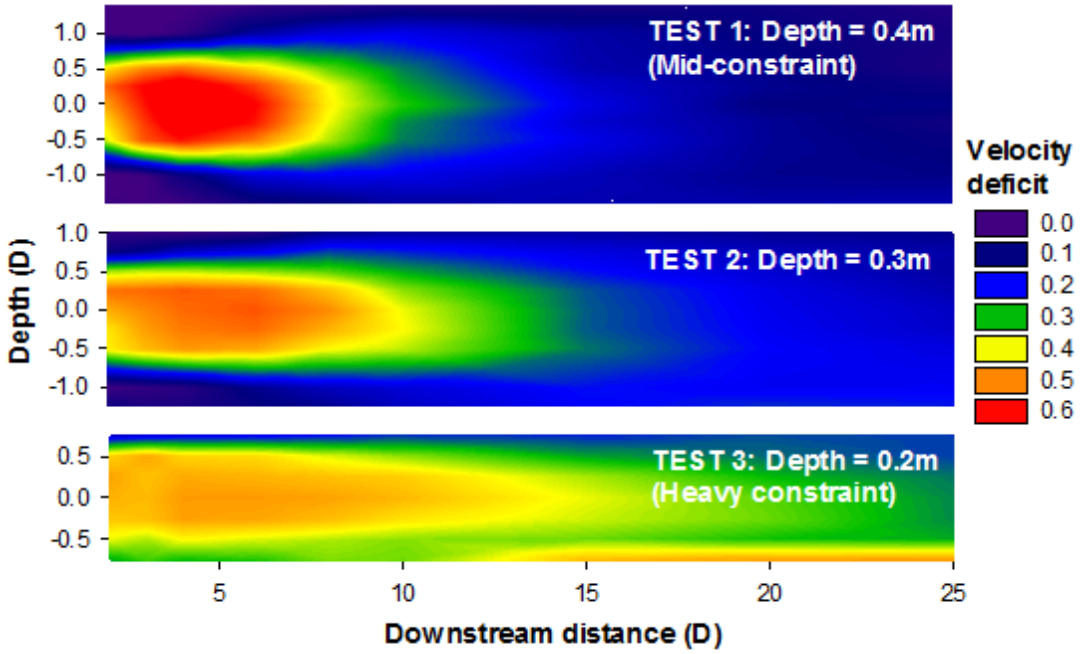

Figure 8-21: Centre plane velocity deficit profiles; PSCD

Although the full benefits of power potential must be considered, tuning the PSCD sweep height to the local flow depth could be a good approach if farm density was the priority. It must be noted that the PSCD will have a wider wake compared with a typical horizontal axis turbine. This is because the swept width of the hydrofoils will be significantly larger than a typical HAT diameter. In addition if the proposed design with two pairs of closely spaced hydrofoils is chosen, it is expected that the two wakes will combine and form one large wake persisting further downstream (Myers and Bahaj, 2012).

8.7 Construction, deployment and recovery strategy

Construction, deployment, recovery and maintenance are critical aspects for the commercialisation of a MCEC operating with a ramp-foundation. A concrete or fabricated steel caisson structure is proposed for the ramp-foundation. Such structures have been extensively used for gravity based foundations.

The principal advantage of using a caisson-type structure is that the bulk of the fabrication can be done onshore or in dry docks. The structure can then be floated and towed to the offshore installation site and gradually sunk into position. If required, additional buoyancy could be added by attaching buoyancy tanks. Gerwick (2000) states that the principal failure mechanism is sliding for water depths of less than 150-200m and this failure can be mitigated by attaching steel skirts or pin piles to the foundation. They effectively penetrate the seabed and force the failure mechanism further below the seafloor and in addition provide extra scour protection. When designing marine structures it is vital to consider loading at every stage of construction, as well as accidental conditions such as unplanned flooding of a buoyancy tank during delivery to site.

A novel deployment and recovery strategy is under development by Pulse Tidal for the PSCD (Figure 8-22). The PSCD has been designed with a "transverse strut" that connects the ramp-foundation to a seabed foundation. The transverse strut is utilised to constrain the position of the base through the water column, as buoyancy and ballast is used to raise and lower the MCEC. This method has significant advantages over a purely gravity-based approach in terms of lateral resistance of loads and providing active control of both deployment and recovery. The proposed deployment and recovery strategy is thus:

1. Deliver assembly to site.
2. Connect MCEC to ramp-foundation.
3. Install seabed foundation, i.e. install piles, grouting or swaging.
4. Connect transverse strut to seabed foundation.
5. Float ramp-foundation/MCEC towards the floating free-end of the transverse strut and connect.
6. Lower device to seabed using ballast tanks.
7. When required expel ballast and raise device to surface for maintenance. For large maintenance/repair procedures, the device would be disconnected and towed to a suitable port or dry dock.

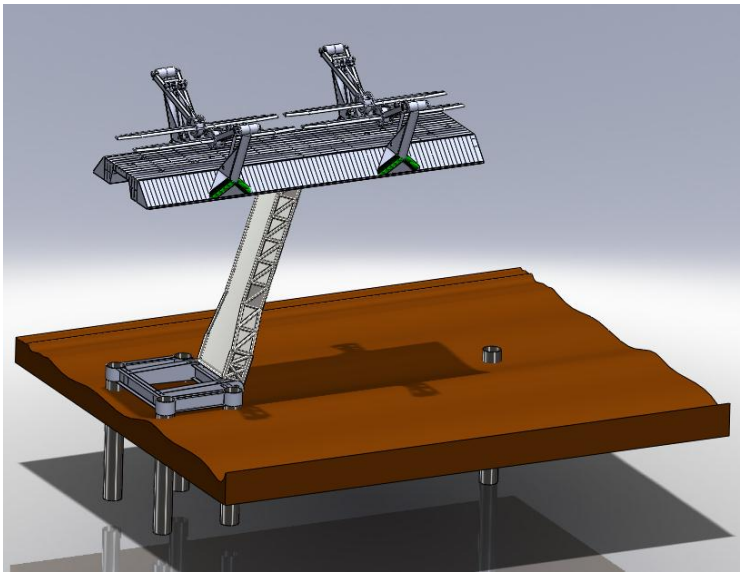

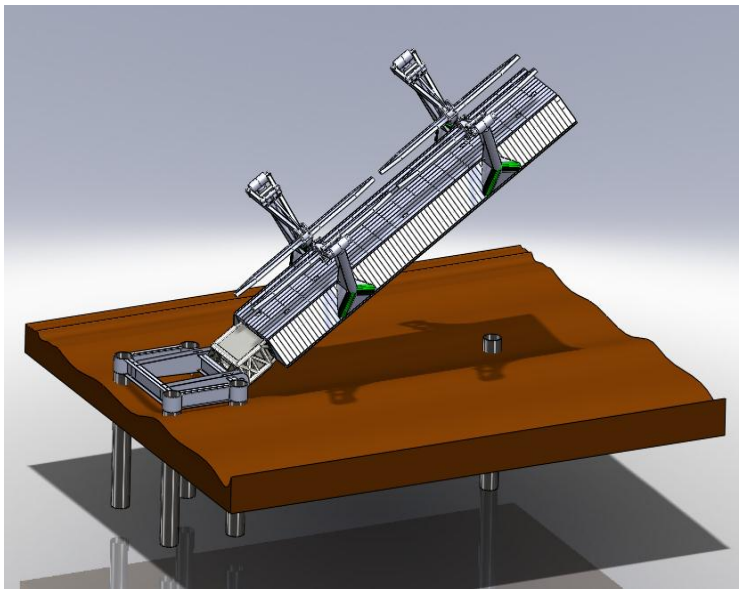

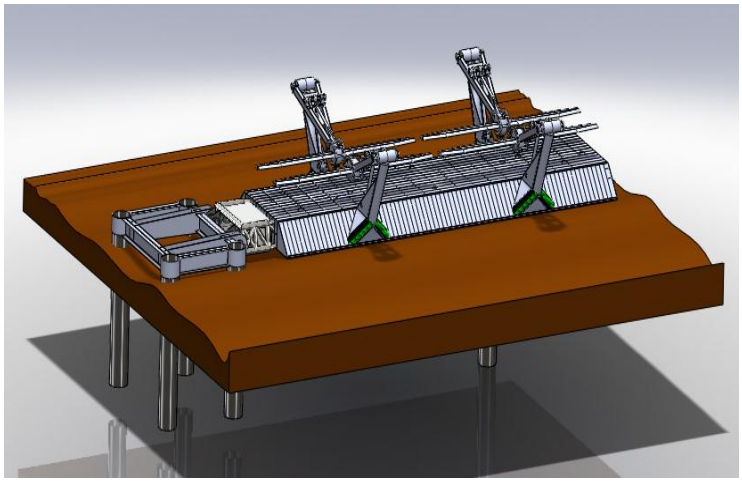

Figure 8-22: Deployment and recovery strategy: (a) surface maintenance height. (b) mid-water depth. (c) operating height

8.8 Stability calculations

8.8.1 Concrete foundation

Concrete caisson structures have been extensively used for gravity-based foundations. Full structural calculations will be conducted as part of the PSCD project, but presented here are preliminary stability calculations for a general ramp-foundation operating with a horizontal axis MCEC.

The factor of safety for the overturning moment and bed shear resistance were computed for horizontal axis turbines of varying diameters. Forces contributing to failure mechanisms include turbine thrust, drag from the support structure/foundation and the buoyancy force. The force that prevents failure is the mass weight of the ramp-foundation and the MCEC.

The buoyancy force (equation 8.3) is the resultant of the upward force on the foundation's lower surface minus the downward force on the upper surface of the foundation (Archimedes' principle). The resultant of this is the weight of the fluid displaced by the body (or ramp-foundation in this case).

$$Buoyancy = \rho g \times ramp\ volume \tag{8.3}$$

The drag force (equation 8.4) on the support structure and ramp-foundation results from the viscous flow exerting a force as it passes the structure. The magnitude of the force depends on many factors, including a drag coefficient C_d and the cross-sectional area of the support structure or leading edge profile. The drag coefficient C_d is determined by the body shape, surface roughness and Reynolds number. For the support structure the C_d value of 0.31 for a cylinder in turbulent flow is used. For the ramp a C_d value of 0.75 for an inclined plane of 45° is used.

$$Drag\ force = \frac{1}{2} C d \rho A U^2 \tag{8.4}$$

Turbine thrust is calculated from equation 3.25 presented in chapter 3 and a turbine power conversion coefficient of 0.4. The mass weight of the foundation is calculated assuming a concrete density of 2400kg/m^3. Sea water density was assumed to be 1025 kg/m^3.

The ramp height was 10% of the mean flow depth in each case. The ramp width was conservatively presumed to be the same width as the turbine diameter and the length was assumed to be 10m (optimum dimensions found in chapter 5).

Factors of safety against sliding were calculated by taking the resisting force (bed friction) and dividing it by the sum of the disturbing forces (turbine thrust, foundation drag and support structure drag). The resisting force from bed friction was calculated using a bed friction coefficient (μ) of 0.25. This coefficient was chosen from marine industry experience and from work by Yan et al. (2009).

The factor of safety against overturning was calculated by dividing the resisting moments (foundation weight) by the disturbing moments (buoyancy, thrust, support structure and ramp drag). Moments are taken about the far downstream edge of the ramp-foundation.

Provided these factors are in excess of unity the concept can be assumed to be stable, in reality for detailed design extreme loading conditions will need to be investigated. Results are presented in Table 8-6 and all factors of safety for overturning and bed shear resistance were in excess of unity.

Turbine diameter	Flow depth	Spring peak velocity	**Ramp dimensions**			**Overturning**			**Bed shear resistance**		
			Height	Width	Length	Resisting moment	Disturbing moment	Factor of safety	Resisting force	Disturbing force	Factor of safety
m	m	m/s	m	m	m	kNm	kNm		kN	kN	
5	**10**	**3.0**	**1.0**	**5**	**10**	**5886**	**3104**	**1.90**	**169**	**134**	**1.26**
7.5	**15**	**3.0**	**1.5**	**7.5**	**10**	**13244**	**7486**	**1.77**	**379**	**279**	**1.36**
10	**20**	**3.0**	**2.0**	**10**	**10**	**23544**	**14202**	**1.66**	**674**	**477**	**1.41**
15	**30**	**3.0**	**3.0**	**15**	**10**	**52974**	**35975**	**1.47**	**1517**	**1030**	**1.47**

Table 8-6: Concrete ramp-foundation stability calculation results

If further resistive capacity was required then the ramp length/width could be increased or pin piles could be added for increased overturning resistance and bed shear capacity. Results for concrete foundations are very encouraging. It can be concluded that even with a purely gravity-based foundation, the concept appears structurally viable.

8.8.2 Steel foundation

The preliminary structural calculations from section 8.9.1 were modified for a fabricated steel plate foundation. The density of steel was assumed to be 8000 kg/m^3 and the weight of the entrained water within the base was included in the calculations. The foundation height was again assumed to be 10% of the mean flow depth. Once again factors of safety against overturning and sliding failures were in excess of unity, ranging from 1.28-1.91 depending on the flow depth (Table 8-7).

Turbine diameter	Flow depth	Spring peak velocity	Ramp dimensions			Overturning			Bed shear resistance		
			Height	Width	Length	Resisting moment	Disturbing moment	Factor of safety	Resisting force	Disturbing force	Factor of safety
m	m	m/s	m	m	m	kNm	kNm		kN	kN	
5	**10**	**3.0**	**1.0**	**5**	**10**	**5935**	**3104**	**1.91**	**171**	**134**	**1.28**
7.5	**15**	**3.0**	**1.5**	**7.5**	**10**	**13354**	**7486**	**1.78**	**385**	**279**	**1.38**
10	**20**	**3.0**	**2.0**	**10**	**10**	**23740**	**14202**	**1.67**	**684**	**477**	**1.43**
15	**30**	**3.0**	**3.0**	**15**	**10**	**53415**	**35975**	**1.48**	**1540**	**1030**	**1.49**

Table 8-7: Steel ramp-foundation stability calculation results

Both results from the concrete and steel calculations are very promising. It can once again be concluded that even with a purely gravity-based foundation, the concept appears structurally viable. With the increased lateral restraint from any potential transverse strut connection between the seabed and base ramp (as with the PSCD) or pin piles these factors of safety would increase dramatically.

8.9 Techno-economic analysis

8.9.1 Introduction

For the ramp-foundation concept to be commercially attractive it must be technically feasible but equally it must be economically viable. The presence of the ramp-foundation will increase the device power output across the tidal cycle and hence increase the revenue generated from the exported energy. Despite the ramp-foundation being of multi-use, such as acting as an integral foundation, there will be an increased capital cost involved compared with a conventional MCEC. A techno-economic analysis has been conducted for the PSCD, which considers a breakdown of the capital cost of components, installation cost, operation and maintenance costs and the electricity revenue generated across a full tidal cycle. A Net Present Value (NPV) analysis has been applied (equation 8.1). The method is used to analyse the viability/profitability of the project taking into account the various costs (a NPV of greater than zero indicates a project is viable and profitable). NPV analysis uses “discount factors” to take into account that the value of money today will not be the same as its value at the end of the project. The design life of the PSCD concept is 25 years and hence this is considered the overall project duration. The Carbon Trust (2006a) recommended a discount factor of 15% for “1st commercial marine energy schemes” and 8% for “matured marine energy technology”. During the analysis a range of discount factors from 15-8% were considered to model the PSCD concept at various stages of commercial development. The current demonstration project is

considered to have a discount factor of 15%. As a demonstrator it is not designed to be a highly profitable project, but the analysis can still be used to estimate the general financial benefit of ramp-foundations.

$$NPV = PV(income) - PV(Expenses) \quad (8.1)$$

8.9.2 Project costs

8.9.2.1 Capital cost

Capital costs have been generated by estimating the cost of each component of the PSCD and the costs associated with installation. It is assumed that these costs are all incurred at the beginning of the project (year 0); hence no discount rates are applied. The total capital cost of the PSCD is estimated at £5,506,000.

8.9.2.2 Operation and maintenance costs

Operation and maintenance costs are assumed to be a constant annual expenditure during the course of the project. The estimated cost is £50,000 per year. As this is an annual expense throughout the project the discount rate must be applied to this as well as the income generated through the sale of electricity. Before the discount rate is applied the operation and maintenance costs are discounted from the income created by electricity generation. The discount factor is then applied to the result of the annual income minus expenses sum.

8.9.2.3 Energy generation income

The revenue generated from one year's operation was calculated based on a typical daily tidal cycle and a calculated energy conversion factor of 40%. The revenue from 1kWh of electricity is estimated at 20p based on an anticipated purchase price from a utility company and the added value from the ROCs (Renewables Obligation Certificate). It is assumed that the same amount of electricity is generated each year and hence the relative income will be the same. To account for deprecation of the value of money a discount factor is applied.

8.9.3 Results

Results are presented in non-dimensional form by dividing the NPVs by the estimated capital cost of the project.

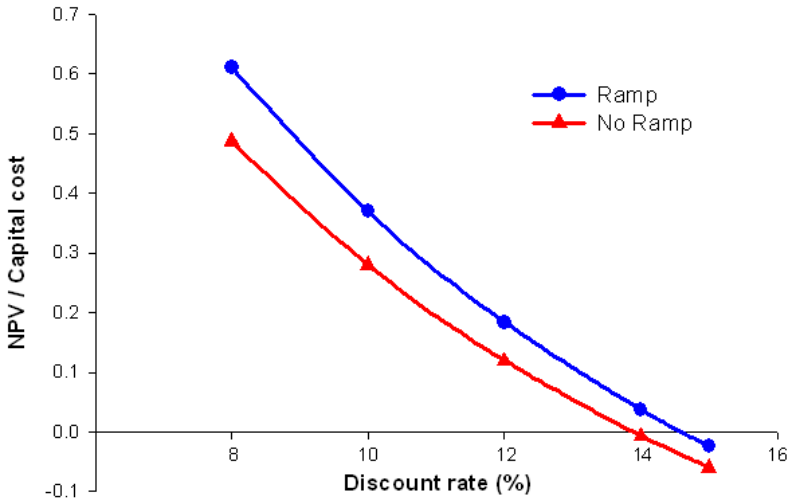

Figure 8-23: PSCD NPV analysis (25 year design life)

Figure 8-23 displays the results from the NPV analysis. It can be clearly seen that ramp-foundations offer financial benefits. By integrating the area under the curves using equation 8.2, an impression of the average overall financial benefit of a ramp-foundation is estimated at 23%. This takes into account the increased revenue from the sale of electricity and also the added capital cost of the ramp-foundation. Here the PSCD was modelled with a ramp-foundation occupying 25% of the channel width; of course with smaller lateral blockage ratios the financial benefit will reduce (see section 5.4). For example with a ramp occupying 10% of the channel width these benefits are predicted at 13%.

$$F(x) = y = A.\ln(x) + B \tag{8.2}$$

$$Area = \int_8^{12} F(x) = \int_8^{12} A.\ln(x) + B = A.[x.\ln(x) - x]_8^{12} + B[x]_8^{12}$$

These financial gains clearly show that ramp-foundations could be a financial reality as well as being technically viable provided the lateral ramp width to channel width ratio is sufficient. Figure 8-23 shows that in its current commercial state the PSCD is unlikely to be profitable (not unexpected for a demonstration device). However with zero NPV values occurring at discount factors of 14.6% for a ramp-foundation and 13.9% without a ramp-foundation, it is anticipated that with a small amount of development the next generation PSCD device would be a fully profitable concern.

Chapter 9

9 Conclusions

The key objective of this project was to investigate the topic of energy extraction from shallow tidal flows. In particular to research and model the application of ramp-foundations for MCECs and the effects of MCEC height to flow depth ratio on wake length. The Pulse Stream Commercial Demonstrator is also the first full scale commercial MCEC to be designed with an integral ramp-foundation to augment the flow. Here the key conclusions from the project are summarised:

- **Extracting energy from shallow tidal flows:** shallow tidal flows are generally more accessible for energy extraction and hence make a good location for first generation tidal stream arrays. Their close location to shore improves the construction feasibility and economic prospects. In addition in deeper sites it may be technically difficult to harness the full site potential, whereas in shallow areas a MCEC can be designed to occupy a greater proportion of the vertical water column. This project identified two key limiting factors for deploying MCECs in shallow flows, one being suitably high velocities for economic energy extraction and the second being the close proximity of the seabed/free-surface to the MCEC and its subsequent influence on downstream wake length (farm/array spacing). In addition close seabed and free-surface proximity may limit the applicability of horizontal axis turbines in very shallow flows because the swept area is equal to π times the square of the turbine's radius and cross flow turbines or oscillating hydrofoils may become desirable.

- **The use of ramp-foundations:** ramp-foundations increase the available power per unit channel cross sectional area by physically constraining the tidal flow. Low velocity shallow currents can thus be constrained and the velocity increased to an exploitable level, resulting in increased MCEC power output across a tidal cycle. In the UK alone if the local flow velocity could be artificially magnified by 15% the exploitable shallow resource area could be increased by up to 72% (see Figure 5-22). The foundation would be of multi-use, acting as a flow augmenter increasing device power potential, providing scour protection, acting as an integral gravity based foundation and potentially providing an engine room for machinery.

- **Ramp length and width:** the optimum ramp-foundation length is dependent on the ratio of ramp height to flow depth. For a ratio of 0.1 the optimum ramp length is approximately equal to the flow depth. This means a well-developed flow profile with a constant velocity upper energy extraction region occurs at half the flow depth downstream from the ramp's leading edge. The optimum ramp-foundation length therefore enables bi-directional tidal flows to be exploited. The width of the ramp-foundation would not need to considerably exceed the width of a MCEC for tidal currents with strong bi-directional characteristics as the bulk flow is in the downstream direction and no significant velocity reductions are likely to occur near the ramp side edges. For tidal currents with a degree of misalignment between flood and ebb flow the foundation footprint might need to be increased.

- **Ramp height/flow depth ratio:** a ramp-foundation occupying 10% of the flow depth is recommended as an applicable solution in terms of maximising power gain potential, abating the ramp-foundation's capital cost and maintaining its ability to operate as a gravity-based structure with an acceptable factor of safety against a global overturning or bed-shear sliding failure. A lower ratio will abate the capital cost but also reduce the degree of ramp flow augmentation and hence power gain, whilst a ramp that occupies a large proportion of the total depth will cost more to construct and may also limit the feasible rotor diameter that can be deployed.

- **Shear stress/turbulence intensity:** the extent of the sheared boundary layer region does not significantly increase with the presence of a ramp-foundation; due to mass flow continuity it is effectively compressed by the increased flow velocity in the upper region of the profile. Turbulence intensities were slightly reduced in the flow across the ramp-foundation, which would be beneficial to device operation and survival. It is postulated that the increase in flow speed and the associated increase in shear stress close to the ramp-foundation reduces a proportion of the smaller length-scale turbulent motion in the upper energy extraction region. Additionally the lower surface roughness of the ramp compared to the channel bed could be supporting this effect.

- **Leading and trailing edge profile:** a 45° leading and trailing edge profile at both ends of the foundation to exploit bi-directional flows would be recommended. This provides a compromise between increased velocity and minimising turbulence/shear stress near the foundation. Alternative leading and trailing edge profiles were tested but offered no measurable benefits in terms of performance.

- **Power gain potential and lateral extent of ramp-foundation:** increased velocity and power potential across a ramp-foundation result because of two key factors. Firstly continuity and localised flow streaming force the flow velocity to increase with flow area reduction across the ramp. Secondly the optimum energy extraction region occurs because of boundary layer redevelopment over the ramp surface. At low lateral ramp blockage ratios if just continuity principles from the reduction in channel cross sectional area were considered, velocity increase would be negligible, but localised streaming effects from the bulk downstream flow momentum yield tangible velocity benefits. The degree of flow velocity increase is hence dependent on the lateral ramp span to channel width ratio. Thus when considering the use of ramp-foundations the ramp width or overall array width must be tuned to the channel breadth to maximise power benefits. Clearly a ramp-foundation occupying the entire width of the channel would not be feasible except perhaps in a tidal fence application. Therefore the power gain potential of ramp-foundations is dependent on vertical ramp blockage, lateral ramp blockage and the MCEC solidity. For a typical MCEC, power gain prospects from installing a ramp-foundation would be 5-22% for a fixed vertical ramp height to flow depth ratio of 0.1 and varying with the lateral ramp span to channel width ratio in the range of 0.04 - 1. Until large arrays are deployed and occupy large widths of tidal channels, lateral blockage ratios for initial tidal stream developments are likely to be at the lower end of the spectrum with ramp-foundation power benefits of <10% across a tidal cycle.

- **Prediction of ramp-foundation power performance:** the velocity and power gain potential for ramp-foundations for different vertical (ramp height/flow depth) and lateral ramp blockage ratios (ramp width/channel width) is best described through empirical relationships developed from fundamental theory and validated using experimental data. The relationships described by equation 5.4 and 5.8 provide a good correlation with the experimental results for lateral ramp blockage ratios in the range of 0 to 0.5 (Figure 5-37). The empirical formula is a function of the ratio of above ramp flow area to side bypass channel area and the velocity/power gain from a full channel width ramp (with a corresponding ramp height to flow depth ratio). For lateral ratios greater than 0.5 the empirical fit breaks down and it appears that velocity gain reaches a constant peak value equal to that of a full channel width ramp. This effect could be characterised by further experimental testing but is of little concern as tidal deployment sites are anticipated to fall within the lower end of the lateral ramp blockage range. Larger lateral ramp spans would require farms to occupy the majority of a tidal channel which is unlikely to be feasible due to economic, navigational and construction constraints.

- **Potential flow ramp model:** the ramp-foundation potential flow model acts as a useful validation tool for experimental modelling and a means of efficiently analysing different ramp flow configurations. Although not yielding the accuracy of CFD analysis, results can be arrived at within reasonable tolerances without the requirement of extensive validation, multiple user input parameters or large computing times. Limitations of the potential model include; irrotational flow, inviscid fluid, lack of boundary layer characterisation and its 2-dimensional nature. The presence of the MCEC is also neglected because potential flow cannot directly model turbulent mixing between the wake and its surrounding flow. But in summary the potential flow model solves part of the scenario well and critically the important energy extraction region above the ramp is solved very quickly and efficiently. With further development the model could be developed into 3-dimensions but this was considered beyond the scope of this experimental project.

- **Full scale significance of ramp-foundations:** because of physical lateral channel restrictions ramp-foundations will only be technically viable in relatively narrow channels or in arrays or tidal fences (lateral ramp blockage ratio > 0.1) due to diminishing power returns at very low ramp span to channel width ratios. Analysis of some potential deployment sites showed that ramp-foundations appear viable in Strangford Narrows, Kyle Rhea and the Menai Strait provided a row of 10 or more turbines are installed (12-15% power gain). The concept could also be viable with a single MCEC provided the smaller returns of power were accepted and the ramp-foundation did not add significant capital cost to the device.

- **Financial benefits:** following a Net Present Value (NPV) analysis of the Pulse Stream Commercial Demonstrator (PSCD) concept and ramp-foundation, it can be anticipated that ramp-foundations will offer financial benefits taking into account the increased capital investment and the increased power potential across a full tidal cycle provided the lateral ramp to channel width ratio is sufficient. In the case of the PSCD, overall ramp financial benefits are predicted to be in the region of 13-23% (for a ramp-foundation occupying 10-25% of the channel width) compared with a PSCD operating without a ramp-foundation.

- **Vertical flow constraint and wake length:** it is critical that tidal stream farms or arrays are optimised in terms of their downstream spacing and packing density. It has been demonstrated that a flow depth of four times the turbine diameter is the optimum to reduce wake length, and either side of this depth ratio the wake length will increase. Hence wake length is directly related to the device height to flow depth ratio (Figure 7-8) and the

downstream spacing of MCECs must be tuned to the local flow depth to maximise the power potential of downstream turbine rows. In a deep unconstrained flow MCECs might only occupy a small percentage of the flow depth and local flow enhancement around the wake and hence shear forces at the wake boundary are reduced. In very constrained shallow flows MCECs could occupy the majority of the water column and flow above and below the MCEC would be restricted because the wake cannot expand fully and occupies the majority of the vertical water column. Furthermore, below the disk the highly turbulent and slow-moving wake combines with the channel boundary layer which has similar properties. Differential shear is thus low and there is little mass flow between the disk and bed. Both unconstrained and heavily constrained flow cases result in less wake flow mixing and resulting increased wake lengths. Intermediate-depth tidal sites will offer the shortest wake lengths due to the higher velocity augmentation of flow surrounding the wake. This flow serves to break down the wake in a shorter distance through higher turbulent mixing and wake boundary shear forces. This work highlights the importance of decoupling vertical and lateral MCEC blockage effects and could be developed into a full validated 3D experimental flow constraint model with an additional experimental programme to characterise lateral blockage effects in more detail.

It is hoped that the ramp-foundation concept and the relationship between vertical flow constraint and wake length will continue to help with the development of shallow depth tidal stream farms. It seems clear that ramp-foundations will only be commercially viable when deployed in shallow channels with high lateral ramp blockage ratios (device or array width to channel width ratio). The relationship between MCEC diameter to channel depth ratio and the downstream wake length will be critical for optimising future large-scale tidal stream arrays.

Appendix A

GILES, J., MYERS, L., BAHAJ, A. S., O'NIANS, J. & SHELMERDINE, B. 2011a. Foundation-based flow acceleration structure for marine current energy converters. IET Renewable Power Generation, 5, 287-298.

[12 pages]

Published in IET Renewable Power Generation
Received on 23rd November 2009
Revised on 3rd December 2010
doi: 10.1049/iet-rpg.2009.0181

ISSN 1752-1416

Foundation-based flow acceleration structures for marine current energy converters

J. Giles[1] L. Myers[1] A. Bahaj[1] J. O'Nians[2] B. Shelmerdine[2]

[1]Sustainable Energy Research Group, School of Civil Engineering and the Environment, University of Southampton, SO17 1BJ, UK
[2]IT Power Ltd., St Brandon's House, 29 Great George Street, Bristol BS1 5QT, UK
E-mail: jack.giles@soton.ac.uk

Abstract: This study presents a preliminary experimental study investigating the potential benefits of foundation-based flow acceleration structures for marine current energy converters (MCECs). Such structures would provide multiple benefits, including; increased device power output, increased foundation footprint and scour protection. Two phases of experimental testing have been conducted. The first series of tests investigated the flow acceleration caused by a ramp foundation without the presence of a MCEC. They were scaled from a shallow tidal flow site and provide evidence that these structures could give power benefits of 12–25% depending on ramp size and flow depth. An optimum ramp size was established based on the suitability of the vertical velocity profiles for energy extraction. The second phase of testing modelled a commercial marine current energy convertor with a gravity-based ramp foundation. The device was modelled using actuator plates to represent the interaction between the device and the surrounding flow field. A proposed single-operation installation method using a concrete ramp foundation is proposed and preliminary stability calculations are presented.

Nomenclature

C_p	power coefficient
ρ	water density
U_0	rotor centre flow velocity
A_d	turbine swept area
F_r	Froude number
d	flow depth
d_1	upstream flow depth
d_2	flow depth across ramp
U_1	upstream depth-averaged velocity
U_2	depth-averaged velocity across ramp
ΔZ	ramp foundation height
L	ramp length
W	ramp width
H	ramp height
I	ambient turbulence intensity
σ	standard deviation of sample
U	3D mean velocity of sample
u, v, w	instantaneous velocity
$\bar{u}, \bar{v}, \bar{w}$	sample mean velocity
u'	$u - \bar{u}$
v'	$v - \bar{v}$
w'	$w - \bar{w}$

1 Introduction

A critical limiting factor for the commercialisation and deployment of large-scale tidal energy is the availability of suitable sites. Suitable locations need to be easily accessible for device installation and maintenance, close to grid connections and most importantly have sufficient tidal flow velocities. Power from a tidal turbine is proportional to the cube of the flow velocity hence any small increase in velocity will result in considerable power benefits [1]. Power output from a free-stream tidal turbine is defined as

$$\text{power} = \frac{1}{2} C_p \rho U_o^3 A_d \tag{1}$$

where C_p is the fraction of the kinetic energy captured across the swept area of the turbine rotor. It has a maximum (limiting) value of 0.593 for an un-augmented rotor as defined by Betz [2]. In practice it also includes blade, drivetrain and other losses. Peak C_p values for megawatt (MW) class wind turbines are now approaching 0.5. Many suitable sites for marine current energy converters (MCECs) are located in shallow tidal flows such as those found close to the shore and in estuaries. Shallow flows have a reduced cross-sectional area suitable for energy extraction compared with deeper channels, but they have other benefits including close proximity to the shore with many sites situated away from shipping channels. This could make construction and grid connection both easier and economically feasible. Regions of flow that currently have insufficient velocities

for economic power generation could also be made economically viable with the use of artificial flow acceleration structures.

Present literature related directly to flow acceleration in tidal flows is limited, but some open-channel hydraulics such as submerged objects and bedforms may be applied. Two methods of flow acceleration have been identified. Flow concentrators that surround tidal turbines could be used to locally accelerate the flow, such as the shrouded Rotech turbine designed by Lunar Energy [3, 4] and the two-way diffuser detailed by Setoguchi *et al.* [5]. Klaptocz *et al.* [6] and Roddier *et al.* [7] present studies of vertical side wall concentrators for tidal stream turbines and both conclude that these structures are beneficial in terms of power generation. An alternative concept that is proposed and developed in this paper is a seabed mounted tidal flow acceleration structure.

Ramp or apron structures placed on the seabed could be used to locally accelerate the flow while also offering scour protection and an increased foundation footprint (Fig. 1). Increasing the footprint area and hence foundation mass would increase the downforce created by the foundation and hence increase the bed shear capacity. With careful design of the leading edge it may also be possible to smooth the vertical velocity profile that will serve to reduce rotor loading. These structures would form an integral part of the MCEC foundation and would be most applicable to shallow tidal flows with depths ranging from 10 to 20 m. Foundations could be gravity based and constructed using reinforced concrete caissons that are floated out from shore and sunk in the required position. The concept could be used for deeper flows but ramp height would need to be considerably greater to accelerate the flow, hence leading to increased construction cost.

Salter and Taylor [8] stated that a high local flow acceleration would occur for any reduction in channel width or depth. This reinforces the anticipated benefits of ramp accelerators. Although there is a lack of work directly related to marine energy extraction, open-channel hydraulics, channel bed obstructions and possibly submerged weirs could be applied. Starting with simple open-channel hydraulics texts [9, 10], which describe principles of specific energy and continuity, it is obvious that in a laterally constrained domain the introduction of a bed ramp will accelerate the flow and cause a small surface drop in the case of subcritical flows. This theory cannot be directly applied to tidal flows, except for perhaps in a tidal fence application, because flows are generally laterally unconstrained. A number of authors [11–15] specifically address open-channel bedforms and describe velocity profile development, turbulence characteristics, the importance of avoiding critical depth conditions and flow separation. Weir flow theory can be found in the text Chow [9], and Wu and Rajaratnam [16] present an experimental study into submerged weir flow; however, the study focuses on sharp-crested weirs that bear few similarities to a long submerged foundation ramp. A submerged bed obstruction has a clearer resemblance to a ramp foundation structure than a submerged weir mainly owing to the ratio of flow depth to ramp height.

It may seem intuitive that a ramp spanning the full channel width will accelerate the velocity; in reality however, it would not be feasible to construct and install such a huge structure. The ramp foundation would only occupy a small lateral (cross flow) proportion of the channel hence the interaction effects of the bounding flows are critical. In addition, minimising the ramp's dimensions will reduce the construction costs and improve concept viability.

The combined effect of a MCEC and a ramp foundation on the flow field is of paramount importance. The benefits of the ramp foundation may be reduced if the MCEC has a higher coefficient of thrust, and hence an increased thrust loading, meaning higher device solidity and resulting higher flow blockage. This flow impedance will force more flow around the side of the device and hence a higher solidity MCEC will reduce the velocity acceleration effect across the ramp. This needs to be quantified but the ramp is still expected to provide considerable flow enhancement and hence power benefits compared with a MCEC operating in free-flow conditions.

For efficient energy capture and reduced rotor loading the vertical velocity profile ideally needs to be relatively constant with depth, certainly in the region of flow swept by the rotor [17]. Vertical velocity profiles have been measured at a few locations in UK waters [18, 19]. One of these shows a very close resemblance to the modified 1/7th power law [20], with a sheared boundary layer region near the bed and an approximately linear upper section. When the flow encounters the upstream edge of a ramp structure the lower sheared section of the vertical velocity profile will effectively be removed [11] and the profile will start to re-develop across the ramp. Fig. 2 shows some measured vertical velocity profiles across a scaled ramp in a water channel facility. Ideally the MCEC would be located at the optimum location along the ramp where the maximum velocity increase occurs coupled with a more uniform vertical profile.

It is preferable to avoid the sheared region of flow near the sea bed as the differing mass flow rates will cause disparate rotor loadings. It has been previously estimated that the top 8 m and bottom 25% of the depth should be avoided owing to surface wave effects and the steeper section of the boundary layer, respectively, [20]. It is also important to

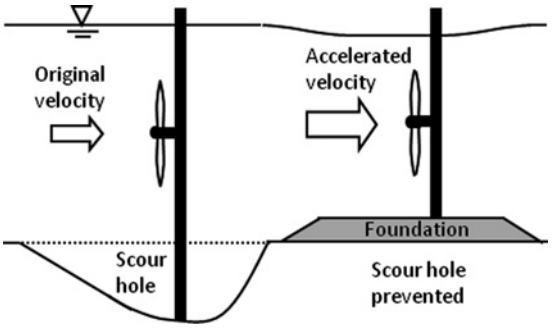

Fig. 1 *Proposed ramp foundation benefits*

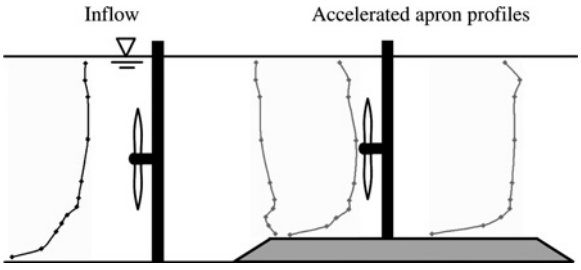

Fig. 2 *Boundary layer redevelopment*

doi: 10.1049/iet-rpg.2009.0181

ensure the ramp will not induce more turbulence that could have a negative effect on MCEC loading and performance.

When analysing the flow using specific energy estimations a significant surface drop would be expected across the ramp. However, results from previous work indicate that unless flow speeds become very rapid and the flow is confined by solid boundaries there may not be any measurable change in water surface elevation [21]. The reduction in water surface elevation can be derived from Bernoulli's equation (2). Specific energy analysis assumes no friction, a theoretical model which takes account of these effects and the presence of the MCEC is under development.

$$\text{surface drop} = d_1 - d_2 = \frac{U_2^2}{2g} - \frac{U_1^2}{2g} + \Delta Z \qquad (2)$$

As with any new concept the cost/benefit will be important to the commercial viability. The construction of an extensive ramp foundation will add cost to the construction and this added cost must be recouped in the additional power generated and through reduced construction costs associated with any reduction in dynamic loading offered by the ramp.

2 Materials and methods

In order to test the concept at a manageable scale, scaled ramps and actuator plates were constructed and tested in circulating water channels at the University of Southampton and HR Wallingford Ltd., UK. The working section of the Southampton channel is 21 m in length, 1.35 m wide and a maximum 0.4 m depth for steady operation with a maximum flow rate of 0.2 m^3/s. For the Wallingford channel the dimensions are as follows: 25 m in length, 2.4 m wide and a maximum 0.7 m depth for steady operation with a maximum flow rate of 0.28 m^3/s.

Using Froude scaling, the experimental flow domain was scaled from a prototype MCEC deployment site with an average full-scale depth of 10–20 m. Spring peak and neap peak tidal flow velocities are in the range of 0–3 m/s. It was assumed that a feasible full-scale ramp foundation height would be 10% of the average flow depth.

A range of different flow parameters and ramp dimensions were investigated. These included varying; Froude number, ramp height to flow depth ratio, ramp width and length. The angled sections at the upstream and downstream ramp ends are termed 'approach ramps' and were angled at 30° to the horizontal.

A range of flow and ramp configurations were tested for the ramp only tests, dimensions of key ramps are shown schematically in Fig. 3 and tests are detailed in Table 1.

The tests conducted at HR Wallingford used actuator plates to represent a commercial demonstrator (Fig. 5, right). The porous aluminium actuator plate's impedance was designed using an empirical relationship between thrust coefficient (C_t) and plate porosity. This relationship was developed from a combination of experimental findings from the University of Southampton and from equations presented by Whelan *et al.* [22]. Four plates termed LOW, MID, HIGH and V.HIGH solidity were tested to represent the device in different operating conditions.

Actuator plates are now an accepted method for modelling MCECs and have been extensively used for horizontal axis turbines, but the method can equally be used to model vertical axis and oscillating hydrofoil devices. Actuator and momentum theory is discussed extensively by Burton *et al.*

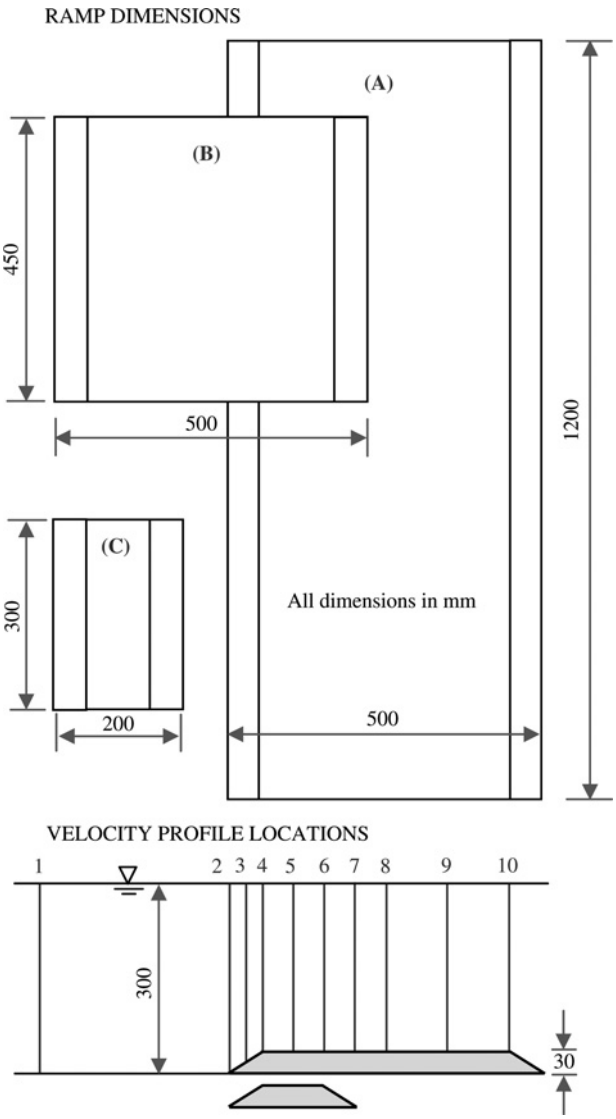

Fig. 3 *Ramp dimensions and centreline velocity profile locations for ramp only testing*

[23]. Work concerning the use of small-scale actuator plates for the representation of far wake conditions has been addressed by a number of authors [21, 24] and experimental work has been conducted which involves the modelling of MCECs using actuator plates and disks [25–27]. The principle difference between flow fields around actuator plates and full-scale MCECs is the representation of the near wake and these differences are generally known to dissipate in less than four rotor diameters downstream [28, 29].

In order to determine the potential benefits of the ramp, velocity profiles were measured upstream of the ramp and at various locations along the ramp's length; numbered in Fig. 3. This method was also used for the HR Wallingford actuator plate tests with the additional measurement of the actuator plate thrust.

In order to measure the velocity profiles and visualise the flow field around the ramps and actuator plates, samples were taken using a high-frequency acoustic Doppler velocimeter (ADV). Operational issues and the accuracy of ADVs have been addressed at length in many publications [30–33]. The ADV was set to sample at 50 Hz. For each data point 7500 readings were taken over a 150 s period.

Table 1 Experimental parameters and full-scale dimensions for ramp only testing

Test	Froude	Experimental scale					Ramp	Full scale			
		Depth, mm	Mean vel., m/s	Ramp size, mm				Mean vel., m/s	Ramp size, m		
				L	*W*	*H*			*L*	*W*	*H*
1	0.25	300	0.43	500	1200	30	A	2.48	16.5	39.6	1
2	0.35	300	0.60	500	1200	30	A	3.47	16.5	39.6	1
3	0.15	300	0.26	500	1200	30	A	1.49	16.5	39.6	1
4	0.15	300	0.26	500	1200	30	A	1.49	16.5	39.6	1
5	0.2	300	0.34	500	1200	30	A	1.98	16.5	39.6	1
6	0.3	300	0.50	500	1200	30	A	2.97	16.5	39.6	1
7	0.15	400	0.30	500	1200	30	A	1.49	16.5	39.6	1
8	0.15	200	0.21	500	1200	30	A	1.49	16.5	39.6	1
9	0.25	200	0.35	500	1200	30	A	2.48	16.5	39.6	1
10	0.2	400	0.40	500	1200	30	A	1.98	16.5	39.6	1
11	0.2	200	0.28	500	1200	30	A	1.98	16.5	39.6	1
12	0.2	300	0.34	500	600	30	–	1.98	16.5	19.8	1
13	0.2	300	0.34	500	450	30	B	1.98	16.5	14.9	1
14	0.2	300	0.34	300	450	30	–	1.98	9.9	14.9	1
15	0.15	300	0.26	300	450	30	–	1.49	9.9	14.9	1
16	0.2	300	0.34	200	450	30	–	1.98	6.6	14.9	1
17	0.2	300	0.34	200	300	30	C	1.98	6.6	9.9	1

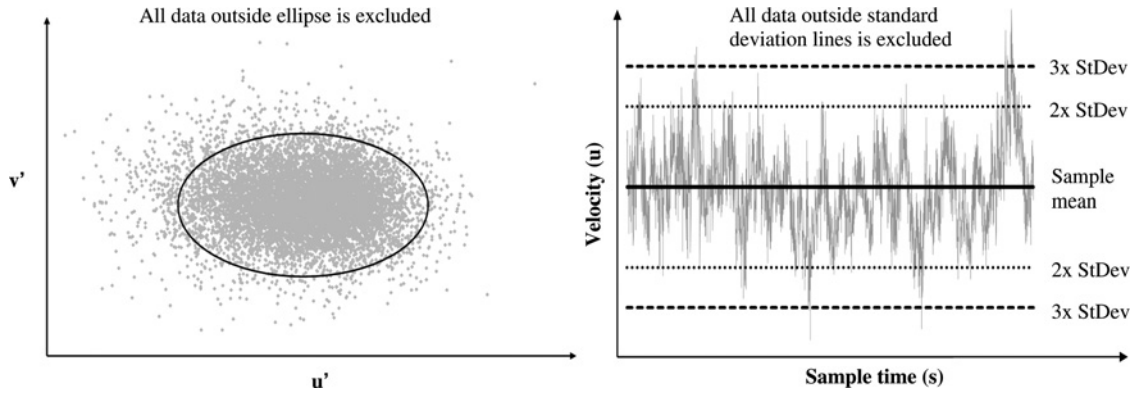

Fig. 4 *Velocity correlation filtering method (left) and minimum/maximum filter (right)*

Thrust was measured using a lever arm rig and 10 N button load cell. Thrust was measured by recording applied voltage to the load cell and from this the actual disk thrust in Newtons was calculated.

Data were filtered to remove noise and spurious points (Fig. 4, shows data spikes) although the large quantity of suspended particles in both the circulating channels minimised sample errors. Filtering is required to improve measurements of higher-order flow effects such as turbulence intensity and shear stresses as spikes in the data give the impression of increasing energy within the flow. However, filtering has a very small effect for mean flow velocities as spikes are generally equally positive and negative. All samples were filtered using a velocity cross-correlation filter ultimately chosen owing to ease of use and effectiveness after a single pass [34]. This method plots the

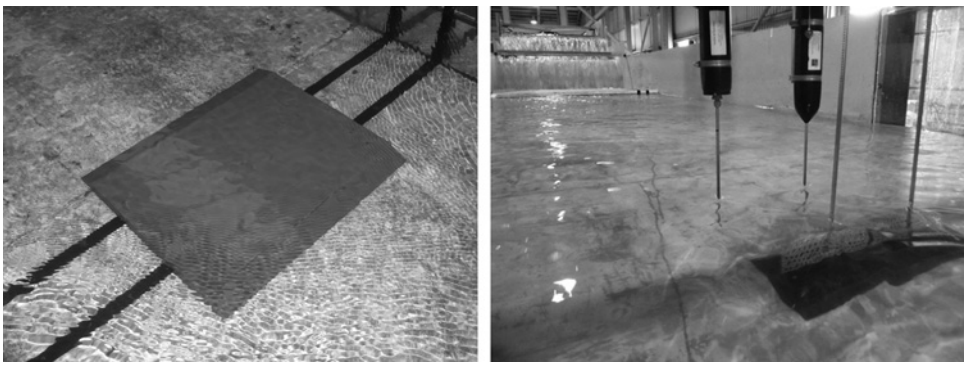

Fig. 5 *Experimental testing: ramp foundation testing (left) and MCEC model testing (right)*

doi: 10.1049/iet-rpg.2009.0181

varying components of velocity against each other and constructs an ellipse in three-dimensional space to exclude any data points that deviate significantly from the sample mean (Fig. 4, left). Similar filters can be set up to remove statistically or physically improbable values. The former can be based on the removal of data points more than three sample standard deviations from the mean sample value assuming that the dataset is normally distributed; this type of simple filter is commonly referred to as a minimum/maximum filter (Fig. 4, right). Physically improbable criteria include techniques such as removing data points where the varying velocity component exceeds the acceleration owing to gravity (highly improbable in a viscous fluid such as water). The importance of filtering for higher-order flow effects is illustrated by Table 2, it can be seen that the percentage change from the raw data values to the filtered values (velocity correlation filter) is much higher for the turbulence intensity compared with the mean velocity. Hence, as stated by Cea *et al.* [34] filtering is required to compute the correct turbulence parameters.

When conducting small-scale tests in a circulating water channel, there will be limitations. These include replicating full-scale channel bathymetry, the temporal dynamics of a tidal cycle (such as varying depth, flow velocity and direction), lateral blockage effects and Reynolds and Froude number parity. These parameters must be considered when interpreting results but should not effect the general conclusions presented in this paper and it would be virtually impossible to fully represent all the features found in a natural tidal channel at this scale. It will not be possible to achieve Reynolds number parity between model and full scale although for the experimental tests presented here the model Reynolds number was fully turbulent. Lateral blockage is of concern but both channels are significantly wider than they are deep so effects should be minimised, particularly in the wide HR Wallingford channel.

Characterisation of ambient turbulence levels is important as long length scale turbulence may lead to increases in dynamic rotor and structure loading. The ambient turbulence intensities in the circulating channels used during this study were ~6–8% and were calculated in all three planes (u, v, w) Turbulence intensity is commonly defined as the root-mean-squared of the turbulent velocity fluctuations divided by the mean velocity of the sample.

$$I = \frac{\sigma}{U} \tag{3}$$

High shear stress can be detrimental to MCEC survival. Horizontal shear stress should be approximately zero throughout the channel depth as lateral velocity components are small. Vertical shear stress will increase towards the channel bed owing to increased shear in the boundary layer. Horizontal and vertical shear stresses are defined as

$$\text{horizontal shear stress} = u'v'\rho \tag{4}$$

$$\text{vertical shear stress} = u'w'\rho \tag{5}$$

Normalised results for velocity measurements and turbulence intensity are presented by normalising ramp profiles with the depth-averaged values from the upstream profile.

3 Ramp foundation results

This phase of testing was conducted to fully understand the behaviour and benefits of a ramp foundation without the presence of a MCEC.

3.1 Full channel width ramp

The initial set of tests involved a ramp spanning the full channel width. A range of Froude numbers with a fixed flow depth of 300 mm were investigated. Velocity profiles were taken at the locations detailed in Fig. 3.

Fig. 6 shows how the u-plane and w-plane velocity profiles developed across the ramp for a flow depth of 300 mm and a Froude number of 0.25. The profile taken 150 mm downstream of the ramp leading edge shows the best profile for energy extraction, in terms of acceleration and a linear upper section. The sheared boundary layer region does not seem to increase considerably with the presence of the ramp. In general these conclusions are true for all tests conducted with the full width ramp at a flow depth of 300 mm. The u-plane velocity was increased by ~10% in all cases.

Velocities in the v-plane (lateral) and w-plane (vertical) were found to be approximately equal to zero throughout the flow depth. With the exception of profiles 2–4 (Fig. 3) taken across the upstream approach ramp where small w-plane velocity components were introduced near the ramp (Fig. 6). This is likely to have resulted from a small back eddy forming at the start of the ramp.

Turbulence intensities reduced slightly across the ramp for all planes (u, v, w). This is significant as it was previously stated that turbulence can have negative effects on MCEC performance. It is postulated that the acceleration in flow speed and the associated increase in shear stress close to the ramp structure may have reduced some of the smaller length scale turbulent motion.

The horizontal and vertical shear stresses were calculated throughout the water depth. Horizontal shear stress was found to be approximately zero throughout the depth (Fig. 7). This was expected as there are no significant lateral components of velocity to cause shear in this direction, both for the ambient upstream flow and that across the ramp structure. The vertical shear stress increased

Table 2 Minimum/maximum and velocity correlation filter comparison

Sample	u-plane velocity, m/s				u-plane turbulence intensity, %			
	Raw	Min/max	Vel. Cor.	% Change from raw	Raw	Min/max	Vel. Cor.	% Change from raw
1	0.2446	0.2448	0.2459	0.54	9.56	9.56	7.43	−22.24
2	0.2949	0.2949	0.2911	−1.29	18.86	18.86	15.17	−19.54
3	0.2863	0.2863	0.2860	−0.11	10.59	10.59	8.91	−15.83
4	0.2869	0.2863	0.2843	−0.93	11.55	11.55	10.05	−12.94
5	0.2456	0.2457	0.2470	0.56	9.26	9.26	7.31	−20.99

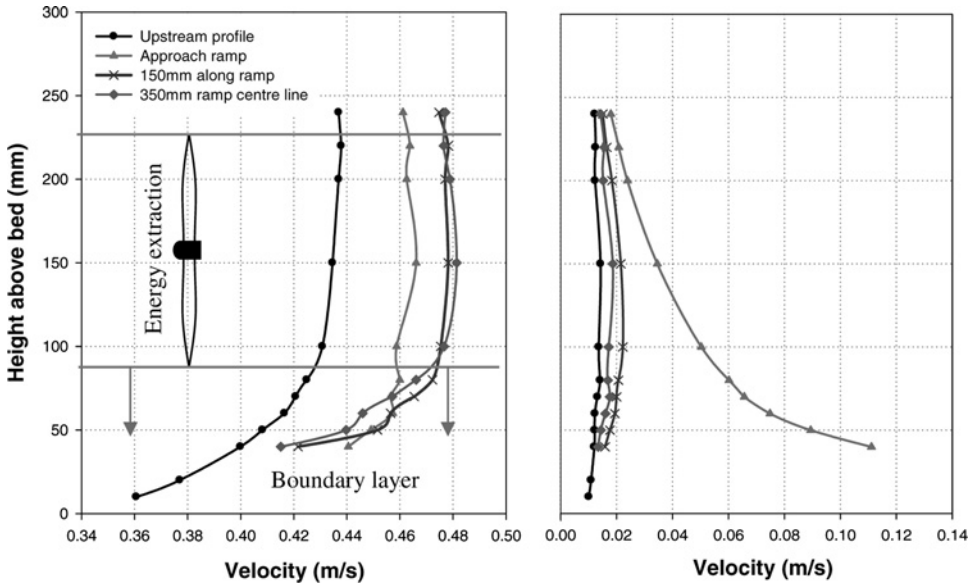

Fig. 6 *u-plane (left) and w-plane (right) velocity profiles: full channel width ramp, $F_r = 0.25$, $d = 300$ mm*

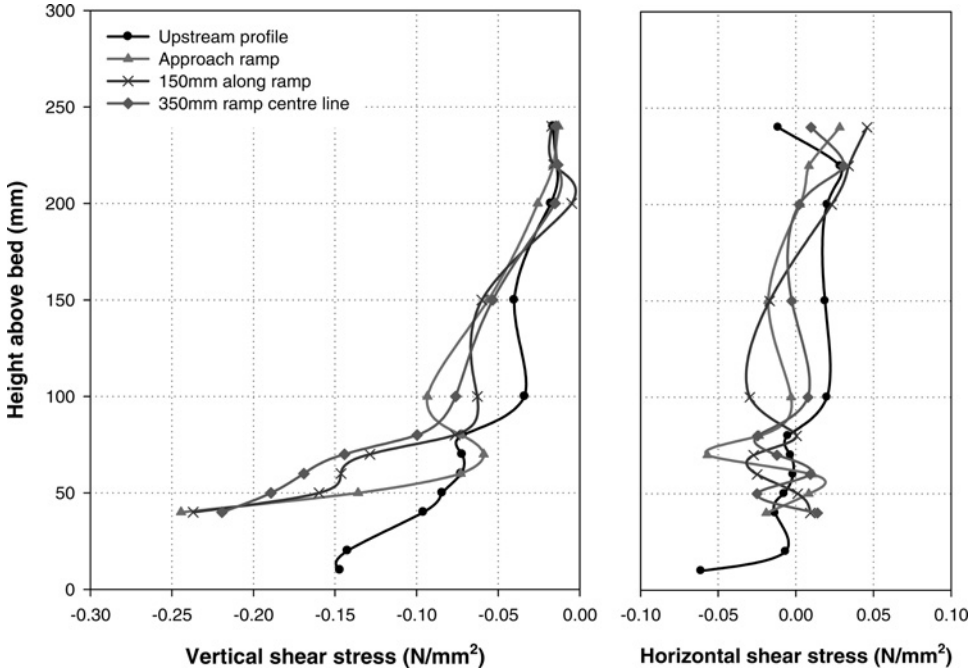

Fig. 7 *Vertical and horizontal shear stress profiles: full channel width ramp, $F_r = 0.25$, $d = 300$ mm*

significantly close to the ramp as would be expected for a flow that is accelerating. The vertical extent of this increase was limited to the lower part of the water column and it did not seem to adversely influence the shape of the vertical velocity profile in the region where a tidal turbine rotor might be located (Fig. 6).

A series of tests were run to investigate the effects of changing the ramp height/flow depth ratio.

$$\text{ramp height/depth ratio} = \frac{\text{ramp height}}{\text{flow depth}} \tag{6}$$

Here the ramp height was kept constant, but the flow depth in the channel was varied. The results are illustrated in the normalised graphs (Figs. 8–10). It can be seen that if the ratio is increased (i.e. flow depth reduced) the benefits of the ramp are greater in terms of velocity gain. If the ratio is reduced the velocity gain decreases. This highlights the fact that this technology might be difficult to implement in deep tidal flows because the ramp height would need to be considerable.

These ramp height/depth ratio experiments were conducted with ramps effectively spanning the whole width of the channel but in reality this is unlikely to occur. A final set of experiments were conducted to understand the effects of reducing ramp width and length.

3.2 Ramp width and length reduction

Ramp length and widths were progressively reduced to establish an optimum ramp size and to understand the effects of the ramp side edges on the flow.

doi: 10.1049/iet-rpg.2009.0181

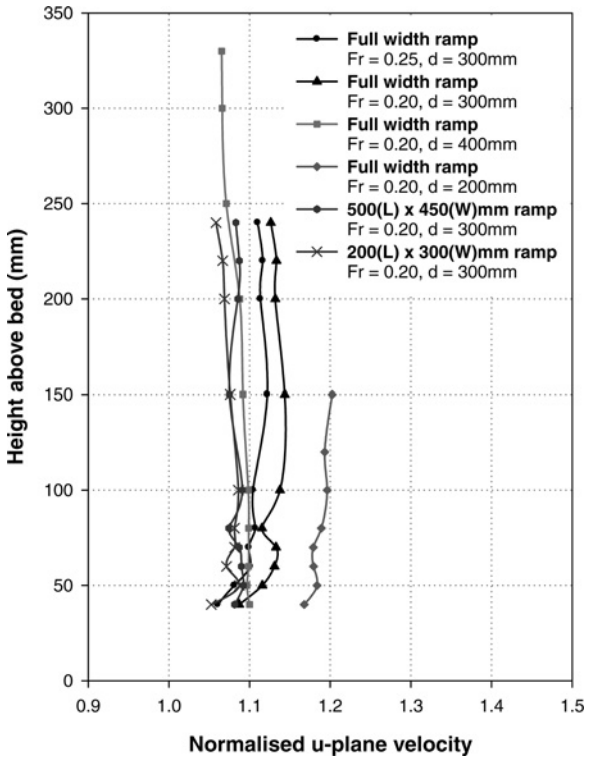

Fig. 8 *Normalised u-plane, point 4, velocity profiles: top of approach ramp*

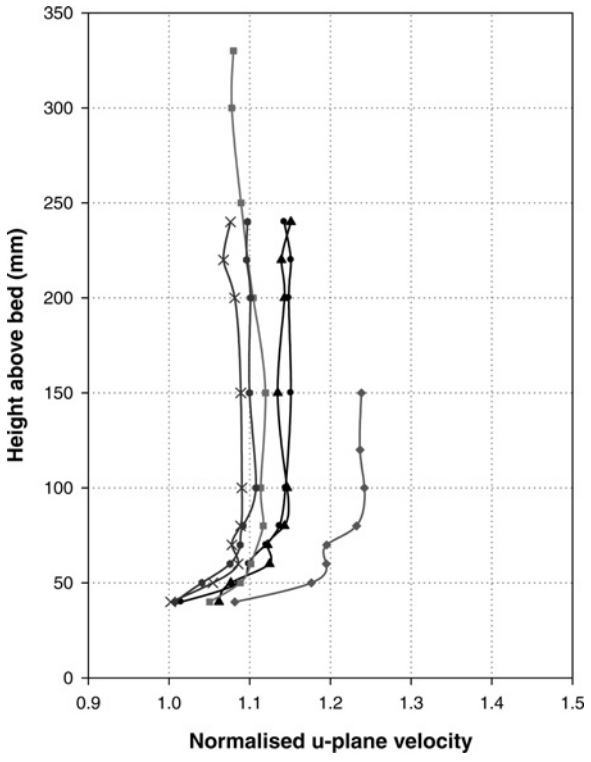

Fig. 9 *Normalised u-plane, point 6, velocity profiles: 150 mm along ramp*

In general, the conclusions from the full width tests held but with the benefits reduced. Fig. 11 shows the *u*-plane velocity profiles from two of the reduced width/length ramps. For this set-up velocity was still accelerated but by only 5%.

For all the tested ramps at a flow depth of 300 mm the optimum vertical velocity profile remained at 150 mm downstream (or six ramp depths) from the leading edge of the ramp. However, for the smallest ramp this point is at the very end of the ramp, so it can be concluded that this ramp was insufficient in length. The optimum ramp length would thus be 300 mm so that the optimum profile will occur at the ramp centreline allowing a device to benefit from the increased energy flux from both directions in a bi-directional tidal flow. This would equate to a 10 m long ramp at full scale.

There were no significant velocity reductions seen near the side edges of the ramp, as shown by the vertical profiles measured 20 mm from the side of the ramp structure in Fig. 11. Some side edge velocities were slightly reduced; however, this would be expected as velocity generally reduces away from the channel centreline. This would mean full-scale ramps would not need to exceed the device width, reducing construction costs.

At Froude numbers of ~0.2 there was no observed change in water surface elevation over the apron structure. According to (2) a reduction in water surface elevation should occur for subcritical flows ($F_r < 1$) leading to an even shallower and faster moving flow over the apron. However, this is clearly not observed by experiment under what are relatively and hydraulically defined as tranquil conditions. It is expected that Froude numbers approaching 1 (or critical condition) may be required to observe and quantify any reduction in water surface elevation over the apron structures. This could be achieved by increased flow speed or a reduction in total water depth.

3.3 Optimal downstream distance for energy extraction

Fig. 8 shows a normalised comparison between point 4 located at the top of the approach ramp. It shows how the sheared boundary layer is initially removed by the ramp to give an almost completely vertical profile. This would be an ideal profile for energy extraction; however, the velocity is not yet fully accelerated and power gains would be less.

Fig. 9 shows velocity profiles taken at the optimum energy extraction location. It highlights how increasing the ramp height/flow depth ratio increases the velocity gain and how reduced ramp size reduces the velocity gain. Profiles exhibit compressed sheared boundary regions and good vertical profiles for energy extraction.

Turbulence intensities showed similar trends for all tests (Fig. 10). Both the *u* and *v*-plane profiles were an inverse of the *u*-plane velocity profile with a constant upper section equal to 6–7%. *w*-plane turbulence intensity was generally constant with depth, with slightly lower values of ~5%. Fig. 10 shows how the turbulence intensity was slightly reduced across the ramp compared with the average upstream values.

In essence the lower section of the flow depth should be avoided for energy extraction for both increased shear stress and turbulence intensity.

3.4 Velocity, turbulence and shear stress intensity visualisation

The contour plots given in Fig. 12 illustrate how the centreline velocity intensity increases across the ramp, and how the turbulence intensity and shear stress develops. The optimum

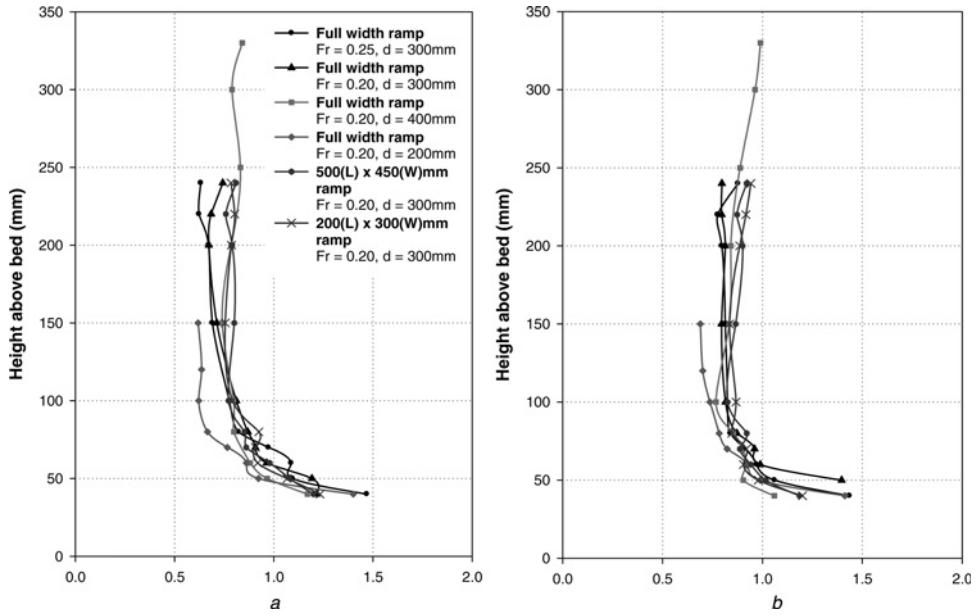

Fig. 10 *Normalised turbulence intensity profiles (optimum profile location)*

a *u*-plane (left)
b *v*-plane (right)

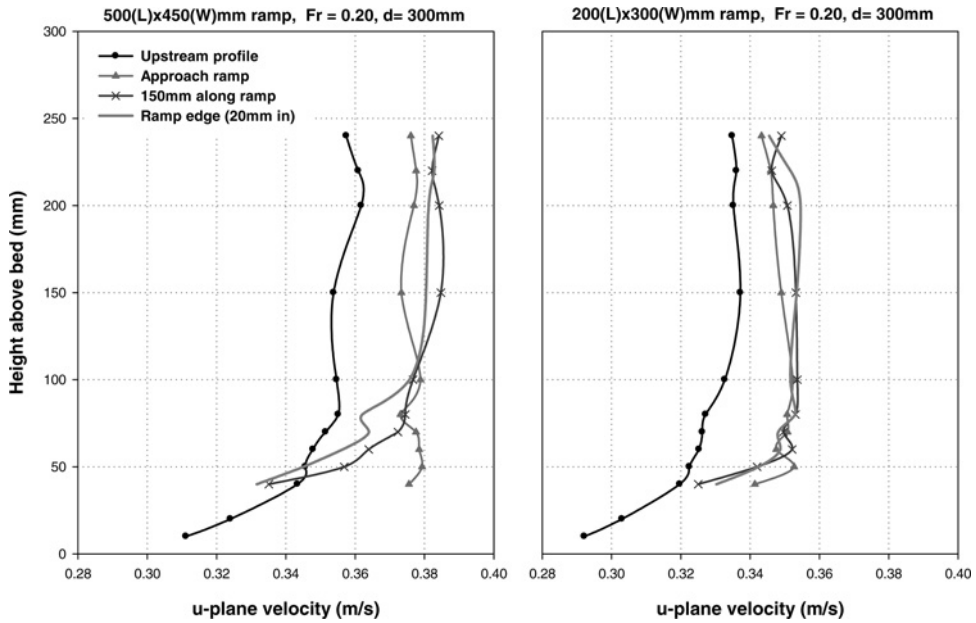

Fig. 11 *u-plane velocity profiles (tests 13 and 17)*

energy extraction point is shown and the redevelopment of the boundary layer along the ramp can be clearly seen.

4 Scaled MCEC results

The scaled commercial demonstrator device and ramp foundation were tested for a range of flow scenarios to represent full-scale conditions at a potential deployment site. Velocities ranged from 0.21 to 0.47 m/s (2.10 to 4.70 m/s full scale) and depth ranged from 0.2 to 0.3 m (20 to 30 m full scale).

Initially testing involved scenarios with a ramp foundation but without the presence of a MCEC. These were designed to validate the work previously presented by Giles *et al.* [35]. The results confirmed potential velocity gains from a ramp foundation of ~10%.

Following on from this a range of tests were conducted with the presence of the twin unit MCEC (actuator plates) working at different operating conditions over a range of flow conditions. Fig. 13 shows a typical flow field around the MCEC operating with a high-frequency rotor/hydrofoil oscillation (high solidity). This solidity case is equivalent to the MCEC operating at peak efficiency/rated power at its rated velocity of 2.5 m/s. The plot clearly shows the wake development behind the device and the reduced inflow velocity owing to axial induction.

From studying the *u*-plane centreline velocity profiles (Fig. 14) it might at first glance appear that the ramp foundation is providing little flow acceleration benefit

doi: 10.1049/iet-rpg.2009.0181

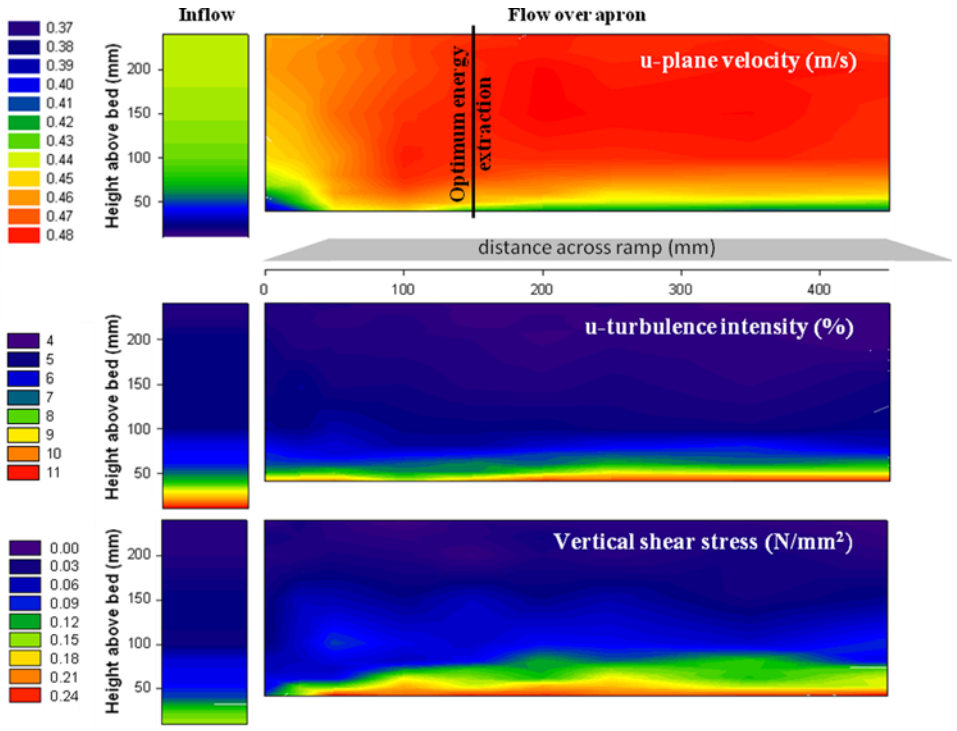

Fig. 12 *Contour plots of u-plane velocity, u-plane turbulence intensity and vertical shear stress: full channel width ramp, $F_r = 0.25$, $d = 300$ mm (test 1)*

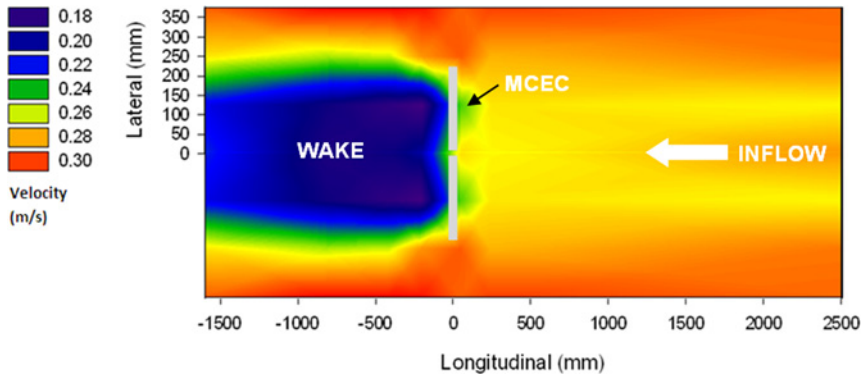

Fig. 13 *Flow field visualisation: uv velocity plane – MCEC operating with high frequency oscillation/high solidity*

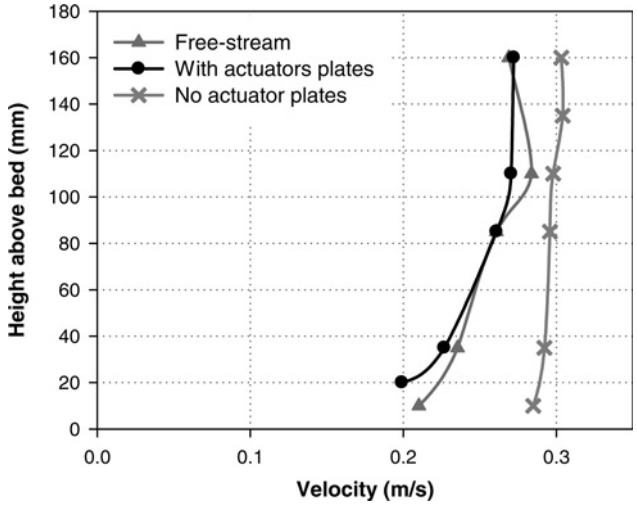

Fig. 14 *Vertical velocity profiles across ramp foundation with and without actuator plates present*

because the free-stream and across ramp profiles are very similar. But this is not the case, as would be expected from momentum theory; when the flow encounters the MCEC it is retarded owing to device blockage. Without the ramps presence the magnitude of the mean velocity would be lower and less energy would be available for extraction. A general rule was established from these tests which is; the free-stream velocity profile and across ramp profile are approximately equal in magnitude. One could say the ramp foundation is effectively removing the negative effects of flow retardation from axial induction compared with the free-stream case.

A more direct measure of ramp performance for these tests is the comparison of thrust exerted on the actuator plate for the situations with and without a ramp foundation. In general from these tests, the ramp achieves an 8% increase in thrust on the actuator plates compared with a MCEC located at the same relative vertical height in the water column but operating without a ramp foundation. This thrust increase can be translated into considerable power benefits of ~12% across a tidal cycle.

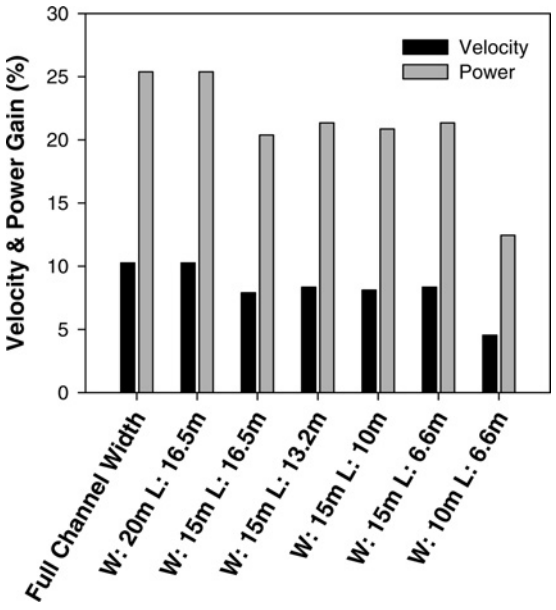

Fig. 15 *Potential velocity and full power percentage gain*

5 Full-scale application

The experimental findings from the phase one tests were scaled to the full-scale tidal site. The benefits of an integral concrete ramp foundation are illustrated by calculating potential power gains obtainable from a 5 m diameter horizontal axis marine current turbine, taking into account that the top and bottom 25% of the flow depth should be avoided.

Power was calculated using (1) where a power conversion efficiency factor of 0.4 was assumed. Results are illustrated in Fig. 15.

Interpretation of the results clearly shows for a small velocity gain the resulting power gains are considerable. Even for the small ramp, 12% power gains could be obtained. This correlates with the result presented at the end of Section 4.

Fig. 16 presents an estimate of the potential area increase of exploitable shallow tidal flow sites around the UK with the addition of ramp foundations. Bathymetry data and mean spring peak velocities were obtained from the Department for Business, Enterprise and Regulatory Reform's (BERR)

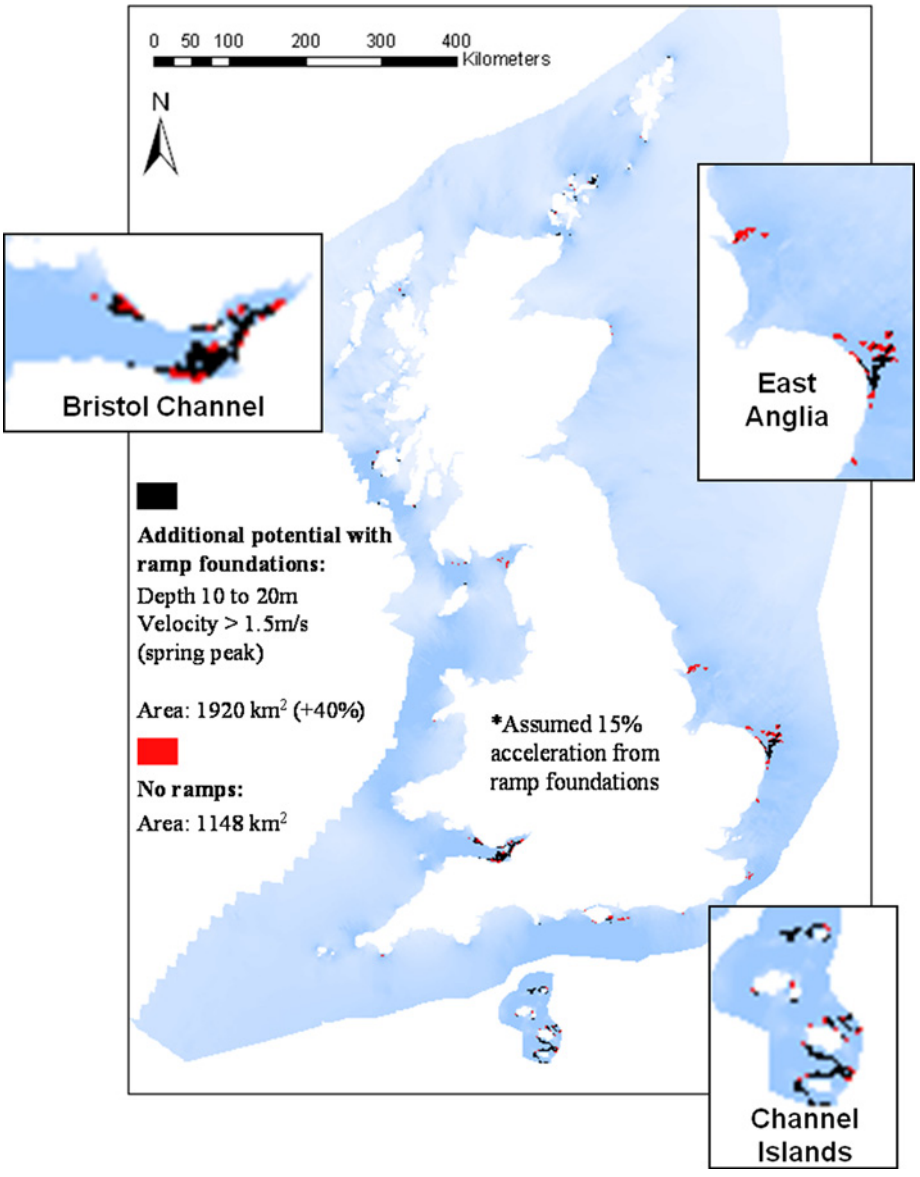

Fig. 16 *Potential shallow flow resource with ramp foundations*

doi: 10.1049/iet-rpg.2009.0181

Table 3 Stability calculations

Turbine diameter, m	Flow depth, m	Spring peak velocity, m/s	Ramp dimensions, m			Overturning			Bed shear resistance		
			Height	Width	Length	Resisting moment, kNm	Disturbing moment, kNm	Factor of safety	Resisting force, kN	Disturbing force, kN	Factor of safety
5	10	3.0	1.0	5	10	5886	3191	1.84	169	151	1.12
7.5	15	3.0	1.5	7.5	10	13 244	7683	1.72	379	305	1.24
10	20	3.0	2.0	10	10	23 544	14 552	1.62	674	512	1.32
15	30	3.0	3.0	15	10	52 974	36 764	1.44	1517	1083	1.40

'Marine Energy Resource Atlas' [36, 37] and the layers were manipulated using ArcGIS geographic information system (GIS) software. Results must be treated with caution owing to the limited data resolution but an exploitable sea area increase of 40% appears promising. Increasing flow speeds at sites already with suitable velocities would allow developers to either increase the rated power of turbines (to increase annual energy yield) or increase the plant load factor to provide steady power production over a greater range of flow speeds. The choice made would depend on any financial premium associated with either strategy.

A concrete caisson structure is proposed for the ramp foundation, these have been extensively used for gravity-based foundations. The principle advantage of using a caisson type structure is that the bulk of the fabrication can be done onshore or in dry docks. The structure can then be floated to the offshore installation site and gradually sunk into position. If required additional buoyancy could be added by attaching buoyancy tanks. Gerwick [38] states that the principle failure mechanism is sliding for water depths of $<150-200$ m and this can be prevented by attaching steel skirts and pin piles to the foundation. They effectively penetrate the seafloor and force the failure mechanism further below the seafloor and in addition provide extra scour protection. When designing marine structures it is vital to consider loading at every stage of construction and accidental conditions such as unplanned flooding of a buoyancy tank during delivery to site.

The proposed stages of construction are as follows:

1. Construction of the caisson gravity-based foundation on-shore.
2. Floatation of foundation at an inshore site.
3. Attachment of steel skirts to resist lateral loads.
4. Attachment of MCEC to floating foundation to form a single structure.
5. Structure towed to the offshore installation site.
6. Structure gradually sunk into place.
7. Placement confirmed by remotely operated vehicle (ROV) camera or divers.
8. Grid connection of MCEC.

A ramped gravity-based foundation is under consideration for a commercial scale MCEC demonstrator and full structural calculations will be conducted as part of this project; however, some initial stability calculations have been conducted and the results are detailed in Table 3.

The factor of safety for the overturning moment and bed shear resistance were computed for horizontal axis turbines of varying diameters. Assuming a concrete density of 2400 kg/m^3, bed friction coefficient of 0.25 (from marine industry experience and Yan *et al.* [39]), water density of 1025 kg/m^3 and a turbine power coefficient equal to 0.4, factors of safety for overturning and bed shear resistance were all in excess of unity (Table 3). Forces contributing to failure mechanisms include; turbine thrust, drag from the support structure/foundation and the buoyancy force. The force which prevents failure is the mass weight of the ramp foundation and the MCEC.

If further resistive capacity was required the ramp length/width could be increased or pin piles could be added for increased overturning resistance and bed shear capacity.

6 Conclusions

Ramp foundation structures could be utilised to accelerate tidal flows and increase MCEC power output. The initial phase of testing with ramp foundations showed these power benefits could be in the region of 12–25%, depending on the ramp size and ramp height/flow depth ratio. The second phase of testing with a model MCEC (actuator plates) and a ramp foundation confirmed the potential benefits of ramp foundations, found in the phase one tests, with power increases in the region of 12%. Data from the BWEA 'Marine Energy Resource Atlas' were manipulated using GIS and it was concluded that with the addition of ramp foundation structures the potential shallow tidal resource with depths of 10–20 m could be increased by ~40%. Further work with higher-resolution data will seek to verify this figure.

It was found that there was an optimum ramp length depending on the ramp height/flow depth ratio. For a ramp height of 1 m and a 10 m tidal flow depth this would be ~10 m.

The width of the ramp would not need to considerably exceed the width of the MCEC, as no significant velocity reductions were measured near the ramp side edges.

The extent of the sheared boundary layer region does not significantly increase with the presence of a ramp foundation; it is effectively compressed by the increased flow velocity.

Turbulence intensities were slightly reduced in the flow across the ramp, which would be beneficial to device operation and survival.

This concept would probably only be commercially viable for shallow tidal flows and the ramp would need to be of multi-use. This means in addition to increasing device power output, it would also need to act as an integral foundation and scour protection.

A proposed construction and installation method using concrete caisson foundation ramps is discussed and it is hoped it would improve the ease and speed of installation of MCECs in shallow flows. It would enable foundations and devices to be installed in one operation. Preliminarily stability calculations, for a range of turbine sizes, provide

good factors of safety against overturning and bed shear failures that are all in excess of unity.

This work is a preliminary study and future work aims to address the effects of changing approach ramp profiles, further studies into varying the ramp height/flow depth ratio, effects of yawed flow (as tidal flows are seldom bi-directional), ramp roughness, construction techniques, modelling with computational fluid dynamics, effectiveness over a full tidal cycle with varying water depth and tidal flow velocities and techno-economic analysis to establish the commercial viability of such structures.

7 Acknowledgments

This work forms part of an Engineering Doctorate study and has been jointly funded by the Engineering and Physical Sciences Research Council (EPSRC) and IT Power Ltd.

8 References

1 Fraenkel, P.L.: 'Power from marine currents'. Proc. Institution of Mechanical Engineers – Part A, 2002, vol. 216, pp. 1–14
2 Betz, A.: 'Das maximum der theoretisch moglichen ausnutzung des windes durch windmotoren'. Z. Gesamte Turbinenwesen, Heft 26, 1920
3 Lunar Energy Ltd.: http://www.lunarenergy.co.uk, accessed November 2009
4 Thorpe, T.: 'The advantages of ducted over unducted turbines'. Sixth European Wave and Tidal Energy Conf., Glasgow, UK, 2005, pp. 523–528
5 Setoguchi, T., Shiomi, N., Kaneko, K.: 'Development of two-way diffuser for fluid energy conversion', *Renew. Energy*, 2004, **29**, pp. 1757–1771
6 Klaptocz, V.R., Rawlings, G.W., Nabavi, Y., Alidadi, M., Li, Y., Calisal, S.M.: 'Numerical and experimental investigation of a ducted vertical axis tidal current turbine'. Proc. Seventh European Wave and Tidal Energy Conf., Porto, Portugal, 2007
7 Roddier, D., Cermelli, C., Aubault, A.: 'Electrical power generation by tidal flow acceleration'. Proc. 26th Int. Conf. on Offshore Mechanics and Arctic Engineering, San Diego, California, 2007
8 Salter, S.H., Taylor, J.R.M.: 'Vertical-axis tidal-current generators and the Pentland Firth', *Proc. IMechE, Power and Energy*, 2007, **221**, pp. 181–199
9 Chow, V.T.: 'Open channel hydraulics' (McGraw-Hill Book Company, London, 1959)
10 Chadwick, A., Morfett, J., Borthwick, M.: 'Hydraulics in civil and environmental engineering' (Spoon Press, Oxon, 2004)
11 Lyn, D.A.: 'Turbulence measurements in open-channel flows over artificial bed forms', *Hydraul. Eng.*, 1993, **119**, pp. 306–326
12 Shen, H.W., Fehlman, H.M., Mendoza, C.: 'Bed form resistances in open channel flows', *Hydraul. Eng.*, 1990, **116**, pp. 799–815
13 Fadda, D., Raad, P.E.: 'Open channel flow over submerged obstructions: an experimental and numerical study', *Trans. ASME*, 1997, **119**, pp. 906–910
14 Dyer, K.R.: 'Coastal and estuarine sediment dynamics' (J. Wiley & Son, 1986)
15 Dewey, R., Richmond, D., Garrett, C.: 'Stratified tidal flow over a bump', *Am. Meteorol. Soc.*, 2005, **35**, pp. 1911–1927
16 Wu, S., Rajaratnam, N.: 'Submerged flow regimes of rectangular sharp-crested weirs', *J. Hydraul. Eng.*, 1996, **122**, pp. 412–414
17 Myers, L.: 'Operational parameters of horizontal axis marine current turbines'. PhD thesis, School of Civil Engineering and the Environment, University of Southampton, 2005
18 Rippeth, T., Williams, E., Simpson, J.: 'Reynolds stress and turbulent energy production in a tidal channel', *J. Phys. Oceanogr.*, 2002, **32**, pp. 1242–1251
19 DTI, DTI report.: 'Development, installation and testing of a large scale tidal current turbine', 2005
20 European Commission: 'The exploitation of the tidal and marine currents'. Technical report EUR 16683 EN, Commission of the European Communities, Directorate-General for Science, Research and Development, 1996
21 Bahaj, A.S., Myers, L., Thomson, M.D., Jorge, N.: 'Characterising the wake of horizontal axis marine current turbines'. Seventh European Wave and Tidal Energy Conf., Porto, Portugal, 2007
22 Whelan, J., Thomson, M., Graham, J.M.R., Peiro, J.: 'Modelling of free surface proximity and wave induced velocities around a horizontal axis tidal stream turbine'. Seventh European Wave and Tidal Energy Conf., Porto, Portugal, 2007
23 Burton, T., Sharpe, D., Jenkins, N., Bossanyi, E.: 'Wind energy handbook' (Wiley, Chichester, 2001)
24 Myers, L., Bahaj, A.S., Rawlinson-Smith, R.I., Thomson, M.D.: 'The effect of boundary proximity upon the wake structure of horizontal axis marine current turbines'. Twenty-Seventh Int. Conf. on Offshore Mechanics and Arctic Engineering, Estoril, Portugal, 2008
25 Myers, L., Bahaj, A.S., Germain, G., Giles, J.: 'Flow boundary interaction effects for marine current energy conversion devices'. World Renewable Energy Congress X Glasgow, 2008
26 Whelan, J.I., Graham, J.M.R., Peiro, J.: 'A free-surface and blockage correction for tidal turbines', *J. Fluid Mech.*, 2009, **624**, pp. 281–291
27 Harrison, M.E., Batten, W.M.L., Myers, L.E., Bahaj, A.S.: 'A comparison between CFD simulations and experiments for predicting the far wake of horizontal axis tidal turbines'. Proc. Eighth European Wave and Tidal Energy Conf., Uppsala, Sweden, 2009
28 Connel, P.J., George, R.L.: 'The wake of the MOD-0A1 wind turbine at two rotor diameters downwind on 3 December 1981' (Pacific Northwest Laboratory, Battelle, USA, 1982)
29 Vermuelen, P.E.J. : 'Mixing of simulated wind turbine wakes in turbulent shear flow'. TNO report 79-09974, Apeldoorn, Holland,1979
30 Lohrmann, A., Cabrera, R., Kraus, N., Asce, M.: 'Acoustic-Doppler velocimeter (ADV) for laboratory use'. Fundamentals and Advancements in Hydraulic Measurements and Experimentation, New York, USA, 1994
31 Voulgaris, G., Trowbridge, J.H.: 'Evaluation of the acoustic Doppler velocimeter (ADV) for turbulence measurements', *J. Atmos. Ocean. Technol.*, 1998, **15**, pp. 272–289
32 Rusello, P.J., Lohrmann, A., Siegel, E., Maddux, T.: 'Improvements in acoustic Doppler velocimetery'. Seventh Int. Conf. on Hydroscience and Engineering, Philadelphia, USA, 2006
33 Blanckaert, K., Lemmin, U.: 'Means of noise reduction in acoustic turbulence measurements', *J. Hydraul. Res.*, 2006, **44**, pp. 3–17
34 Cea, L., Puertas, J., Pena, L.: 'Velocity measurements on highly turbulent free surface flow using ADV', *Exp. Fluids*, 2007, **42**, pp. 333–348
35 Giles, J.W., Myers, L., Bahaj, A.S., O'Nians, J.: 'An experimental study to assess the potential benefits of foundation-based flow acceleration structures for marine current energy converters'. Eighth European Wave and Tidal Energy Conf., Uppsala, Sweden, 2009
36 ABP.: 'Atlas of UK marine renewable energy resources: technical report'. ABP Marine Environmental Research Ltd, Department for Business, Enterprise & Regulatory Reform, 2008
37 Cooper, W.S., Hinton, C.L., Ashton, N., *et al.*: 'An introduction to the UK marine renewable atlas', *Marit. Eng.*, 2005, **159**, pp. 1–7
38 Gerwick, B.C.: 'Construction of marine and offshore structures' (CRC Press, Boca Raton, London, New York, Washington, DC, 2000)
39 Yan, S.W., Chu, J., Fan, Q.J., Yan, Y.: 'Building a breakwater with prefabricated caissons on soft clay', *Geotech. Eng.*, 2009, **GE1**, pp. 3–12

doi: 10.1049/iet-rpg.2009.0181

Appendix B

GILES, J., MYERS, L., BAHAJ, A. S. & SHELMERDINE, B. 2011b. The downstream wake response of marine current energy converters operating in shallow tidal flows. World Renewable Energy Congress 2011. Linkoping, Sweden.

[8 pages]

The downstream wake response of marine current energy converters operating in shallow tidal flows

Jack Giles[1,2*], Luke Myers[1], AbuBakr Bahaj[1], Bob Shelmerdine[2]

[1]*University of Southampton, Southampton, UK*
[2] *IT Power Ltd., Bristol, UK*
** Corresponding author. Tel: +44 7855037885, E-mail: jack.giles@soton.ac.uk*

Abstract: This paper presents findings from an experimental study investigating the downstream wake response from marine current energy convertors operating in various degrees of vertical flow constraint. The paper investigates deep vertically unconstrained sites, mid-depth sites and there is a particular emphasis on shallow tidal stream sites. Shallow tidal resources could be utilised for the deployment of first generation farms. The nature of the downstream wake flow will be a critical factor when determining the farm layout and the wake length is heavily influenced by the flow depth or ratio of rotor diameter to flow depth. A porous actuator disk is used to model the marine current energy convertor and an Acoustic Doppler Velocimeter is used to map the downstream wake. Linear scaling of length ratios suggests mid depth sites of 30-50m will produce the shortest wake lengths and for deeper and shallower sites the wake length increases. It is hoped that these relationships between vertical flow constraint and wake length will help with the layout design of tidal stream farms.

Keywords: *wake, vertical flow constraint, shallow tidal flows, farms.*

Nomenclature

C_t	*thrust coefficient*	$\overline{U}$	*Mean velocity of sample* ..... $m \cdot s^{-1}$
U_{def}	*velocity deficit* ..... $m \cdot s^{-1}$	D	*actuator disk diameter* ..... m
U_w	*wake velocity* ..... $m \cdot s^{-1}$	u	*downstream velocity component* ..... $m \cdot s^{-1}$
U_o	*free-stream velocity at hub height* ..... $m \cdot s^{-1}$	v	*lateral velocity component* ..... $m \cdot s^{-1}$
I	*turbulence intensity* ..... %	w	*vertical velocity component* ..... $m \cdot s^{-1}$

1. Introduction

Shallow tidal flows hold a number of advantages for first generation tidal stream farms. Shallow flows, of depths less than 20m, often have a reduced cross-sectional area suitable for energy extraction compared with deeper channels, but they also have other benefits including close proximity to the shore with many sites situated away from shipping channels. This could make construction and grid connection both easier and more economically feasible. Fig. 1 presents results showing potential sites for device deployments in shallow tidal flows in the UK. The data for bathymetry and mean spring peak velocities was obtained from the BWEA "Marine Energy Resource Atlas" [1] and the layers were manipulated using geographic information system (GIS) software. The highlighted areas show sites with depths between 10-20m and spring peak velocities of greater than 1.5m/s.

When deploying a farm of Marine Current Energy Converters (MCECs), the nature of the downstream wake flow will be a critical factor when determining the farm layout and packing density. It is known that the wake length is heavily influenced by the flow depth or the degree of vertical flow constraint. This paper presents experimental findings of the flow fields around scale MCEC simulators operating in a circulating flume at varying depths to represent the range of depths present at the many sites suitable for MCEC deployment. Examples of shallow tidal sites include; the Bristol Channel, the Humber Estuary and areas around the Channel Islands (see Fig. 1). Deeper flows exist in the Pentland Firth and in various locations around the West of Scotland.

Previous work presented by Myers et al. [2] concluded that MCECs operating in shallow fast-moving flow regimes will see a difference in the downstream flow field compared with devices installed in deeper water. It was stated that the effects of sea bed proximity have shown that wake recovery is not as favourable when the flow field is very deep beneath the rotor disk. This is due to reduced shear forces and lack of accelerated flow generated by the close proximity of the sea bed and surface that serve to drive wake dissipation. This paper presents work developed from the previous study [2] to further investigate the effects of vertical flow confinement on the downstream wake development of MCECs. A thorough understanding of wake development is critical for the optimisation of the downstream device spacing in tidal stream farms. Minimising the downstream spacing will enable a higher farm device density and hence higher yields from a specific site.

For a multiple-row MCEC array, longitudinal spacing of devices is expected to be great enough to ensure that downstream devices have an incoming flow regime (and hence power production) that is comparable to devices located upstream. However, at spatially constrained sites this approach to spacing may be tightened in order to increase energy capture per surface area of the site and to reduce electrical connection costs. It is postulated that there may be an optimum device height to flow depth ratio that will lead to the minimisation of downstream wake length. For sites that are deeper or shallower than this optimum depth range, the downstream wake length is expected to increase. Whilst an explanation has been provided for deeper flows [2] it is expected that in a very shallow flow vertical blockage is high and flow acceleration above and below the MCEC will be restricted. Both of these factors are expected to result in reduced mixing between the wake and ambient flow thus increasing wake length.

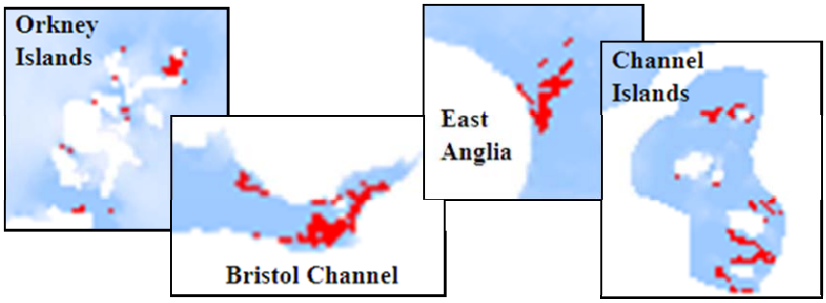

Fig. 1 Potential UK first generation shallow tidal flow sites, not to scale.

2. Methodology

In order to conduct the testing at a reasonable scale a porous mesh disk was used to model a horizontal axis turbine (often referred to as actuator disks). Actuators are now an accepted method for modelling MCECs and have been extensively used for horizontal axis turbines, but the method could equally be used to model vertical axis and oscillating hydrofoil devices. Actuator and momentum theory is discussed extensively by Burton et al. [3]. Work concerning the use of small scale actuator disks for the representation of far wake conditions has been addressed by a number of authors for both wind and tidal energy applications [4,5] . The principle difference between flow fields around actuators and full scale MCECs is the representation of the near wake and these differences are generally known to dissipate in less than four rotor diameters downstream [6,7].

For this work the principle parameters that require replication from large to small scale are [2]:

a) Device thrust force controlled through the level of actuator disk porosity (ratio of open to closed area).
b) Linear scaling of length ratios such as disk diameter to water depth and channel width.
c) Replication of ambient flow field conditions such as Froude number, vertical velocity profile and turbulence intensities. Full-scale and model Reynolds numbers cannot achieve parity at small scale but should lie within the turbulent classification.

Testing was conducted at a scale of 1:100 using actuator disks of 0.1m diameter. The porous actuator's impedance was specified using an empirical relationship between thrust coefficient (C_t) and plate porosity. This relationship was developed from a combination of experimental findings from the University of Southampton and from equations presented by Whelan et al. [8]. The actuator disk used is of the same porosity as that used in Myers et al. [2].

The actuator disk was mounted on a thin stainless steel support arm which made up part of a pivot arrangement to magnify the small thrust forces on the actuator disk. The rig can be seen in Fig. 2, a 10N button load cell was used to measure the total thrust force.

Shallow-depth experiments were conducted in the tilting flume at the Chilworth hydraulics laboratory, University of Southampton, UK. The working section of this flume is 21m in length, 1.37m wide and a maximum depth of 0.4m for steady operation.

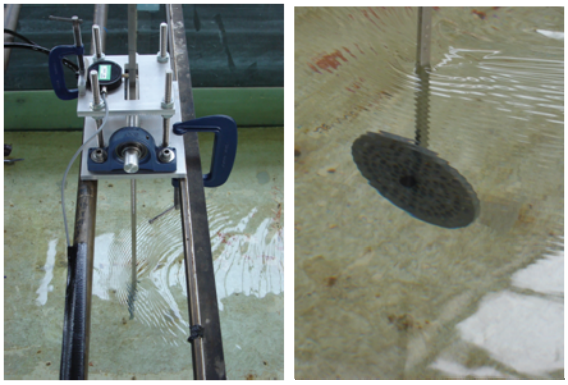

Fig. 2 Actuator lever arm rig (left) actuator disk mounted on lever arm (right)

The vertically unconstrained results which were used to compare with the constrained tests were presented by Myers et al. [2] and were conducted in the IFERMER circulating channel, Boulogne sur Mer, France. The channel has a working section of 18m in length, 4m wide and 2m deep. The downstream wake was mapped using a high frequency Acoustic Doppler Velocimeter (ADV). Operational issues and the accuracy of ADVs have been addressed at length in many publications [9-11]. The ADV was set to sample at 50Hz. For each data point 7500 readings were taken over a 150 second period.

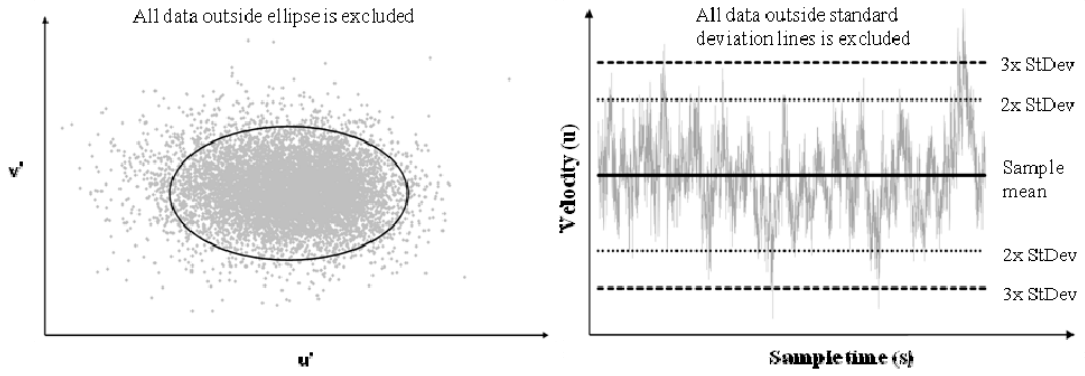

Fig. 3 Velocity correlation filtering method (left) and minimum/maximum filter (right).

Data was filtered to remove noise and spurious points (Fig. 3, shows data spikes) although the large quantity of suspended particles in the Chilworth channel minimised sample errors. Filtering is required to improve measurements of higher order flow effects such as turbulence intensity and shear stresses as spikes in the data give the impression of increasing energy within the flow. However filtering has a very small effect for mean flow velocities as spikes are generally equally positive and negative. All samples were filtered using a velocity cross-correlation filter ultimately chosen due to ease of use and effectiveness after a single pass [12]. This method plots the varying components of velocity against each other and constructs an ellipsoid in 3-dimensional space to exclude any data points that deviate significantly from the sample mean (Fig. 3, left). Similar filters can be set up to remove statistically or physically improbable values. Table 1 compares the velocity cross-correlation filter to a minimum-maximum filter (Fig. 3, right) that removes time-series values ±3 standard deviations from the sample mean. The effectiveness of the cross-correlation filter for the turbulence data is apparent.

Table 1 Minimum/maximum and velocity correlation filter comparison.

Sample	u-plane velocity ($m.s^{-1}$)				u-plane turbulence intensity (%)			
	Raw	Min/ max	Vel. Cor.	% Change from raw	Raw	Min/ max	Vel. Cor.	% Change from raw
1	0.245	0.245	0.246	+0.54	9.80	9.56	7.43	-24.18
2	0.295	0.295	0.291	-1.29	18.86	18.86	15.17	-19.54
3	0.286	0.286	0.286	-0.11	11.30	10.59	8.91	-21.14
4	0.287	0.286	0.284	-0.93	13.47	11.55	10.05	-25.41
5	0.246	0.246	0.247	+0.56	9.31	9.26	7.31	-21.45

The recovery of the wake is defined in terms of velocity deficit; this is a non-dimensional number relative to the free-stream flow speed at hub height and the wake velocity, defined by Eq. (1).

$$U_{def} = 1 - U_w / U_o \tag{1}$$

The ambient turbulence intensities in the circulating channel used during this study were approximately 6-8% and were calculated in all three planes (u,v,w). Turbulence intensity is commonly defined as the root-mean-squared of the turbulent velocity fluctuations divided by the mean velocity of the sample. Table 2 details the parameters of the constrained flow tests conducted as part of this work and the previously conducted unconstrained flow tests conducted at the IFERMER facility. Dimensions are detailed in disk diameters (D).

Table 2 experimental test parameters.

Test	Water depth	Channel width	Actuator centre from surface	Depth-averaged Froude No.	Depth-averaged Reynolds No.	Disk height/depth ratio
1	4.0	13	2.00	0.15	$1.2x10^5$	0.25
2	3.0	13	1.50	0.15	$7.8x10^4$	0.33
3	2.5	13	1.25	0.15	$5.7x10^4$	0.40
4	2.0	13	1.00	0.15	$4.2x10^4$	0.50
5	1.5	13	0.75	0.15	$2.7x10^4$	0.66
6*	20	40	2.00	0.113	$9.9x10^5$	0.05

*unconstrained test conducted at IFERMER, France.

Myers et al. [2] showed experimentally for a constant depth the wake velocity deficit is independent of velocity (for a representative range of Froude numbers).

3. Results and Discussion

Three cases from Table 2 will be addressed herein; A deep-unconstrained tidal site (test #6), a mid-depth tidal site (test #1) and a shallow-depth tidal site (test #4).

3.1. Free-stream results

Fig. 4 (left) shows the normalised vertical velocity profiles for the three cases, these are the free-stream results from the Chilworth and IFREMER facilities. Depth is expressed in terms of disk (or rotor, full scale) diameters (D). The velocity profile at Chilworth is well developed but the close proximity of the bed induces a more pronounced gradient that leads to disparate mass flow rates above and below the disk, this is most noticeable in the shallow-depth scenario. Flow speed in the deep site case is similar above and below the disk.

Fig. 4 (right) shows the ambient turbulence intensities in all three planes (u,v,w) for the deep-unconstrained and mid-depth scenarios (IFERMER and Chilworth channels, respectively). At the Chilworth facility the presence of the flume bed 2-diameters below the disk causes an increase in turbulence intensity immediately above the bed. u and v components are of a similar magnitude at 6-7% whilst turbulence intensity in the vertical plane is slightly greater. The IFERMER channel turbulence intensity is more constant with depth close to the disk. The turbulence intensity in the vertical plane is much lower than at Chilworth. The difference occurs due to the nature with which water is delivered to the upstream end of the working section.

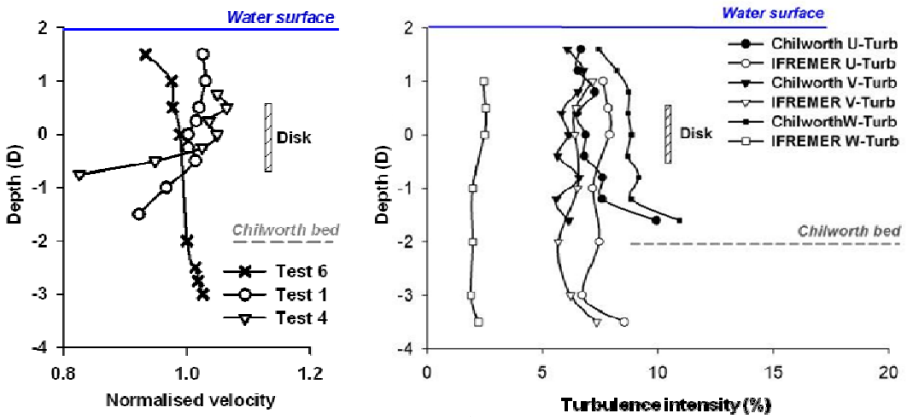

Fig. 4 Normalised vertical velocity profiles at the Chilworth and IFERMER water channels (left) and Turbulence intensities (right).

3.2. Wake length

Fig. 5 shows the longitudinal centre plane velocity deficits for the three depth cases. It is clear that in the mid-depth case the wake is broken down in a significantly shorter downstream distance than in the deeper and shallower cases (approximately 6D). This results from flow acceleration above and below the actuator disk that acts to break the wake down through greater lateral turbulent mixing. This effect was postulated by Myers et al. [2] and is reinforced following analysis of these results.

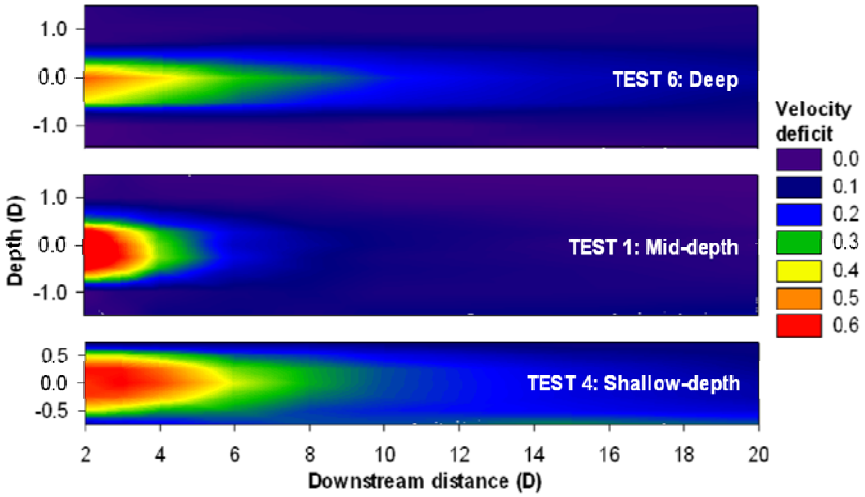

Fig. 5 Centre plane velocity deficit profiles; deep-site, mid-depth site & shallow-depth site.

The wake persists much further downstream in the deep-unconstrained and shallow depth cases (10-12D downstream), this results from restrictions in flow acceleration around the MCEC. In the deep-unconstrained case vertical blockage is low and hence flow acceleration is reduced, thus allowing the wake to persist further downstream. In the shallow flow scenario vertical blockage is high and hence local flow acceleration above and below the MCEC is restricted, again allowing wake to persist further downstream.

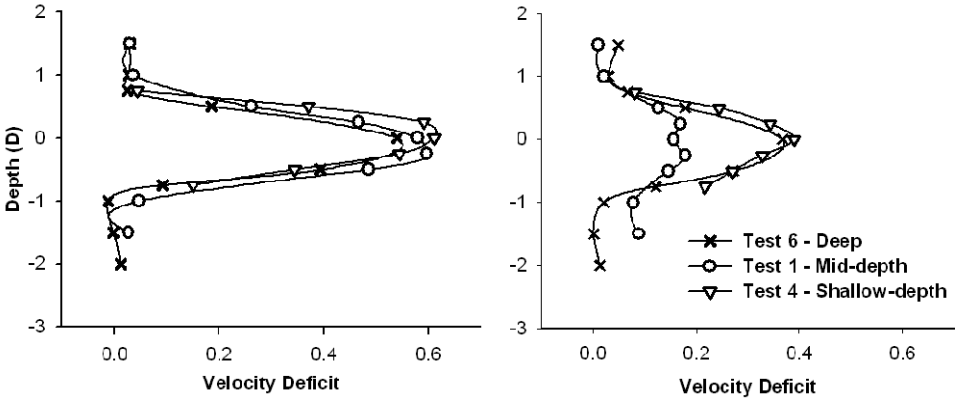

Fig. 6 Vertical velocity deficits at 3 diameters downstream (left) and 6 diameters (right)

Fig. 6 shows vertical line plots of velocity deficit at two downstream locations for all three depth cases. Looking at the 3D downstream graph it is clear that the initial velocity deficits directly behind a MCEC are similar irrespective of the vertical flow constraint; this is because wake is re-energised by turbulent mixing from the surrounding flow and in the near wake this effect is less pronounced. Further downstream e.g. 6D, the effects of varying degrees of vertical blockage can be seen. The deep and shallow cases give similar profiles, whereas the velocity deficits for the mid-depth case are reduced considerably because of increased turbulent mixing between the wake and accelerated surrounding flow. The effects of flow acceleration in the mid-depth case can be observed.

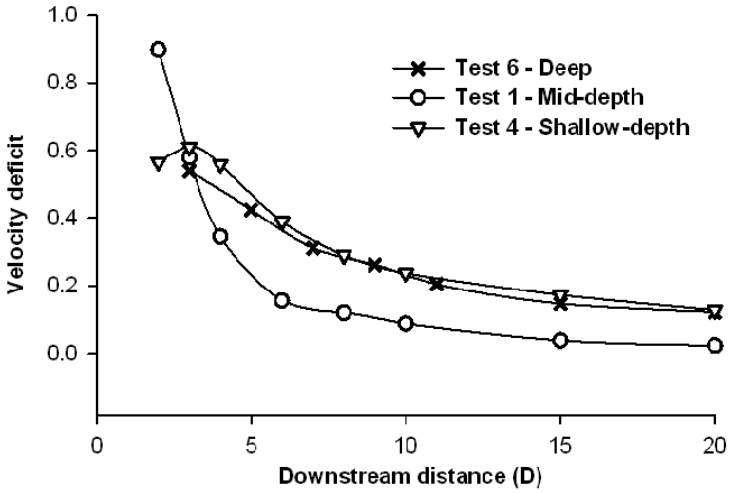

Fig. 7 Disk centreline velocity deficit comparison.

Fig. 7 shows the downstream centreline deficits. As suggested by Fig. 5 the wake recovers much more quickly in the mid-depth case. Again the principal mechanism for this is flow acceleration around the disk which serves to break up the wake more rapidly. In Fig. 7 the similarities in terms of downstream velocity deficits between the shallow and deep cases are clearly illustrated.

3.3. Farm row optimisation

This section highlights the significance and importance of this work to tidal stream farm design and optimisation. Fig. 8 shows there is an optimum rotor diameter/flow depth ratio in terms of wake recovery and minimising downstream wake length. Three different downstream location cases are compared for all the tests detailed in Table 2. It appears that 0.25 is the optimum rotor diameter/flow depth ratio for minimising downstream spacing. At full scale this might equate to a site with a depth range of 30-50m depending on the rotor diameter.

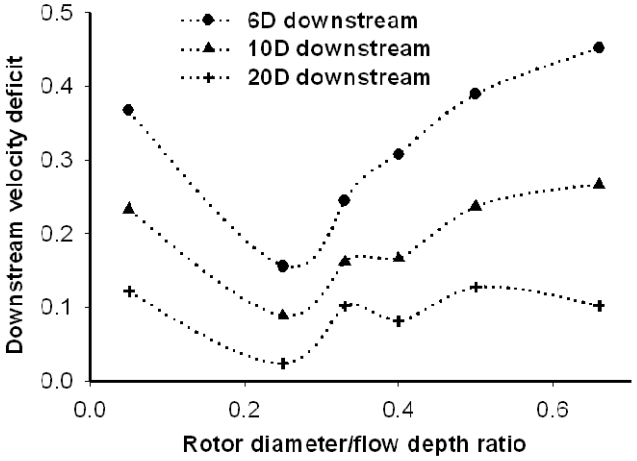

Fig. 8 Optimum rotor diameter/flow depth ratio in terms of wake recovery

4. Conclusions

From the results presented in this paper, it is critical that tidal stream farms or arrays are optimised in terms of downstream spacing and packing density, it will thus be important to tune the downstream device spacing to the local flow depth. Although at spatially constrained sites the spacing may be tightened in order to increase energy capture per surface area of the site and to reduce electricity connection costs. It is anticipated that many first generation sites will be located in shallow tidal flows and hence the longer wake lengths compared with mid-depth sites must be factored into the design process. In terms of the full scale significance and to reduce wake length, the optimum rotor diameter/flow depth ratio is 0.25. This would equate to a flow depth range of 30-50m depending on the rotor diameter.

The wake length is controlled by the degree of lateral flow mixing between the retarded wake flow and the surrounded accelerated free-stream flow. Increased wake length in very deep and very shallow flows result from vertical blockage, in a deep flow vertical blockage is minimal and hence local flow acceleration around the wake is reduced. In a very shallow flow vertical blockage is high and flow acceleration above and below the MCEC is restricted. Both these

factors result in less lateral flow mixing and thus increased wake length. It is hoped that the relationship between vertical flow constraint and wake length will help with the layout design of future tidal stream farms.

Acknowledgements

This work has been conducted as part of an Engineering Doctorate study and has been jointly funded by the European and Physical Sciences Research Council (EPSRC) and IT Power Ltd. Work at IFERMER was funded by the Marine Environment Tests and Research Infrastructure (METRI II) programme and the UK Technology Strategy Board. “Performance characteristics and optimisation of marine current energy converter arrays”, project number T/06/00241/00/00.

References

[1] ABP, ‘Atlas of UK Marine Renewable Energy Resources: Technical Report’, ABP Marine Environmental Research Ltd, Department for Business, Enterprise & Regulatory Reform, 2008.

[2] L. Myers, A.S. Bahaj, G. Germain, J. Giles, ‘Flow boundary interaction effects for marine current energy conversion devices’, World Renewable Energy Congress X, Glasgow, 2008.

[3] T. Burton, D. Sharpe, N. Jenkins, E. Bossanyi, ‘Wind Energy Handbook’, Wiley, 2001

[4] A.S. Bahaj, L. Myers, M.D. Thomson, N. Jorge, ‘Characterising the wake of horizontal axis marine current turbines’, 7th European Wave and Tidal Energy Conference, Porto, Portugal, 2007.

[5] L. Myers, A.S. Bahaj, R.I. Rawlinson-Smith, M.D. Thomson, ‘The effect of boundary proximity upon the wake structure of horizontal axis marine current turbines’, 27th International Conference on Offshore Mechanics and Arctic Engineering, Estoril, Portugal, 2008.

[6] P. J. Connel, R.L. George, ‘The wake of the MOD-0A1 wind turbine at two rotor diameters downwind on 3 December 1981’, Pacific Northwest Laboratory, Battelle, U.S., 1982.

[7] P.E.J. Vermuelen, ‘Mixing of simulated wind turbine wakes in turbulent shear flow’, TNO Rep. 79-09974, Apeldoorn, Holland, 1979.

[8] J. Whelan, M. Thomson, J.M.R. Graham, J. Peiro, ‘Modelling of free surface proximity and wave induced velocities around a horizontal axis tidal stream turbine’, 7th European Wave and Tidal Energy Conference, Porto, Portugal, 2007.

[9] A. Lohrmann, R. Cabrera, N. Kraus, M. ASCE, ‘Acoustic-Doppler Velocimeter (ADV) for Laboratory Use’, Fundamentals and Advancements in Hydraulic Measurements and Experimentation, New York, USA, 1994.

[10] G. Voulgaris, J.H. Trowbridge, ‘Evaluation of the Acoustic Doppler Velocimeter (ADV) for Turbulence Measurements’, Journal of Atmospheric and Oceanic Technology, 1998, 15, pp. 272 – 289.

[11] P.J. Rusello, A. Lohrmann, E. Siegel, T. Maddux, ‘Improvements in Acoustic Doppler Velocimetery’, The 7th Int. Conf. on Hydroscience and Engineering, Philadelphia, USA, 2006.

[12] L. Cea, J. Puertas, L. Pena, ‘Velocity measurements on highly turbulent free surface flow using ADV’, Experiments in Fluids, 2007, 42, pp. 333 – 348.

Appendix C

GILES, J., MYERS, L., BAHAJ, A. S., SHELMERDINE, B. & PAISH, M. 2011c. The Commercialisation of Foundation-based Flow Acceleration Structures for Marine Current Energy Converters. 9th European Wave and Tidal Energy Conference. Southampton, UK.

[7 pages]

The Commercialisation of Foundation-based Flow Acceleration Structures for Marine Current Energy Converters

Jack Giles[#1], Luke Myers[#2], AbuBakr Bahaj[#3], Bob Colclough[*4], Marc Paish[**5]

[#]*Sustainable Energy Research Group, University of Southampton, SO17 1BJ, UK*

[1]jack.giles@soton.ac.uk

[*]*IT Power Ltd.*
St Brandon's House, 29 Great George Street, Bristol, BS1 5QT, UK

[**]*Pulse Tidal Ltd.*

***Abstract*—This paper presents further work regarding the development and commercialisation of foundation-based flow structures for marine current energy converters (MCECs). Such ramp structures could provide multiple benefits, including: increased device power output, increased foundation footprint and scour hole protection. Experimental studies have confirmed appreciable power benefits are obtainable across a full tidal cycle with the addition of ramp foundations. The extent of the benefit depends on the ratio of ramp width to channel width.**

Key barriers to the commercialisation of the concept are discussed. To become a commercial reality the structure will need to produce a net gain in energy yield to offset the additional capital costs. The multi-purpose nature of the concept is expected to improve the commercial viability. A novel method of construction, deployment and recovery is presented and preliminary structural stability calculations conclude that sufficient factors of safety are achievable.

***Keywords*— shallow tidal flows, flow acceleration, ramp foundation, power gain.**

I. Introduction

A critical limiting factor for the commercialisation of tidal stream energy is the availability of suitably energetic deployment sites. Suitable locations need to be easily accessible for device installation and maintenance; close to grid connections and most importantly have sufficient tidal flow velocities to yield meaningful amounts of energy. For these reasons, it is anticipated that many first generation tidal stream sites will be located in shallow tidal flows, in depths of 10-30m, which are generally located closer to shore and away from shipping channels. Their location makes both construction and grid connection easier and improves economic viability. Many shallow flow sites do not currently have sufficient tidal flow velocities for economic power generation but it is proposed many of these sites could be made viable with the integration of artificial flow acceleration structures. Examples of shallow tidal sites include; the Bristol Channel, the Humber Estuary and areas around the Channel Islands (Fig. 1).

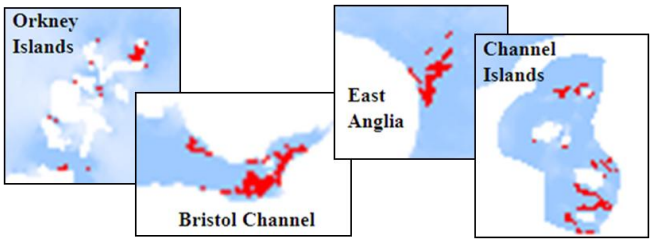

Fig. 1 Potential UK first generation shallow tidal flow sites

The fundamental application of ramp-based foundations (Fig. 2) to artificially increase energy yield across a tidal cycle, whilst working as an integral foundation and scour hole protection has been discussed by Giles et al. [1-2]. Fundamental work concluded that ramps could provide power benefits of 12-30% across a tidal cycle, depending on ramp size and flow depth. Geographic information system (GIS) mapping has shown that ramp foundations have the potential to increase the exploitable sea area by up to 40% in the UK [1]. The concept is most applicable to shallow tidal flows with depths of 10-30m. Structures could be utilised in deeper flows, but the increased ramp height required would only be commercially viable with an associated increase in device capacity.

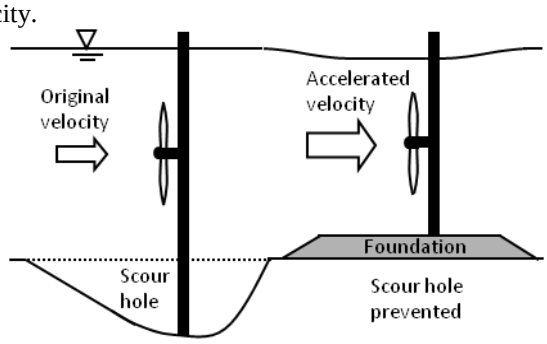

Fig. 2 Ramp based foundation concept

The bulk of the previous fundamental study considered ramp foundations operating without a MCEC, but this work aims to address some of the uncertainty surrounding the flow modification and resulting power yield benefits when a base ramp is combined with a MCEC simulator. Extending the modelling study to include the blockage effects of a MCEC is expected to slightly reduce the power benefits of ramp foundations and it is critical that this fundamental operation is understood. The overarching objective of this paper is to provide evidence that base ramps have potential to be a commercial reality rather than just an academic concept. A commercial demonstrator device with an integral ramp foundation is currently being developed by Pulse Tidal Ltd. [3].

II. Commercial Development

Following the successful deployment and operation of Pulse Tidal's 100kW device in the Humber Estuary, during 2009, their next generation device is under development, the Pulse Stream Commercial Demonstrator (PSCD) [3]. This will be a 1.2MW oscillating hydrofoil device with an integral foundation ramp (Fig. 3).

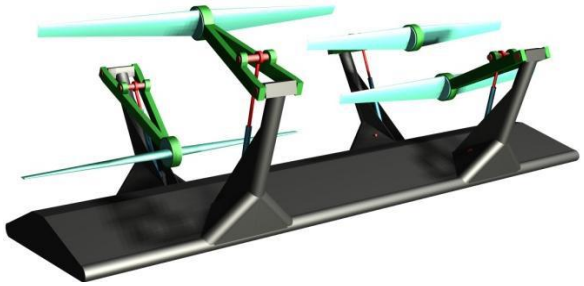

Fig. 3 PSCD with a ramp foundation

The decision to include an integral base foundation ramp was supported by the fundamental work presented by Giles et al. [2]. The PSCD shows a direct commercial application of a ramp foundation at full scale, but the concept could equally be applied to horizontal and vertical axis type devices (Fig. 2).

III. Experimental Modelling

A. *Introduction*

Fundamental experimental results have been presented in Giles et al. [1]. The results presented here build on the fundamental studies to further include the influence of the MCEC on the flow field. In order to test the concept at a manageable scale, 1:100 scale ramps and actuator disks/plates (Fig. 4) were constructed and tested at the University of Southampton and HR Wallingford Ltd.

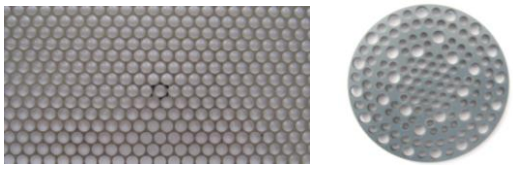

Fig. 4 Actuator plate (PSCD) & disk (HAT)

Actuator disks were used to model a horizontal axis turbine and actuator plates were used to model Pulse Tidal's PSCD (Fig. 5). The actuator porosity represents the speed of turbine blade rotation and hydrofoil oscillation respectively at full scale. The actuator plates impedances, used to represent the PSCD, were designed using an empirical relationship between thrust coefficient and plate porosity. This relationship was developed from a combination of experimental findings from the University of Southampton and from equations presented by Whelan et al. [4]. Four plates termed LOW, MID, HIGH and V.HIGH solidity were tested to represent the PSCD in different operating conditions. The HIGH solidity plate is discussed in this paper as it represents normal operating conditions for the PSCD. Actuator modelling of MCECs is now an accepted technique [4-6]. The principle difference between flow fields around actuators and full scale MCECs, is the representation of the near wake and these differences are known to dissipate in less than four diameters downstream [7-8]. The ramp foundation was modelled using machined HDPE plastic.

Fig. 5 PSCD 1:100 scale testing

The working section of the University of Southampton channel is 21m in length, 1.35m wide and a maximum 0.4m depth for steady operation. For the Wallingford channel the dimensions are; 25m in length, 2.4m wide and a maximum 0.7m depth for steady operation. Using Froude scaling, the experimental flow domain was scaled from a prototype MCEC deployment site with an average full scale depth of 15-30m. Spring peak and neap peak tidal flow velocities are in the range of 0-3m/s. It was assumed that a feasible full-scale ramp foundation height would be 10-15% of the average flow depth.

To determine the potential benefits of the ramp foundation, the velocity was mapped upstream of the MCEC, across the ramp and also downstream of the MCEC in order to characterise the wake. In addition to this the actuator plate thrust was recorded to provide a direct measure of the ramp benefits in terms of thrust and resulting power gain. The actuators were mounted on a thin stainless steel support arm which made up part of a pivot arrangement to magnify the small thrust forces on the actuators. A 10N button load cell was used to measure the total thrust force. In order to measure the velocity and visualise the flow field around the ramps and actuator plates, samples were taken using a high frequency

Acoustic Doppler Velocimeter (ADV). Operational issues and the accuracy of ADVs have been addressed at length in many publications [9-10]. Data was filtered to remove noise and spurious points, although the large quantity of suspended particles in both channels minimised sample errors, again filtering techniques have been addressed in many publications [11-12]. Filtering is required to improve measurements of higher order flow effects such as turbulence intensity and shear stresses, as spikes in the data give the impression of increasing energy within the flow. However filtering has a very small effect for mean flow velocities as spikes are generally equally positive and negative. All samples were filtered using a velocity cross-correlation filter ultimately chosen due to ease of use and effectiveness after a single pass [12].

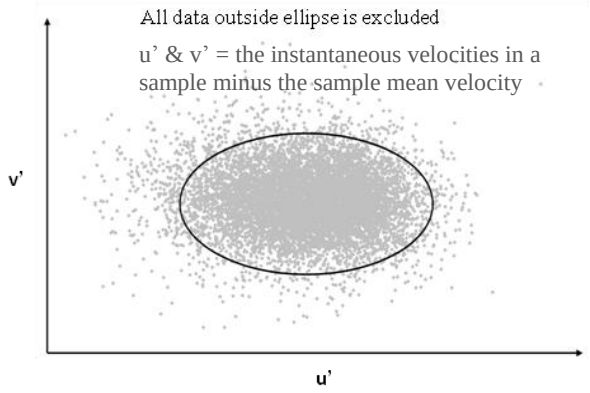

Fig. 6 Velocity correlation filtering method

Velocities (u,v,w) in all three planes (x,y,z) are defined as a non-dimensional number relative to the average free-stream velocity. Eq. (1) is for velocities (u) in the downstream x-plane

$$u_{non\text{–}\dim} = u / u_o \qquad (1)$$

The ambient turbulence intensities in the circulating channels used during these studies were approximately 6-10% and were calculated in all three planes (u,v,w). Turbulence intensity is commonly defined as the root-mean-squared of the turbulent velocity fluctuations divided by the mean velocity of the sample.

B. *Horizontal axis and hydrofoil device tests*

Table I describes the ramp foundation and MCEC interaction tests presented in this paper (Fd represents the Froude Number). Tests 1-6 are for the 1:100 scale horizontal axis turbine (HAT) tested in the University of Southampton's Chilworth channel. Tests 7-10 are for the 1:100 scale Pulse Stream Commercial Demonstrator device (oscillating hydrofoils), tested in HR Wallingford's general purpose flume.

C. *Free-stream ramp augmentation benefits*

Fig. 7 shows across ramp velocity gains and predicted power gains from previous experimental work without the presence of a MCEC simulator [1]. These ramp only tests clearly show that the degree of flow acceleration and hence power gain is dependent on the lateral channel blockage of the ramp structure. Clearly a ramp occupying the entire width of the channel would not be feasible except perhaps in a tidal fence application [13]. Thus when considering the use of ramp foundations the ramp width or overall array width must be tuned to the channel width to maximise the power benefits.

TABLE I
RAMP FOUNDATION AND MCEC INTERACTION TESTS

Test	Device	Fd	Flow Depth (m)	Ramp Height (m)
1	HAT	0.15	0.30	0.03
2	HAT	0.20	0.30	0.03
3	HAT	0.25	0.30	0.03
4	HAT	0.22	0.30	0.03
5	HAT	0.17	0.30	0.03
6	HAT	0.20	0.20	0.03
7	PSCD	0.15	0.25	0.025
8	PSCD	0.20	0.25	0.025
9	PSCD	0.25	0.25	0.025
10	PSCD	0.20	0.20	0.025

The following sections consider new work where the ramp foundations are modelled with the presence of MCEC simulators (actuators).

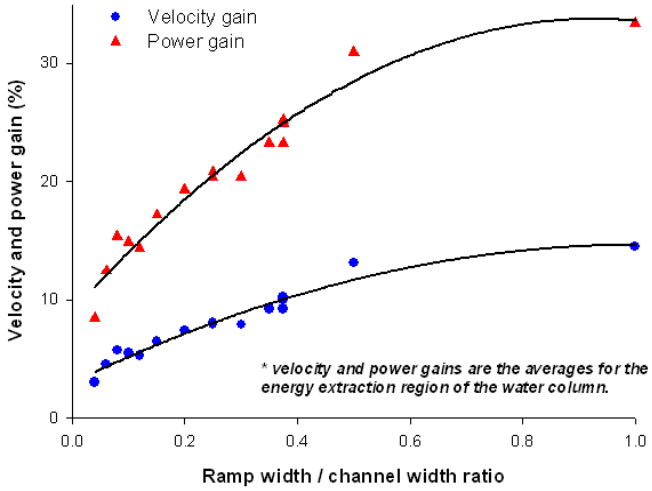

Fig. 7 Potential velocity and power gain - preliminary testing without MCECs presence

D. *Horizontal axis device*

Tests 1-6 (Table I) involved mapping the flow around the model horizontal axis tidal turbine in various flow conditions. An actuator disk was used with a solidity to match a MCEC operating at peak efficiency/rated power, at its rated velocity of 3m/s (optimum thrust coefficient is 0.9 for a horizontal axis turbine [5]). This section discusses the non-dimensional trends found from the ADV flow mapping. Thrust and power measurements are discussed in section F.

Fig. 8 shows the variation of the horizontal velocity component, u, with height above the bed, h, for the free-stream flow profile and the across ramp profile with and

without a MCEC present. At a first glance it might appear that the ramp foundation is providing little flow acceleration benefit to the MCEC because the free-stream and across ramp profiles are similar, but this is not the case, as would be expected from momentum theory; when flow encounters the MCEC it is retarded due to device blockage. Without the ramps presence the magnitude of the velocities would be lower and less energy would be avaiable for extraction (this is confirmed when comparing the thrust in section F).

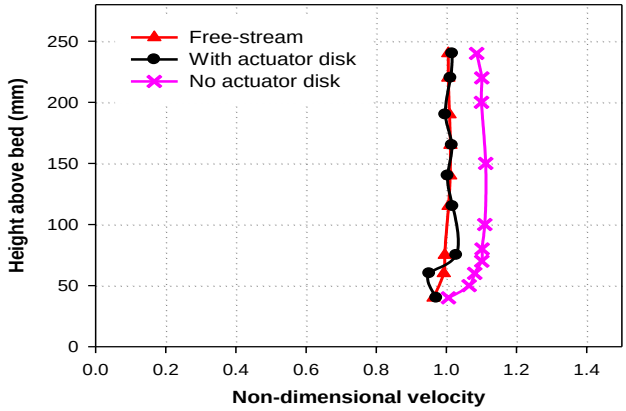

Fig. 8 Typical vertical velocity profiles across ramp foundation with and without actuator disk present.

Fig. 9 shows a typical horizontal plane flow field around a horizontal axis MCEC. The plot clearly shows the reduced velocity flow immediately upstream of the device, the flow acceleration around the MCEC and the downstream wake development. It seems that the majority of the downstream wake is broken down within 20 disk diameters; this agrees with work presented by Myers and Bahaj. [5] which showed significant velocity recovery (up to 95%) at 20-diameters downstream, for a turbulence intensity of ≈8%, suggesting faster recovery at full-scale sites. It is also encouraging in terms of farm spacing that the addition of a ramp foundation does not appear to significantly increase the wake length.

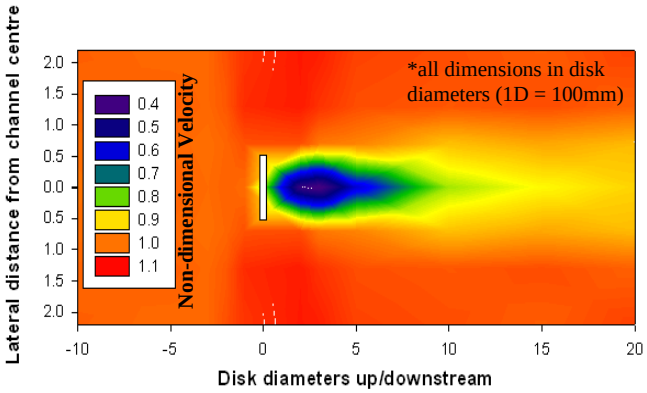

Fig. 9 mid-depth horizontal non-dimensional velocity flow map around the PSCD.

E. *Hydrofoil device*

Tests 7-10 (Table I) involved mapping the flow around the model PSCD oscillating hydrofoil device. Again the actuator plate's porosity was chosen to match the device's solidity over a range of operating conditions. Presented here are the results from a PSCD operating at peak efficiency/rated power, at its rated velocity of 2.5m/s.

Fig. 10 shows the vertical velocity profiles for the PSCD. The same trend can be seen in Fig. 8 and other results not presented in this paper, with the free-stream and across ramp (with MCEC) profiles coninciding. A general rule can thus be established; the free-stream velocity profile and across ramp profiles are approximately equal in magnitude. One could perhaps say the ramp foundation is effectively removing the negative effects of flow retardation from axial induction.

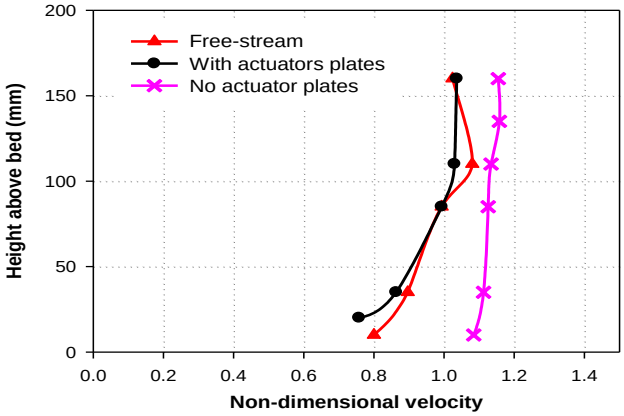

Fig. 10 Typical vertical velocity profiles across ramp foundation with and without actuator plates present.

Fig. 11 shows the typical flow field around the PSCD in the horizontal plane. The structure of the flow field is almost idential to that of the horizontal axis MCEC; with the retarded flow region immediately upstream of the device, flow acceleration around the PSCD and the downstream wake development region.

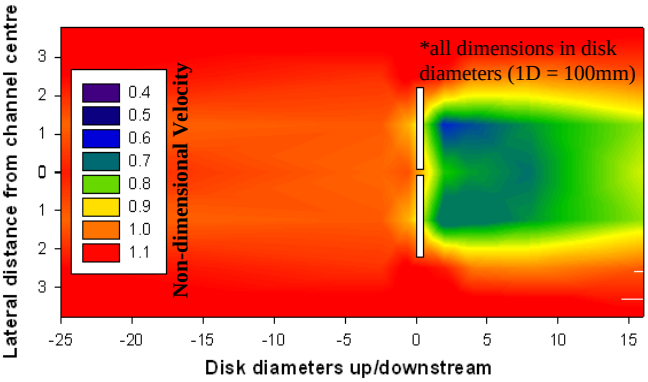

Fig. 11 mid-depth horizontal non-dimensional velocity flow map around the PSCD.

F. *MCEC thrust and power benefits*

Previous experimental work [1-2] has focused on the velocity augmentation effects of a ramp foundation without the presence of a MCEC simulator. In order to establish the true device thrust and power gains further testing with actuator disks and plates mounted above a scaled ramp foundation were conducted. Some key results from these are presented in Table II for a model HAT and the PSCD.

TABLE II
RAMP FOUNDATION AND MCEC INTERACTION RESULTS

Test	R	No MCEC thrust gain (%)	Calc. No MCEC power gain (%)	Measured thrust gain with MCEC (%)	Calc. power gain with MCEC (%)
2	0.22	13.34	19.28	8.63	12.66
3	0.22	13.34	19.28	8.06	11.84
4	0.22	13.34	19.28	8.87	13.00
9	0.20	12.65	18.32	6.10	9.01
10	0.20	12.65	18.32	5.87	8.67

It can be concluded from these tests that when modelling ramp foundations with the presence of a MCEC the thrust and power benefits will be reduced. Resulting power benefits are found to be in the region of 8-15% for lateral blockage ratios (R) of 0.20-0.22. ('R' is defined as the ratio of ramp width to channel width). These values are approximately 35% less than those presented in section C. The justification for this reduction in potential is the fact that the combined blockage effect of the MCEC device and ramp will force a proportion of the flow around and away from the influence of the ramp.

Table II also highlights the importance of lateral blockage. With increased blockage (e.g. a wider ramp/device width or a wider array) the power gain potential of ramp foundations increases significantly.

Although these results reveal that the potential for power/thrust amplification is less than previously thought, it must be re-iterated that ramp foundations have multiple benefits in addition to increasing energy yield; they make up a large proportion of the foundation down-force, can aid scour protection and provide an engine room for machinery.

IV. TECHNO-ECONOMIC ANALYSIS

For the ramp concept to be commercially viable it must primarily be technically feasible but equally as important, it must be economically viable. The presence of the ramp will increase the device power output across the tidal cycle and hence increase the revenue generated from the exported energy. But despite the ramp foundation being of multi-use, such as acting as an integral foundation, there will be an increased capital cost involved compared with a conventional MCEC. A techno-economic analysis has been conducted for Pulse Tidal's commercial demonstrator which considers a break down of the capital costs of components, installation costs, operation and maintenance costs and the electricity revenue generated across a full tidal cycle. A Net Present Value (NPV) analysis has been applied to the PSCD. The method is used to analyse the viability/profitability of the project taking into account the various costs (a NPV of greater than zero indicates a project is viable and profitable). NPV analysis uses "discount factors" to take into account that the value of money today will not be the same as its value at the end of the project. The design life of the PSCD is 25 years and hence this is considered the overall project duration. The Carbon Trust [14] recommends a discount factor of 15% for "1st commercial marine energy schemes" and 8% for "matured marine energy technology". During the analysis a range of discount factors from 15-8% were considered to model the PSCD at various stages of commercial development. The current demonstration project is considered to have a discount factor of 15%. As a demonstrator it is not designed to be a highly profitable project, but the analysis can still be used to estimate the general financial benefit of ramp foundations.

Results are presented in non-dimensional form by dividing the NPVs by the estimated capital cost of the project.

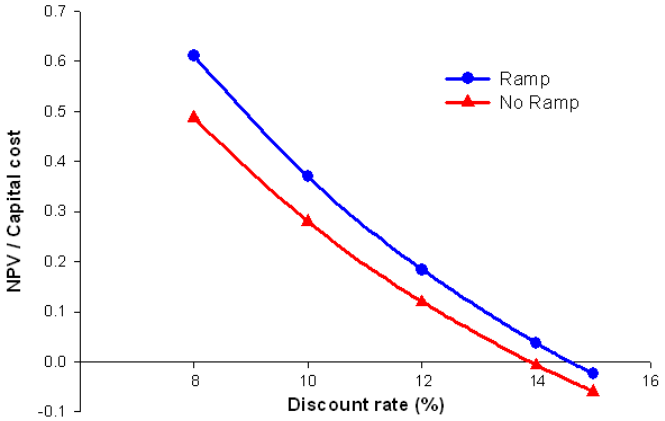

Fig. 12 PSCD NPV analysis (25 year design life)

Fig. 12 displays the results from the NPV analysis, it can be clearly seen that ramp foundations offer significant financial benefits. By integrating the area under the curves, an impression of the average overall financial benefit of a ramp foundation is estimated at 23%. This is a significant financial gain and clearly shows ramp foundations could be a financial reality as well as being technically viable. Fig. 12 shows that in its current commercial state the PSCD is unlikely to be profitable (not unexpected for a demonstration device), but with zero NPV values occurring with discount factors of 14.6% with a ramp and 13.9% without a ramp, it is anticipated with a small amount of development that the next generation PSCD device would be a fully profitable concern.

V. CONSTRUCTION, DEPLOYMENT AND RECOVERY

Construction, deployment, recovery and maintenance are critical aspects for the commercialisation of a MCEC operating with a ramp foundation. A concrete or fabricated steel caisson structure is proposed for the ramp foundation, these have been extensively used for gravity based foundations.

The principle advantage of using a caisson type structure is that the bulk of the fabrication can be done onshore or in dry docks. The structure can then be floated and towed to the offshore installation site and gradually sunk into position. If required additional buoyancy could be added by attaching buoyancy tanks. Gerwick [15] states that the principle failure mechanism is sliding for water depths of less than 150-200m and this can be prevented by attaching steel skirts and pin piles to the foundation. They effectively penetrate the seabed and force the failure mechanism further below the seafloor and in addition provide extra scour protection. When

designing marine structures it is vital to consider loading at every stage of construction and accidental conditions such as unplanned flooding of a buoyancy tank during delivery to site.

A novel deployment and recovery strategy is under development for a full scale commercial demonstrator (Fig. 13). The MCEC has been designed with an integral ramp foundation. A "transverse strut" which connects the base ramp to a seabed foundation is utilised to constrain the position of the base through the water column as buoyancy and ballast is used to raise and lower the MCEC. This method has significant advantages over a purely gravity based approach in terms of; lateral resistance of loads and providing active control of both deployment and recovery. The proposed deployment and recovery is thus:

1. Deliver assembly to site.
2. Float base ramp and connect MCEC.
3. Install seabed foundation, i.e. install piles, grouting or swaging.
4. Connect transverse strut to seabed foundation.
5. Float base ramp towards the floating free-end of the transverse strut and connect.
6. Lower device to seabed using ballast tanks.
7. When required expel ballast and raise device to surface for maintenance. For large maintenance/repair procedures, device would be disconnected from the transverse strut and towed to a suitable port or dry dock.

Preliminary structural calculations for a concrete caisson ramp foundation were presented in [1]. These calculations were for a purely gravity based foundation and considered the forces that contribute to failure mechanisms, including; MCEC thrust, drag from the support structure/foundation and the buoyancy force. The force which prevents failure is the mass weight of the foundation and the MCEC. Factors of safety were calculated by dividing the magnitude of the forces/moments resisting failure by those which contribute to failure. Provided these factors are in excess of unity the concept can be assumed to work, in reality in detailed design the factors may need to be greater to resist extreme loading conditions. Factors of safety against overturning and bed shear failure (sliding) ranged from 1.12-1.84, all in excess of unity.

These preliminary structural calculations were modified for a fabricated steel plate foundation (Fig. 13). The density of steel was assumed to be 8000 kg/m^3 and the weight of the entrained water within the base was included in the calculations. The foundation height was assumed to be 10% of the mean flow depth. Again factors of safety against overturning and sliding failures were in excess of unity, ranging from 1.13-1.86 depending on the flow depth (Table III).

Both the results from the concrete and steel calculations are very encouraging, it can be concluded that even with a purely gravity based foundation, the concept is structurally viable. With the increased lateral restraint from a transverse strut connection between the seabed and base ramp these factors of safety would increase dramatically.

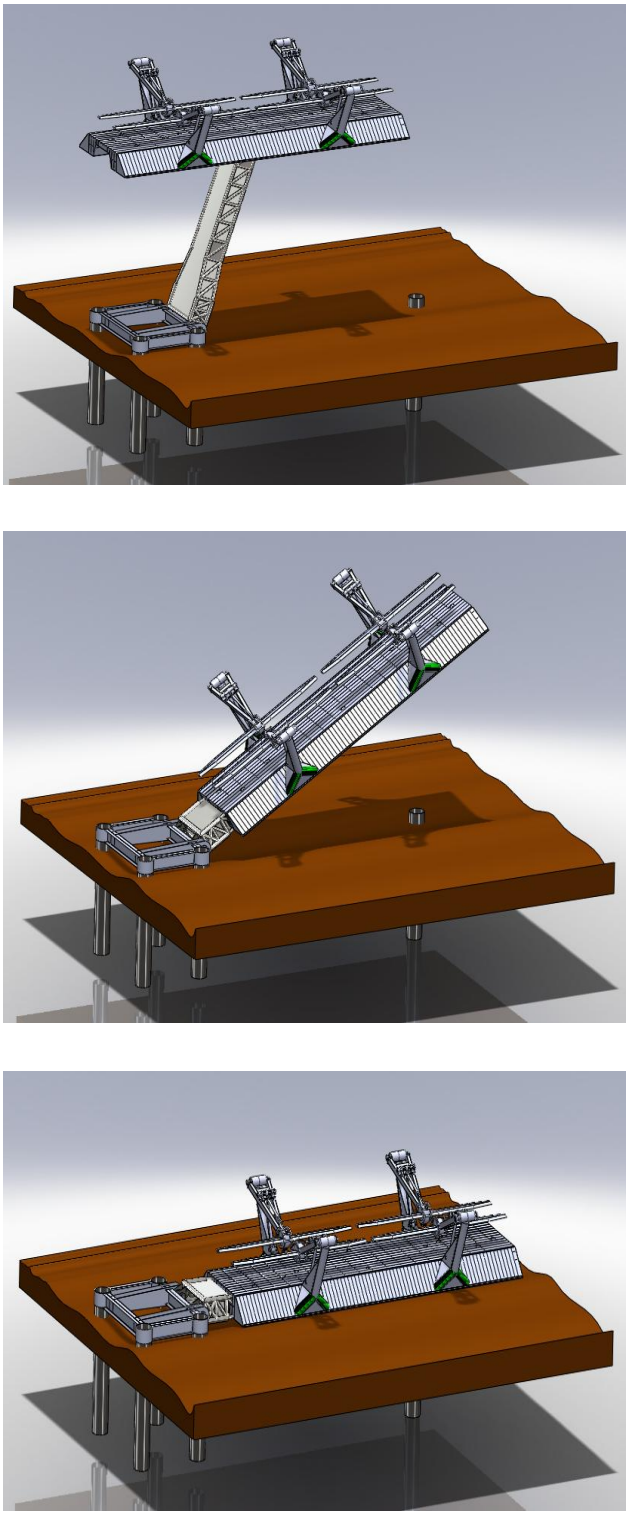

Fig. 13 deployment and recovery strategy: (a) surface maintenance height. (b) mid-water depth. (c) operating height

TABLE III
STABILITY CALCULATIONS – DEVICE WITH A STEEL RAMP

Turbine diameter	**Flow depth**	**Spring peak velocity**	**Overturning factor of safety**	**Sliding factor of safety**
m	m	m/s		
5	10	3.0	1.86	1.13
7.5	15	3.0	1.74	1.26
10	20	3.0	1.63	1.34
15	30	3.0	1.45	1.42

VI. CONCLUSIONS

Ramp based foundations could be utilised to increase MCEC power outputs and to improve the economic viability of shallow tidal stream sites (10-30m) that currently have insufficient velocities for economic energy extraction. Fundamental work, without the presence of a MCEC simulator, concluded that ramps could provide power benefits of 12-30% depending on ramp size and flow depth [1,2]. On the basis of this fundamental work Pulse Tidal Ltd. are designing their commercial demonstration device with an integral base foundation ramp. Another key conclusion from the fundamental testing is that the degree of flow enhancement and hence power gain is dependant on the lateral channel blockage of the ramp structure. When considering the use of ramp foundations, the ramp width or array width must be tuned to the channel width to maximise the power benefits.

The combined ramp and MCEC simulator experimental testing presented in this paper concludes that the thrust and power benefits of ramp foundations decreases from 12-30% to 8-15% when a MCEC is interacting with a ramp. This is important as this combination represents the full scenario and this reduction in benefit can be attributed to the increased channel blockage presented by the MCEC. The MCEC blockage is effectively forcing a proportion of flow away from the ramp/MCEC. Despite this reduction it must be re-iterated that ramp foundations offer multiple benefits other than increased energy yield, including; added foundation down-force, scour protection and an engine room for machinery.

A general rule is established for MCECs operating with a ramp foundation; the free-stream vertical velocity profile and the across ramp profile are approximately equal in magnitude. One could perhaps say ramp foundations effectively remove the negative flow retardation effects from axial induction.

A NPV techno-economic analysis for Pulse Tidal's PSCD device concluded that ramp foundations could be a financial reality as well as a technical reality. The overall financial benefit of ramp foundations was estimated at 23.7%.

A novel deployment and recovery strategy is proposed which is currently being developed for the PSCD. Preliminary structural calculations for both a concrete and steel fabricated ramp foundation concluded that factors of safety against sliding and over turning would all be in excess of unity for a purely gravity based foundation.

In summary it appears that ramp based foundations have the potential to be both a technical and commercial reality provided they are deployed in suitable locations. Suitable locations would be constrained to shallow flows (10-30m) and channels with a suitable lateral blockage ratio.

ACKNOWLEDGMENT

The project has been jointly funded by the Engineering and Physical Sciences Research Council (EPSRC) and IT Power Ltd. Thanks must be given to HR Wallingford Ltd. for allowing access and providing support for the testing in their general purpose flume.

REFERENCES

[1] J. Giles, L. Myers, A. Bahaj, J. O'Nians and B. Shelmerdine, "Foundation-based flow acceleration structures for marine current energy converters", *IET Renewable Power Generation,* awaiting publication.

[2] J. Giles, L. Myers, A. Bahaj and J. O'Nians, "An experimental study to assess the potential benefits of foundation-based flow acceleration structures for marine current energy converters", *8th European Wave and Tidal Energy Conference,* Uppsala, Sweden, 2009.

[3] M. Paish, J. Giles and B. Panahandeh, "The Pulse Stream concept, and the development of the Pulse Stream Commercial Demonstrator", *3rd International Conference on Ocean Energy,* Bilbao, Spain, 2010.

[4] J. Whelan, J. Graham and J. Peiro, "A free-surface and blockage correction for tidal turbines", *Journal of Fluid Mechanics,* vol. 624, pp. 281-291, 2009.

[5] L. Myers and A. Bahaj, "Experimental analysis of the flow field around horizontal axis tidal turbines by use of scale mesh disk rotor simulators", *Ocean Engineering,* vol. 37, pp. 218–227, 2010.

[6] J. Giles, L. Myers, A. Bahaj and B. Shelmerdine, "The downstream wake response of marine current energy converters operating in shallow tidal flows", *World Renewable Energy Congress 2011,* Linköping, Sweden, 2011.

[7] L.Vermeer, J. Sorensen and A. Crespo, "Wind turbine wake aerodynamics", *Progress in Aerospace Sciences,* vol. 39, pp. 467-510, 2003.

[8] P. Sforza, P. Sheerin and M. Smorto, "Three-dimensional wakes of simulated wind turbines", *AIAA Journal,* vol. 19, pp. 1101-1107, 1981.

[9] A. Lohrmann, R. Cabrera and N. Kraus, "Acoustic-Doppler Velocimeter (ADV) for Laboratory Use", Fundamentals and Advancements in Hydraulic Measurements and Experimentation", *ASCE,* pp. 351-365, 1994.

[10] G. Voulgaris and J. Trowbridge, "Evaluation of the Acoustic Doppler Velocimeter (ADV) for Turbulence Measurements", *Journal of Atmospheric and Oceanic Technology,* vol. 15, pp. 272-289, 1998.

[11] H. Chanson, M. Trevethan and S. Aoki, "Acoustic Doppler velocimetry (ADV) in a small estuarine system. Field experience and despiking", *XXXI IAHR Congress, Seoul, Korea, 2005.*

[12] L. Cea, J. Puertas and L. Pena, "Velocity measurements on highly turbulent free surface flow using ADV", *Experiments in Fluids,* vol. 42, pp. 333-348, 2007.

[13] J. Giles, I. Godfrey, I. Bryden, L. Myers, J. O'Nians, A. Bahaj and J. Griffiths, "An innovative tidal fence development for the Severn Estuary, UK", *3rd International Conference on Ocean Energy,* Bilbao, Spain, 2010.

[14] Entec UK Ltd, "Cost estimation methodology, the Marine Energy Challenge approach to estimating the cost of energy produced by marine energy systems", *The Carbon Trust,* May 2006.

[15] B. Gerwick, "Construction of marine and offshore structures", Boca Raton, London, New York, Washington D.C.: CRC Press, 2000.

References

ABD-EL-MALEK, M. B. & MASOUD, S. Z. 1987. Linearized solution of a flow over a ramp. *Applied Mathematical Modelling,* 12**,** 406-410.

ABP 2008. Atlas of UK Marine Renewable Energy Resources: Technical Report. ABP Marine Environmental Research Ltd, Department for Business, Enterprise & Regulatory Reform.

ADAMS, N., RANFORD, D. & LIVINGSTON, D. 2011. Modelling and Optimisation of Tidal Arrays. *In:* Proceedings of the 9th European Wave and Tidal Energy Conference, 2011 Southampton, UK.

ANDERSEN, O. B., EGBERT, G. D., EROFEEVA, S. Y. & RAY, R. D. 2006. Mapping nonlinear shallow-water tides: a look at the past and future. *Ocean Dynamics,* 56**,** 416-429.

AUBERTINE, C. D., EATON, J. K. & SONG, S. 2004. Parameters controlling roughness effects in a separating boundary layer. *International Journal of Heat and Fluid Flow,* 25**,** 444-450.

BAHAJ, A. S. 2008. The Status of Tidal Stream Energy Conversion. Southampton: IEA-OES Annual Report 2008.

BAHAJ, A. S. 2011. Generating electricity from the oceans. *Renewable and Sustainable Energy Reviews,* 15**,** 3399-3416.

BAHAJ, A. S., BATTEN, W. M. J., MOLLAND, A. F. & CHAPLIN, J. R. 2005. Experimental Investigation into the Hydrodynamic Performance of Marine Current Turbines. *Sustainable Energy Series: Report 3.* Southampton: University of Southampton.

BAHAJ, A. S., MOLLAND, A. F., CHAPLIN, J. R. & BATTEN, W. M. J. 2007a. Power and thrust measurements of marine current turbines under various hydrodynamic flow conditions in a cavitation tunnel and a towing tank. *Renewable Energy,* 32**,** 407-426.

BAHAJ, A. S. & MYERS, L. 2004. Analytical estimates of the energy yield potential from the Alderney Race (Channel Islands) using marine current energy converters. *Renewable Energy,* 29**,** 1931-1945.

BAHAJ, A. S., MYERS, L. E., THOMSON, M. D. & JORGE, N. 2007b. Characterising the wake of horizontal axis marine current turbines. *In:* Proceedings 7th European Wave and Tidal Energy Conference, 2007 Porto, Portugal. 11-14.

BAHAJ, A. S. & MYERS, L. E. 2013. Shaping array design of marine current energy converters through scaled experimental analysis. *Energy,* 59**,** 83-94.

BAI, K. J. 1979. Blockage correction with a free surface. *Fluid Mechanics,* 94**,** 433-452.

BAI, L., SPENCE, R. R. G. & DUDZIAK, G. 2009. Investigation of the Influence of Array Arrangement and Spacing on Tidal Energy Converter (TEC) Performance using a 3-Dimensional CFD Model. *In:* Proceedings of the 8th European Wave and Tidal Energy Conference, 2009 Uppsala, Sweden.

BAKER, R. W., WALKER, S. N. & KATEN, P. C. 1985. Wake measurements around operating wind turbines. *Journal of Solar Energy Engineering,* 107**,** 183-185.

BARNSLEY, M. J. & WELLICOME, J. F. 1990. Final Report on the 2nd Phase of Development and testing of a horizontal axis wind turbine test rig for the investigation of stall regulation aerodynamics, Carried out under ETSU Agreement.

BATTEN, W. M. J. & BAHAJ, A. S. 2006. CFD simulation of a small farm of horizontal axis marine current turbines. *In:* World Renewable Energy Congress IX, 2006 Florence, Italy. Elsevier.

BELLONI, C. S. K. & WILLDEN, R. H. J. 2011. Flow Field and Performance Analysis of Bidirectional and Open-centre Ducted Tidal Turbines. *In:* Proceedings of the 9th European Wave and Tidal Energy Conference, 2011 Southampton, UK.

BETZ, A. 1920. Das maximum der theoretisch moglichen ausnutzung des windes durch windmotoren. *Z. Gesamte Turbinenwesen,* Heft 26.

BLACK AND VEATCH CONSULTING LTD 2004. UK, Europe and global tidal stream energy resource assessment. Carbon Trust.

BLACK AND VEATCH CONSULTING LTD 2005. Phase II UK tidal stream energy resource assessment. Carbon Trust.

BLANCKAERT, K. & LEMMIN, U. 2006. Means of Noise Reduction in Acoustic Turbulence Measurements. *Journal of Hydraulic Research,* 44**,** 3-17.

BLUNDEN, L. S. 2009. *New approach to tidal stream energy analysis at sites in the English Channel.* Doctor of Philosophy, University of Southampton.

BLUNDEN, L. S. & BAHAJ, A. S. 2006. Initial evaluation of tidal stream energy resources at Portland Bill, UK. *Renewable Energy,* 31**,** 121-132.

BLUNDEN, L. S. & BAHAJ, A. S. 2007. Tidal energy resource assessment for tidal stream generators. *Proceedings of the Institution of Mechanical Engineers,* 221**,** 137-146.

BLUNDEN, L. S., BATTEN, W. M. J., HARRISON, M. E. & BAHAJ, A. S. 2009. Comparison of boundary-layer and field models for simulation of flow through multiple-row tidal fences. *In:* Proceedings of the 8th European Wave and Tidal Energy Conference, 2009 Uppsala, Sweden.

BONAKDARI, H., LARRARTE, F., LASSABATERE, L. & JOANNIS, C. 2008. Turbulent velocity profile in fully-developed open channel flows. *Environ Fluid Mech,* 8, 1-17.

BOUSSINESQ, J. 1877. Théorie de l'Écoulement Tourbillant, Mem. Présentés par Divers Savants Acad. *Sci. Inst. Fr.,* 23**,** 46-50.

BOYLE, G. 2004. *Renewable Energy, Power for a Sustainable Future,* Oxford, Oxford University Press.

BP 2010. BP Statistical Review of World Energy.

BRETON, S.-P. & MOE, G. 2009. Status, plans and technologies for offshore wind turbines in Europe and North America. *Renewable Energy,* 34**,** 646-654.

BROWN, E., COLLING, A., PARK, D., PHILLIPS, J., ROTHERY, D. & WRIGHT, J. 1999. *Waves, Tides and Shallow-water Processes,* Oxford, Reed Educational and Professional Publishing Ltd.

BRYDEN, I. G. 2006. The marine energy resource, constraints and opportuntities. *Maritime Engineering,* 159**,** 55-65.

BRYDEN, I. G. & COUCH, S. J. 2006. ME1-marine energy extraction: tidal resource analysis. *Renewable Energy,* 31**,** 133-139.

BRYDEN, I. G., COUCH, S. J., OWAN, A. & MELVILLE, G. T. 2007. Tidal current resource assessment. *Proceedings of the Institution of Mechanical Engineers, Power and Energy,* 221**,** 125-135.

BRYDEN, I. G., GRINSTED, T. & MELVILLE, G. T. 2005. Assessing the potential of a simple tidal channel to deliver useful energy. *Applied Ocean Research,* 26**,** 198-204.

BRYDEN, I. G. & MELVILLE, G. T. 2004. Choosing and evaluating sites for tidal current development. *Proceedings of the Institution of Mechanical Engineers, Part A: Journal of Power and Energy,* 218**,** 567-577.

BRYDEN, I. G., NAIK, S., FRAENKEL, P. L. & BULLEN, C. R. 1998. Matching tidal current plants to local flow conditions. *Energy,* 23**,** 699-709.

BUCHHAVE, P. & GEORGE, W., K. 1979. The measurement of turbulence with the laser-doppler anemometer. *Annual Review Fluid Mechanics,* 11**,** 443-503.

BUILTJES, P. J. 1978. The interaction of windmill wakes. *Proceedings of the 2nd Int. Symposium on wind energy systems, Amsterdam*.

BUKREEV, V. I., GUSEV, A. V. & LYAPIDEVSKII, V. Y. 2002. Transcritical Flow over a Ramp in an Open Channel. *Fluid Dynamics,* 37**,** 896-902.

BURTON, T., SHARPE, D., JENKINS, N. & BOSSANYI, E. 2001. *Wind Energy Handbook,* Chichester, Wiley.

CARBON TRUST 2006a. Cost estimation methodology. Entec UK Ltd.

CARBON TRUST 2006b. Future Marine Energy: results of the marine energy challenge: cost competitiveness and growth of wave and tidal stream energy. London: The Carbon Trust.

CEA, L., PUERTAS, J. & PENA, L. 2007. Velocity measurements on highly turbulent free surface flow using ADV. *Experiments in Fluids,* 42**,** 333-348.

CHADWICK, A., MORFETT, J. & BORTHWICK, M. 2004. *Hydraulics in Civil and Environmental Engineering,* Oxon, Spoon Press.

CHANSON, H., TREVETHAN, M. & AOKI, S.-I. 2005. Acoustic Doppler velocimetry (ADV) in a small estuarine system. Field experience and "despiking". *In:* Proceedings of the XXXI IAHR Congress, 2005 Seoul, Korea.

CHOW, V. T. 1959. *Open Channel Hydraulics,* London, McGraw-Hill Book Company.

CLEAN-CURRENT. 2011. *Clean Current* [Online]. Available: http://www.cleancurrent.com/ [Accessed 16.09.11].

CLÉMENT, A., MCCULLEN, P., FALC˜AO, A., FIORENTINO, A., GARDNER, F., HAMMARLUND, K., LEMONIS, G., LEWIS, T., NIELSEN, K., PETRONCINI, S., PONTES, M.-T., SCHILD, B.-O., SJÖSTRÖM, P., SØRESEN, H. C., & THORPE,T. 2002. Wave energy in Europe: current status and perspectives. *Renewable and Sustainable Energy Reviews,* 6(5)**,** 405-431.

CONNEL, P. J. & GEORGE, R. L. 1982. The wake of the MOD-0A1 wind turbine at two rotor diameters downwind on 3 December 1981. Battelle, U.S.: Pacific Northwest Laboratory.

COOPER, W. S., HINTON, C. L., ASHTON, N., SAULTER, A., MORGAN, C., PROCTOR, R., BELL, C. & HUGGETT, Q. 2005. An introduction to the UK marine renewable atlas. *Maritime Engineering,* 159**,** 1-7.

COUCH, S. J. & BRYDEN, I. G. 2006. Tidal current energy extraction: hydrodynamic resource chacteristics. *Proceedings of the Institution of Mechanical Engineers, Engineering for the Maritime Environment,* 220**,** 185-194.

DECC 2010. 2050 Pathways Analysis. London.

DECC 2011. Planning our electric future: a White Paper for secure, affordable and low carbon electricity.

DECC 2012. Digest of United Kingdom Energy Statistics 2012.

DEWEY, R., RICHMOND, D. & GARRETT, C. 2005. Stratified Tidal Flow over a Bump. *American Meteorological Society,* 35**,** 1911-1927.

DOMARATSKII, A. N., DUBNISHCHEV, Y. N., KORONKEVICH, V. P., SOBOLEV, V. S., STOLPOVSKII, A. A., UTKIN, E. N. & SHMOILOV, N. F. 1972. Comparson of readings from a laser Doppler velocimeter and a hot-wire anemometer in the wake behind a cylinder. *Journal of Applied Mechanics and Technical Physics,* 13**,** 114-116.

DONG, L., SHUJIE, W. & PENG, Y. 2010. An overview of development of tidal current in China: Energy resource, conversion technology and opportunities. *Renewable and Sustainable Energy Reviews,* 14**,** 2896-2905.

DOODSON. 1921. The Harmonic Development of the Tide-Generating Potential. *Proceedings of the Royal Society of London, Series A,* 100**,** 305-329.

DOUGLAS, J. F., GASIOREK, J. M., SWAFFIELD, J. A. & JACK, L. B. 2005. *Fluid Mechanics,* Harlow, Pearson Education Limited.

DRAPER, S., BORTHWICK, A. G. L. & HOULSBY, G. T. 2011. Energy Potential of a Tidal Fence Deployed Near a Coastal Headland. *In:* Proceedings of the 9th European Wave and Tidal Energy Conference, 2011 Southampton, UK.

DRAPER, S., HOULSBY, G. T., OLDFIELD, M. L. G. & BORTHWICK, A. G. L. 2010. Modelling tidal energy extraction in a depth-averaged coastal domain. *Renewable Power Generation, IET,* 4**,** 545-554.

DRAPER, S., STALLARD, T., STANSBY, P., WAY, S. & ADCOCK, T. 2013. Laboratory scale experiments and preliminary modelling to investigate basin scale tidal stream energy extraction. *In:* Proceedings of the 10th European Wave and Tidal Energy Conference, 2013 Aalborg, Denmark.

DTI 2003. Energy White Paper, Our energy future, creating a low carbon economy. *In:* DTI (ed.).

DTI 2005. DTI report, Development, installation and testing of a large scale tidal current turbine.

DTI 2007. Meeting the Energy Challange, A White Paper on Energy. *In:* DTI (ed.).

DURGUN, O. & KAFALI, K. 1991. Blockage Correction. *Ocean Engineering,* 18**,** 269-282.

DWORAK, J. A. & GOMEZ-VALDES, J. 2005. Modulation of shallow water tides in an inlet-basin system with mixed tidal range. *Journal of Geophysical Research,* 110.

DYER, K. R. 1986. *Coastal and Esturine Sediment Dynamics,* J. Wiley & Son.

ELLIOTT, D. 2009. Marine Renewables: a new innovation frontier. *Technology Analysis & Strategic Management,* 21**,** 267-275.

ETSU 1993. Tidal stream energy review. Hartwell Laboratory, Energy Technology Support Unit, DTI.

EUROPEAN COMMISSION 1996. The exploitation of tidal and marine currents. Commission of the European Communities.

EVANS, E. M. 1987. *Tidal stream energy.* Doctor of Philosophy, Plymouth Polytechnic.

EWEA 2007. European Wind Energy Association's response to the European Commission's Green Paper towards a future maritime policy for the Union: a European vision for the oceans and seas. Brussels.

FADDA, D. & RAAD, P. E. 1997. Open Channel Flow Over Submerged Obstructions: An Experimental and Numerical Study. *Journal of Fluids Engineering,* 119**,** 906-910.

FALCONER, R. A., JUNQIANG, X., BINLIANG, L. & ABMADIAN, R. 2009. The Severn Barrage and other tidal energy options: Hydrodynamic and power output modelling. *Science in China, Series E: Technological Sciences,* 52**,** 3413-3424.

FERRO, V. & BAIAMONTE, G. 1994. Flow velocity profiles in gravel-bed rivers. *Journal of Hydraulic Engineering,* 120**,** 60-78.

FINELLI, M., HART, D. D. & FONSECA, D. M. 1999. Evaluating the spatial resolution of an acoustic Doppler velocimeter and the consequences for measuring near-bed flows. *Limnology and Oceanography,* 44**,** 1793-1810.

FRAENKEL, P. L. 2002. Power from marine currents. *Proceedings of the Institution of Mechanical Engineers,* Part A 216**,** 1-14.

FRAENKEL, P. L. 2010. Development and testing of Marine Current Turbine's SeaGen 1.2MW tidal stream turbine. *In:* Proceedings of the 3rd International Conference on Ocean Energy, 2010 Bilbao, Spain.

FRAENKEL, P. L. & MUSGROVE, P. J. 1979. Tidal and river current energy systems. *In:* Proceedings of the International Conference on Future Energy Concepts, 1979 London, UK.

FRAU, J. P. 1993. Tidal Energy: Promising Projects. *IEEE Transactions on Energy Conversion,* 8**,** 552-558.

FRID, C., ANDONEGI, E., DEPESTELE, J., JUDD, A., RIHAN, D., ROGERS, S. I. & KENCHINGTON, E. 2012. The environmental interactions of tidal and wave energy generation devices. *Environmental Impact Assessment Review,* 32**,** 133-139.

FUNKE, S.W., FARRELL, P.E. & PIGGOTT, M.D. 2014. Tidal turbine array optimisation using the adjoint approach. *Renewable Energy,* 63**,** 658-673.

GARCIA, C. M., CANTERO, M. I., NINO, Y. & GARCIA, M. H. 2004. Acoustic Doppler Velocimeters (ADV) Performance Curves (APCs) sampling the flow turbulence. *In:* proceedings of the 2004 world water and environmental resources congress, 2004 Salt Lake City.

GARRETT, C. & CUMMINS, P. 2004. Generating Power from Tidal Currents. *Journal of waterway, port, coastal and ocean engineering,* 130**,** 114-118.

GARRETT, C. & CUMMINS, P. 2005. The power potential of tidal currents in channels. *Royal Society of London Proceedings* 461**,** 2563-2572.

GARRETT, C. & CUMMINS, P. 2007. The efficiency of a turbine in a tidal channel. *Journal of Fluid Mechanics,* 588**,** 243-251.

GARRETT, C. & CUMMINS, P. 2008. Limits to tidal current power. *Renewable Energy,* 33**,** 2485-2490.

GAUDIOSI, G. 1999. Offshore wind energy prospects. *Renewable Energy,* 16**,** 828-834.

GERWICK, B. C. 2000. *Construction of marine and offshore structures,* Boca Raton, London, New York, Washington D.C., CRC Press.

GILES, J., GODFREY, I., BRYDEN, I. G., MYERS, L., O'NIANS, J., BAHAJ, A. S. & GRIFFITHS, J. 2010. An innovative tidal fence development for the Severn Estuary, UK. *In:* Proceedings of the 3rd International Conference on Ocean Energy, 2010 Bilbao, Spain.

GILES, J., MYERS, L., BAHAJ, A. S. & SHELMERDINE, B. 2011. The downstream wake response of marine current energy converters operating in shallow tidal flows. *In:* Proceedings of the World Renewable Energy Congress, 2011 Linkoping, Sweden.

GILES, J. W., MYERS, L., BAHAJ, A. S. & O'NIANS, J. 2009. An experimental study to assess the potential benefits of foundation based flow acceleration structures for marine current energy converters. *In:* Proceedings of the 8th European Wave and Tidal Energy Conference, 2011. Uppsala, Sweden.

GORDON, L. 2000. Acoustic Doppler Velocimeter Performance in a Laboratory Flume. Mississippi: National Sedimentation Laboratory.

GORING, D. G. & NIKORA, V. I. 2002. Despiking Acoustic Doppler Velocimeter Data. *Journal of Hydraulic Engineering,* 128**,** 117-126.

GRABBE, M., LALANDER, E., LUNDIN, S. & LEIJON, M. 2009. A review of the tidal current energy resource in Norway. *Renewable and Sustainable Energy Reviews,* 13**,** 1898-1909.

GREAT BRITAIN. 2008. Climate Change Act 2008. (c.27). *London: The Stationery Office.*

HAMILL, L. 2001. *Understanding Hydraulics,* Basingstoke, Palgrave.

HAMMERFEST-STRØM. 2013. *Hammerfest Strøm AS* [Online]. Available: http://www.hammerfeststrom.com/ [Accessed 24.11.2013].

HAMMONS, T. J. 1993. Tidal Power. *Proceedings of the IEEE,* 8**,** 419-433.

HAMMONS, T. J. 2011. Tidal Power in the UK and Worldwide to Reduce Greenhouse Gas Emissions. *International Journal of Engineering Business Management,* 3**,** 16-28.

HARDISTY, J. 2007. Assessment of tidal current resources: case studies of estuarine and coastal sites. *Energy and Environment,* 18**,** 233-249.

HARDISTY, J. 2009. *The Analysis of Tidal Stream Power,* Chichester, John Wiley & Sons Ltd.

HARRIES, D., MCHENRY, M., JENNINGS, P. & THOMAS, C. 2006. Hydro, tidal and wave energy in Australia. *International Journal of Environmental Studies,* 63**,** 803-814.

HARRISON, M. E., BATTEN, W. M. J., BLUNDEN, L. S., MYERS, L. E. & BAHAJ, A. S. 2008. Comparisons of a Large Tidal Turbine Array Using the Boundary Layer and Field Wake Interaction Models. *In:* Proceedings of the 2nd International Conference on Ocean Energy, 2008 Brest, France.

HARRISON, M. E., BATTEN, W. M. J., MYERS, L. E. & BAHAJ, A. S. 2009. A comparison between CFD simulations and experiments for predicting the far wake of horizontal axis tidal turbines. *In:* Proceedings of the 8th European Wave and Tidal Energy Conference, 2009 Uppsala, Sweden.

HARRISON, M. E., BATTEN, W. M. J., MYERS, L. E. & BAHAJ, A. S. 2010. Comparison between CFD simulations and experiments for predicting the far wake of horizontal axis tidal turbines. *Renewable Power Generation, IET,* 4**,** 613-627.

HM GOVERNMENT 2009. The UK Renewable Energy Strategy. Norwich: TSO.

HSE 2002. Offshore Technology Report: Environment considerations. Norwich: Health & Safety Executive.

ISAACS, J. D. & SEYMOUR, R. J. 1973. The ocean as a power resource. *International Journal of Environmental Studies,* 4**,** 201-205.

IYER, A. S., COUCH, S. J., HARRISON, G. P. & WALLACE, A. R. 2009. Analysis and Comparision of Tidal Datasets. *In:* Proceedings of the 8th European Wave and Tidal Energy Conference, 2009 Uppsala, Sweden. 228-236.

JO, C. H., LEE, K. H. & RHO, Y. H. 2010. Recent TCP (Tidal Current Power) projects in Korea. *Science China,* 53**,** 57-61.

JONSSON, C., JOHNSON, P. B. & EAMES, I. 2011. Energy Extractors in Turbulent Flow: Wake Decay and Implications for Farm Layout. *In:* Proceedings of the 9th European Wave and Tidal Energy Conference, 2011 Southampton, UK.

KAWANISI, K. 2004. Structure of Turbulent Flow in a Shallow Tidal Estuary. *Journal of Hydraulic Engineering,* 130**,** 360-370.

KIRKGOZ, M. S. & ARDICHOGLU, M. 1997. Velcocity Profiles of Developing and Developed Open Channel Flow. *Hydraulic Engineering,* 3, 333-348.

KLAPTOCZ, V. R., RAWLINGS, G. W., NABAVI, Y., ALIDADI, M., LI, Y. & CALISAL, S. M. 2007. Numerical and Experimental Investigation of a Ducted Vertical Axis Tidal Current Turbine. *In:* Proceedings of the 7th European Wave and Tidal Energy Conference, 2007 Porto, Portugal.

KNIGHT, O. & HILL, K. 2007. Turning the tide: tidal power in the UK. Sustainable Development Commission.

KOBOLD. 2009. *Ponte di Archimede International* [Online]. Available: http://pontediarchimede.com [Accessed 17.09.09].

KRAUS, N., ASCE, M., LOHRMANN, A. & CABRERA, R. 1993. New Acoustic Meter for Measuring 3D Laboratory Flows. *Journal of Hydraulic Engineering,* 120**,** 406-412.

LALANDER, E. & LEIJON, M. 2009. Numerical modeling of a river site for in-stream energy converters. *In:* Proceedings of the 8th European Wave and Tidal Energy Conference, 2009.

LANE, S. N., BIRON, P. M., BRADBROOK, K. F., BUTLER, J. B., CHANDLER, J. H., CROWELL, M. D., MCLELLAND, S. J., RICHARDS, K. S. & ROY, A. G. 1998. Three-dimensional measurement of river channel flow processes using Acoustic Doppler Velocimetry. *Earth Surface Processes and Landforms,* 23**,** 1247-1267.

LANGE, C. F., DURST, F. & BREUER, M. 1999. Correction of hot-wire measurements in the near-wall region. *Experiments in Fluids,* 26**,** 475-477.

LE DUFF, A., PLANTIER, G., VALIERE, J.-C. & BOSCH, T. 2002. Velocity Measurement in a Fluid Using LDV: Low-Cost Sensor and Signal Processing Design. *In:* Proceedings of the First IEEE Interantional Conference on Sensors, 2002.

LOHRMANN, A., CABRERA, R., GELFENBAUM, G. & HAINES, J. 1995. Direct Measurements of Reynolds Stress with an Acoustic Doppler Velocimeter. *In:* Proceedings of the IEEE Fifth Working Conference on Current Measurement, 1995 St. Petersburg, Florida, USA.

LOHRMANN, A., CABRERA, R., KRAUS, N. & ASCE, M. 1994. Acoustic-Doppler Velocimeter (ADV) for Laboratory Use. *Fundamentals and Advancements in Hydraulic Measurements and Experimentation.* New York.

LUNAR ENERGY. 2011. *Lunar Energy* [Online]. Available: www.lunarenergy.co.uk [Accessed 17.09.11].

LYN, D. A. 1993. Turbulence Measurements in Open-Channel Flows Over Artificial Bed Forms. *Hydraulic Engineering,* 119.

MACLEOD, A. J., BARNES, S., RADOS, K. G. & BRYDEN, I. G. 2002. Wake effects in tidal current turbine farms. *In:* Proceedings of the International Conference on Marine Renewable Energy, 2002 Newcastle, UK.

MYCEK, P., GAURIER, B., GERMAIN, G., FACQ, J-V., BACCHETTI, T., PINON, G. & RIVOALEN, É. 2013. Characterisation of the Interactions between Horizontal Axis Turbines Aligned with the Flow. *In:* Proceedings of the 10th European Wave and Tidal Energy Conference, 2013 Aalborg, Denmark.

MALKI, R., MASTERS, I., WILLIAMS, A. J. & CROFT, T. N. 2011. The Influence of Tidal Stream Turbine Spacing on Performance. *In:* Proceedings of the 9th European Wave and Tidal Energy Conference, 2011 Southampton, UK.

MASON-JONES, A., O'DOHERTY, D. M., MORRIS, C. & O'DOHERTY, T. 2013. Influence of a velocity profile & support structure on tidal stream turbine performance. *Renewable Energy,* 52**,** 23-30.

MASSEY, B. 2006. *Mechanics of Fluids,* Oxon, Taylor & Francis.

MCCOMBES, T., JOHNSTONE, C. & GRANT, A. 2009. Unsteady 3D Wake Modelling for Marine Current Turbines. *In:* Proceedings of the 8th European Wave and Tidal Energy Conference, 2009 Uppsala, Sweden.

MCLELLAND, S. J. & NICHOLAS, A. P. 2000. A new method for evaluating errors in high-frequency ADV measurements. *Hydrological Processes,* 14**,** 351-366.

MCT. 2013. *Marine Current Turbines Ltd* [Online]. Available: www.marineturbines.com [Accessed 24.11.2013].

MEILE, T., DE CESARE, G., BLANCKAERT, K. & SCHLEISS, A. J. 2008. Improvement of Acoustic Doppler Velocimetry in steady and unsteady turbulent open-channel flows by means of seeding with hydrogen bubbles. *Flow Measurement and Instrumentation,* 19**,** 215-221.

MILNE, I. A., SHARMA, R. N., FLAY, R. G. J. & BICKERTON, S. 2010. The Role of Waves on Tidal Turbine Unsteady Blade Loading. *In:* Proceedings of the 3rd International Conference on Ocean Energy, 2010 Bilbao, Spain.

MOLLAND, A. F. & TURNOCK, S. R. 2007. *Marine Rudders and Control Surfaces,* Oxford, Butterworth-Heinemann.

MYERS, L. 2005. *Operational parameters of horizontal axis marine current turbines.* Doctor of Philosophy, University of Southampton.

MYERS, L. & BAHAJ, A. S. 2005. Simulated elcetrical power potential harnessed by marine current turbine arrays in the Alderney Race. *Renewable Energy,* 30**,** 1713-1731.

MYERS, L. & BAHAJ, A. S. 2007. Wake studies of a 1/30th scale horizontal axis marine current turbine. *Ocean Engineering,* 34**,** 758-762.

MYERS, L. & BAHAJ, A. S. 2009. Near wake properties of horizontal axis marine current turbines. *In:* Proceedings of the 8th European Wave and Tidal Energy Conference, 2009 Uppsala, Sweden.

MYERS, L., BAHAJ, A. S., GERMAIN, G. & GILES, J. 2008. Flow boundary interaction effects for marine current energy conversion devices. *In:* Proceedings of the World Renewable Energy Congress X, 2008 Glasgow, UK.

MYERS, L., GALLOWAY, P. & BAHAJ, A. S. 2011a. Operational issues surrounding the use of towing tanks for performance quantification of marine current energy converters. *In:* Proceedings of the 9th European Wave and Tidal Energy Conference, 2011 Southampton, UK.

MYERS, L. E. & BAHAJ, A. S. 2010. Experimental analysis of the flow field around horizontal axis tidal turbines by use of scale mesh disk rotor simulators. *Ocean Engineering,* 37**,** 218-227.

MYERS, L. E. & BAHAJ, A. S. 2012. An experimental investigation simulating flow effects in first generation marine current energy converter arrays. *Renewable Energy,* 37**,** 28-36.

MYERS, L. E., KEOGH, B. & BAHAJ, A. S. 2011b. Layout Optimisation of 1st -Generation Tidal Energy Arrays. *In:* Proceedings of the 9th European Wave and Tidal Energy Conference, 2011 Southampton, UK.

NEILL, S. P., JORDAN, J. R. & COUCH, S. J. 2012. Impact of tidal energy converter (TEC) arrays on the dynamics of headland sand banks. *Renewable Energy,* 37**,** 387-397.

NEPTUNE RENEWABLE ENERGY. 2010. *Neptune Proteus device* [Online]. Available: www.neptunerenewableenergy.com [Accessed 05.06.08].

NEWTON. 1687. *Philosophiæ Naturalis Principia Mathematica, Latin for "Mathematical Principles of Natural Philosophy.*

NIKORA, V. I. & GORING, D. G. 1998. ADV Measurements of Turbulence: can we improve their interpretation? *Journal of Hydraulic Engineering,* 124**,** 630-634.

NIKORA, V. I. & GORING, D. G. 2000. Flow Turbulence over Fixed and Weakly Mobile Gravel Beds. *Journal of Hydraulic Engineering,* 126**,** 679-690.

NORRIS, J. V. & DRONIOU, E. 2007. Update on EMEC activities, resource description, and characterisation of wave-induced velocities in a tidal flow *In:* Proceedings of the European Wave and Tidal Energy Conference, 11-13 Sept. 2007 Porto, Portugal.

NORTEK 2004. *Vectrino Velocimeter User Guide*.

O'DOHERTY, D. M., MASON-JONES, A., MORRIS, C., O'DOHERTY, T., BYRNE, C., PRICKETT, P. W. & GROSVENOR, R. I. 2011. Interaction of Marine Turbines in Close Proximity. *In:* Proceedings of the 9th European Wave and Tidal Energy Conference, 2011 Southampton, UK.

O'DOHERTY, T., EGARR, D. A., MASON-JONES, A. & O'DOHERTY, D. M. 2009. An assessment of axial loading on a five-turbine array. *Proceedings of the Institution of Civil Engineers, Energy,* 162**,** 57-65.

OPEN HYDRO. 2013. *OpenHydro* [Online]. Available: www.openhydro.com [Accessed 24.11.2013].

OPSI 2008. Energy Act 2008, Chapter 32. Office of Public Sector Information.

PAISH, M., GILES, J. & PANAHANDEH, B. 2010. The Pulse Stream concept, and the development of the Pulse Stream Commercial Demonstrator. *In:* Proceedings of the 3rd International Conference on Ocean Energy, 2010 Bilbao, Spain.

PELC, R. & FUJITA, R. M. 2002. Renewable energy from the ocean. *Marine Policy,* 26**,** 471-479.

PETHICK, J. S., MORRIS, R. K. A. & EVANS, D. H. 2009. Nature conservation implications of a Severn tidal barrage - A preliminary assessment of geomorphological change. *Journal for Nature Conservation,* 17**,** 183-198.

POGGI, D., PORPORATO, A. & RIDOLFI, L. 2002. An experimental contribution to near-wall measurements by means of a special laser Doppler anemometry technique. *Experiments in Fluids,* 32**,** 366-375.

POINDEXTER, C., RUSELLO, P. & VARIANO, E. 2011. Acoustic Doppler velocimeter-induced acoustic streaming and its implications for measurement. *Experiments in Fluids,* 50**,** 1429-1442.

POSTNOTE 2007. Electricity in the UK. *In:* TECHNOLOGY, P. O. O. S. A. (ed.).

POSTNOTE 2009. Marine Renewables. *In:* TECHNOLOGY, S. A. (ed.). Parliamentary Office.

PRANDLE, D. 1997. The influence of bed friction and vertical eddy viscosity on tidal propagation. *Continental Shelf Research,* 17**,** 1367-1374.

PRANDTL. 1904. On The Motion of Fluids with Very Little Friction.

PRANDTL, L. 1925. Bericht über Untersuchungen zur ausgebildeten Turbulenz, *Z. Angew. Math, Meth.,* 5**,** 136-139.

PRECHT, E., JANSSEN, F. & HUETTEL, M. 2006. Near-bottom performance of the Acoustic Doppler Velocimeter (ADV) - a comparative study. *Aquatic Ecology,* 40**,** 481-492.

RAMASAMY, M. & LEISHMAN, J. G. 2007. Benchmarking Particle Image Velocimetry with Laser Doppler Velocimetry for Rotor Wake Measurements. *AIAA Journal,* 45**,** 2622-2633.

RAUPACH, M. R., ANTONIA, R. A. & RAJAGOPALAN, S. 1991. Rough-wall turbulent boundary layers. *Applied Mechanics Reviews, American Society of Mechanical Engineers,* 44, 1-25.

REEVE, D. 2004. *Coastal engineering : processes, theory and design practice,* London, Spoon Press.

REYNOLDS, O. 1883. On the experimental investigation of the circumstances which determine whether the motion of water shall be direct or sinuous, and the law of resistance in parallel channels. *Phil. Trans. Roy. Soc. London Ser. A,* 174**,** 935-982.

RIPPETH, T., WILLIAMS, E. & SIMPSON, J. 2002. Reynolds Stress and Turbulent Energy Production in a Tidal Channel. *Journal of Physical Oceanography,* 32**,** 1242-1251.

ROBERSON, J. A. & CROWE, C. T. 1997. *Engineering Fluid Mechanics,* Canada, John Wiley & Sons.

ROC, T., GREAVES, D., CONLEY, D. C. & LEYBOURNE, M. 2013. Optimising commercial-scale TEC arrays: genetic algorithm, Fractal & Eco-mimicry. *In:* Proceedings of the 10th European Wave and Tidal Energy Conference, 2013 Aalborg, Denmark.

RODDIER, D., CERMELLI, C. & AUBAULT, A. 2007. Electrical power generation by tidal flow acceleration. *In:* Proceedings of the 26th International Conference on Offshore Mechanics and Arctic Engineering, 2007 San Diego, California.

RUSELLO, P. J. & COWEN, E. A. 2011. Turbulent dissipation estimates from pulse coherent doppler instruments. *In:* Proceedings of Current, Waves and Turbulence Measurements (CWTM), 2011 IEEE/OES 10th, 20-23 March 2011 2011. 167-172.

RUSELLO, P. J., LOHRMANN, A., SIEGEL, E. & MADDUX, T. 2006. Improvements in Acoustic Doppler Velocimetery. *In:* Proceedings of the 7th International Conference on Hydroscience and Engineering, 2006 Philadelphia, USA.

SALTER, S. H. & TAYLOR, J. R. M. 2007. Vertical-axis tidal-current generators and the Pentland Firth. *Proceedings of the Institution of Mechanical Engineers, Power and Energy,* 221**,** 181-199.

SETOGUCHI, T., SHIOMI, N. & KANEKO, K. 2004. Development of two-way diffuser for fluid energy conversion. *Renewable Energy,* 29**,** 1757-1771.

SFORZA, P. M., SHEERIN, P. & SMORTO, M. 1981. Three-dimensional wakes of simulated wind turbines. *AIAA Journal,* 19**,** 1101-7.

SHAFIEE, S. & TOPAL, E. 2009. When will fossil fuel reserves be diminished? *Energy Policy,* 37**,** 181 - 189.

SHANAHAN, G. 2009. Tidal Range Technologies. *IEA-OES Annual Report 2008*.

SHARPE, D. J. 2004. A general momentum theory applied to an energy-extracting actuator disc. *Wind Energy,* 7**,** 177-188.

SHEN, H. W., FEHLMAN, H. M. & MENDOZA, C. 1990. Bed Form Resistances in Open Channel Flows. *Hydraulic Engineering,* 116**,** 799-815.

SHIVES, M. & CRAWFORD, C. 2010. Overall Efficiency of Ducted tidal current turbines. *In:* Proceedings of OCEANS 2010, 20-23 September 2010 Seattle, USA.

SMITH, J. A. 2006. Wave–Current Interactions in Finite Depth. *Journal of Physical Oceanography,* 36**,** 1403-1419.

SNYDER, W. H. & CASTRO, I. P. 1999. Acoustic Doppler Velocimeter Evaluation in Stratified Towing Tank. *Journal of Hydraulic Engineering,* 125**,** 595-603.

SONG, S., DEGRAAFF, D. B. & EATON, J. K. 2000. Experimental study of a separating, reattaching, and redeveloping flow over a smoothly contoured ramp. *International Journal of Heat and Fluid Flow,* 21**,** 512-519.

SONG, S. S. & EATON, J. E. 2002. The effects of wall roughness on the separated flow over a smoothly contoured ramp. *Experiments in Fluids,* 33**,** 38-46.

SONG, T. & GRAF, W. H. 1996. Velocity and turbulence distribution in unsteady open-channel flows. *Journal of Hydraulic Engineering,* 122**,** 141-154.

SQW ENERGY 2008. Modelling Changes to the Renewables Obligation. *In:* SCOTTISH GOVERNMENT, E. (ed.).

SROKOSZ, M. A. 1987. Models of Wave-Current Interaction. *Modelling the Offshore Environment: Proceedings of an International Conference.* London, UK: The Society for Underwater Technology.

STALLARD, T., COLLINGS, R., FENG, T. & WHELAN, J. I. 2011. Interactions Between Tidal Turbine Wakes: Experimental Study of a Group of 3-Bladed Rotors. *In:* Proceedings of the 9th European Wave and Tidal Energy Conference, 2011 Southampton, UK.

SULLIVAN, P. & MCCOMBIE, P.. 2013. Optimisation of tidal power arrays using a genetic algorithm. *Proceedings of the Institution of Civil Engineers, Energy,* 166**,** 19-28.

SUN, X., CHICK, J. P. & BRYDEN, I. G. 2008. Laboratory-scale simulation of energy extraction from tidal currents. *Renewable Energy,* 33**,** 1267-1274.

SWAN, C. & JAMES, R. L. 2000. A simple analytical model for surface water waves on a depth-varying current. *Applied Ocean Research,* 22**,** 331-347.

TGL. 2013. *Tidal Generation Ltd* [Online]. Available: http://www.tidalgeneration.co.uk/ [Accessed 24.11.2013].

THORPE, T. 2005. The advantages of ducted over unducted turbines. *In:* Proceedings of the 6th European Wave and Tidal Energy Conference, 2005 Glasgow, UK. 523-528.

TOKE, D. 2011. The UK offshore wind power programme: A sea-change in UK energy policy? *Energy Policy,* 39**,** 526-534.

TROWSE, G. C. & EL-HAWARY, M. E. 2009. A review of methods for determining average available power from a tidal current. *In:* Proceedings of the Electrical Power & Energy Conference (EPEC), 22-23 Oct. 2009 Montreal, Canada.

TURNOCK, S. R., PHILLIPS, A. B., BANKS, J. & NICHOLLS-LEE, R. 2011. Modelling tidal current turbine wakes using a coupled RANS-BEMT approach as a tool for analysing power capture of arrays of turbines. *Ocean Engineering,* 38**,** 1300-1307.

TWIDELL, J. & WEIR, T. 2006. *Renewable Energy Resources,* London, Taylor & Francis.

VALLENTINE, H. R. 1969. *Applied Hydrodynamics,* London, Butterworth & Co. Limited.

VENABLES, M. 2008. Nuclear dawn. *Engineering and Technology,* 3**,** 50-53.

VENNELL, R. 2010. Tuning turbines in a tidal channel. *Journal of Fluid Mechanics,* 663**,** 253-267.

VENNELL, R. 2011a. Estimating the power potential of tidal currents and the impact of power extraction on flow speeds. *Renewable Energy,* 36**,** 3558-3565.

VENNELL, R. 2011b. Tuning tidal turbines in-concert to maximise farm efficiency. *Journal of Fluid Mechanics,* 671**,** 587-604.

VERDANT-POWER. 2012. *Verdant Power* [Online]. Available: www.verdantpower.com [Accessed 16.09.12].

VERMEER, L. J., SORENSEN, J. N. & CRESPO, A. 2003. Wind turbine wake aerodynamics. *Progress in Aerospace Sciences,* 39**,** 467-510.

VERMUELEN, P. E. J. 1979. Mixing of simulated wind turbine wakes in turbulent shear flow.

VOULGARIS, G. & TROWBRIDGE, J. H. 1998. Evaluation of the Acoustic Doppler Velocimeter (ADV) for Turbulence Measurements. *Journal of Atmospheric and Oceanic Technology,* 15**,** 272-289.

WATSON, J. & SCOTT, A. 2009. New nuclear power in the UK: A strategy for energy security? *Energy Policy,* 37**,** 5094-5104.

WHELAN, J., THOMSON, M., GRAHAM, J. M. R. & PEIRO, J. 2007. Modelling of free surface proximity and wave induced velocities around a horizontal axis tidal stream turbine. *In:* Proceedings of the 7th European Wave and Tidal Energy Conference, 2007 Porto, Portugal.

WHELAN, J. I., GRAHAM, J. M. R. & PEIRO, J. 2009. A free-surface and blockage correction for tidal turbines. *Journal of Fluid Mechanics,* 624**,** 281-291.

WHELAN, J. I. & STALLARD, T. 2011. Arguments for modifying the geometry of a scale model rotor. *In:* Proceedings of the 9th European Wave and Tidal Energy Conference, 2011 Southampton, UK.

WILSON, S. & DOWNIE, S. 2003. A review of possible marine renewable energy development projects and their natural hertiage impacts from a Scottish perspective. Scotish Natural Heritage.

WOLF, J. & PRANDLE, D. 1999. Some observations of wave-current interaction. *Coastal Engineering,* 37**,** 471-485.

WOODROFFE, C. D. 2002. *Coasts: Form, process and evolution,* Cambridge, Cambridge University Press.

WORLD ENERGY COUNCIL 1994. *New Renewable Energy Resources,* London, Kogan Page.

WU, S. & RAJARATNAM, N. 1996. Submerged Flow Regimes of Rectangular Sharp-Crested Weirs. *Journal of Hydraulic Engineering,* 122**,** 412-414.

WYATT, L. R. 2009. Wave and Tidal Power measurements using HF radar. *In:* Proceedings of the 8th European Wave and Tidal Energy Conference, 2009 Uppsala, Sweden.

WYMAN, P. R. & PEACHEY, C. J. 1979. Tidal current energy conversion. *In:* Proceedings of the International Conference on Future energy concepts, 1979 London, UK.

YAN, S. W., CHU, J., FAN, Q. J. & YAN, Y. 2009. Building a breakwater with prefabricated caissons on soft clay. *Geotechnical Engineering,* GE1**,** 3-12.

YUE, Z. & MALMSTROM, T. G. 1998. A simple method for low-speed hot-wire anemometer calibration. *Measurement Science and Technology,* 9**,** 1506-1510.

ZHIXIN, W., CHUANWEN, J., QIAN, A. & CHENGMIN, W. 2009. The key technology of offshore wind farm and its new development in China. *Renewable and Sustainable Energy Reviews,* 13**,** 216–222.